Brno University of Technology
Faculty of Mechanical Engineering
Institute of Machine and Industrial Design

Vysoké učení technické v Brně
Fakulta strojního inženýrství
Ústav konstruování

PERFORMANCE AND SAFETY IMPROVEMENT OF LARGE-SCALE HYDROSTATIC BEARINGS

Ing. Michal Michalec
Author
Autor práce

doc. Ing. Petr Svoboda, Ph.D.
Supervisor
Vedúci práce

Dissertation thesis
Dizertačná práca

Brno 2024

STATEMENT

I hereby declare that I have written the PhD thesis *Performance and safety improvement of large-scale hydrostatic bearings* on my own according to the advice of my supervisor doc. Ing. Petr Svoboda, Ph.D., and using the sources listed in the references.

…….
Michal Michalec

BIBLIOGRAPHICAL REFERENCE

MICHALEC, Michal. *Performance and safety improvement of large-scale hydrostatic bearings*. Brno, 2024. 104 p., PhD thesis. Brno University of Technology, Faculty of Mechanical Engineering, Institute of Machine and Industrial Design. Supervisor doc. Ing. Petr Svoboda, Ph.D.

ACKNOWLEDGEMENT

I would like to express my deepest appreciation to my supervisor, doc. Ing. Petr Svoboda, Ph.D., who supported and encouraged me throughout my study. I would like to extend my sincere thanks to the Head of our Tribology Research Group, prof. Ing. Ivan Křupka, Ph.D., as well as to our Department Director prof. Ing. Martin Hartl, Ph.D. for their support during my studies.

I could not have undertaken this journey without my colleagues at the Institute of Machine and Industrial Design for a supportive, friendly and creative atmosphere. Special thanks to the colleagues with whom I shared an office during my studies. I am also grateful to all the people and colleagues who made my internships abroad more enjoyable.

Words cannot express my gratitude to my family and friends, who accompanied me and brought joy to my life. Their belief in me fuelled me and kept my spirits high during this process.

ABSTRACT

This dissertation thesis deals with the experimental and numerical study of large-scale hydrostatic bearings. Such bearings are used to carry and manipulate large structures precisely and smoothly, as the sliding surfaces of the bearing are completely separated by an externally pressurized lubricating film. Since its first official introduction in 1852, extensive research has been conducted on performance improvement. Nonetheless, the researchers primarily focused on hydrostatic bearings of small sizes, while very little research focused on larger dimensions of this type of bearing. In such cases, completely different challenges arise, which are connected with higher energetic demands, the bearing parts manufacturability, transportation and assembly. Manufacturing errors, improper bearing alignment or non-optimal design can worsen the bearing performance, and even cause its malfunction. This thesis aims to introduce performance and safety improvements into large-scale hydrostatic bearing design methodology. The bearing performance improvement is performed using a numerical model of the fluid domain that is validated using experimental and theoretical data. This study presents a completely new approach based on optimizing multiple geometric parameters of the hydrostatic bearing pad independently. The safety improvement is performed purely experimentally. The attention is aimed at pad and slider misalignment, and their influence on the bearing performance. Moreover, the self-aligning ability of the pad using compliant support is examined. The experimental part was carried out using testing hydrostatic bearing consisting of two pads with full diagnostics. As the results indicate, the proposed optimization methodology of geometric parameters of a hydrostatic bearing can improve the bearing performance by as much as 20 %. The investigation of misalignment effects on the performance shows certain range, within the bearing can still operate safely, while compliant support can extend this range. This study presents original research expanding the knowledge of large-scale hydrostatic bearing systems towards better performance and higher safety.

KEYWORDS

hydrostatic lubrication, design optimization, assembly errors, misalignment, compliant support

ABSTRAKT

Táto dizertačná práca sa zaoberá experimentálnym a numerickým štúdiom veľkorozmerných hydrostatických ložísk. Takéto ložiská sa používajú na presné a plynulé polohovanie veľkých konštrukcií, pretože klzné plochy ložiska sú úplne oddelené externe tlakovaným mazacím filmom. Od jeho prvého oficiálneho predstavenia v roku 1852 prebehol rozsiahly výskum na zlepšenie výkonnosti. Napriek tomu sa výskumníci primárne zameriavali na hydrostatické ložiská malých rozmerov, zatiaľ čo len veľmi malá časť výskumu sa zameriavala na väčšie rozmery tohto typu ložísk. V takýchto prípadoch vznikajú úplne iné výzvy, ktoré sú spojené s vyššou energetickou náročnosťou, výrobou dielov ložísk, dopravou a montážou. Výrobné chyby, nesprávne zarovnanie ložísk alebo neoptimálna konštrukcia môžu zhoršiť výkonnosť ložiska, čo môže viesť až k jeho poruche. Cieľom tejto dizertačnej práce je predstaviť vylepšenia výkonu a bezpečnosti do rozsiahlej metodiky návrhu hydrostatických ložísk. Zlepšenie výkonu ložiska sa vykonáva pomocou numerického modelu oblasti tekutiny, ktorý je overený pomocou experimentálnych a teoretických údajov. Táto štúdia predstavuje úplne nový prístup založený na nezávislej optimalizácii viacerých geometrických parametrov hydrostatickej ložiskovej kapsy. Zlepšenie bezpečnosti sa vykonáva čisto experimentálne. Pozornosť je zameraná na nesúosovosť klzných plôch kapsy a bežca a ich vplyv na výkon ložísk. Okrem toho je skúmaná schopnosť samo-vyrovnávania podložky s použitím poddajnej podstavy. Experimentálna časť bola vykonaná pomocou testovania hydrostatického ložiska pozostávajúceho z dvoch káps s plnou diagnostikou. Ako ukazujú výsledky, navrhovaná metodika optimalizácie geometrických parametrov hydrostatického ložiska môže zlepšiť výkon ložiska až o 20 %. Skúmanie vplyvov nesúosovosti na výkonnosť ložiska ukazuje určitý rozsah, v rámci ktorého môže ložisko stále bezpečne fungovať, zatiaľ čo poddajná podpora môže tento rozsah ešte predĺžiť. Táto štúdia predstavuje originálny výskum rozširujúci poznatky o rozsiahlych hydrostatických ložiskových systémoch smerom k lepšiemu výkonu a vyššej bezpečnosti.

KĽÚČOVÉ SLOVÁ

hydrostatické mazanie, optimalizácia konštrukcie, montážne chyby, nesúososť, poddajná podstava

CONTENT

1 INTRODUCTION

Hydrostatic (HS) lubrication principle was firstly introduced in 1852 by L. D. Girard. Since Rowe patented the HS bearing (HSB) in 1985, the interest in HS lubrication research has been rising over the years [1]. The HS lubrication principle is based on supplying pressurized fluid into HS pad to separate solid bodies and create thick lubricating film, thus the bearing can be operated even when standstill. HSB are key parts of machines requiring long durability, minimum downtime, and smooth and precise movement. This type of bearing is can be used in a wide range of applications – from small milometer-sized spindles up to large-scale machines and structures exceeding tens of metres.

With the increasing demand for large-scale machines of high precision, HS lubrication regime offers huge scalability. Compared to rolling bearings (RB) HSB can be utilized for moving structures exceeding tens of metres while keeping relatively high precision [2]. Achieving high precision with RB at large scales would lead to extremely increased costs, while the HS lubricating film can even work properly with certain magnitude of surface error that is compensated with changing the hydraulic circuit performance. Another issue emerges with rolling elements wear that leads to necessary service. Moreover, HSB can be operated at low-speed and even in stationary conditions, unlike hydrodynamic (HD) or rolling element bearings working in elastohydrodynamic (EHD) lubrication regime.

HSB offer long durability, minimal downtime and high precision. However, large-scale HSB encounter issues with the manufacturing precision and challenging manipulation. Therefore, HSB is usually divided into smaller segments to simplify manufacturing, transport and assembly processes. This might generate problems linked with the assembly precision of the segmented sliders and misalignment of the bearing pads. Moreover, the electricity consumption of the HSB pump required for proper operation is proportionally rising with its size, thus it is necessary to reduce the energetic demands and electricity consumption.

1.1 Motivation

The purpose of this research is to extend the hydrostatic (HS) bearing design knowledge and to improve the bearing performance, reduce energy consumption and improve its safety. The focus is aimed at large-scale HS bearings (HSB) that can exceed tens of metres (Figure 1). Areas of particular interest are assembly precision assessment and improvement, and pad geometry optimization.

The immediate motivation for this research is for moving large-scale HSB with high precision and efficiency. Structures of large sizes, however, encounter many challenges, such as assembly and manufacturing precision. Securing extremely high manufacturing and assembly precision leads to high costs, or might be very challenging. Other option is to establish higher film thickness to compensate the errors, what does, however, increase the hydraulic pump electric energy consumption. This research is therefore aimed at assessing HSB assembly errors.

Another challenge for large-scale HSB is the necessity of hydraulic circuit constant supply of pressurized lubricant during operation. The HSB pad shape is closely related to the pressurized lubricant flow rate requirement and load carrying capacity. Frequently used one-parameter optimization approach, which was based on experimental measurement using electric field analogy provides a useful tool to determine basic shape of the pad geometry. Nonetheless, as the latest research in this area shows, the HSB pad geometry can be further improved using modern tools, such as computational fluid dynamics (CFD).

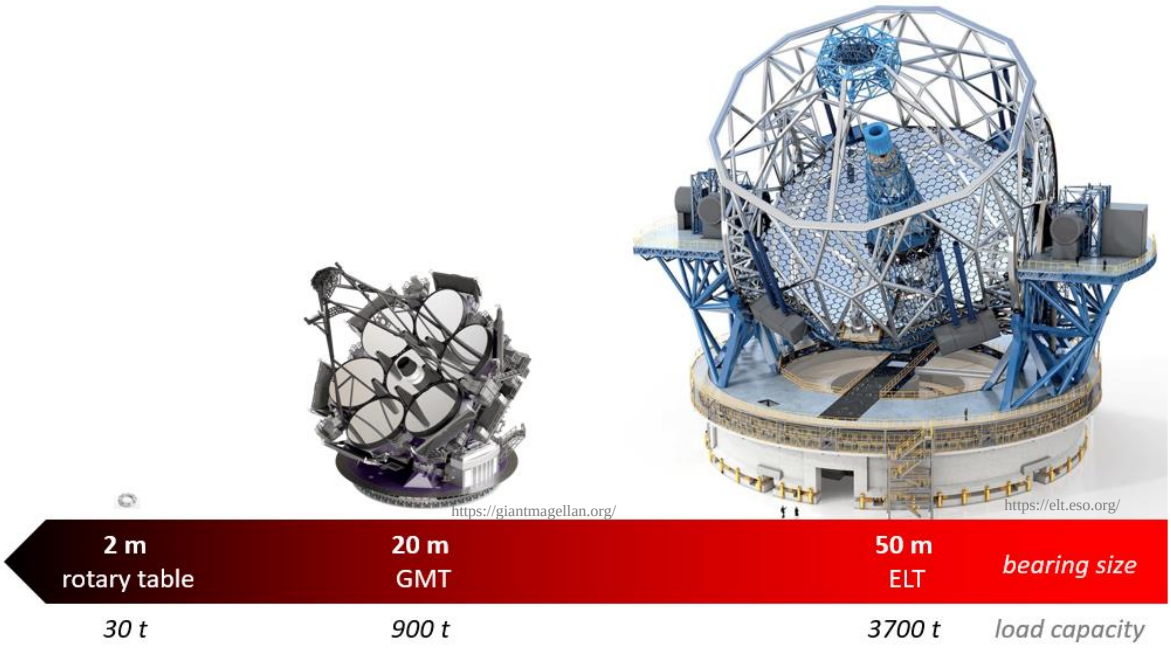

Figure 1 Hydrostatic bearings size and load capacity comparison of various applications

2 STATE OF THE ART

The state of the art is summarized in the following review article that was published in 2021, entitled: *"A review of the design and optimization of large-scale hydrostatic bearing systems"*. The review is based on 209 references including original research articles, reviews and books on topic of HS lubrication and large-scale HSB. The article is divided into the following sections:

1. Introduction to the issue & motivation
2. Overview of a large HSB system
3. Calculation and optimization
4. Sliding surfaces
5. HSB supply system
6. Summary
7. Future challenges

The main outcome of the review article was to provide a literature scan focused on large-scale hydrostatic bearing-oriented research. Considered were not only mechanical parts of the bearing, but also supply and materials and modifications of bearing solid bodies. Relevant available published research was described and discussed. Subsequently, a summary was provided to highlight the current research trends and spotlights. Finally, future challenges were defined based on the knowledge derived from the published research to help researchers aim their research efforts at current issues and demands in the industrial and academical fields. The review article can be found on the following pages. The available relevant research, published in the period after the submission of the review article, until the submission of this dissertation thesis, is discussed in the following paragraphs.

Engineering Science and Technology, an International Journal 24 (2021) 936–958

HOSTED BY

Contents lists available at ScienceDirect

Engineering Science and Technology, an International Journal

journal homepage: www.elsevier.com/locate/jestch

Review

A review of the design and optimization of large-scale hydrostatic bearing systems

Michal Michalec [a,*], Petr Svoboda [a], Ivan Křupka [a], Martin Hartl [a]

[a] Department of Tribology, Faculty of Mechanical Engineering, Brno University of Technology, Technická 2896/2, Brno 616 69, Czechia

ARTICLE INFO

Article history:
Received 15 October 2020
Revised 11 January 2021
Accepted 14 January 2021
Available online 13 February 2021

Keywords:
Hydrostatic lubrication
Hydraulic system
Machine design
Fail-safe measures
Geometric errors

ABSTRACT

In the last decades, the demand for hydrostatic bearings application has been rising due to the possibilities and advantages they offer. The advancements in hydrostatic lubrication understanding and computer technology improvement opened new ways for hydrostatic bearing performance and precision improvement. The emergence of the trend Industry 4.0 has brought new challenges and opportunities to the heavy machinery industry. This paper reviews the overall design and optimization processes for large-scale hydrostatic bearing geometry including the hydraulic system. The latest developments in the bearing geometry optimization, pressurized fluid supply components, and flow control devices are discussed. Moreover, possible measures for avoiding costly maintenance and repairs of the hydrostatic bearing are proposed. Finally, potential future research directions in large-scale hydrostatic bearing development are suggested. This review offers a comprehensive summary of potential problems and possible solutions in the large-scale hydrostatic bearing design, and simultaneously, serves as a supporting material to overcome potential obstacles that might emerge during manufacturing, assembly, and service.

Contents

* Corresponding author.
E-mail address: michal.michalec@vut.cz (M. Michalec).
Peer review under responsibility of Karabuk University.

https://doi.org/10.1016/j.jestch.2021.01.010
2215-0986/

1. Introduction

The invention of the water-fed hydraulic bearing in 1852 by L. D. Girard opened new possibilities in the mechanical engineering industry. The development process has advanced enormously ever since. Reynold's publication on the theory of lubrication [1] based on Tower's discovery of the hydrodynamic lubrication in 1886 significantly contributed to the fluid flow understanding. In 1918, Lord Rayleigh [2] discussed the optimal step bearing geometry for maximum load capacity, now referred to the Rayleigh step bearing. In the next period, the development process and application of externally pressurized bearings were continuously growing, as well as numerous patents were proposed. A review paper on hydrostatic and hybrid bearings was presented by Rowe [3] in 1989 that summarized previous advances in this field. Later in 1992, Bassani and Piccigallo [4] wrote a comprehensive book describing all the important aspects of the hydrostatic bearing design and optimization based on the latest research. Research progress in the field of large hydrostatic bearings was further reviewed by Li et al. [5] in 2014. Later, an insight into hydrostatic bearing system research and applications was presented by Liu et al. [6], proving that hydrostatic lubrication was still an increasingly significant topic. Despite all the previous significant contributions in the field of hydrostatic lubrication, the latest technology developments offer new opportunities for further hydrostatic bearing improvement.

Hydrostatic lubrication works on the principle of feeding pressurized fluid in between sliding surfaces to secure their separation [4] as shown in Fig. 1. The fluid is supplied from a hydraulic circuit through an inlet hole and evenly distributed by a recess. The turntable is floating and is ready for operation once the lubricating film is fully developed. The fluid pressure is gradually decreasing from the recess area to the atmospheric pressure, and the outlet fluid is collected and returned to the circulation.

The key advantages of the hydrostatic bearing are very low friction only generated by the fluid shear forces and negligible wear of sliding surfaces that are completely separated by pressurized fluid film. In comparison to the hydrodynamic bearings, which require higher rotating speeds, the hydrostatic bearing is working even when standstill since the surface separation is maintained externally. Since the bearing clearance is filled with the pressurized fluid, the hydrostatic bearing shows a high damping ability and high stiffness while the noise emission and vibration transfer is very low. On account of solid contact absence, the hydrostatic bearing exhibits very high moving accuracy and stability without any undesirable stick–slip effect [7,8]. Nevertheless, there are also several disadvantages that must be considered before selecting the hydrostatic bearing for a specific application. High precision of sliding surfaces is required; thus, the initial manufacturing costs can be considerably higher. The initial cost is increased by the necessity of an external pressurized fluid supply, considering all the elements of hydraulic circuit needed for proper functioning. Considering the complexity of the hydrostatic bearing system, a larger bedding space is required for piping, hydraulic and electric energy supply. Despite the low noise emission generated in between the sliding surfaces, the hydrostatic bearing system noise emission generated by the motor of the pump should not be overlooked. However, the noise transmitted by air, fluid, and structure [9] can be reduced by insulating material or by hydrogenerator confinement in an insulated space. The fluid-transmitted vibrations [10] can be dampened by the hydraulic accumulator [11], while structural vibrations can be reduced using silentblocks or shock absorbers.

Large-scale bearings are fundamental supporting elements of heavy rotary parts. The use of rolling elements is limited by the maximal diameter and load capacity. The size of rolling bearings is mostly only a few millimetres. However, large rolling bearings for wind turbines can reach 5 m [12]. The issue with large rolling bearing is not only the size and required precision of rolling elements, but also fatigue [13] and raceway/ball damage due to high contact stress [14]. In contrast to the rolling bearings, the hydrostatic bearings are beneficial for their applicability in wide constructions, large load carrying capacity, and uniform stress distribution. Hence, the hydrostatic bearings have been used for large tunnel drilling machines [15], large ship shafts and journal bearings [16], thrust bearings [17], and antenna or telescope structures carrying and operation, such as Giant Magellan telescope [18,19]. Possibly, this type of bearing can be used for large ships propellers, crushing machines, large rotating blades [15], heavy

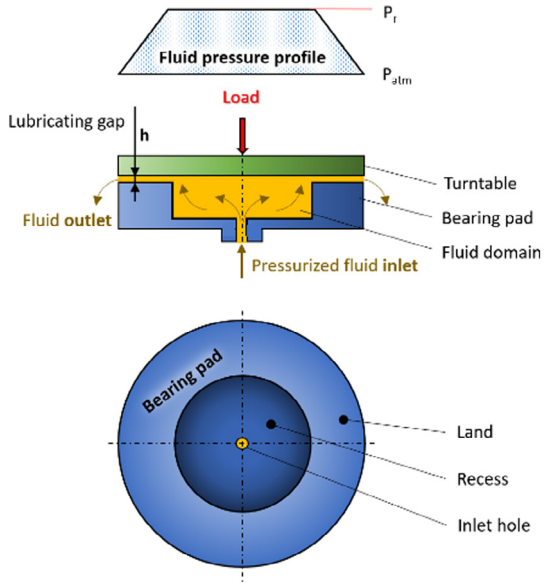

Fig. 1. Scheme of the open-type hydrostatic bearing pad and fluid pressure distribution.

Fig. 2. Lift pockets on pad of a tilting pad turbine hydrodynamic journal bearing (reprinted from [27] under licence CC BY 3.0).

transportation turning, or stage and assembly line manipulation and accurate positioning. Another important applications of hydrostatic bearings are CNC turntables for dimensional workpieces [20], and dampers [21,22] thanks to the characteristics of fluid during compression, and impact loading and vibration damping, which is also a great advantage for use in grinding machines [23]. One of the most significant uses of hydrostatic bearings is hydropower units [24]; when the hydroelectric turbine [25] of the hydrogenerator [26] needs to start spinning without contacting surface damage, the hydrodynamic (HD) bearing is combined with hydrostatic bearing pockets [27], as seen in Fig. 2, when a hybrid bearing is started, stopped, or reversed without damaging the contacting surfaces of the bearing. Moreover, the high load and the possibility of pumping water is advantageous for ship sealift lock-gate hinge where the sea level difference needs to be overcome [28]. Additionally, the working principle can be used for a rotary recovery device for the desalination process and reverse osmosis [29]. As introduced above, hydrostatic bearings have a great application potential that will be increasing with the development of modern technologies and trends [30], such as Industry 4.0 [31].

Lately, detailed books and papers on hydrostatic bearing design [4,5,32-34] have been published and the recency of some publications show that the topic of hydrostatic bearings is still a relevant issue [6]. However, the publications focused mainly on hydrostatic pad and flow control at the input into the hydrostatic pad or at externally pressurized journal bearing design [35], but very little of them aimed at the most significant limitations and issues connected with large hydrostatic bearings, such as manufacturing, transportation, and assembly. Moreover, the publications mostly did not cover the whole bearing incorporating the hydraulic circuit and the significance of its characteristics and optimal parameter design. Furthermore, the operation of hydrostatic bearings in critical conditions might lead to serious damage and costly repair. However, such complications can be safely avoided during the designing process. This review paper presents a comprehensive insight into the design and optimization of large hydrostatic bearings, to make the design process of hydrostatic bearings more accessible and to enable further development of large-scale machines, help creating modern technologies and build a healthier environment.

2. Overview of a large hydrostatic bearing system

A suitable type of bearing is an essential step in machine design. Previously, several selection strategy guides were introduced for hydrostatic bearings [35] including a decision-making process and a selection guide [33] according to required characteristics for automotive industry. Hydrostatic bearings are divided into three basic groups according to load support direction – axial (thrust), radial (journal), and combined. The calculation for both axial and radial types is similar, yet in different coordinate systems. The bearings can be characterized according to construction type: open type (Fig. 3a) and closed type (Fig. 3b), where opposed recesses act on turntable or shaft, respectively. Journal bearings can be either fully closed, e.g. for spindles [36] that represent the majority, or open for the positioning of large structures [18], such as azimuth rotation. Contrastingly, open type is the most frequently used thrust hydrostatic bearing type, which is simple in construction but provides lower precision and dynamic performance [20,37]. In the enclosed type the opposed pads act on turntable, resulting in higher precision [38], stiffness [39], and dynamic performance [40]. On the contrary, closed type bearings are more expensive and demanding on hydraulic circuit components. When both radial and axial loads need to be supported, another type of hydrostatic bearings is the combination of radial and axial bearings [41], whose shape can be either flat (Fig. 3c) or conical (Fig. 3d). The combined bearing is advantageous for medium to high rotation precision [15] and a relatively small run-out [42]. Another advantage is the ability of self-compensation provided by the conical shape of bearing [43,44]. The conical bearing is especially suitable for higher combined loads as the angle can be adjusted for desired performance [45], where an optimal value was found to be 60° for best radial and 30° for best axial performance. Generally, open-type bearings are the simplest and suitable for unidirectional loading only, while closed-type bearings are desirable for bidirectional loading. The combined type is advantageous in higher precision machines. And finally, conical bearings are superior in compensation ability and suitable for similar loads in radial and axial directions.

In the case of large-scale bearings, manufacturing, transportation, and assembly have become the most important criteria in

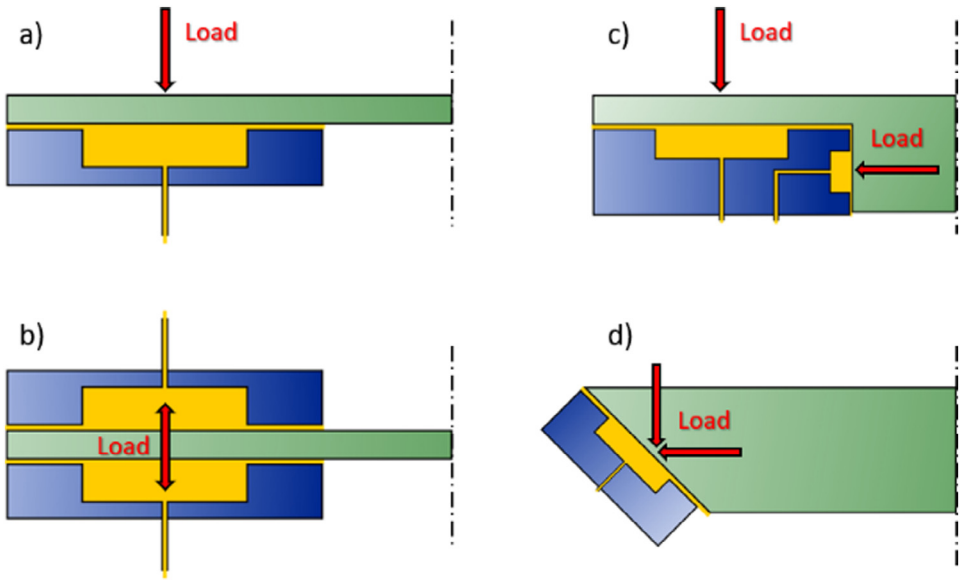

Fig. 3. Types of hydrostatic bearing according to loading direction: a) thrust open type, b) thrust closed type, c) open type combined and d) conical.

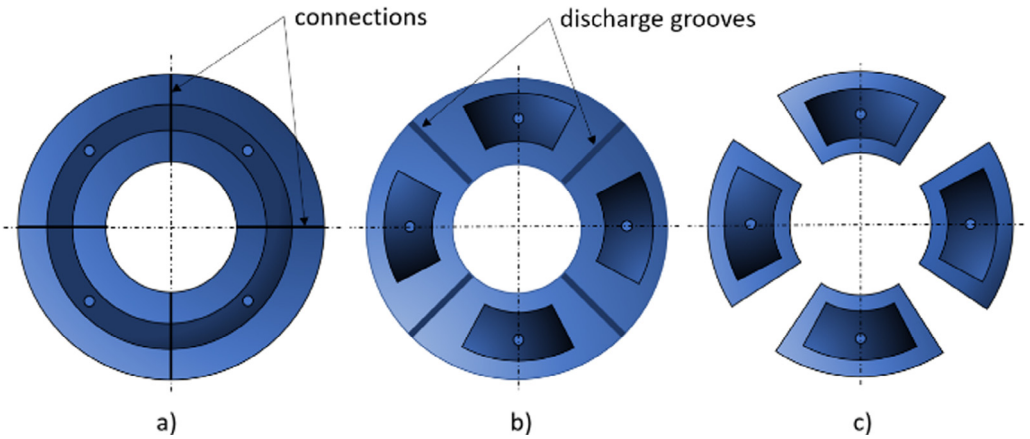

Fig. 4. The geometry of a) single-pad single-recess, b) single-pad multi-recess, and c) multi-pad hydrostatic bearing types.

the design process. In terms of size, the large scale can be understood from several points of view:

a) market availability – diameters greater than standardized bearings offered
b) by companies (occasionally up to 2000 mm diameter),
c) manufacturability – what cannot be made in one piece with satisfactory accuracy of sliding surfaces, manipulation – transport size (e.g., exceptionally large bearing diameters above 10 000 mm) or construction site build up area does not allow moving the bearing in one piece (e.g., limited bearing bedding space, hard-to-reach bearing placement – basement etc.).

Considering all the above-mentioned circumstances, the hydrostatic pad can be either uniform, assembled from ring segments, or divided into separate segments supporting the turntable. **Uniform hydrostatic pad (single pad bearing –** Fig. 4a) is advantageous in the height positioning of turntable segments. However, the manufacturing and transportation process can be much more complicated compared to the other geometry type. Additionally, discharge grooves for hydrostatic recess separation (Fig. 4b) are recommended to avoid mutual recess flow interference [46]; however, the whole workflow will become more complicated. Therefore, a special shape can be derived to avoid flow interference and to make the manufacturing, transportation, and assembly processes simpler – s**eparated hydrostatic pads (multi pad bearing –** Fig. 4c**)**. Moreover, the manipulation throughout the assembly process is greatly improved. Nevertheless, levelling and positioning is more difficult than in the uniform hydrostatic pad. A sealing rubber rib must be included to avoid oil leakage between pads. The distance between separated hydrostatic pads depends on the turntable rigidity and required precision. Basically, for higher precision, such as CNC turntables for machining, the number of hydrostatic pads is generally higher. In Jang and Choi [20] proposed design where the hydrostatic pads were placed in two rows: twenty outside at 1500 mm radius and eight inside at 500 mm radius. However, the circumferential distance between pads is greater for large constructions [4], high rigidity structures, or applications with lower required precision. For instance, the Giant Magellan Telescope azimuth structure is based on 24 axial hydrostatic pads. A master–slave pad variation according to load-sharing ratios [47] is beneficial in multi-pad hydrostatic bearing control. Additionally, considering a constant supply system for multi-pad bearing is very expensive [40], so flow distribution and control devices are recommended.

A full scheme of a large-scale hydrostatic bearing is shown in Fig. 5. The hydrostatic bearing is composed of two main sections: the hydrostatic pad and the hydraulic circuit. The hydrostatic pad is a stationary part supporting the rotating turntable with load. The second fundamental part of hydrostatic bearing is the hydraulic circuit. A constant low supply system has a separate hydrogenerator for each recess; however, supplying many recesses would be a complication because of either space or initial costs. Therefore the multi-pad hydrostatic bearing is supplied by one pump with flow dividers and restrictors [34]. Moreover, large hydrostatic bearings are limited by manufacturing, transportation, and assembly processes, so those types of bearings are frequently composed of a large ring with numerous inlets [18] or numerous pads placed in a desired bearing diameter [20]. The pump supplies the hydrostatic pad with enough pressurized fluid at a higher pressure than required by the pad; thus, the flow volume and pressure is processed using hydraulic valves. Three types of hydraulic valves are included: way-valves to control direction of oil flow, pressure control valves to control pressure in different segments in the circuit, and flow control valves to control the flow rate in the circuit. Flow control valves are especially important components of the hydrostatic bearing because they maintain constant film thickness by compensating pressure differential during impact and non-symmetric loading and vibrations. The hydraulic accumulator significance will be discussed later; however, it acts as a fail-safe measure in case of sudden hydraulic circuit failure. An analogy was found in hydraulic circuit modelling and electrical circuit composition [48] that might simplify the design process using the similarity of physical laws with conversion factors and corresponding dimensions. Suitable filters are necessary for the maintenance of lubricant quality.

In case of insufficient passive cooling, an active cooler must be included in the hydraulic circuit to avoid hydrostatic bearing performance decrease by a significant lubricant temperature increase.

2.1. Hydrostatic bearing working modes

Hydrostatic bearing working modes introduced in [4] are summarized in Table 1. The basic condition for sliding surface separation is to maintain enough lifting force generated by fluid inertia. During the design stage, working conditions must be carefully set to avoid long working periods in a critical state of hydrostatic bearing operation.

The critical states of operation (Table 2) can be avoided when considered in advance, so this review paper focuses on the prevention of such states' occurrence. States of non-symmetrical loading

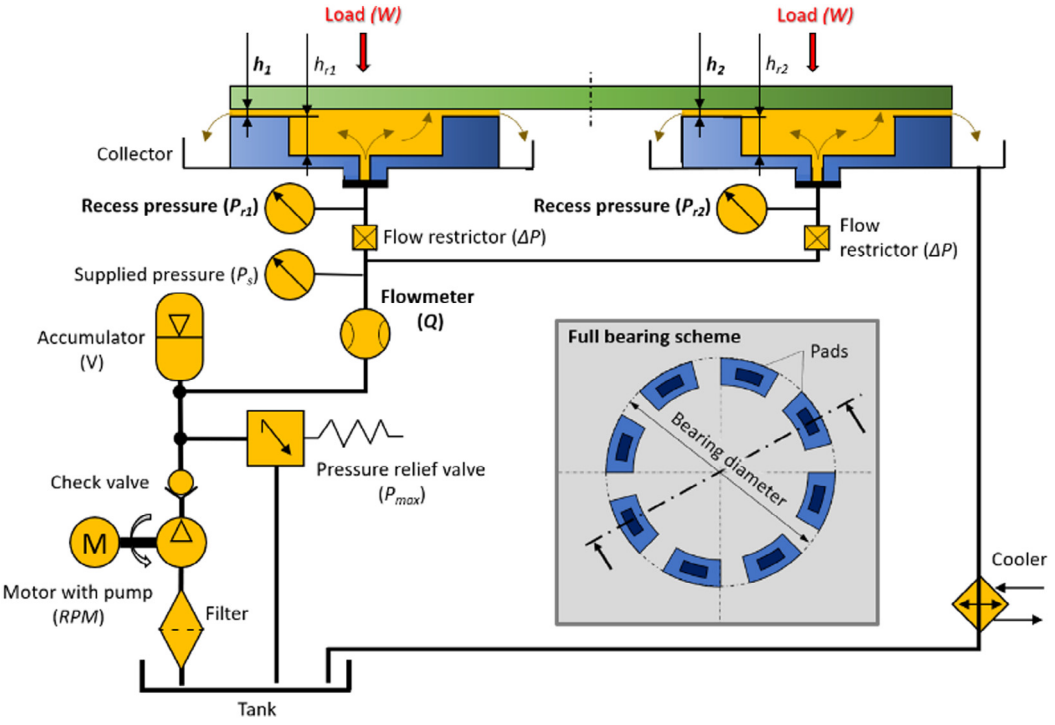

Fig. 5. Full scheme of the hydraulic circuit and cross section of two hydrostatic pads of a large multi-pad hydrostatic bearing.

and sudden load change are a matter of proper pad-shape geometry and flow control. Lubricant behaviour and thermal characteristics can be analysed using computational software. And finally, hydraulic circuit failure can be predicted and prevented by implementing specific measures. The above-mentioned procedures will be discussed in detail in the following parts.

3. Calculation and optimization

Basic requirements for flow investigation in a narrow gap are isotropic and continuous conditions in an elementary volume. Thus Navier—Stokes equation used for viscous fluid flow description is shown in Eq. (1).

$$\rho \frac{Dv}{Dt} = \rho f + \nabla \sigma \tag{1}$$

Table 1
Modes of hydrostatic bearing operation.

State	Description
Non-working state	Hydraulic circuit is not supplying pressurized fluid. Sliding surfaces are in contact. No operating/turning possible.
Introduction to steady state	Hydraulic circuit starts supplying pressurized fluid. Sliding surfaces are being separated. No operating/turning recommended until in steady state.
Steady state	Hydraulic circuit is stable, and lubricating film is fully developed. Ready for operating/turning.
Working state	Hydraulic circuit is stable, and the bearing is operating at normal conditions.
Critical state of operation / bearing failure	Working at/beyond the edge of projected conditions. Possibility of lubricating film collapse or sliding surface damage.

However, the complexity of Navier—Stokes equations may be reduced by applying such simplifications as averaging quantities along one direction, flow linearity and inertia terms [4]. Thus, the Reynolds equation without viscosity variations can be derived as shown in Eq. (2).

Table 2
Critical states of hydrostatic bearing operation.

State	Description
Non-symmetrical loading	Uneven load distribution. Large pressure differences in pads that can lead to tilting or eventually a contact between sliding surfaces.
Sudden load change	Overload can lead to sliding surface contact or hydraulic circuit damage.
Operation at very high rotation speed	Lubricant overheating. Pressure distribution and flow influence the carrying capacity.
Lubricant overheating	Loss of carrying ability of lubricant. Fluid film collapse. Sliding surfaces get into contact.
Hydraulic circuit failure	Sudden contact of moving sliding surfaces without developed lubricating layer.

Table 3
Example of expressed equations for circular hydrostatic pad calculation [4,32,50].

Quantity	Equation
Required lifting pressure in the recess area	$p_r = \frac{W}{A_{min}}$
Total load-carrying capacity	$W = 3\frac{\mu r_2^2}{h^3} Q\left(1 - \frac{r_1^2}{r_2^2}\right)$
Flow rate	$Q = \frac{\pi h^3 p_r}{6\mu \ln(r_2/r_1)}$
Viscous friction	$\tau = \frac{\pi \mu \omega}{2h}\left(r_2^4 - r_1^4\right)$
Fluid power loss	$H_v = \omega \tau$
Pumping power loss	$H_p = p_r Q$

Table 4
Key parameters of hydrostatic bearings.

Parameter	Description	Typical range
Flow (Q)	required steady flow distribution for all bearing pads	5–50 l/min
Recess pressure (p_r)	sufficient working fluid pressure for load carrying and surface separation during introduction to the working state	50–150 bar
Supplied pressure (p_s)	pressurized fluid output from hydrogenerator considering pressure losses	50–200 bar (according to pressure drops at hydraulic circuit elements)
Dynamic viscosity (μ)	stable, low temperature dependency	0.05–0.15 Pa·s (according to oil viscosity grade for expected environment temperatures)
Pad and recess geometry	dependent on selected manufacturing process	calculated for optimal performance and desired load capacity.
Load (W)	Desired or achievable load-carrying capacity	wide range, up to 1000 metric tons in total [18] and more
Film thickness (h)	maintained a constant lubricating gap, high enough to carry load, and to overcome manufacturing and assembly errors	approximately 10–100 μm
Viscous friction torque (τ)	the force acting against bearing rotation generated by viscous forces of the fluid	approximately 300 Nm at 10 rpm and medium viscosity (based on calculation for 1000 t load according to eqns. in Table 3)
Total power loss (H)	given by required performance, lubricant viscosity, choking elements, and fluid friction during operation	pumping power loss up to 3 kW (based on calculation for 1000 t hydrostatic bearing according to eqns. in Table 3), fluid film power loss is negligible.

$$\nabla\left(\frac{h^3}{\eta}\cdot\nabla\overrightarrow{p}\right)=6\nabla\left(\overrightarrow{U}\cdot h\right)+12\frac{\partial h}{\partial t} \tag{2}$$

Alternatively, the complexity of Navier—Stokes equations can be reduced into a 2D problem using the Dirichlet conditions [49] to obtain analytical formulations. Bassani and Piccigallo [4] derived simple-pad and single-recess geometry, such as circular, rectangular, and annular. Several other configurations for multi-recess bearings were introduced by Khonosari and Booser [32]. These are based on pad coefficients, whose values are selected from a graph. In Table 3 equations for circular pad are expressed, showing the key parameters of a hydrostatic bearing. Subsequently, the key parameters of hydrostatic bearings are described in Table 4 with respect to the values of large-scale hydrostatic bearing, either obtained from references or calculated using equations in Table 3.

All conditions and desired parameter specifications must be set at the beginning of the design process. There are several design criteria that are specified in Table 5. When the design criterion is selected and the key parameter is set, the equations from Table 3 are customized to match the calculation aim – the calculated parameters. At this stage, optional parameters are chosen according to budget and availability.

Table 5
Classification of design criteria and bearing parameters.

Design criteria	Key parameter	Optional parameter	Calculated parameter
Required load capacity	Predicted load range (W_{min} – W_{max})	Recess pressure (p_r) Required volumetric flow (Q) Dynamic viscosity (μ)	Hydrostatic pad geometry (pad and recess dimensions) Film thickness (h) Required supplied pressure (p_s)
Error	compensation	Minimal required film thickness with respect to maximum errors (h_{min})	Recess pressure (p_r) Required volumetric flow (Q) Predicted load range (W_{min}-W_{max}) Dynamic viscosity (μ)
Load-carrying capacity (W) Hydrostatic pad geometry (pad and recess dimensions) Required supplied pressure (p_s)			
Limited bedding space	Maximum pad area (A_{max}) considering collector pan and surroundings	Recess pressure (p_r) Required volumetric flow (Q) Dynamic viscosity (μ) Predicted load range (W_{min}-W_{max})	Film thickness (h) Required supplied pressure (p_s) Load-carrying capacity (W_{max})
Hydrogenerator performance	Supplied volumetric flow (Q) Supplied pressure (p_s) Hydrogenerator power (H_p)	Dynamic viscosity (μ) Load-carrying capacity (W)	Hydrostatic pad geometry (pad and recess dimensions) Film thickness (h) Recess pressure (p_r)

The calculation of hydrostatic bearing base parameters is an iterative process that is performed to achieve desired performance and reasonable bearing geometry or hydraulic circuit parameters. The workflow is schematically shown in Fig. 6.

To evaluate the performance of a non-derived hydrostatic bearing shape analytically, an approximation method according to Rippel [51] can be utilized to obtain roughly corresponding load capacity. Calculation generalization was introduced using performance parameters as introduced by Khonosari and Booser [32] to simplify the design process for derived geometry hydrostatic bearing shapes as shown in Eq. (3).

$$W = A_{eff}\cdot p_r = a_p\cdot A_{tot}\cdot p_r \tag{3}$$

where A_{eff} is the effective area of a pad, A_{tot} is the total pad area, and a_p is the pressure coefficient. This form is advantageous for the application of results from the numerical simulation resultant forces [46] and for obtaining of pressure coefficients for a specific geometry. Additionally, Kang et al. [47] provided hydrostatic bear-

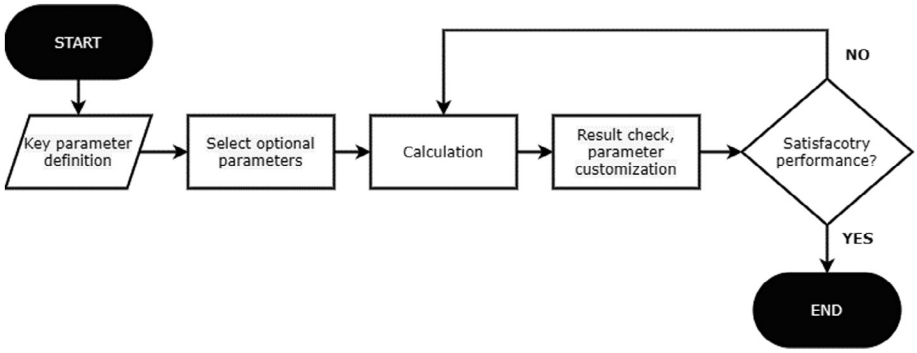

Fig. 6. Bearing parameter calculation process.

Table 6
Comparison of analytical and numerical approaches in hydrostatic bearing calculation.

Analytical	Numerical
Simple and quick calculation of key parameters. Can be used for [4]: • static and dynamic performance analysis, • thermal and flow properties prediction, • optimization of basic shape pads using, nomographs.	Required advanced knowledge of fluid modelling. Can be used for: • static and dynamic performance analysis [52,53], • flow investigation [54,55], • thermal properties evaluation [56,57], • deformation evaluation [24,36], • error modelling [58-60].
Preferred for basic derived pad geometry shapes.	Powerful tool for obtaining resultant force for various pad and recess geometry from simulation [29], including unusual shapes.
Limited to simple geometry configurations.	Suitable for unusual configurations of recess and pad shapes design that is very difficult or impossible to express analytically [61].

Table 7
Overview of CFD discretization methods used in hydrostatic bearing modelling.

	FVM	FEM	FDM
Suitability	pressure distribution [67], heat transfer [68,69], and turbulent flows	mixed formulations and multiphysics problems	pressure distribution [70,71], heat transfer [37]
Computation speed	moderate	slower [38]	quicker [72]
Geometry	regular geometry	any geometry (including curved)	simple and regular domains (required cartesian meshes) [72]
Problems related to **hydrostatic bearings**		relationships among rotation speed, recess pressure and dynamic viscosity [69], high speed and high viscosity conditions [62], flow investigation [55], oil film temperature field in variable viscosity condition and rotation [68,69,73], recess pressure field and investigation of heavy bearing [67]	high rotation speed effects [41], static and dynamic performance of conical bearings and bearings with restrictors [44,45,74,75], non-Newtonian and smart fluid modelling [76-78],
static, dynamic and thermal	characteristics [37], carrying capacity according to pressure distribution considering surface waviness effect [30]		

ing parameters for effective area calibration based on experimental investigation. The analytical calculation process is performed using analytical expressions for the determination of basic parameters and required hydropower unit performance. The numerical approach serves as an auxiliary tool for performance optimization and deformation investigation, which is discussed in this paper in detail later. A summary of both analytical and computation approaches is listed in Table 6.

Numerical methods can be implemented in the hydrostatic bearing design to achieve desired performance and eliminate possible issues in advance. The computational fluid dynamic (CFD) is a powerful tool for fluid flow simulation and investigation. An overview of the most widely used discretization methods, namely the finite volume method (FVM), the finite element method (FEM), and the finite difference method (FDM), is listed in Table 7. In a nutshell, the FVM is most suitable for flow investigation of any geometry. A comparative investigation of the FVM and vortex visualisation for three different Reynolds number at inlet (Fig. 7) presented by Shen et al. [55] showed a good agreement in results. The FEM has more demanding computational requirements, however, it is superior for multiphysics and non-Newtonian fluid modelling. In contrast to the previously described methods, the FDM is a quick computational method that is preferred only for simple and regular domain investigation. Li et al. [62] presented a CFD analysis for a shear cavitation effect influence on the performance of journal bearings that led to a better agreement with experimental results, especially when viscosity, speed, and eccentricity increased. For specific simulations considering also solid interfaces, the fluid–structure interaction (FSI) problems are widely used for multiphysics problems [63], sliding surface deformation and error investigation [64], and thermal analyses. In comparison to CFD, FSI is more demanding on computational requirements [65] and therefore preferred only in predicting solid interface stress and deformation. Additionally, simulation accuracy improvement can be achieved by considering FSI and temperature influence [66], which resulted in significant static stiffness decrease.

In comparison to analytical representation, the proposed exact FEM Reynolds equation formulation by Chasalevris and Sfyris [79] results in a significant design process improvement. Thermal-elastohydrodynamic (TEHD) simulation of hydrodynamic

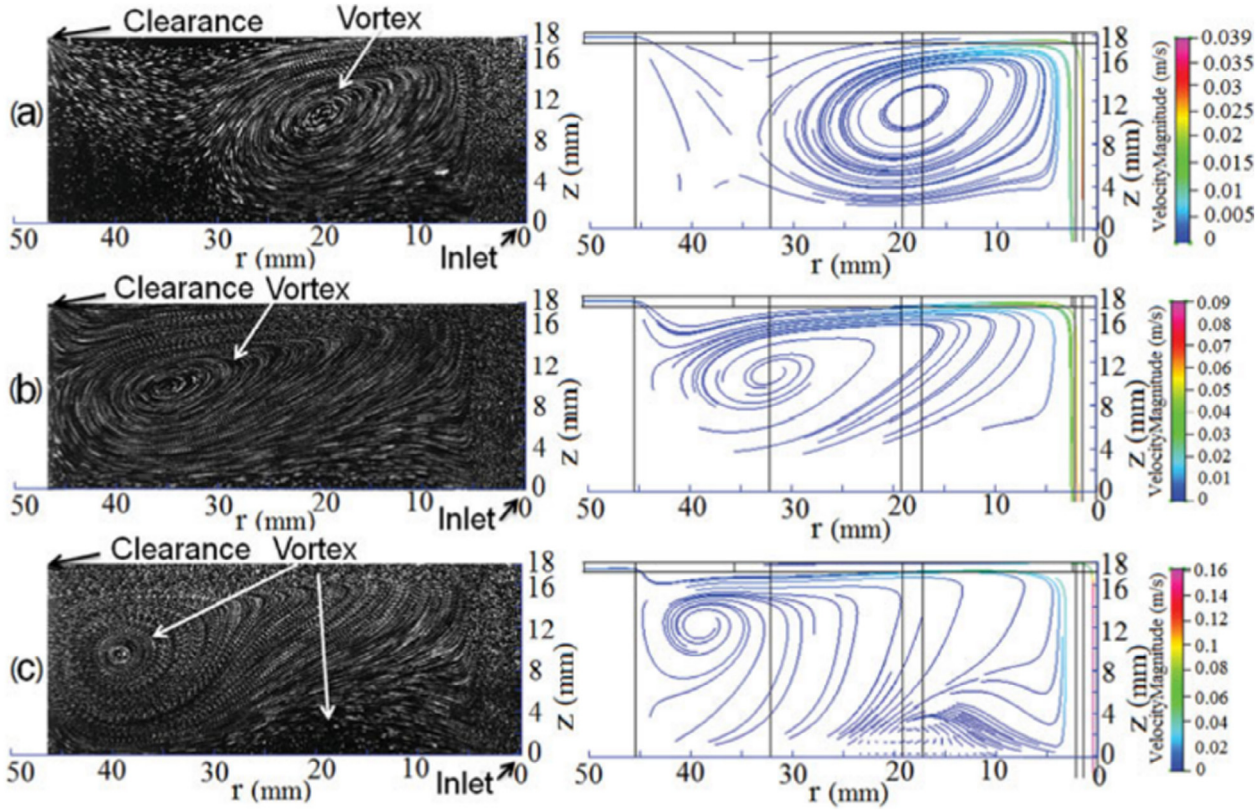

Fig. 7. Comparison of simulation and experiment results of flow patterns in the recess area for Re_{in} a) 140, b) 350, and c) 701 (reprinted from [55] with permission of Taylor & Francis Ltd, http://www.tandfonline.com).

(HD) bearing aimed at film thickness evaluation compared to induced fluorescence measurements [80] showed a relatively good agreement at lower speeds; however, the deviation was higher at higher speeds. Generally, it is necessary to identify the flow regime according to Reynolds number [81] because turbulent flow provides higher load carrying capacity, however, also increases the fluid friction. The resulting accuracy of hydrostatic bearing simulations can be improved using inertia effects [82] and dynamic grid technology [83], where dynamic changes of boundary conditions are implemented. The workflow of numerical investigation provided by Zhang et al. [83] considered symmetric conditions of periodic oil pads to cut down the calculation time and increase result accuracy. Numerical approach based on the CFD simulation was experimentally investigated by Cui [84] for large hydrostatic bearing, where a maximal 9.52% error in results of recess pressure was observed, while measurements of oil film thickness resulted in a 13.8% error, so the simulation results errors should be always considered. However, the results are heavily influenced by mesh quality. A meshless method with radial basis functions was introduced by Nicoletti [72]. It significantly improves the computing time with only a 5% error even with a coarse grid.

Another important demand on simulation is the computational time that significantly affects price and result accuracy. Therefore, a fast thermo-hydrodynamic CFD model was proposed by Novotný et al. [85] that greatly improves computational speed. The proposed computation model accuracy is lower compared to the CFD simulation (Fig. 8), which is caused by the location of the boundary condition of the simplified model. Another dynamic model for rapid static and dynamic characteristics analysis of a closed type bearing that is roughly 10 times faster than the FEM was introduced and experimentally verified by Wang et al. [86]. Another significant computational time improvement in simplified model for static and dynamic performance calculation of hydrostatic bearing with errors lower than 6.5% while taking only 1/603 of the FDM's runtime was proposed by Liang et al. [87].

3.1. Performance optimization

Performance optimization is an important process that includes both optimal control establishment and the whole system energy consumption minimization.

The hydrostatic bearing performance is provided according to a selected design criterion as listed in Table 5. Simple cases deal only with the optimization of one parameter, which is, however, not enough for obtaining high performance, good thermal properties, and economical energy management. Hence, a multicriteria optimization was introduced by Solmaz et al. [88] as an iterative process considering the most important parameters, specifically minimum power and temperature rise. The better required overall performance, the more criteria should be considered. A remarkable 30–60% accuracy [89] can be achieved by considering the influence of design parameters, geometric errors, deformation, temperature, and random parameters. Fedorynenko et al. [90] proposed an innovative design of hybrid bearing achieved a significant efficiency increase, i.e. 1.5 times decreased total energy loss in hydrostatic mode and 4 times in HD mode. Additional details on the performance characteristics optimization are listed in Table 8.

The hydrostatic bearing has a significant advantage in comparison to rolling bearings owing to the fluid film presence when it comes to managing vibrations. It should be stated that damping capacity of a flat pad is higher than a pad with recess of same size and operating parameters. The lubricating film stiffness is proportional to its height (Eq. (4)); however, it differs with the type of flow compensation [32]. Damping coefficient is given by ratio of

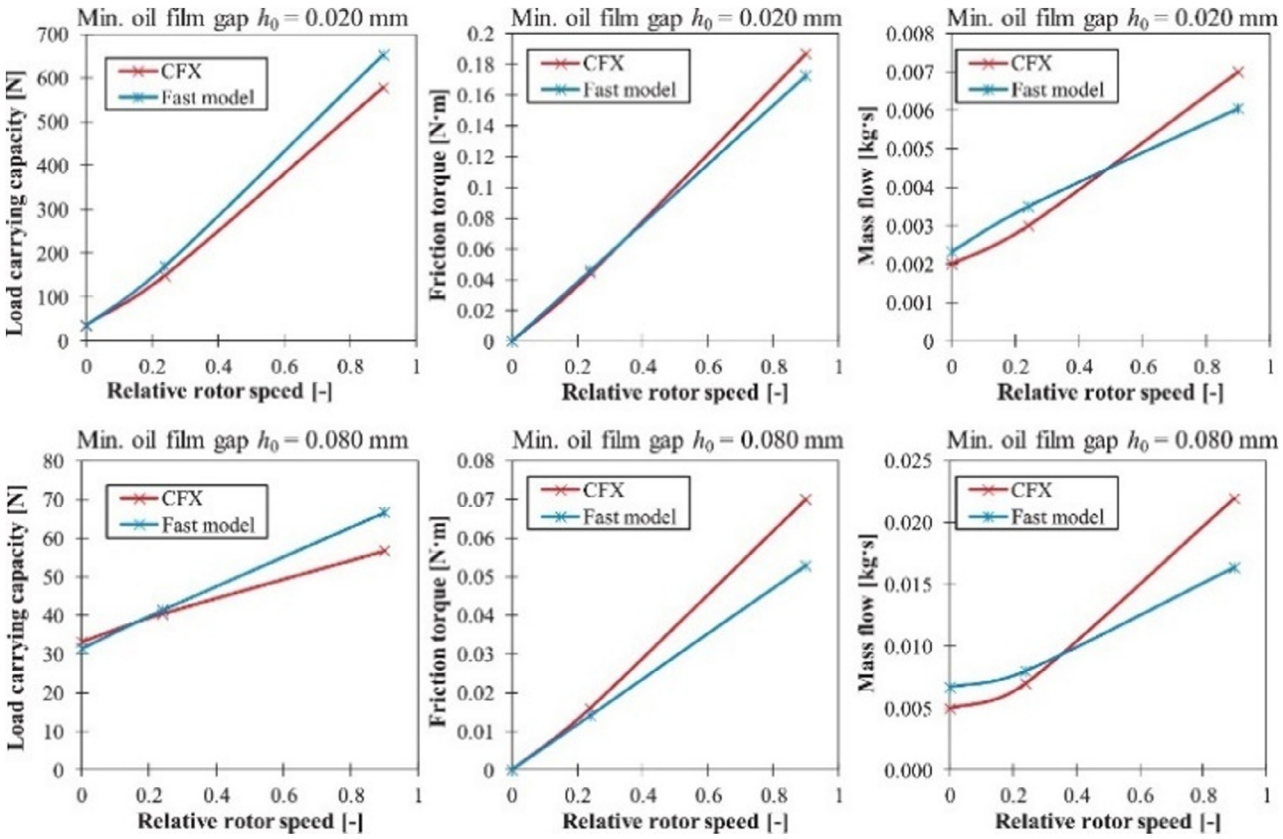

Fig. 8. Results of CFD and proposed fast computation model calculation for load capacity, friction torque, and mass flow in 0.02 mm and 0.08 mm film thicknesses (reprinted from [85] with permission from Elsevier®).

damping load and squeeze velocity [95], which is proportional to lubricant dynamic viscosity, pad geometry and compensation type, and film thickness (Eq. (5)). The required parameters should be reflected in the bearing optimization to achieve desired and optimal performance. Comparative stiffness and damping values can be found in references [86,96]; however, only for small-scale applications.

$$k = \frac{dW}{dh} \tag{4}$$

$$c = \frac{W}{\dot{h}} \tag{5}$$

Table 8
Optimization considerations of selected performance characteristics.

Bearing characteristic	Description
Stiffness	Oil supply rate redistribution among pads according to actual conditions can improve static performance by 17% while maintaining the same dynamic performance without further energy consumption [91].
Damping	Impact resistance is improved by lowering film thickness [70,92].
Friction	The higher the flow rates, the greater the friction torque. The effect is more significant while considering laminar and turbulent conditions [93].
Thermal effects	Considering thermal effects in simulation decreases the load carrying capacity by about 3% and stiffness and damping by up to 10% [94]. Moreover, static stiffness drops significantly when considering temperature influence [66] according to FSI analysis results.

3.2. Pad geometry optimization

The bearing pad recess area provides enough lifting force to the bearing turntable and load. Additionally, the recessed pad has significantly better performance compared to a non-recessed pad [97,98], allowing the bearing to withstand higher rotating speeds and load variations. However, different recess shapes exhibit slightly different characteristics. Generally, mostly preferred are ones conventional shapes [99], such as circular, rectangular and annular, because of derived equations and manufacturability. Nonetheless, unusual and specific hydrostatic bearing recess geometry can be developed using sand casting, as introduced by Kotilainen and Slocum [100]. With the advancement of computational software and manufacturing technologies, triangular and elliptic [101], or even unconventional geometry shapes [102] can be developed. A comparison provided by Sharma et al. [99] summarized the recess shapes as follows: the circular shape is advantageous for the highest pocket pressure and the lowest required flow, annular exhibited highest stiffness and load capacity, and finally rectangular shape showed the highest damping ability. Sing et al. [101] confirmed the previous findings and investigated also a triangular shape, which happened to provide the highest film thickness from all compared shapes. Investigated unconventional shapes using numerical simulations, such as sector or cross shapes [103], can be adjusted to optimal performance and temperature control. Aside from the recess outline, the straightness of the recess cross section provides slightly different performance in aerostatic bearing investigation, as noticed Gao et al. [53]. The conical shape (Fig. 9a) exhibits higher load capacity at higher rotational speeds, while the straight shape (Fig. 9b) maintains higher load capacity

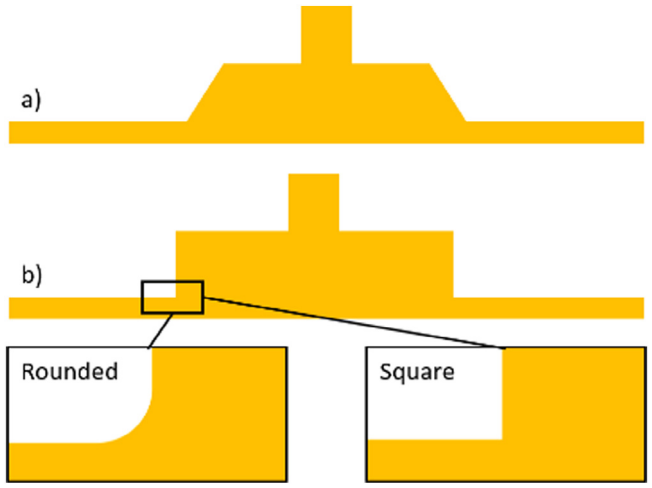

Fig. 9. Recess shape a) conical b) straight with rounded and squared corners.

even at larger film thickness. In the case of straight recess shape, square corners provide higher recess pressure [104], while rounded corners form smoother outlines that maintain better outflow and thermal dissipation of the pressurized fluid.

A lifting pocket can also be included in a HD bearing design. For instance, Fillon et al. [105] performed a numerical investigation of the recess presence for a variation of the recess depth (nominal value – h = 2 mm) and recess diameter (nominal value – d = 170 mm). The results showed a plateau (Fig. 10), a less contrasted distribution, in the pressure field and a small decrease in the temperature field. Thus, the performance of hybrid bearings is improved with the recess presence, while the thermal properties are preserved or slightly enhanced. On the contrary, Wasilczuk et al. [106] observed in field tests, the hybrid bearing maintains a higher film thickness and lower temperature rise, but also greater friction losses due to larger viscosity of oil with lower temperature.

The ration of the hydrostatic pad recess area to the total pad area plays a significant role in the overall performance of the hydraulic supply. For a single recessed hydrostatic pad, the optimal ratio values for circular, annular, and square shapes range from 0.4 to 0.6 [4], depending on the recess outline shape. The outside dimensions of a rectangular pad and the optimal ratio of recess dimensions for best damping and stiffness characteristics were found to be 1 [96], thus the square shape is superior to the rectangular one in terms of required performance. The higher the pocket ratio, the better static and dynamic performance of the pad can be achieved. Yet, higher pumping performance is necessary. However, in case of lower pocket ratios [107], in the range of 0.1–0.4, larger frictional power loss occurs. A multi-recessed hydrostatic pad recess layout is generally symmetrical [32] although it can be customized according to requirements for tilt compliance [43] to achieve best possible performance and accuracy.

The recess depth also plays an important role in the bearing performance. Common design practice for a recess depth design [108] is 50–100 times the expected film thickness. However, for highspeed thrust bearings, the optimal recess depth can be rather smaller, below 25 times the expected film thickness. Horvat and Braun's [109] investigation of two-dimensional flow visualization with an experimental verification confirmed that at low speed operation the Poiseuille pressure forces dominate, while at high speed the Couette shear forces become more influential.

The results clearly show that the pressure forces are dependent on the rotation direction, creating a combined effect at one side of bearing and a counteracting effect at the opposite. Shen et al. [111] investigated a three-dimensional flow, contributing to the increased precision of heavy duty hydrostatic bearing performance prediction.

For very shallow recess with a depth less than 2 mm [73], the dynamic pressure significantly increased even at the low rotational speed of 6 rpm. Recess depths above 2 mm showed constant values of pressure. Tian et al. [111] investigated inertia effects and couple stress in numerical simulations, concluding that the recess depth affects static properties of hydrostatic thrust bearings, while noticing that a recess depth higher than four times the film thickness showed a negligible effect on the performance.

Yu et al. [112] confirmed that the dynamic pressure rise in shallow recess depth is stronger at higher speeds. For heavy bearings operating at 80 rpm [113], the recess depths above 3 mm showed constant oil film pressure, thus the higher the speed, the higher pressure and stiffness can be achieved. However, it is not possible to establish an optimal depth without expected film thickness, and therefore Helene et al. [114] proposed recess depth to film thickness ratio H1/H2 for laminar and turbulent flow regimes, where deep pockets (H1/H2 greater than 16) show a constant pressure level for both regimes. A combination of deep and shallow recess by Hong et al. [41] was introduced to be especially suitable for high speed applications. The oil film temperature increase in recess at static and low speed conditions is negligible [69]; however, the shallow recess as a choking element was observed to a generate greater amount of heat [113] at rotation speeds higher than 20 rpm. An addition of a sealing edge [115,116] can improve the hydrostatic bearing stability when operated at higher speeds by load compensation using dynamic pressure for uni- and bi-directional operation.

Wang et al. [117] confirmed that the higher rotational speed shear forces cause a greater temperature rise in simulation of 10 mm deep recess and film thickness of 0.1 mm, thus the dynamic pressure increase should be higher than the hydrostatic pressure decrease caused by lubricant heating. The oil feed hole position in the recess area does not affect the pressure distribution in the hydrostatic pad [118]. However, for a shallow recess type, high speed, and uneven loading conditions the pressure distribution can differ, thus further investigation is necessary.

4. Sliding surfaces

The requirements on sliding surfaces of hydrostatic bearings are relatively high due to a small gap in maintained by pressurized fluid. Therefore, a precise design and analysis are necessary to avoid any unwanted collisions caused by unexpected thermal or structural deformations, and errors created during the manufacturing and assembly processes.

4.1. Structural deformation analysis and prevention

The lubricating film thickness between the sliding surfaces ranges between hundreds and tens of microns [18,68], so the potential deformations must be considered in advance. Modern software offers great support to the design process by simulations, either structural or fluid. There are three main components generating structural deformations. The first is deformation of the turntable caused by mechanical load when the increasing load causes deformation of the turntable [119]. The second is structural deformation caused by the pressurized fluid. Although the lubricant pressure does not reach critical values compared to material yield strength, especially in small hydrostatic bearings, it has major contribution in the large-scale hydrostatic bearings, where the loads are greatly higher. The resulting deformation is influenced by the turntable thickness and load distribution on the turntable, relative to the position of hydrostatic pads. If necessary, FSI can be used to

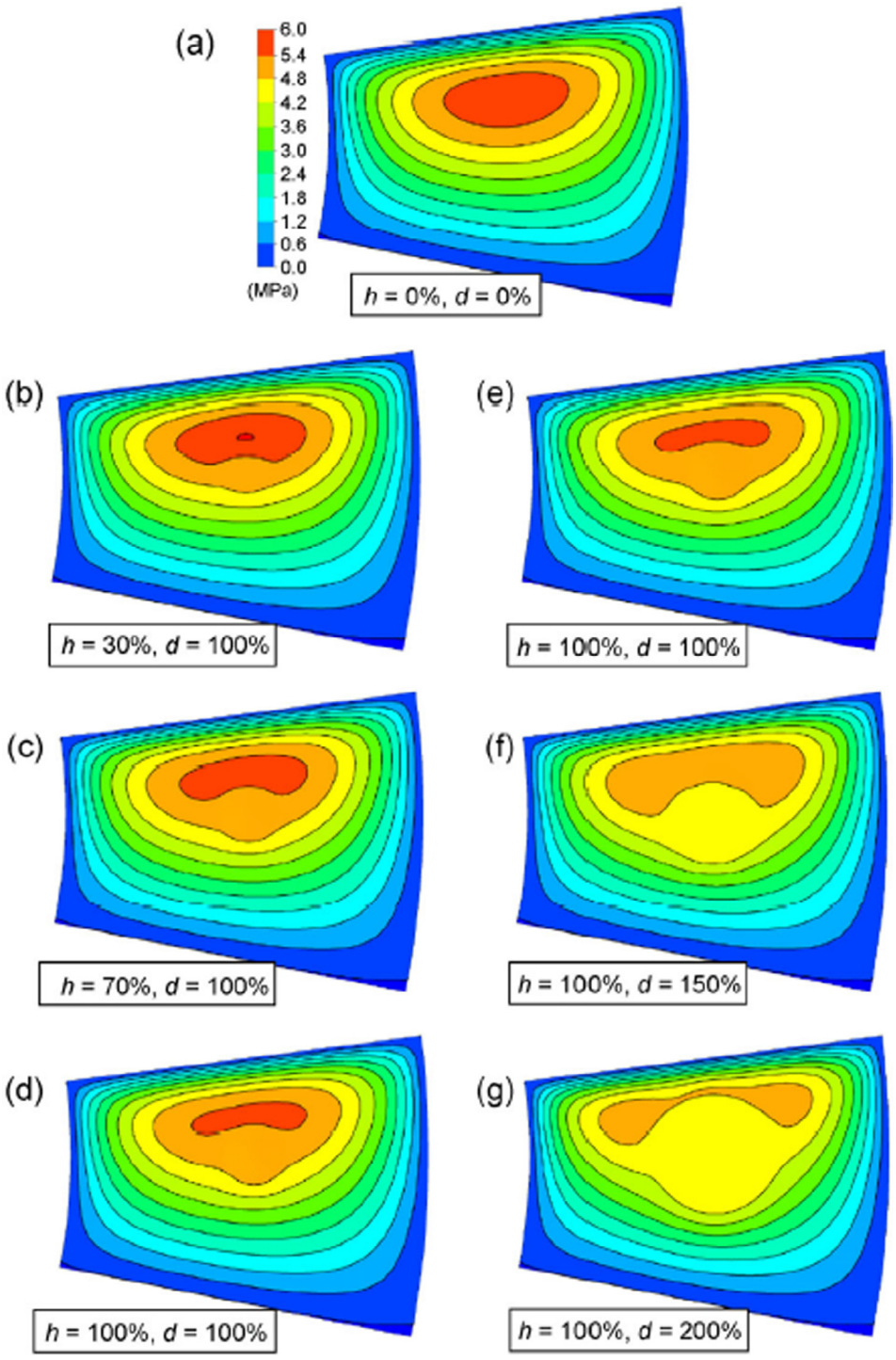

Fig. 10. Effect of pocket presence and size in HD bearing (reprinted from [105] under licence CC BY 3.0).

evaluate the expected deformations. And finally, thermal deformation of the turntable caused by insufficient lubricant cooling or excessive heating at choking elements or at the inlet into the hydrostatic pad [120]. Elastic and thermal distortion effects directly affect the load and error acceptance range [35]. Thermal analyses are widely used for thermo-elastic hydrodynamic (TEHD) models for hydrodynamic and hybrid bearings [56], making it a particularly important task at the design stage of a large hydrostatic pad and turntable. Therefore, numerical methods play an important role during this stage of the development process. Using the FVM and FSI, it is possible to predict the fluid film interface deformation caused by loading [121] or the temperature field of tilted sliding surfaces [94] as a result of asymmetric loading or inaccurate assembly. However, it still seems to be a difficult task to design appropriate boundaries to achieve a good agreement with the measured data [64], especially in large-scale applications. Other specific conditions for inspection are variable working processes with frequent cold/warm starting as it was investigated in study [122] where the film thickness difference was significantly affected by the lubricant temperature.

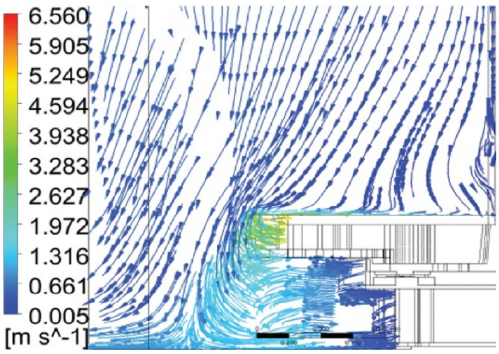

Fig. 11. Flow field of convective heat transfer at 60 r/min (reprinted from [123] under licence CC BY 3.0).

Attention should be particularly directed to large machines and devices built on hydrostatic bearing systems operating at high rotational speeds reaching 70 m/s [117] when the film thickness temperature is significantly increasing. A study by Xu et al. [123] was carried out to establish a temperature rise equation based on heat transfer analysis, simulation and experimental verification with a decent agreement of obtained results, making it a remarkable approach for heat exchange investigation and heat point identification. As stated above, the main transfer modes are heat conduction and natural convection (Fig. 11), significantly affected by the increasing rotational speed.

High rotational speed with a combination of long operation cycles, up to 6 h, increase the temperature even more significantly [124], where the experimental results show 10–30% decrease of hydrostatic bearing clearance. The lubricant heating is a serious issue that must be considered during the designing stage of the hydrostatic pad and turntable. Several investigations into heat dissipation with use of rib plates [125] or into micro heat pipe technology for sufficient cooling of heat generated by shear forces of lubricant film [126] have been carried out. These might help with local lubricant temperature stabilization in the hydrostatic pad. The outlet lubricant cooling process will be further discussed in the hydraulic circuit section.

4.2. Manufacturing and assembly error analysis and prevention

The very thin lubricant film thickness has demanding requirements on the sliding surface precision. The increase of pressure in the recess raises the value of lubricating film thickness only slightly while increasing the required performance strongly. Therefore, it is necessary to achieve a high precision of sliding surfaces. Thermal changes and load effects of machining tools during the manufacturing process always influence the proportions of geometrical errors. Besides structural and thermal deformations, other

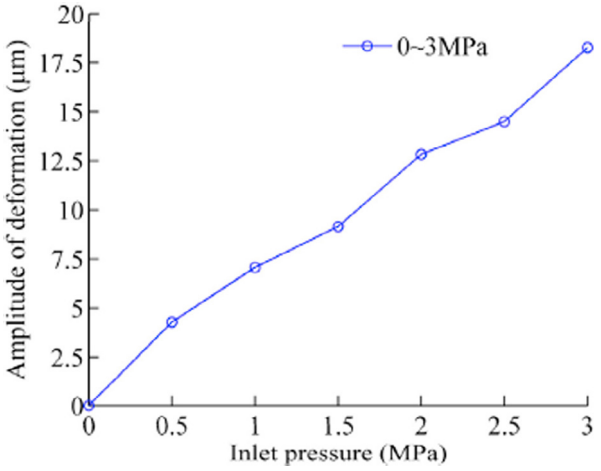

Fig. 13. Amplitude of harmonic wave on the deformed guide rail with wave number 0.5 (reprinted from [130] with permission from Elsevier®).

errors are generated during the manufacturing and assembly. Numerical compensation [127] is frequently used for error reduction. However, it should not be used in machines with notable hysteresis effects. Huang and Kong [128] proposed a new simulation-based method for the simulation and integration of part geometric errors (Fig. 12) that uses tolerances to control the statistical model and enables a tolerance analysis. Wang et al. [129] proposed a model for motion error prediction from the measured geometric errors of hydrostatic guide rails. Recently, an error averaging effect [130–132] for the accuracy improvement and error prediction of the hydrostatic guideway sliding surface, was discussed. Zhang et al. [130] provided a prediction of rail deformation amplitude of a hydrostatic guideway and obtained a good agreement among experimental, approximate, and simulation results.

As shown in Fig. 13, the rail deformation range is comparable to the hydrostatic lubricating film thickness range. The analytical methods and models provide a powerful tool for achieving desirable precision and error reduction. Zha et al. [59] proposed a time-saving error compensation process based on a laser beam measurement without the necessity of guide rail geometric error measurement. For higher rotational speeds in spindles, averaging coefficients become smaller [58], which means that the eccentricity decreases due to a stronger hydrodynamic effect that can also be analogically applied to thrust bearings. Thus, the higher the rotational speed, the lower the sensitivity to geometrical error due to larger hydrodynamic pressure.

The main geometric accuracy parameters [35] are cylindricity and flatness [133] for radial and thrust bearings respectively. As for the case of conical bearings, the perpendicular error should be considered for desired rotation accuracy. Manufacturing errors

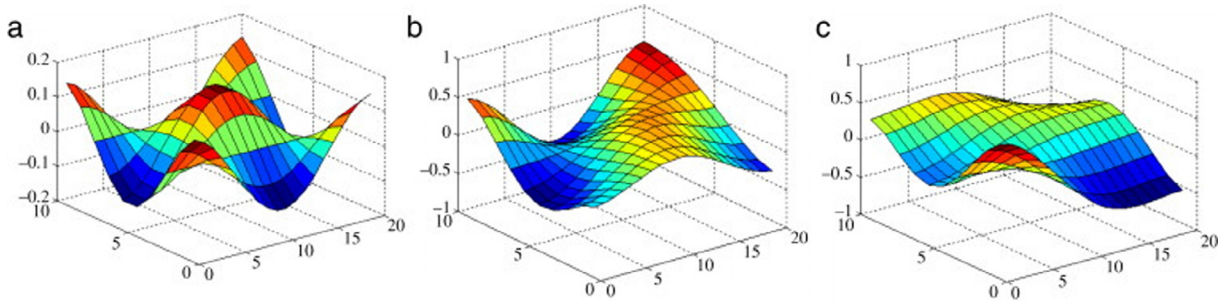

Fig. 12. Part geometric error modes shape illustration (reprinted from [128] with permission from Elsevier®).

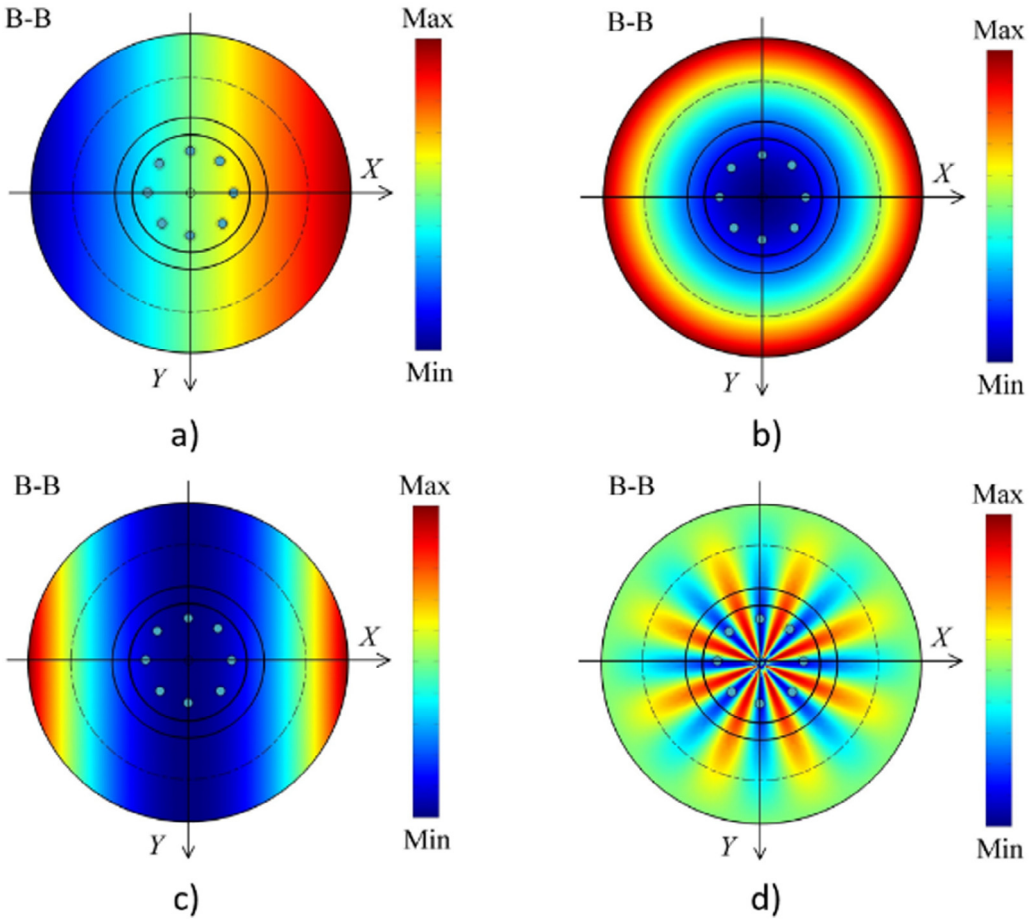

Fig. 14. Diagrams of thrust plate geometric errors: a) tilt errors, b) bowel-shaped errors, c) saddle-shaped errors and d) sinusoidal errors (reprinted from [135] with permission from Elsevier®).

of radial bearings was investigated by Rajput and Sharma [134] numerically, based on the Reynolds equation, to clarify the combined influence of geometric imperfections and axis misalignments on the minimum film thickness for barrel, bellmouth, and undulated journal shapes. Zhang et al. [135] described three types of thrust bearing errors – tilt-, saddle-, and petal-shaped errors (Fig. 14) – and provided approximate formulas for error motions of hydrostatic thrust bearings under quasi-static conditions, considering structure parameters and error motions. Convex and concave shapes modelled by Cui et al. [136] showed a good agreement of calculation, providing a suitable error prediction tool. Generally, a convex shape is always undesirable [137]; however, a concave shape performed with increased load-carrying capacity and lower flow.

Wang et al. [71] investigated the waviness amplitude and wavelength of an aerostatic bearing concluding that higher amplitude generates higher friction, lower load capacity, and stiffness, while it requires a lower flow rate. Zoupas et al. [138] proposed a numerical model for large HD thrust bearing lubricating film investigation in relationship to the effect of surface errors on performance parameters.

Waviness modelling can be related to surface roughness as well. Lin [139] investigated the surface roughness effect numerically, while noticing that in comparison to a smooth surface, confidering surface roughness creates a difference in the dynamic behaviour of a hydrostatic bearing. Yacout et al. [97] confirmed that this type of bearings is sensitive to surface roughness. Generally, the greater the minimum film thickness, the greater roughness is permissible. However, the bearing characteristics are only slightly influenced by the surface roughness [98], except for the stiffness that can be notably enhanced. Therefore, the influence of surface roughness should be considered to improve the accuracy of a turbulent lubrication performance analysis [140], especially in highspeed conditions. Wang et al. [141] presented a stochastic model for surface modelling with utilization of non-dimensional parameters. The circumferential roughness provided higher load capacity, while the radial roughness showed the opposite effect. Moreover, the surface roughness effect is more significant for greater bearing radius and higher operating speed conditions.

Large-scale bearing mounting encounters complications connected with the inaccuracy of their foundations. Therefore, additional measures for proper positioning are necessary. Error compensation proposed by Zha et al. [59] based on a laser interferometer provides a timely effective measurement process, but not greatly suitable for large turnables. A different approach to measuring is photogrammetry [142] that has previously been used for large sites, (as large as 10–20 m with only 10–26 mm error). Its main advantage is the simplicity of the measurement system and portability. However, the required precision for assembly error of large hydrostatic bearings might not be satisfactory and nowadays can only be used for partial measurements. A frequently used mechanism for uniform hydrostatic pad leveling was introduced by Johns et al. [19] in the Giant Magellan Telescope design where there are adjustment screws between track and pier (Fig. 15). The leveling compensation of hydrostatic Lock-gate proposed by Ostayen et al. [28] was based on rubber support. Another example

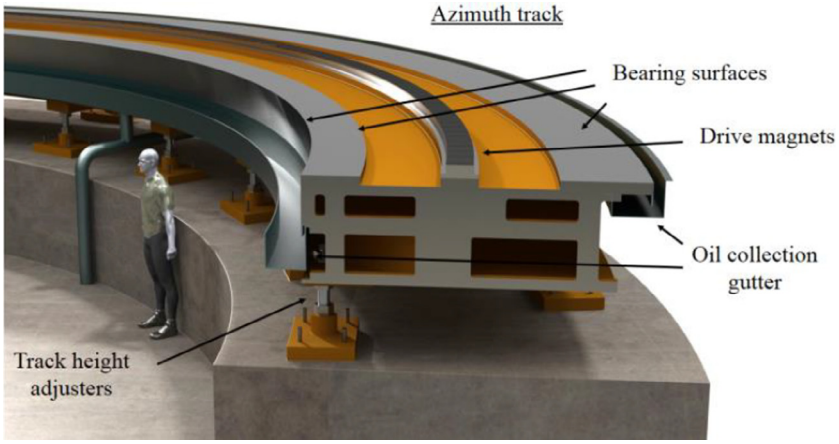

Fig. 15. Azimuth track of the Giant Magellan Telescope (reprinted from [19] with permission from SPIE).

of rubber support in a hydrostatic thrust bearing was provided by Beek and Segal [143] who used material with the compressibility of $51{\cdot}10^6$ bar^{-1}. The results showed that when a local strain becomes greater than 10%, nonlinear elastic behaviour might occur; thus the strain and symmetric pressure distribution [144] should be carefully checkced to avoid unacceptably large or unpredicted elastic deformation. Elastomer materials are widely used in concrete bridge bearings [145], expansion joints [146], and pot bearings of dimensions up to 1200 × 1200 × 360 mm with a load capacity reaching 10 MN. Therefore, the use of such support is possible for stable and lower ambient temperatures because the elastomer material aging process [147,148] at temperatures above 70 °C decreases the rebound resilience, tensile strength, and elastic modulus, while the hardness increases. Higher temperatures can eventually lead to swelling [149] and an increase in the volume of up to 2.4 times. Hassine et al. [150] proposed failure criteria and failure time prediction for lower operation temperatures to minimize the impact of rubber ageing and degradation on its mechanical performance.

4.3. Materials, surface treatment, and modification

Proper material selection of the hydrostatic bearing pad is an essential step in the machine design process, where price, manufacturability, and mechanical and chemical properties are considered. To achieve specific properties, bimetallic or trimetallic bearings are used [151]. An important material characteristic of hydrostatic bearing sliding surfaces is material compatibility. Materials [151] should be selected to resist physical joining when the sliding surfaces sit on each other while in a non-working state. Subsequently, when the bearing is in a working state, cavitation resistance plays a significant role, especially at higher rotation speeds. When using lubricants that promote corrosion, such as water or seawater [152], corrosion resistant materials, such as bronze, should be considered to avoid costly surface treatment and frequent maintenance. Summer et al. [153] experimentally investigated friction and wear properties of journal bearings with various polymer coatings composed of silicon, intermetallic, and tin phases (Fig. 16). With respect to fail-safe measures, friction reduction and wear prevention surface treatment might help to reduce repairs and maintenance in case of hydropower unit failure. The selection of what is needed and what is possible to perform was summarized by Matthews et al. [154], as well as the application requirements according to the dominating phenomenon.

In case of high hydropower unit failure and surface error compensation, thick elastic coatings [144] could be applied onto the sliding surfaces. Along with surface material selection and treatment, surface texturing has its significance in numerous areas of mechanical engineering, including hydrostatic bearings. As presented in reference [155], in a full-fluid-film and mixed lubrication regime surface texturing can serve as storage pockets for lubrication, acting as a fail-safe measure for large bearings. Additionally, grooves are able to trap wear debris in case of lubricant contamination, prevent minor surface damage or conserve micro particles of smart fluid particle-based lubricants [156-158]. The groove shape, size, density, and texture fraction play an important role in the bearing performance optimization [159]. Higher groove density results in better performance at higher speeds, but proper

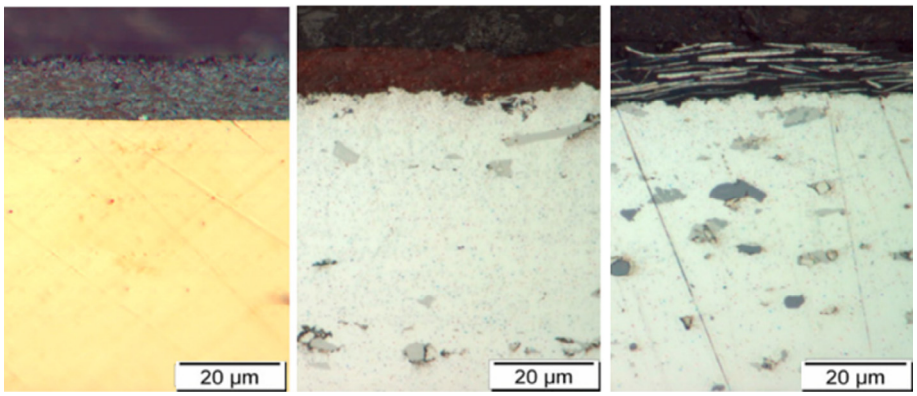

Fig. 16. Microscopy analysis of bearing shells showing the cross section of various polymer coatings and thicknesses (reprinted from [153] under licence CC BY 3.0).

selection of bearing operating conditions must be known and set in advance [160]. Along with full texturing, partial texturing [161] has shown several advantages because of pressure build-up at grooves at higher rotational speeds, leading to higher load capacity and lower friction torque at optimal dimple depth and density ratio [162]. High speed conditions of textured surfaces are especially sensitive to cavitation occurrence at a critical dimple depth [163]. Cavitation is generally considered a negative effect, although it can increase the load-carrying capacity and decrease the friction force. To keep the positive effect of cavitation on performance, wall erosion reduction can be achieved by welding a cavitation-resistant-alloy layer onto the surface [164]. Fluid performance at specific conditions, including cavitation effects, can be efficiently investigated using a numerical approach considering roughness and special averaging methods providing information about local flow losses [165]. A frequently used tool for investigation is the FSI, providing more accurate results [166]. An advanced tool is the thermal-FSI (TFSI) [167] that includes high temperature rise condition and results in a complex insight into texture performance evaluation. The higher the groove depth is, the larger the load capacity and temperature increase. Modern technologies allow us to consider unusual groove shapes that can be made with unconventional processes, such as laser texturing. An example is generic algorithm optimization according to Zhang et al. [61] where bullet-like grooves exhibited the lowest coefficient of friction in comparison to circular and fish-like shapes (Fig. 17); however, only at higher rotation speeds and appropriate rotating direction.

5. Hydrostatic bearing supply system

The hydraulic circuit is the second, equally important part of the hydrostatic bearing (Fig. 5). A pressurized fluid supply is necessary for proper working of the hydrostatic lubrication. Preferably, the design process of the hydraulic circuit is defined by performance requirements. The recommended design flow of a hydraulic circuit is shown in Fig. 18. With respect to large dimensions and numerous hydrostatic pads required to supply with pressurized fluids, the use of flow compensators is necessary and will be described in detail in the following chapter.

5.1. Flow compensation

In case of large hydrostatic bearings, numerous hydrostatic pads will be usually used due to the previously stated size-related limitations (as shown in Fig. 5). Therefore, pressurized fluid flow must be supplied into all pads either by using separate pump for each pad, or by using a common source of pressurized fluid. While the first type is advantageous from the point of maintaining a constant lubricating film, the second option using common source of pressurized fluid is preferred since it does not require large number of pumps. However, when using a common source of pressurized fluid, a compensating device is necessary for maintaining a constant lubricating film thickness in all pads for uneven loading and error compensation. There are numerous options of flow control compensation devices available, all described in Table 9. Restrictor types can be divided according to geometry into fixed or variable. Adams and Shapiro [95] provided damping-load design charts for different recess-to-pad ratios for constant flow (highest), orifice and capillary (lowest) flow compensation. An unusual restriction type was proposed by Xu et al. [168] where a combination of numerous orifice restrictors in the hydrostatic hinge inner compensation led to significantly better performance than only orifice-compensated hydrostatic hinge. Nonetheless, the latest trends in flow compensation aim at intelligent control [64] to maximize the performance and cut down friction losses. A particularly important advancement in flow control is variable viscosity monitoring [169] according to actual oil temperature in the recess to avoid the loss of a load-carrying capacity due to lubricant overheating. Recently, preview control based on a prediction of the machining force for ultraprecision CNC machine tools was proposed by Liu et al. [38], resulting in very high sensitivity to lubricant pressure and displacement. Wang et al. [37] introduced an intelligent monitoring system based on data acquisition that is capable of online diagnostics of measured parameters to provide maximal control and safety of a hydrostatic bearing operation via abnormal data dynamic control. Furthermore, the collected data [130] can be used for real-time performance improvement of the whole hydrostatic bearing system, including carrying ability, variable viscosity conditions, dynamic load influence on film fluctuations, and any other measured and controllable properties. Thus, maintenance can be predicted and prioritized [170] to cut down downtime-related costs.

5.2. Accumulator units

Accumulator units serve as temporary supply of pressurized fluid in the hydraulic circuit, for example in case of hydrogenerator supply failure [179], making it an important element for sliding surface damage. The accumulator price is a small sacrifice considering costly maintenance and repairs [180] that could emerge from electricity drop-out and other possible disturbances. Hydraulic accumulators are often connected with energy recovery systems and energy transformation [181]. However, they also play an important role in energy saving and storage [182], pressure fluctuation reduction [183], and shock absorbing element in fast heavy forging machines [184]. As observed by Xue et al. [60], the fluctuation of the supply pressure increases the linear motion errors. Moreover, inclusion of hydraulic accumulators leads to pulsation pressure reduction. However, the accumulator unit should not be overdimensioned because the volume increase causes a slight increase in pressure pulsations [185]. The accumulator optimal design in case of large hydrostatic bearings is to last for at least as long as the moving part stopping time from full speed to zero, so in case of an emergency the sliding surfaces will get into a contact when they become stationary. Besides the fail-safe measures, accumulator units can be helpful for thermal expansion and leakage compensation in extreme conditions [182], considering relatively small changes in the pressure at a wide range of volume increase as shown at Fig. 19.

5.3. Lubricants

As previously mentioned, lubricant characteristics directly influence the overall performance of the hydrostatic bearing. Viscosity-pressure dependence is normally not considered even though liquids under extreme pressure often show an increase in viscosity, thus only the pumping performance will be affected. However, experimental results of Zhang et al. [186] showed an increase in bearing performance with high bulk (low compressibility) fluid. The viscosity-temperature dependence is far more important since the pump and choking members generate heat. An unexpectedly high temperature rise could even lead to a serious decrease in load-carrying capacity [187] and eventually to a loss of the load-carrying ability. Therefore, a cooling system is usually used for keeping the stable performance of a hydrostatic bearing with restricted flow [188]. Constant viscosity is generally considered in the design process. However, for achieving a higher calculation accuracy, a variable viscosity should be taken into account [68], while an expected ambient temperature range and internal fluid heating on choking elements must be included in the design

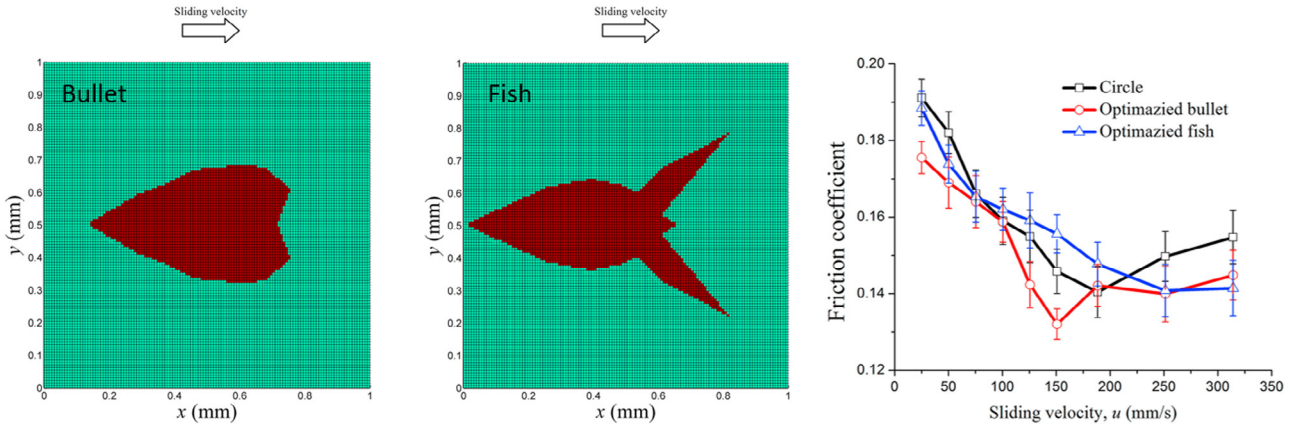

Fig. 17. Final shapes of generated textures based on genetic algorithm and their performance compared to basic circular shape (reprinted from [61] with permission from Elsevier®).

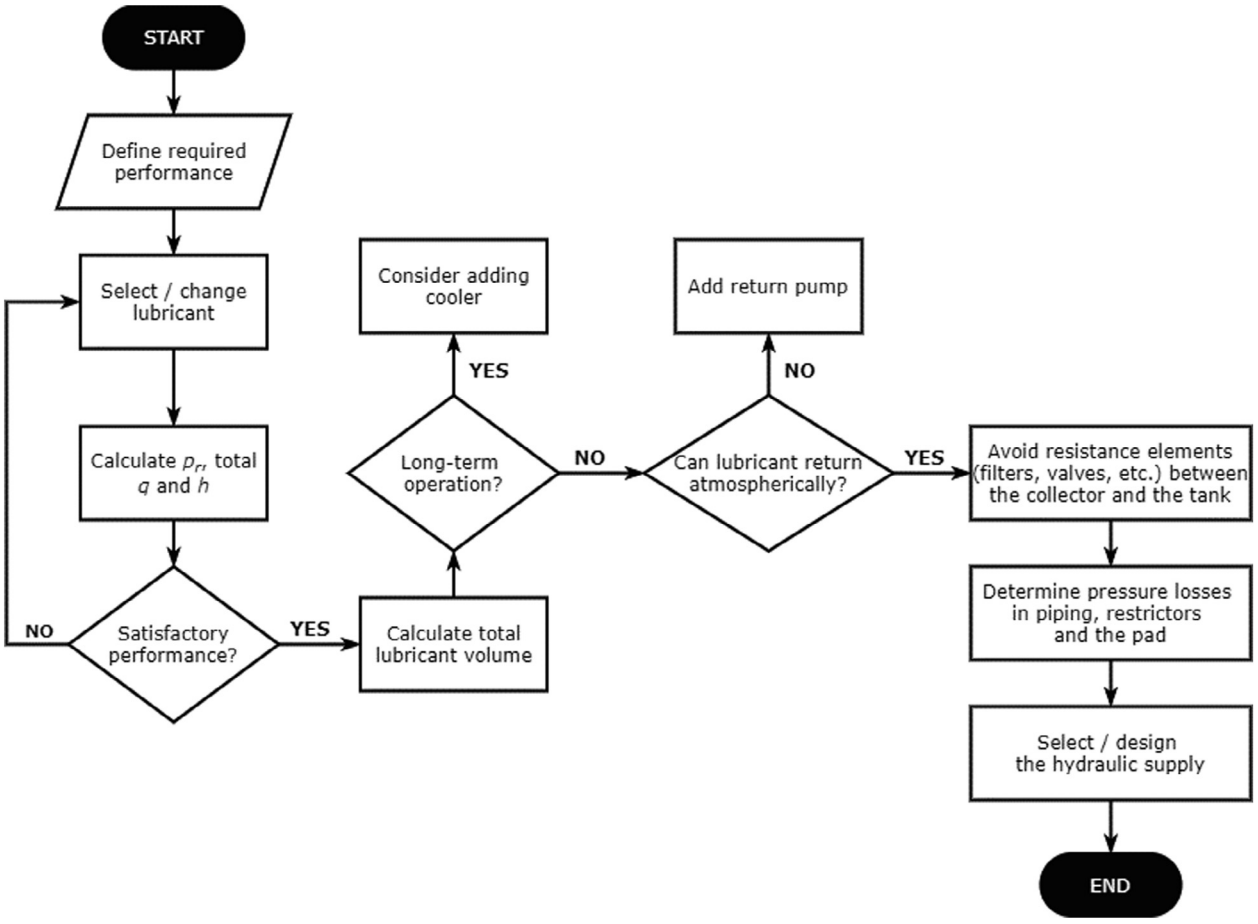

Fig. 18. Flowchart of a hydraulic circuit design process and considerations.

stage. Moreover, viscosity-shear dependence should also be taken into account, especially at rotational speeds above 60 r/min and heavy loads, because the hot oil carrying phenomenon occurs [189]. Basically, a higher viscosity fluid carries more load; however, it requires a higher pumping power, and generates more fluid friction. A low viscosity fluid might not reach desired load carrying capacity of the hydrostatic bearing [54]. Therefore, the lubricant should be selected for the optimal supply power and load-carrying ability. Mostly used lubricants are oils because of certified classification of viscosity index (VI) according to ISO VG. In order to modify the performance or lubricant characteristics, VI improvers are used [190]. However, the NMR (Nuclear magnetic resonance) spectroscopy for the viscosity-temperature relation prediction offers more accurate results than standard measurements, which makes it beneficial mainly for high-precision bearings [191]. Basically, mineral oils are of satisfactory performance and relatively reasonable price. ISO VG 10/15/22/32/46/68/100/150 are chosen according to expected working and surrounding temperatures, and the hydrogenerator performance. Oils of these grades are advantageous due to low friction performance and a neutral effect

Table 9
Comparison of compensating devices types for hydrostatic bearings flow control.

Geometry type	Restriction type	Restrictor device	Flow maintenance	Stiffness	Variable load range	Film thickness compensation	Power losses	Cost	Suitability
Fixed geometry	Constant flow [40]	None	High	Medium	Medium	Medium	Low	High	High accuracy systems Small hydrostatic bearing systems Pump needed for each pad (for multi-pad bearings)
	Capillary [101]	Capillary tube	Low	Low	Low	Low	High	Low	Low accuracy systems Any size
	Orifice [40,54,171,172]	Orifice plate	Low	Low	Low	Low	Medium/ high	Low	Low accuracy systems Any size
	Self-regulating [15]	Flow divider	High	High	High	High	Medium/ High	High	High viscous damping No restrictor needed Only for closed-type bearings
Variable geometry	Elastic member	Elastic tube [4]	Low	Low	Low	Low	Medium/ high	Low	Rubber capillary Limited pressure range
		Elastic surface plate [144]	Low	High	High	Low	Medium/ high	Low/medium (dependent on size)	Inaccurate design for optimal compensation
	Inherent	Membrane [101,173-176]	Medium	High	High	High	Medium	Medium/high	High accuracy systems
	Feedback system	Servo valve [177,178]	High	High	High	High	Medium (depended on load)	High	Variable loads – quick response (≈ 0.1 s) Long-term operation machines (variable viscosity condition) Feedback system (PID) – variable viscosity compensation

on sealing elements. Standard hydraulic oils are providing protection of the hydraulic circulation system components and are suitable for use at high pressures, up to 350 bar. Hydraulic oils performance is usually enhanced using lubricant additives [192], such as viscosity/temperature stabilizers, anti-wear and oxidation inhibitors and extreme pressure additives, which are often used for increased protection of extremely stressed contact surfaces. However, they might act aggressively when used in lubricating copper-based metals [193], especially at higher temperatures. Therefore, the lubricant should be selected regarding the material selection of hydrostatic bearing components. Obviously, the lubricant properties should be also controlled throughout the service life of the hydrostatic bearing since its working principle and performance relies on the lubricant properties. An important approach to bearing diagnostics is an oil monitoring technique, which is, however, difficult for ball bearings [194]. On the other hand, hydrostatic bearings have hydraulic circulation that can be easily modified for oil diagnostics and special filter addition.

For specific environments other fluids could be used, based on their applicability and suitability. An example is water [36,175,195,196] and saltwater [28,29] that are beneficial for use in mechanism manipulation with a difficulty of oil sealing. However, in such aggressive conditions materials must be carefully selected and treated [152]. In case of extreme operating conditions, such as high vacuum, ionic liquid can be a suitable choice [197]. In terms of performance improvement, non-Newtonian fluids have been recently investigated in numerous applications. As reported, a micropolar lubricant can improve the hydrostatic bearing performance [78] in terms of film thickness and stiffness. Yet, the restrictor performance is decreased, which influences the overall performance of the micropolar fluid-lubricated hydrostatic bearing. To find the optimal performance, fluid modelling is induced for the simplification of the design and development processes of hydrostatic bearing [198], such a model is, for example, the Rabinowitch fluid model that can be used for pseudoplastic, Newtonian, and dilatant fluids by changing a single parameter. The application of fluid modelling showed that a pseudoplastic lubricant has lower load-carrying capacity and higher frictional torque than Newtonian fluids, while dilatant fluids were reported [157] to exhibit a lower frictional power loss. In contrast, investigations on additive percentage included an improvement of the VI [199], which can be beneficial in environments with a large temperature difference. Compared to pseudoplastic fluids, fluid modelling of non-Newtonian fluids for the Bingham type showed higher load capacity [200] compared to conventional hydrostatic bearings. This type of fluid can describe the behaviour of smart fluids whose rheology can be modified [158] by electric and magnetic fields. Surface modification, such as magnetic texturing [201] (Fig. 20), can help to increase the load capacity of an magnetorheological fluid and improve the sealing ability [202] of the land, but it also increases the fluid friction. However, the required amount of hydrostatic bearing lubricant exceeds hundreds of litres. While the smart fluid price is very high [203], they have only been investigated in small applications. Other limitations are high required voltage for inducing a noticeable difference in electrorheological fluid performance [204] and an abrasive effect of magnetorheological particles [205,206] caused by high-pressure flow on sliding surfaces and hydraulic circuit components. Besides the abrasive effect, another limitation introduced by Urreta et al. [207] suggested the active compensation of unbalanced machine tool spindle shaft cannot be used due to slow response of hybrid bearing lubricated with magnetorheological fluid.

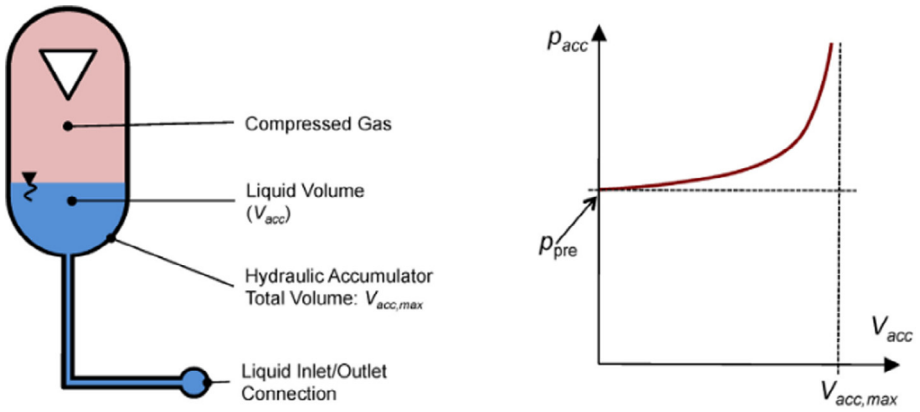

Fig. 19. Pressure-volume relationship for compressed gas in a hydraulic accumulator (reprinted from [182] with permission from Elsevier®).

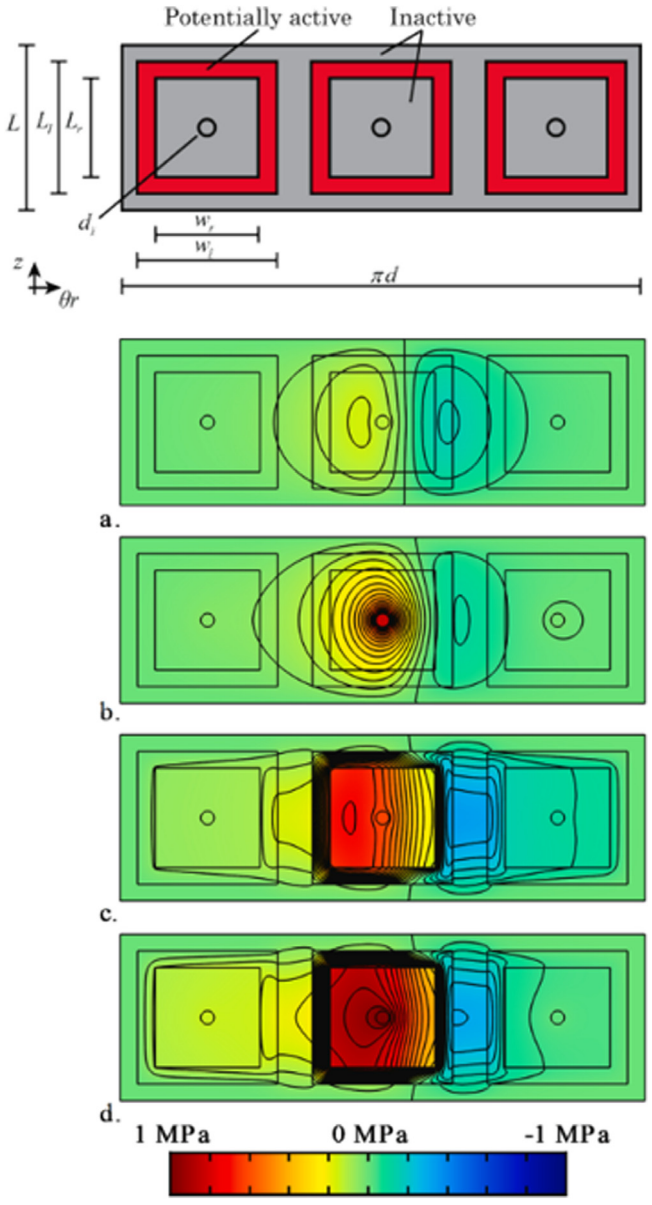

Fig. 20. Pressure distribution of a magnetic texture in hybrid bearing system (reprinted from [201] under licence CC BY 3.0).

6. Summary

This review has summarized the design and optimization process of large-scale hydrostatic bearings. This paper has also highlighted the latest improvements and challenges including hydraulic circuit components and modern advancements in digital technology. The hydrostatic bearing types are selected according to the expected loading direction and designed for the required static and dynamic performance. Analytical calculation provides the pad geometry and approximate static performance, while numerical simulations are utilized for geometry optimization, dynamic performance evaluation, and investigation of thermal properties. Analytical calculation provides a quick estimation of the bearing geometry and supply performance. In contrast, numerical analyses provide a critical insight into the possible future problem minimization, such as structural deformations and thermal influence effects on the performance and lubricating film stability. The bearing land texturing can improve the dynamic properties at higher speeds. As it turned out, the manufacturing process does influence the final bearing performance. It is required to achieve high bearing straightness, which is, however, difficult for large-scale structures. Therefore, a suitable compensation method must be applied – either flow compensation using restrictors, or surface compensation using compliant materials. Latest advancements in control technology offer a wide range of possibilities for bearing performance monitoring, management, and diagnostics. Hydraulic accumulators offer both fail-safe and vibration damping effects. Special lubricant additives can improve the bearing performance. As found out, smart fluids are not yet suitable for large-scale hydrostatic bearings, especially due to high price. The stated remarks can be applied both to radial and axial hydrostatic bearings of all sizes.

7. Future challenges

Some of the greatest challenges will be the design of new large-scale structures based on the hydrostatic lubrication principle, and the replacement of existing old rail turntables with silent hydrostatic bearings. A substantial part of future development will be aimed at numerical simulations improvement and combination, such as FSI etc. The future research might be oriented towards tolerable error specification to simplify the manufacturing and assembly processes of large-scale hydrostatic bearings. Error compensation can be improved using durable and stable compliant materials. Further improvement can be made in optical scanning of sliding surfaces during manufacturing and assembly to speed

up the whole construction process. To avoid costly repairs, a fail-safe surface texturing that act like lubricant reservoirs in case of sliding surface collision can be developed. A significant advancement can be achieved in real-time hydraulic circuit monitoring and adaptive regulation to provide optimal maintenance and condition prediction and adaptation based on big data analysis [208]. The emerging trend of utilizing modern progressive technologies of the Industry 4.0. era, such as Digital Twin (DT) and Internet of Things (IoT), open new ways in machine design, manufacturing [209] and control in the mechanical engineering industry. Possibly, the next industrial epoch might bring fully automated design, optimization and eventually also manufacturing using artificial intelligence (AI) that could exceptionally improve future technologies and satisfy increasing societal demands.

Declaration of Competing Interest

The authors declare that they have no known competing financial interests or personal relationships that could have appeared to influence the work reported in this paper.

Acknowledgments

This research was carried out under the project FSI-S-17-4415 with financial support from the Ministry of Education, Youth and Sports of the Czech Republic.

References

[1] O. Reynolds, On the theory of lubrication and its application to Mr. Lowe's experiments, Philos. Trans. R. Soc. London. 177 (1886) 157–234.
[2] O.M.F.R.S. Lord Rayleigh, Notes on the theory of lubrication, London, Edinburgh, Dublin Philos, Mag. J. Sci. 35 (1918) 1–12, https://doi.org/10.1080/14786440108635730.
[3] W.B. Rowe, Advances in hydrostatic and hybrid bearing technology, Proc. Inst. Mech. Eng. Part C J. Mech. Eng. Sci. 203 (1989) 225–242. https://doi.org/10.1243/PIME_PROC_1989_203_110_02.
[4] R. Bassani, B. Piccigallo, Hydrostatic Lubrication, 22nd ed.,., Elsevier B.V, 1992.
[5] X.B. Li, X. Wang, M. Li, Y.S. Ma, Y. Huang, The Research Status and Progress of Heavy/Large Hydrostatic Thrust Bearing, Adv. Mech. Eng. (2014), https://doi.org/10.1155/2014/982584.
[6] Z.F. Liu, Y.M. Wang, L.G. Cai, Y.S. Zhao, Q. Cheng, X.M. Dong, A review of hydrostatic bearing system: Researches and applications, Adv. Mech. Eng. 9 (2017), https://doi.org/10.1177/1687814017730536.
[7] R. Mahdi, K. Stephan, B. Friedrich, Experimental investigations on stick-slip phenomenon and friction characteristics of linear guides, Procedia Eng. 100 (2015) 1023–1031, https://doi.org/10.1016/j.proeng.2015.01.462.
[8] J. Awrejcewicz, P. Olejnik, The Occurrence of Stick-Slip Phenomenon, (2017).
[9] A. Bonanno, F. Pedrielli, a Study on the structureborne noise of hydraulic gear pumps, Proc. JFPS Int. Symp. Fluid Power. 2008 (2008) 641–646, https://doi.org/10.5739/isfp.2008.641.
[10] V. Induced, I.F. Flow, Vibrations induced by internal fluid flow, Flow-Induced Vib. (2014) 157–195, https://doi.org/10.1016/b978-0-08-098347-9.00004-7.
[11] H. Ortwig, Experimental and analytical vibration analysis in fluid power systems, Int. J. Solids Struct. 42 (2005) 5821–5830, https://doi.org/10.1016/j.ijsolstr.2005.03.028.
[12] G. Chen, J. Wen, Load performance of large-scale rolling bearings with supporting structure in wind turbines, J. Tribol. 134 (2012), https://doi.org/10.1115/1.4007349.
[13] G. Chen, J. Wen, Effects of size and raceway hardness on the fatigue life of large rolling bearing, J. Mech. Sci. Technol. 29 (2015) 3873–3883, https://doi.org/10.1007/s12206-015-0833-3.
[14] L. Chen, X.T. Xia, H. tian Zheng, M. Qiu, Rework solution method on large size radial roller bearings, J. Brazilian Soc. Mech. Sci. Eng. 38 (2016) 1249–1260. https://doi.org/10.1007/s40430-015-0364-y.
[15] R. Bassani, Hydrostatic self-regulating multipad journal and integral bearings, Tribol. Trans. 56 (2013) 187–195, https://doi.org/10.1080/10402004.2012.737501.
[16] J.Y. Jang, M.M. Khonsari, On the characteristics of misaligned journal bearings, Lubricants. 3 (2015) 27–53, https://doi.org/10.3390/lubricants3010027.
[17] E.A. Novikov, I.A. Shitikov, V.A. Maksimov, Calculation of the characteristics of a hydrostatic ring thrust bearing for refrigeration compressors, Chem. Pet. Eng. 40 (2004) 222–228, https://doi.org/10.1023/B:CAPE.0000033680.91322.0f.
[18] M. Sheehan, S. Gunnels, C. Hull, J. Kern, C. Smith, M. Johns, S. Shectman, Progress on the structural and mechanical design of the Giant Magellan Telescope, Ground-Based Airborne Telesc. IV. 8444 (2012) 84440N, https://doi.org/10.1117/12.926469.
[19] M. Johns, C. Hull, G. Muller, B. Irarrazaval, A. Bouchez, T. Chylek, C. Smith, A. Wadhavkar, B. Bigelow, S. Gunnels, B. McLeod, C. Buleri, Design of the giant magellan telescope, Ground-Based Airborne Telesc. 9145 (2014) 91451F, https://doi.org/10.1117/12.2057286.
[20] S.-H. Jang, Y.-H. Choi, S.-T. Kim, H.-S. An, H.-B. Choi, J.-S. Hong, Development of core technologies of multi-tasking machine tools for machining highly precision large parts, J. Korean Soc. Precis. Eng. 29 (2012) 129–138, https://doi.org/10.7736/kspe.2012.29.2.129.
[21] Z. Guo, T. Hirano, R.G. Kirk, Application of CFD analysis for rotating machinery - Part I: Hydrodynamic, hydrostatic bearings and squeeze film damper, J. Eng. Gas Turbines Power. 127 (2005) 445–451, https://doi.org/10.1115/1.1807415.
[22] A. Bouzidane, M. Thomas, Nonlinear dynamic analysis of a rigid rotor supported by a three-pad hydrostatic squeeze film dampers, Tribol. Trans. 56 (2013) 717–727, https://doi.org/10.1080/10402004.2013.788238.
[23] W.B. Rowe, Grinding Machine Developments, in: Princ. Mod. Grind. Technol., Elsevier, 2009: pp. 163–210. https://doi.org/10.1016/b978-0-8155-2018-4.50016-1.
[24] Z. Liming, L. Yongyao, W. Zhengwei, L. Xin, X. Yexiang, A review on the large tilting pad thrust bearings in the hydropower units, Renew. Sustain. Energy Rev. 69 (2017) 1182–1198, https://doi.org/10.1016/j.rser.2016.09.140.
[25] D.V. De Pellegrin, D.J. Hargreaves, An isoviscous, isothermal model investigating the influence of hydrostatic recesses on a spring-supported tilting pad thrust bearing, Tribol. Int. 51 (2012) 25–35, https://doi.org/10.1016/j.triboint.2012.02.008.
[26] M. Wasilczuk, Friction and lubrication of large tilting-pad thrust bearings, Lubricants. 3 (2015) 164–180, https://doi.org/10.3390/lubricants3020164.
[27] X. Raud, M. Fillon, M. Helene, Numerical modelling of hydrostatic lift pockets in hydrodynamic journal bearings – Application to low speed working conditions of highly loaded tilting pad journal bearings, Mech. Ind. 14 (2013) 327–334, https://doi.org/10.1051/meca/2013073.
[28] R.A.J. Van Ostayen, A. Van Beek, M. Ros, A mathematical model of the hydro-support: An elasto-hydrostatic thrust bearing with mixed lubrication, Tribol. Int. 37 (2004) 607–616, https://doi.org/10.1016/j.triboint.2004.01.008.
[29] E. Xu, Y. Wang, J. Wu, S. Xu, Y. Wang, S. Wang, Investigations on the applicability of hydrostatic bearing technology in a rotary energy recovery device through CFD simulation and validating experiment, Desalination. 383 (2016) 60–67, https://doi.org/10.1016/j.desal.2016.01.018.
[30] Z. Liu, Y. Wang, L. Cai, Q. Cheng, H. Zhang, Design and manufacturing model of customized hydrostatic bearing system based on cloud and big data technology, Int. J. Adv. Manuf. Technol. 84 (2016) 261–273, https://doi.org/10.1007/s00170-015-8066-2.
[31] I.F. Santos, Controllable sliding bearings and controllable lubrication principles-an overview, Lubricants. 6 (2018), https://doi.org/10.3390/lubricants6010016.
[32] M.M. Khonsari, E.R. Booser, Applied Tribology: Bearing Design and Lubrication, John Wiley & Sons Ltd, Chichester, UK (2017), https://doi.org/10.1002/9781118700280.
[33] T. Seperamaniam, N.A.A. Jalil, Z.A. Zulkefli, Hydrostatic Bearing Design Selection for Automotive Application Using Pugh Controlled Convergence Method, Procedia Eng. 170 (2017) 422–429, https://doi.org/10.1016/j.proeng.2017.03.068.
[34] A. Harnoy, Bearing design in machinery, Eng. Tribol. Lubrication (2003), https://doi.org/10.1201/9780203909072.ch6.
[35] K. Cheng, W.B. Rowe, A selection strategy for the design of externally pressurized journal bearings, Tribol. Int. 28 (1995) 465–474, https://doi.org/10.1016/0301-679X(95)00011-R.
[36] D. Fedorynenko, R. Kirigaya, Y. Nakao, Dynamic characteristics of spindle with water-lubricated hydrostatic bearings for ultra-precision machine tools, Precis. Eng. 63 (2020) 187–196, https://doi.org/10.1016/j.precisioneng.2020.02.003.
[37] Y. Wang, Z. Liu, Y. Zhao, X. Dong, L. Hun, L. Cai, Design of an intelligent monitoring system for hydrostatic turntable service performance evaluation, J. Ambient Intell. Humaniz. Comput. (2018), https://doi.org/10.1007/s12652-018-1027-5.
[38] C. Liu, J. Hu, Q. Hu, Preview Control of Hydrostatic Guideway for Ultraprecision CNC Machine Tools, Iran. J. Sci. Technol. - Trans, Mech. Eng. 43 (2019) 749–759, https://doi.org/10.1007/s40997-018-0192-7.
[39] X. Zuo, S. Li, Z. Yin, J. Wang, Design and Parameter Study of a Self-Compensating Hydrostatic Rotary Bearing, Int. J. Rotating Mach. 2013 (2013) 1–10, https://doi.org/10.1155/2013/638193.
[40] Y. Kang, J.L. Lee, H.C. Huang, C.Y. Lin, H.H. Lee, D.X. Peng, C.C. Huang, Design for static stiffness of hydrostatic plain bearings: Constant compensations, Ind. Lubr. Tribol. 63 (2011) 178–191, https://doi.org/10.1108/00368791111126608.
[41] G. Hong, L. Xinmin, W. Xiaoling, C. Shaoqi, Performance of flat capillary compensated deep/shallow pockets hydrostatic/hydrodynamic journal-thrust floating ring bearing, Tribol. Trans. 52 (2009) 204–212, https://doi.org/10.1080/10402000802354061.
[42] X.O. Zuo, J.M. Wang, Z.Q. Yin, S.Y. Li, Self-compensated precision hydrostatic rotary bearing, Adv. Mater. Res. 662 (2013) 674–677, https://doi.org/10.4028/www.scientific.net/AMR.662.674.
[43] N.R. Kane, J. Sihler, A.H. Slocum, A hydrostatic rotary bearing with angled surface self-compensation, Precis. Eng. 27 (2003) 125–139, https://doi.org/10.1016/S0141-6359(02)00194-0.

[44] S.C. Sharma, V.M. Phalle, S.C. Jain, Performance analysis of a multirecess capillary compensated conical hydrostatic journal bearing, Tribol. Int. 44 (2011) 617–626, https://doi.org/10.1016/j.triboint.2010.12.012.
[45] X. Zuo, J. Wang, Z. Yin, S. Li, Comparative performance analysis of conical hydrostatic bearings compensated by variable slot and fixed slot, Tribol. Int. 66 (2013) 83–92, https://doi.org/10.1016/j.triboint.2013.04.013.
[46] M. Kozdera, S. Drbáková, Numerical modelling of the flow in the annular multi-recess hydrostatic thrust bearing using CFD methods, EPJ Web Conf. 45 (2013), https://doi.org/10.1051/epjconf/20134501051.
[47] Y. Kang, S.Y. Hu, Y.P. Chang, T.P. Wang, Identification of Characteristic Parameters for Hydrostatic Bearings, J. Mech. 31 (2015) 227–240, https://doi.org/10.1017/jmech.2014.91.
[48] N.G. Chikurov, Modeling of hydrostatic bearings by electrical analogy, Russ. Eng. Res. 37 (2017) 517–522, https://doi.org/10.3103/S1068798X17060107.
[49] B.M.A. Maher, Performance characteristics of an elliptic hydrostatic bearing and comparative analysis based on Stokes' conditions, Acta Mech. 223 (2012) 1187–1198, https://doi.org/10.1007/s00707-012-0647-7.
[50] B.J. Hamrock, S.R. Schmid, B.O. Jacobson, Fundamentals of Fluid Film Lubrication, 2nd ed., Marcel Dekker, New York, 2004.
[51] H.C. Rippel, Cast bronze bearing design manual, Cast Bronze Bearing Institute (1960).
[52] D. Chen, S. Zhou, L. Dong, J. Fan, Performance evaluation and comparative analysis of hydrostatic spindle affect by the oil film slip, J. Manuf. Process. 20 (2015) 128–136, https://doi.org/10.1016/j.jmapro.2015.09.002.
[53] S. Gao, K. Cheng, S. Chen, H. Ding, H. Fu, CFD based investigation on influence of orifice chamber shapes for the design of aerostatic thrust bearings at ultra-high speed spindles, Tribol. Int. 92 (2015) 211–221, https://doi.org/10.1016/j.triboint.2015.06.020.
[54] F. Ghezali, A. Bouzidane, M. Thomas, 3D Numerical investigation of pressure field of an orifice compensated hydrostatic bearing, Mech. Ind. 18 (2017), https://doi.org/10.1051/meca/2016008.
[55] F. Shen, C.L. Chen, Z.M. Liu, Effect of pocket geometry on the performance of a circular thrust pad hydrostatic bearing in machine tools, Tribol. Trans. 57 (2014) 700–714, https://doi.org/10.1080/10402004.2014.906694.
[56] S. Yang, C. Li, M. Jiang, S. Pei, A study of inlet temperature models of a large size tilting thrust bearing comparison between theory and experiment, Tribol. Int. 140 (2019), https://doi.org/10.1016/j.triboint.2019.105881 105881.
[57] X. Li, X. Wang, M. Li, Y. Ma, Y. Huang, The research status and progress of heavy/large hydrostatic thrust bearing, Adv. Mech. Eng. 2014 (2014), https://doi.org/10.1155/2014/982584.
[58] Y.T. Zhang, C.H. Lu, H.X. Zhao, W.J. Shi, P. Liang, Error Averaging Effect of Hydrostatic Journal Bearings Considering the Influences of Shaft Rotating Speed and External Load, IEEE Access. 7 (2019) 106346–106358, https://doi.org/10.1109/ACCESS.2019.2931948.
[59] J. Zha, F. Xue, Y. Chen, Straightness error modeling and compensation for gantry type open hydrostatic guideways in grinding machine, Int. J. Mach. Tools Manuf. 112 (2017) 1–6, https://doi.org/10.1016/j.ijmachtools.2016.10.002.
[60] F. Xue, W. Zhao, Y. Chen, Z. Wang, Research on error averaging effect of hydrostatic guideways, Precis. Eng. 36 (2012) 84–90, https://doi.org/10.1016/j.precisioneng.2011.07.007.
[61] H. Zhang, M. Hua, G. zhong Dong, D. ya Zhang, W. jian Chen, G. neng Dong, Optimization of texture shape based on Genetic Algorithm under unidirectional sliding, Tribol. Int. 115 (2017) 222–232. https://doi.org/10.1016/j.triboint.2017.05.017.
[62] Q. Li, S. Zhang, Y. Wang, W.W. Xu, Z. Wang, Z. Wang, Principal normal stress cavitation criterion for CFD analysis of loading capacity in journal bearings, Ind. Lubr. Tribol. 71 (2019) 1047–1054, https://doi.org/10.1108/ILT-01-2019-0013.
[63] X.D. Yu, X. Zuo, C. Liu, X.H. Zheng, H. Qu, T.F. Yuan, Oil film shape prediction of hydrostatic thrust bearing under the condition of high speed and heavy load, Ind. Lubr. Tribol. 70 (2018) 1243–1250, https://doi.org/10.1108/ILT-07-2017-0220.
[64] M. Wodtke, A. Schubert, M. Fillon, M. Wasilczuk, P. Pajaczkowski, Large hydrodynamic thrust bearing: Comparison of the calculations and measurements, Proc. Inst. Mech. Eng. Part J J. Eng. Tribol. 228 (2014) 974–983. https://doi.org/10.1177/1350650114528317.
[65] M. Badshah, S. Badshah, S. Jan, Comparison of computational fluid dynamics and fluid structure interaction models for the performance prediction of tidal current turbines, J. Ocean Eng. Sci. 5 (2020) 164–172, https://doi.org/10.1016/j.joes.2019.10.001.
[66] L. Lu, H. Su, Y. Liang, Q. Zhang, Research on static stiffness of hydrostatic bearing using fluid-structure interaction analysis, Procedia Eng. 29 (2012) 1304–1308, https://doi.org/10.1016/j.proeng.2012.01.131.
[67] Y.Q. Zhang, L.G. Fan, R. Li, C.X. Dai, X.D. Yu, Simulation and experimental analysis of supporting characteristics of multiple oil pad hydrostatic bearing disk, J. Hydrodyn. 25 (2013) 236–241, https://doi.org/10.1016/S1001-6058(13)60358-3.
[68] Y.Q. Zhang, X.Q. Xu, X.D. Yang, H.M. Li, H. Jiang, X.Y. Yu, Z.M. Shi, Analysis on influence of oil film thickness on temperature field of heavy hydrostatic bearing in variable viscosity condition, Adv. Mater. Res. 239–242 (2011) 1418–1421, https://doi.org/10.4028/www.scientific.net/AMR.239-242.1418.
[69] J.P. Shao, C.X. Dai, Y.Q. Zhang, X.D. Yu, X.Q. Xu, Y.F. Wang, The effect of oil cavity depth on temperature field in heavy hydrostatic thrust bearing, J. Hydrodyn. 23 (2011) 676–680, https://doi.org/10.1016/S1001-6058(10)60164-3.
[70] L.G. Cai, Y.M. Wang, Z.F. Liu, Q. Cheng, Carrying capacity analysis and optimizing of hydrostatic slider bearings under inertial force and vibration impact using finite difference method (FDM), J. Vibroengineering. 17 (2015) 2781–2794.
[71] X. Wang, Q. Xu, B. Wang, L. Zhang, H. Yang, Z. Peng, Effect of surface waviness on the static performance of aerostatic journal bearings, Tribol. Int. 103 (2016) 394–405, https://doi.org/10.1016/j.triboint.2016.07.026.
[72] R. Nicoletti, Comparison between a meshless method and the finite difference method for solving the reynolds equation in finite bearings, J. Tribol. 135 (2013) 1–9, https://doi.org/10.1115/1.4024752.
[73] Y. Zhang, X. Yang, H. Li, H. Jiang, X. Yu, Z. Shi, Research on influence of cavity depth on load capacity of heavy hydrostatic bearing in variable viscosity condition, Adv. Mater. Res. 129–131 (2010) 1181–1185, https://doi.org/10.4028/www.scientific.net/AMR.129-131.1181.
[74] P.G. Khakse, V.M. Phalle, S.S. Mantha, Comparative performance of a non-recessed hole-entry hybrid/hydrostatic conical journal bearing compensated with capillary and orifice restrictors, Tribol. Ind. 38 (2016) 133–148.
[75] P.G. Khakse, V.M. Phalle, S.S. Mantha, Performance Analysis of a Nonrecessed Hybrid Conical Journal Bearing Compensated With Capillary Restrictors, J. Tribol. 138 (2016) 1–9, https://doi.org/10.1115/1.4030808.
[76] V. Kumar, S.C. Sharma, Magneto-hydrostatic lubrication of thrust bearings considering different configurations of recess, Ind. Lubr. Tribol. 71 (2019) 915–923, https://doi.org/10.1108/ILT-10-2018-0370.
[77] C.B. Khatri, S.C. Sharma, Influence of textured surface on the performance of non-recessed hybrid journal bearing operating with non-Newtonian lubricant, Tribol. Int. 95 (2016) 221–235, https://doi.org/10.1016/j.triboint.2015.11.017.
[78] E. Rajasekhar Nicodemus, S.C. Sharma, Orifice compensated multirecess hydrostatic/hybrid journal bearing system of various geometric shapes of recess operating with micropolar lubricant, Tribol. Int. 44 (2011) 284–296, https://doi.org/10.1016/j.triboint.2010.10.026.
[79] A. Chasalevris, D. Sfyris, Evaluation of the finite journal bearing characteristics, using the exact analytical solution of the Reynolds equation, Tribol. Int. 57 (2013) 216–234, https://doi.org/10.1016/j.triboint.2012.08.011.
[80] X. Liang, X. Yan, W. Ouyang, R.J.K. Wood, F. Kuang, Z. Liu, X. Zhou, Comparison of measured and calculated water film thickness of a water-lubricated elastically supported tilting pad thrust bearing, Surf. Topogr. Metrol. Prop. 7 (2019), https://doi.org/10.1088/2051-672X/ab47a6.
[81] B.S. Shenoy, R. Pai, Effect of turbulence on the static performance of a misaligned externally adjustable fluid film bearing lubricated with couple stress fluids, Tribol. Int. 44 (2011) 1774–1781, https://doi.org/10.1016/j.triboint.2011.06.025.
[82] D. Dowson, Inertia effects in hydrostatic thrust bearings, J. Fluids Eng. Trans. ASME. 83 (1961) 227–234. https://doi.org/https://dx.doi.org/10.1115/1.3658931.
[83] Y.Q. Zhang, Z.Q. Zhang, X.B. Kong, R. Li, H. Jiang, Application of dynamic mesh technology in the oil film flow simulation for hydrostatic bearing, Ind. Lubr. Tribol. 71 (2019) 74–82, https://doi.org/10.1108/ILT-08-2017-0222.
[84] C. Cui, T. Guo, Y. Wang, Q. Dai, Research on carrying capacity of hydrostatic slideway on heavy-duty gantry CNC machine, AIP Conf. Proc. 1839 (2017), https://doi.org/10.1063/1.4982524.
[85] P. Novotný, J. Hrabovský, J. Juračka, J. Klíma, V. Hort, Effective thrust bearing model for simulations of transient rotor dynamics, Int. J. Mech. Sci. 157–158 (2019) 374–383, https://doi.org/10.1016/j.ijmecsci.2019.04.057.
[86] Z. Wang, Y. Liu, F. Wang, Rapid calculation method for estimating static and dynamic performances of closed hydrostatic guideways, Ind. Lubr. Tribol. 69 (2017) 1040–1048, https://doi.org/10.1108/ILT-01-2017-0003.
[87] P. Liang, C.H. Lu, W. Pan, S.Y. Li, A new method for calculating the static performance of hydrostatic journal bearing, Tribol. Int. 77 (2014) 72–77, https://doi.org/10.1016/j.triboint.2014.04.019.
[88] E. Solmaz, F.C. Babalik, F. Öztürk, Multicriteria optimization approach for hydrostatic bearing design, Ind. Lubr. Tribol. 54 (2002) 20–25, https://doi.org/10.1108/00368790210415338.
[89] D. Fedorynenko, S. Sapon, S. Boyko, Accuracy of spindle units with hydrostatic bearings, Acta Mech. Autom. 10 (2016) 117–124, https://doi.org/10.1515/ama-2016-0019.
[90] D. Fedorynenko, S. Sapon, S. Boyko, A. Urlina, Increasing of energy efficiency of spindles with fluid bearings, Acta Mech. Autom. 11 (2017) 204–209, https://doi.org/10.1515/ama-2017-0031.
[91] Y. Wang, Z. Liu, Q. Cheng, Y. Zhao, Y. Wang, L. Cai, Analysis and optimization of nonlinear carrying performance of hydrostatic ram based on finite difference method and Runge-Kutta method, Adv. Mech. Eng. 11 (2019) 1–12, https://doi.org/10.1177/1687814019856128.
[92] X.C. Zhu, W.G. Gao, T. Liu, S.H. Zhao, G.W. Zhang, D.W. Zhang, Analysis on dynamic characteristics of closed hydrostatic guideway throttled by capillary, Appl. Mech. Mater. 607 (2014) 594–599, https://doi.org/10.4028/www.scientific.net/AMM.607.594.
[93] L.J. Nypan, B.J. Hamrock, H.W. Scibbe, W.J. Anderson, Optimization of Conical Hydrostatic Bearing for Minimum Friction, J. Lubr. Technol. 94 (1972) 136–142, https://doi.org/10.1115/1.3451656.
[94] Z.F. Liu, C.P. Zhan, Q. Cheng, Y.S. Zhao, X.Y. Li, Y.D. Wang, Thermal and tilt effects on bearing characteristics of hydrostatic oil pad in rotary table, J. Hydrodyn. 28 (2016) 585–595, https://doi.org/10.1016/S1001-6058(16)60662-5.

[95] M.L. Adams, W. Shapiro, Squeeze film characteristics in flat hydrostatic bearings with incompressible flow, ASLE Trans. 12 (1969) 183–189, https://doi.org/10.1080/05698196908972260.
[96] A. Bouzidane, M. Thomas, Equivalent stiffness and damping investigation of a hydrostatic journal bearing, Tribol. Trans. 50 (2007) 257–267, https://doi.org/10.1080/10402000701309745.
[97] A.W. Yacout, A.S. Ismaeel, S.Z. Kassab, The surface roughness effect on the hydrostatic thrust spherical bearing performance (part 2 of 5, clearance type of bearings), Am. Soc. Mech. Eng. Tribol. Div. TRIB. (2006), https://doi.org/10.1115/imece2006-13004.
[98] A.W. Yacout, The surfacse roughness effect on the hydrostatic thrust spherical bearings performance (part 3 of 5, recessed clearance type of bearings), ASME Int, Mech. Eng. Congr. Expo. Proc. 9 (2007) 431–447, https://doi.org/10.1115/IMECE2007-41013.
[99] S.C. Sharma, S.C. Jain, D.K. Bharuka, Influence of recess shape on the performance of a capillary compensated circular thrust pad hydrostatic bearing, Tribol. Int. 35 (2002) 347–356, https://doi.org/10.1016/S0301-679X(02)00013-0.
[100] M.S. Kotilainen, A.H. Slocum, Manufacturing of cast monolithic hydrostatic journal bearings, Precis. Eng. 25 (2001) 235–244, https://doi.org/10.1016/S0141-6359(01)00075-7.
[101] N. Singh, S.C. Sharma, S.C. Jain, S.S. Reddy, Performance of membrane compensated multirecess hydrostatic/hybrid flexible journal bearing system considering various recess shapes, Tribol. Int. 37 (2004) 11–24, https://doi.org/10.1016/S0301-679X(03)00110-5.
[102] S.C. Sharma, R. Sinhasan, S.C. Jain, N. Singh, S.K. Singh, Performance of hydrostatic/hybrid journal bearings with unconventional recess geometries, Tribol. Trans. 41 (1998) 375–381, https://doi.org/10.1080/10402009808983761.
[103] M.B. Yu, X.D. Yu, X.H. Zheng, H. Qu, T.F. Yuan, D.G. Li, Influence of recess shape on comprehensive lubrication performance of high speed and heavy load hydrostatic thrust bearing, Ind. Lubr. Tribol. 71 (2019) 301–308, https://doi.org/10.1108/ILT-05-2018-0204.
[104] M. Dzodzo, M.J. Braun, R.C. Hendricks, Pressure and flow characteristics in a shallow hydrostatic pocket with rounded pocket/land joints, Tribol. Int. 29 (1996) 69–76, https://doi.org/10.1016/0301-679X(95)00036-4.
[105] M. Fillon, M. Wodtke, M. Wasilczuk, Effect of presence of lifting pocket on the THD performance of a large tilting-pad thrust bearing, Friction. 3 (2015) 266–274, https://doi.org/10.1007/s40544-015-0092-4.
[106] M. Wasilczuk, M. Wodtke, L. Dabrowski, Field tests on hydrodynamic and hybrid operation of a bidirectional thrust bearing of a pump-turbine, Lubricants. 5 (2017), https://doi.org/10.3390/lubricants5040048.
[107] F. Canbulut, C. Sinanoğlu, E. Koç, Experimental analysis of frictional power loss of hydrostatic slipper bearings, Ind. Lubr. Tribol. 61 (2009) 123–131, https://doi.org/10.1108/00368790910953631.
[108] O.J. Bakker, R.A.J. van Ostayen, Recess depth optimization for rotating, annular, and circular recess hydrostatic thrust bearings, J. Tribol. 132 (2010) 1–7, https://doi.org/10.1115/1.4000545.
[109] F.E. Horvat, M.J. Braun, Comparative experimental and numerical analysis of flow and pressure fields inside deep and shallow pockets for a hydrostatic bearing, Tribol. Trans. 54 (2011) 548–567. https://doi.org/10.1080/10402004.2011.575535.
[111] Z. Tian, M. Zhao, Y. Huang, Static properties of hydrostatic thrust bearing considering couple stress, DEStech Trans. Eng. Technol. Res. (2017) 29–33.
[112] X. Yu, D. Liu, X. Meng, X. Fu, Z. Wang, Q. Zhou, B. Wu, Y. Zhang, B. Qin, X. Dong, Numerical Simulation of the Effects of Recess Depth on Dynamic Effect of Hydrostatic Thrust Bearing, 31 (2013) 1–5. https://doi.org/10.14257/astl.2013.31.01.
[113] J.P. Shao, G.D. Liu, X.D. Yu, Y.Q. Zhang, X.L. Meng, H. Jiang, Effect of recess depth on lubrication performance of annular recess hydrostatic thrust bearing by constant rate flow, Ind. Lubr. Tribol. 70 (2018) 68–75, https://doi.org/10.1108/ILT-03-2017-0066.
[114] M. Helene, M. Arghir, J. Frene, Numerical study of the pressure pattern in a two-dimensional hybrid journal bearing recess, laminar, and turbulent flow results, J. Tribol. 125 (2003) 283–290, https://doi.org/10.1115/1.1537233.
[115] X. Xu, J. Shao, X. Yang, Y. Zang, X. Yu, B. Gao, Simulation on multi-oil-cavity and multi-oil-pad hydrostatic bearings, Appl. Mech. Mater. 274 (2013) 274–277, https://doi.org/10.4028/www.scientific.net/AMM.274.274.
[116] J. Peng Shao, G. dong Liu, X. Yu, Simulation and experiment on pressure field characteristics of hydrostatic hydrodynamic hybrid thrust bearings, Ind. Lubr. Tribol. 71 (2019) 102–108. https://doi.org/10.1108/ILT-02-2018-0063.
[117] S. Wang, X. Du, D. Li, Q. Hu, Characteristic study on temperature field of hydrostatic bearing of hydroforming machine, Adv. Mater. Res. 605–607 (2013) 630–635, https://doi.org/10.4028/www.scientific.net/AMR.605-607.630.
[118] M. Weck, Werkzeugmaschinen 2 - Konstruktion und Berechnung, Springer, Berlin Heidelberg, Berlin, Heidelberg (2006), https://doi.org/10.1007/978-3-540-30438-8.
[119] J.P. Shao, Y.Q. Zhang, Y.H. Li, X.D. Yu, H. Jiang, Influence of load capcaity on hydrostatic journal support deformation in finite element calculation, J. Cent. South Univ. Technol. 15 (2008) 245–249, https://doi.org/10.1007/s11771−008−0465−1.
[120] T. Liu, W. Gao, Y. Tian, K. Mao, G. Pan, D. Zhang, Thermal simulation modeling of a hydrostatic machine feed platform, Int. J. Adv. Manuf. Technol. 79 (2015) 1581–1595, https://doi.org/10.1007/s00170-015-6881-0.
[121] Y.Q. Zhang, L.G. Fan, Y. Chen, R. Li, T.Z. Wu, X.D. Yu, Deformation analysis of hydrostatic thrust bearing under different load, Appl. Mech. Mater. 494–495 (2014) 583–586, https://doi.org/10.4028/www.scientific.net/AMM.494-495.583.
[122] P. Pajaczkowski, A. Schubert, M. Wasilczuk, M. Wodtke, Simulation of large thrust-bearing performance at transient states, warm and cold start-up, Proc. Inst. Mech. Eng. Part J J. Eng. Tribol. 228 (2014) 96–103. https://doi.org/10.1177/1350650113500483.
[123] X.D. Yu, Y. Wang, D.F. Zhou, G.P. Wu, W.K. Zhou, H.W. Bi, Heat Transfer Characteristics of High Speed and Heavy Load Hydrostatic Bearing, Ieee Access. 7 (2019) 110770–110780, https://doi.org/10.1109/ACCESS.2019.2933471.
[124] M.B. Yu, X.D. Yu, X.H. Zheng, H. Jiang, Thermal-fluid-solid coupling deformation of hydrostatic thrust bearing friction pairs, Ind. Lubr. Tribol. 71 (2019) 467–473, https://doi.org/10.1108/ILT-07-2018-0262.
[125] Y.Q. Zhang, Z. Quan, M. Shi, H.D. Feng, Y.L. Liu, Improvement of hydrostatic bearing workbench structure based on the thermal deformation, 10th Int, Conf. Comput. Sci. Educ. ICCSE 2015 (2015) 528–531, https://doi.org/10.1109/ICCSE.2015.7250303.
[126] X.B. Li, W.X. Li, X.Y. Chen, M. Li, H.Y. Chen, X. Yue, Design and performance analysis on heat pipe hydrostatic thrust bearings based on rectangular oil pad, Ind. Lubr. Tribol. 70 (2018) 1251–1257, https://doi.org/10.1108/ILT-10-2017-0303.
[127] H. Schwenke, W. Knapp, H. Haitjema, A. Weckenmann, R. Schmitt, F. Delbressine, Geometric error measurement and compensation of machines-An update, CIRP Ann. - Manuf. Technol. 57 (2008) 660–675, https://doi.org/10.1016/j.cirp.2008.09.008.
[128] W. Huang, Z. Kong, Simulation and integration of geometric and rigid body kinematics errors for assembly variation analysis, J. Manuf. Syst. 27 (2008) 36–44, https://doi.org/10.1016/j.jmsy.2008.06.004.
[129] Z. Wang, W. Zhao, Y. Chen, B. Lu, Prediction of the effect of speed on motion errors in hydrostatic guideways, Int. J. Mach. Tools Manuf. 64 (2013) 78–84, https://doi.org/10.1016/j.ijmachtools.2012.07.011.
[130] P. Zhang, Y. Chen, C. Zhang, J. Zha, T. Wang, Influence of geometric errors of guide rails and table on motion errors of hydrostatic guideways under quasi-static condition, Int. J. Mach. Tools Manuf. 125 (2018) 55–67, https://doi.org/10.1016/j.ijmachtools.2017.10.006.
[131] E. Qi, Z. Fang, T. Sun, J. Chen, C. Liu, J. Wang, A method for predicting hydrostatic guide error averaging effects based on three-dimensional profile error, Tribol. Int. 95 (2016) 279–289, https://doi.org/10.1016/j.triboint.2015.11.032.
[132] J. Zha, Y. Chen, Z. Wang, A tolerance design method for hydrostatic guideways motion accuracy based on error averaging effect, Procedia CIRP. 75 (2018) 196–201, https://doi.org/10.1016/j.procir.2018.04.054.
[133] P.H. Zhang, Y.L. Chen, X.T. Liu, Relationship between roundness errors of shaft and radial error motions of hydrostatic journal bearings under quasi-static condition, Precis. Eng. Int. Soc. Precis. Eng. Nanotechnol. 51 (2018) 564–576, https://doi.org/10.1016/j.precisioneng.2017.10.012.
[134] A.K. Rajput, S.C. Sharma, Combined influence of geometric imperfections and misalignment of journal on the performance of four pocket hybrid journal bearing, Tribol. Int. 97 (2016) 59–70, https://doi.org/10.1016/j.triboint.2015.12.049.
[135] P.H. Zhang, Y.L. Chen, J. Zha, Relationship between geometric errors of thrust plates and error motions of hydrostatic thrust bearings under quasi-static condition, Precis. Eng. Int. Soc. Precis. Eng. Nanotechnol. 50 (2017) 119–131, https://doi.org/10.1016/j.precisioneng.2017.04.020.
[136] H. Cui, Y. Wang, X. Yue, M. Huang, W. Wang, Effects of manufacturing errors on the static characteristics of aerostatic journal bearings with porous restrictor, Tribol. Int. 115 (2017) 246–260, https://doi.org/10.1016/j.triboint.2017.05.008.
[137] N.D. Manring, R.E. Johnson, H.P. Cherukuri, The Impact of Linear Deformations on Stationary Hydrostatic Thrust Bearings, J. Tribol. 124 (2002) 874–877, https://doi.org/10.1115/1.1482118.
[138] L. Zoupas, M. Wodtke, C.I. Papadopoulos, M. Wasilczuk, Effect of manufacturing errors of the pad sliding surface on the performance of the hydrodynamic thrust bearing, Tribol. Int. 134 (2019) 211–220, https://doi.org/10.1016/j.triboint.2019.01.046.
[139] J.R. Lin, Surface roughness effect on the dynamic stiffness and damping characteristics of compensated hydrostatic thrust bearings, Int. J. Mach. Tools Manuf. 40 (2000) 1671–1689, https://doi.org/10.1016/S0890-6955(00)00012-2.
[140] S. Zhu, J. Sun, B. Li, G. Zhu, Thermal turbulent lubrication analysis of rough surface journal bearing with journal misalignment, Tribol. Int. 144 (2020), https://doi.org/10.1016/j.triboint.2019.106109 106109.
[141] Y. Wang, Y. Zhao, L. Cai, Z. Liu, Q. Cheng, Effects of thermal and hydrodynamic characteristics of heavy-duty rotary table on the hydrostatic circular pads, J. Vibroengineering. 18 (2016) 4193–4206. https://doi.org/10.21595/jve.2016.17079.
[142] P. Sapirstein, Accurate measurement with photogrammetry at large sites, J. Archaeol. Sci. 66 (2016) 137–145, https://doi.org/10.1016/j.jas.2016.01.002.
[143] A. Van Beek, A. Segal, Rubber supported hydrostatic thrust bearings with rigid bearing surfaces, Tribol. Int. 30 (1997) 47–52, https://doi.org/10.1016/0301-679X(96)00021-7.
[144] A. Van Beck, L. Lepic, Rubber supported hydrostatic thrust bearings with elastic bearing surfaces of infinite length, 201 (1996) 45–50.

[145] Y.C. Shiau, M.T. Wang, C.M. Huang, J.Y. Zeng, Discussion of pot bearing for concrete bridge, ISARC 2008 - Proc. from 25th Int. Symp. Autom. Robot. Constr. (2008) 213–223. https://doi.org/10.3846/isarc.20080626.213.
[146] A. Niemierko, Modern Bridge Bearings and Expansion Joints for Road Bridges, Transp. Res. Procedia. 14 (2016) 4040–4049, https://doi.org/10.1016/j.trpro.2016.05.501.
[147] K. Ahmed, S.S. Nizami, N.Z. Raza, K. Mahmood, Mechanical, swelling, and thermal aging properties of marble sludge-natural rubber composites, Int. J. Ind. Chem. 3 (2012) 1–12, https://doi.org/10.1186/2228-5547-3-21.
[148] T. Susanto, R. Affandy, G. Katon, Rahmaniar, Thermal aging properties of natural rubber-styrene butadiene rubber composites filled with modified starch from Dioscorea Hispida Denst extract prepared by latex compounding method, AIP Conf. Proc. 2049 (2018), https://doi.org/10.1063/1.5082421.
[149] B. Moon, J. Lee, S. Park, C.S. Seok, Study on the aging behavior of natural rubber/butadiene rubber (NR/BR) blends using a parallel spring model, Polymers (Basel). 10 (2018), https://doi.org/10.3390/polym10060658.
[150] M. Ben Hassine, M. Naït-Abdelaziz, F. Zaïri, X. Colin, C. Tourcher, G. Marque, Time to failure prediction in rubber components subjected to thermal ageing: A combined approach based upon the intrinsic defect concept and the fracture mechanics, Mech. Mater. 79 (2014) 15–24, https://doi.org/10.1016/j.mechmat.2014.07.015.
[151] N.D.S.A. Santos, V.R. Roso, M.T.C. Faria, Review of engine journal bearing tribology in start-stop applications, Eng. Fail. Anal. 108 (2020), https://doi.org/10.1016/j.engfailanal.2019.104344 104344.
[152] J. Alcántara, D. de la Fuente, B. Chico, J. Simancas, I. Díaz, M. Morcillo, Marine atmospheric corrosion of carbon steel: A review, Materials (Basel). 10 (2017), https://doi.org/10.3390/ma10040406.
[153] F. Summer, F. Grün, E.R. Ravenhill, Friction and wear performance of various polymer coatings for journal bearings under stop start sliding, Lubricants. 8 (2020), https://doi.org/10.3390/lubricants8010001.
[154] A. Matthews, S. Franklin, K. Holmberg, Tribological coatings: Contact mechanisms and selection, J. Phys. D. Appl. Phys. 40 (2007) 5463–5475, https://doi.org/10.1088/0022-3727/40/18/S07.
[155] A. Vencl, L. Ivanović, B. Stojanović, E. Zadorozhnaya, S. Miladinović, P. Svoboda, Surface texturing for tribological applications: a review, Proc. Eng. Sci. 1 (2019) 227–239. https://doi.org/10.24874/PES01.01.029.
[156] S.C. Sharma, S.K. Yadav, Performance analysis of a fully textured hybrid circular thrust pad bearing system operating with non-Newtonian lubricant, Tribol. Int. 77 (2014) 50–64, https://doi.org/10.1016/j.triboint.2014.04.013.
[157] S.K. Yadav, S.C. Sharma, Performance of Hydrostatic Textured Thrust Bearing with Supply Holes Operating with Non-Newtonian Lubricant, Tribol. Trans. 59 (2016) 408–420, https://doi.org/10.1080/10402004.2015.1083065.
[158] M. Michalec, P. Svoboda, I. Krupka, M. Hartl, Tribological Behaviour of Smart Fluids Influenced by Magnetic and Electric Field – A Review, Tribol. Ind. 40 (2018) 515–528. https://doi.org/10.24874/ti.2018.40.04.01.
[159] J. Ji, Y. Fu, Q. Bi, Influence of geometric shapes on the hydrodynamic lubrication of a partially textured slider with micro-grooves, J. Tribol. 136 (2014), https://doi.org/10.1115/1.4027633.
[160] D. Gropper, T.J. Harvey, L. Wang, Numerical analysis and optimization of surface textures for a tilting pad thrust bearing, Tribol. Int. 124 (2018) 134–144, https://doi.org/10.1016/j.triboint.2018.03.034.
[161] I. Etsion, G. Halperin, A laser surface textured hydrostatic mechanical seal, Tribol. Trans. 45 (2002) 430–434, https://doi.org/10.1080/10402000208982570.
[162] V. Brizmer, Y. Kligerman, I. Etsion, A laser surface textured parallel thrust bearing, Tribol. Trans. 46 (2003) 397–403, https://doi.org/10.1080/10402000308982643.
[163] F.M. Meng, On influence of cavitation in lubricant upon tribological performances of textured surfaces, Opt. Laser Technol. 48 (2013) 422–431, https://doi.org/10.1016/j.optlastec.2012.10.020.
[164] F. Avellan, Introduction to cavitation in hydraulic machinery, 6th Int, Conf. Hydraul. Mach. Hydrodyn. (2004) 11–22.
[165] D. Gropper, L. Wang, T.J. Harvey, Hydrodynamic lubrication of textured surfaces: A review of modeling techniques and key findings, Tribol. Int. 94 (2016) 509–529, https://doi.org/10.1016/j.triboint.2015.10.009.
[166] Q. Li, Y. Wang, S. Zhang, W.W. Xu, Z. Wang, Z. Wang, Optimal design of parallel sliders with square-shaped textures considering fluid-structure interaction, Ind. Lubr. Tribol. 71 (2019) 620–627, https://doi.org/10.1108/ILT-09-2018-0366.
[167] Y. Zhang, G. Chen, L. Wang, Effects of thermal and elastic deformations on lubricating properties of the textured journal bearing, Adv. Mech. Eng. 11 (2019) 1–12, https://doi.org/10.1177/1687814019883790.
[168] C. Xu, S. Jiang, Analysis of the Static Characteristics of a Self-Compensation Hydrostatic Spherical Hinge, J. Tribol. 137 (2015) 1–5, https://doi.org/10.1115/1.4030712.
[169] W.U.R. Rehman, Y.X. Luo, Y.Q. Wang, G.Y. Jiang, N. Iqbal, S.U.R. Rehman, S. Bibi, Fuzzy logic-based intelligent control for hydrostatic journal bearing, Meas. Control. 52 (2019) 229–243, https://doi.org/10.1177/0020294019830110.
[170] W.J. Moore, A.G. Starr, An intelligent maintenance system for continuous cost-based prioritisation of maintenance activities, Comput. Ind. 57 (2006) 595–606, https://doi.org/10.1016/j.compind.2006.02.008.
[171] D.W. Childs, P. Esser, Measurements Versus Predictions for a Hybrid (Hydrostatic Plus Hydrodynamic) Thrust Bearing for a Range of Orifice Diameters, J. Eng. Gas Turbines Power-Transactions Asme. 141 (2019), https://doi.org/10.1115/1.4042721.
[172] M.S. Shah, J.B. Joshi, A.S. Kalsi, C.S.R. Prasad, D.S. Shukla, Analysis of flow through an orifice meter: CFD simulation, Chem. Eng. Sci. 71 (2012) 300–309, https://doi.org/10.1016/j.ces.2011.11.022.
[173] D.C. Chen, M.F. Chen, C.H. Pan, J.Y. Pan, Study of membrane restrictors in hydrostatic bearing, Adv. Mech. Eng. 10 (2018) 1–8, https://doi.org/10.1177/1687814018799604.
[174] T.H. Lai, T.Y. Chang, Y.L. Yang, S.C. Lin, Parameters design of a membrane-type restrictor with single-pad hydrostatic bearing to achieve high static stiffness, Tribol. Int. 107 (2017) 206–212, https://doi.org/10.1016/j.triboint.2016.11.037.
[175] M. Gohara, K. Somaya, M. Miyatake, S. Yoshimoto, Static characteristics of a water-lubricated hydrostatic thrust bearing using a membrane restrictor, Tribol. Int. 75 (2014) 111–116, https://doi.org/10.1016/j.triboint.2014.03.016.
[176] H. Sawano, Y. Nakamura, H. Yoshioka, H. Shinno, High performance hydrostatic bearing using a variable inherent restrictor with a thin metal plate, Precis. Eng. Int. Soc. Precis. Eng. Nanotechnol. 41 (2015) 78–85, https://doi.org/10.1016/j.precisioneng.2015.02.001.
[177] W.U. Rehman, G. Jiang, Y. Luo, Y. Wang, W. Khan, S.U. Rehman, N. Iqbal, Control of active lubrication for hydrostatic journal bearing by monitoring bearing clearance, Adv. Mech. Eng. 10 (2018) 1–17, https://doi.org/10.1177/1687814018768142.
[178] W.U. Rehman, L. Yuanxin, J. Guiyun, W. Yongqin, X. Yun, M.N. Iqbal, M.A. Zaheer, I. Azhar, H. Elahi, Y. Xiaogao, Control of an oil film thickness in a hydrostatic journal bearing under different dynamic conditions, Proc. 29th Chinese Control Decis. Conf. CCDC 2017 (2017) 5072–5076, https://doi.org/10.1109/CCDC.2017.7979395.
[179] K.E. Rydberg, Hydraulic accumulators as key components in energy efficient mobile systems, Proc. 6th Int, Conf. Fluid Power Transm. Control. ICFP 2005 (2005,) 124–129.
[180] M. Xian-ting, Review of the present status of hydraulic accumulator, Appl. Mech. Mater. 246–247 (2013) 629–634, https://doi.org/10.4028/www.scientific.net/AMM.246-247.629.
[181] W. Latas, J. Stojek, A new type of hydrokinetic accumulator and its simulation in hydraulic lift with energy recovery system, Energy. 153 (2018) 836–848, https://doi.org/10.1016/j.energy.2018.04.040.
[182] D. Buhagiar, T. Sant, Modelling of a novel hydro-pneumatic accumulator for large-scale offshore energy storage applications, J. Energy Storage. 14 (2017) 283–294, https://doi.org/10.1016/j.est.2017.05.005.
[183] D. Zhao, W. Ge, X. Mo, B. Liu, D. Dong, Design of a new hydraulic accumulator for transient large flow compensation, Energies. 12 (2019), https://doi.org/10.3390/en12163104.
[184] M. Dai, S. Zhao, X. Yuan, The application study of accumulator used in hydraulic system of 20MN fast forging machine, Appl. Mech. Mater. 80–81 (2011) 870–874, https://doi.org/10.4028/www.scientific.net/AMM.80-81.870.
[185] S. Mamčic, M. Bogdevičius, Simulation of dynamic processes in hydraulic accumulators, Transport. 25 (2010), https://doi.org/10.3846/transport.2010.26.
[186] K. Kuze, H. Sawano, H. Yoshioka, H. Shinno, Hydrostatic bearing with high bulk modulus fluid, Key Eng. Mater. 523–524 (2012) 532–537, https://doi.org/10.4028/www.scientific.net/KEM.523-524.532.
[187] Y. Zhang, X. Yu, X. Yang, G. Sun, X. Yu, Z. Shi, Viscosity influence research on load capacity of heavy hydrostatic bearing, Key Eng. Mater. 450 (2011) 63–66, https://doi.org/10.4028/www.scientific.net/KEM.450.63.
[188] Y.W. Liu, S.C. Lin, C.H. Chang, P.S. Lan, Design and test of hydrostatic built-in spindle compensated by orifice restrictors, Proc. 2018 IEEE Int. Conf. Adv. Manuf. ICAM 2018. (2019) 302–305. https://doi.org/10.1109/AMCON.2018.8614907.
[189] Y.Q. Zhang, P.R. Kong, Y.A. Feng, L.L. Guo, Hot oil carrying characteristic about hydrostatic bearing oil film of heavy vertical lathe in high speed, Ind. Lubr. Tribol. 71 (2019) 126–132, https://doi.org/10.1108/ILT-03-2018-0091.
[190] E.F. Jordan, S. Smith, R.E. Koos, W.E. Parker, B. Artymyshyn, A.N. Wrigley, Viscosity index. I. Evaluation of selected copolymers incorporating n-octadecyl acrylate as viscosity index improvers, J. Appl. Polym. Sci. 22 (1978) 1509–1528, https://doi.org/10.1002/app.1978.070220606.
[191] S. Verdier, J.A.P. Coutinho, A.M.S. Silva, O.F. Alkilde, J.A. Hansen, A critical approach to viscosity index, Fuel. 88 (2009) 2199–2206, https://doi.org/10.1016/j.fuel.2009.05.016.
[192] P.D. Srivyas, M.S. Charoo, Effect of lubricants additive: Use and benefit, Mater. Today Proc. 18 (2019) 4773–4781, https://doi.org/10.1016/j.matpr.2019.07.465.
[193] R.W. Wilson, S.B. Lyon, Corrosion in lubricants/fuels, in, Shreir's Corros., Elsevier (2010) 1299–1307, https://doi.org/10.1016/B978-044452787-5.00059-7.
[194] X. Bai, H. Xiao, L. Zhang, The condition monitoring of large slewing bearing based on oil analysis method, Key Eng. Mater. 474–476 (2011) 716–719, https://doi.org/10.4028/www.scientific.net/KEM.474-476.716.
[195] A. Yui, G. Okahata, S. Okuyama, H. Kobayashi, A.H. Slocum, Development of a linear-motor-driven table supported by hydrostatic water bearings: Effect of air volume contained in water-supply tube on pitching motion of table slider, Key Eng. Mater., Trans Tech Publications Ltd (2010) 508–512, https://doi.org/10.4028/www.scientific.net/KEM.447-448.508.
[196] A.H. Slocum, P.A. Scagnetti, N.R. Kane, C. Brunner, Design of self-compensated, water-hydrostatic bearings, Precis. Eng. 17 (1995) 173–185, https://doi.org/10.1016/0141-6359(94)00015-R.

[197] T. Okabe, S. Sasaki, Y. Kondo, M. Miyatake, S. Yoshimoto, Hydrostatic ionic liquid-lubricated fluid film bearing for a rotational electron-beam lithography system, Precis. Eng. 61 (2020) 194–203. https://doi.org/10.1016/j.precisioneng.2019.10.008.
[198] Y. Huang, Z. Tian, A new derivation to study the steady performance of hydrostatic thrust bearing: Rabinowitch fluid model, J. Nonnewton. Fluid Mech. 246 (2017) 31–35, https://doi.org/10.1016/j.jnnfm.2017.04.012.
[199] U.P. Singh, R.S. Gupta, V.K. Kapur, On the steady performance of hydrostatic thrust bearing: Rabinowitsch fluid model, Tribol. Trans. 54 (2011) 723–729, https://doi.org/10.1080/10402004.2011.597541.
[200] S.G.E. Lampaert, R.A.J. van Ostayen, Load and stiffness of a hydrostatic bearing lubricated with a Bingham plastic fluid, J. Intell. Mater. Syst. Struct. (2019), https://doi.org/10.1177/1045389X19873426.
[201] S.G.E. Lampaert, F. Quinci, R.A.J. van Ostayen, Rheological texture in a journal bearing with magnetorheological fluids, J. Magn. Magn. Mater. 499 (2020), https://doi.org/10.1016/j.jmmm.2019.166218 166218.
[202] H. Urreta, G. Aguirre, P. Kuzhir, L.N. Lopez De Lacalle, Seals Based on Magnetic Fluids for High Precision Spindles of Machine Tools, Int. J. Precis. Eng. Manuf. 19 (2018) 495, https://doi.org/10.1007/s12541-018-0060-9.
[203] J. Hesselbach, C. Abel-Keilhack, Active hydrostatic bearing with magnetorheological fluid, J. Appl. Phys. 93 (2003) 8441–8443, https://doi.org/10.1063/1.1555850.
[204] C.B. Khatri, S.C. Sharma, Analysis of textured multi-lobe non-recessed hybrid journal bearings with various restrictors, Int. J. Mech. Sci. 145 (2018) 258–286, https://doi.org/10.1016/j.ijmecsci.2018.07.014.
[205] W.L. Song, C.H. Lee, S.B. Choi, Sliding wear behavior of magnetorheological fluid for brass with and without magnetic field, Trans. Nonferrous Met. Soc. China (English Ed. 23 (2013) 400–405, https://doi.org/10.1016/S1003-6326(13)62476-0.
[206] H.W. Sun, S.C. Yang, Revolved Surface Finishing with Smart Fluid Abrasives, Key Eng. Mater. 304–305 (2006) 579–583, https://doi.org/10.4028/www.scientific.net/KEM.304-305.579.
[207] H. Urreta, G. Aguirre, P. Kuzhir, L.N. Lopez de Lacalle, Actively lubricated hybrid journal bearings based on magnetic fluids for high-precision spindles of machine tools, J. Intell. Mater. Syst. Struct. 30 (2019) 2257–2271, https://doi.org/10.1177/1045389X19862358.
[208] Q. Qi, F. Tao, Y. Zuo, D. Zhao, Digital Twin Service towards Smart Manufacturing, Procedia CIRP. 72 (2018) 237–242, https://doi.org/10.1016/j.procir.2018.03.103.
[209] V. Alcácer, V. Cruz-Machado, Scanning the Industry 4.0: A Literature Review on Technologies for Manufacturing Systems, Eng. Sci. Technol. an Int. J. 22 (2019) 899–919, https://doi.org/10.1016/j.jestch.2019.01.006.

Later in 2021, Breńkacz et al. [3] published a review article focused on different controllable journal bearings, including comparisons and possible future development in the field of controllable bearings. Bouyer et al. [4] experimentally investigated the effect of HS lubrication in HD bearings. It is evident that the HS regime helps during the start and stop phases to eliminate wear and reduce friction. Moreover, the externally supplied lubricant significantly reduced the temperature rise in the lubricating film area. Nonetheless, the hybrid regime (HS + HD) has greater energetic demands, and it is not suitable for operation at very high speeds.

Majority of the published available research, which focused on HSB was devoted to numerical modelling of the bearing performance. Shang et al. [5] proposed a CFD-based model considering viscosity-temperature dependence and validated it using experimental data to improve the precision of an internal grinding machine HS spindle. The results show a good agreement with the experimental data, when compared to a conventional model. CFD was further implemented by Liu et al. [6] for investigation of HSB performance with microgroove surface. As seen in Figure 2, the microgroove depth might change the heat generation within the lubricating film, eventually to lead to a lower heat generation in high depths compared with smooth surfaces. Moreover, a larger groove spacing can further decrease the heat generation rate.

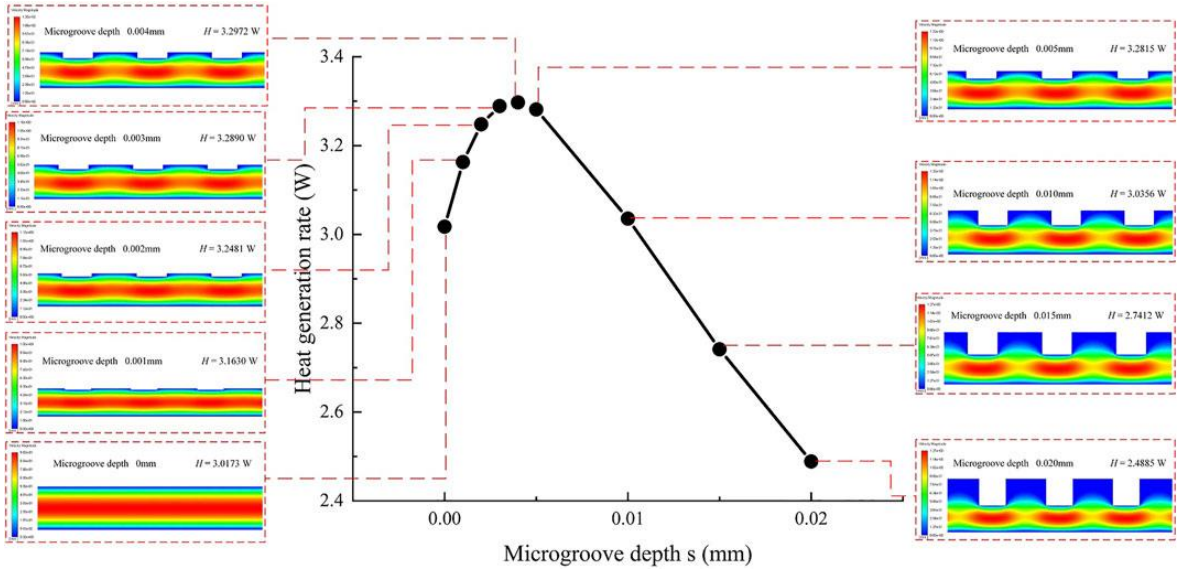

Figure 2 Heat generation for different microgroove depths [6].

Li et al. [7] investigated the influence of supporting grooves in aerostatic bearings. The results show good agreement of the CFD model and experimental data. The supporting grooves improve bearing stability and increase load carrying capacity (Figure 3). Nonetheless, the CFD boundary conditions for inlet were set to constant pressure supply, thus even though a greater load capacity was observed, it required higher supplied flow.

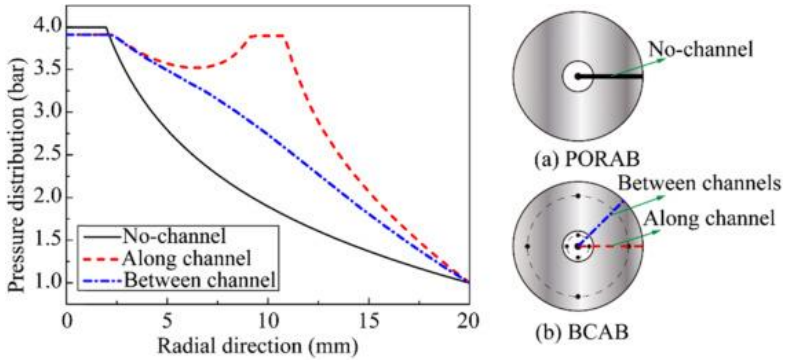

Figure 3 Pressure distribution comparison of a) flat pad and b) pad with supporting channels [7].

HSB fluid domains were usually modelled using Finite Difference Methods (FDM), which require structured meshes [8–10]. Wang et al. [11] used Finite Volume Method (FVM) with unstructured mesh to analyse the performance of HSB pocket with orifice using k-ε turbulence model. The unstructured mesh allowed for higher agreement for experimental data compared with analytical formulae.

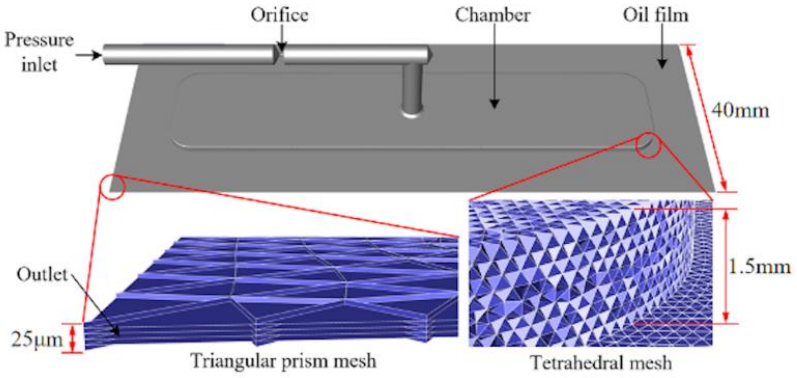

Figure 4 Computational domain of the CFD analysis with details on unstructured mesh regions [11].

Another numerical modelling technique, which has been frequently combined with the CFD approach is Fluid-Structure Interaction (FSI). This method has a great importance when it comes to evaluation of bearing precision considering structural deformations and thermal effects. Liu et al. [12] investigated solid body deformation of an aerostatic bearing, concluding that the deformation can be as high as 53 % of the film thickness depending on the supplied flow and film thickness, what can lead to an undesirable decrease of the bearing precision.

3 ANALYSIS AND CONCLUSION OF LITERATURE REVIEW

HS lubricating film is created between sliding surfaces by an external hydraulic supply. It secures complete separation of the conformal surfaces, resulting in very low friction, almost no wear, very high precision without occurrence of stick-slip effect, high stiffness and vibration damping ability. The use of fluid bearings might lead to higher energy efficiency compared to rolling or sliding bearings with direct contact [13], even though HS lubrication requires continuous external supply of pressurized lubricant. HS lubrication is a unique type of lubrication regime that is suitable for a wide range of applications – from millimetres up to tens of metres [2] – for small high precision bearings, through medium-sized machining centres, or even for moving large structures, such as giant telescopes, radio antennas, or large-scale machining centres. In the case of large-scale applications, the slider and pad bodies are not possible to be manufactured in one piece, because of manufacturing space, transportation, and assembly. The performance, precision and safety of large-scale HSB can be heavily influenced by assembly precision, which has not yet been specified in the available literature. Moreover, HSB require pressurized oil supply for proper function, therefore the energetic demands for operation are higher than other types of bearings, thus energy consumption should be minimized as much as possible. A comprehensive methodology on HSB design and optimisation was published by Bassani & Piccigallo [14]. This book provides a strong foundation for HSB design engineers. Nonetheless, some of the challenges and issues that are linked with large-scale machines and structures show new challenges and issues, especially regarding assembly precision and the use of computational software for bearing geometry optimization, which has been remarkably improved over the last few years.

3.1 Bearing safety

Geometric errors negatively influence the lubricating layer of sliding bearings, whose performance is decreasing with the magnitude of surface irregularities [15]. Misalignment in hydrodynamic (HD) bearings is strongly influencing the lubricating film. HS bearings are often combined with HD bearings to reduce wear during start and stop phase [16], and compensate misalignment and are frequently mounted on tilting support of the pad [17]. HS lubrication regime increases the film thickness and improves lubricant circulation and cooling [18], thus improving its performance. This is one of the main reasons why HS lubrication is used for bearings of high-precision machines. Nonetheless, HS bearings have also certain limits to compensate the geometric errors. The energetic demands needed to compensate the geometric precision of the solid bodies surrounding the lubricating film [19] are rising with the error magnitude. An unconventional way of error compensation, by using

compliant members was employed for slider surface [20] and pad support [21]. The previous research was aimed at the pad misalignment compensation modelling using compliant support numerically [22]. Numerical modelling was also used for geometric error investigation. Model for motion error analysis of closed guideways lubricated by HS regime, based on kinetic equilibrium of the table with squeeze film effect consideration was proposed by Wang et al. [23], who found out that with increasing speed the error is more significant, but can be compensated with higher lubricant supply. Rajput and Sharma [24] investigated different geometric imperfections of defined shapes and misalignment of journal bearing lubricated with HS regime using FEM formulation. All imperfections caused observably lower minimal film thickness, while the minimal film thickness was as twice as much lower in all cases with journal misalignment. As later observed by Zoupas et al. [25] using CFD analysis, different manufacturing error types (convex, concave, sine wave) have similar effects on the HD thrust bearings, as it was in the case of journal bearings. A new design of adjustable HS bearing with improved precision was proposed by Fedorynenko et al. [26]. Zhang et al. [27] presented a model based on formulations describing the relationship between geometric errors and motion errors in bearings lubricated with HS regime with an experimental validation. Zha et al. [28] later proposed tolerance design method for HS guideways based on error averaging effect, considering geometric parameters of guide rails with experimental validation.

KNOWLEDGE GAP:

The previous published available research provided insight into manufacturing error modelling and the use of compliant members. Nonetheless, an experimentally validated approach for investigation of compliant support applicability, and estimation of allowable assembly errors is missing.

3.2 Bearing efficiency

Unlike in case of small HSB, the power economy becomes a serious issue. The power consumption of HSB increases with the size. Therefore, it is crucial to optimize the bearing performance to reduce the operational costs. The calculation of a HSB performance and characteristics can be derived from N-S equations considering simplifications that lead to Reynolds equation for pressure distribution calculation. Based on the derived equations, analytical solutions for simple geometries, such as single recess rectangular or circular pad, were derived. In case of more complicated pad geometries, such as multi-recess pads, it is merely impossible, or extremely difficult to obtain analytical formulation. Therefore, experimental approach was used to obtain performance factors for a variety of pad proportions [29,30] based on electric analogy. This classical simplistic, yet effective approach has been used for decades to determine the pad geometry [31]. Nonetheless, with the advances in computational fluid dynamics, numerical modelling approach allowed to

improve the design process of any bearing shape, while allowing to investigate flow characteristics and parameters that are difficult or even impossible to be measured experimentally. This approach has been increasingly applied on HS lubrication modelling [1]. It was successfully used for comparison of recess shapes by Yadav and Sharma [32] using FEM formulations. Helene et al. [8] used full Navier-Stokes equations in 2D geometry with structured mesh, including modelling turbulence effects to determine an optimal recess depth of HS journal bearings. 3D geometries are harder to be discretized into a structured mesh, therefore, an analysis of unstructured mesh for HS bearing performance was conducted by Wang et al. [11]. The presented results show that the CFD approach results are far closer to the experimental results than the analytical formulae.

KNOWLEDGE GAP:

As shown in the provided state-of-the-art summary, many works aimed at numerical investigation of various recess shapes [33–37], but none of the available published research focused on assessing HSB performance by varying recess size and position of multi-recess HSB pad independently.

4 AIMS OF THE THESIS

The main aim of this PhD thesis is to introduce performance and safety improvements to the large-scale hydrostatic bearing design methodology. The thesis is focused on experimental and numerical analysis of hydrostatic bearing performance for different pad geometries and under bearing misalignment conditions. To achieve the main goal of this thesis, the necessary sub-aims are as follows:

- development and design of the experimental device,
- design of the methodology of experiments,
- design of data processing and evaluating,
- development of the methodology for pad shape optimization,
- series of experiments focused on the analysis of the bearing performance for the investigated cases and conditions,
- data analysis,
- discussion and publication of obtained results.

4.1 Scientific questions & Hypotheses

Q1: *What is the influence of HSB recess position and size on the bearing performance?*

- **H1:** Recess size and layout optimization are usually done according to one parameter classical approach, in which the geometric parameters are linked together [14,29,38,39]. Separating the two parameters, size and layout, can lead to improved pad performance and lower energetic losses.

Q2: *How is the HS lubricating film affected by assembly errors of the bearing bodies?*

- **H2:** Pad misalignment can significantly affect the generation and uniformity of the HS lubricating film [15,24,40]. The lubricating film is able to compensate certain magnitude of pad misalignment. The bearing performance during eccentric loading can be improved using a compliant member [41]. But the compliant support is also able to compensate larger misalignment compared to rigid support.
- **H3:** Manufacturing errors were studied due to their influence on the bearing precision [5,42,43]. Assembly errors were not studied, even though HS bearings have a great potential in large-scale applications. Assembly errors of a segmented slider can lead to HS lubricating film non-uniformity and disruption. The maximal allowed error of the segmented sliders must be smaller than the film thickness to secure safe operation of the bearing.

4.2 Thesis layout

The PhD thesis is composed of three original research papers published in peer-reviewed journals with impact factor. The content of the thesis is reflecting the scientific questions from chapter 4.1. As shown in Figure 5, two main parts of the conducted research were determined: bearing efficiency and bearing safety, respectively. The two parts are further described in publications [I-III] in detail.

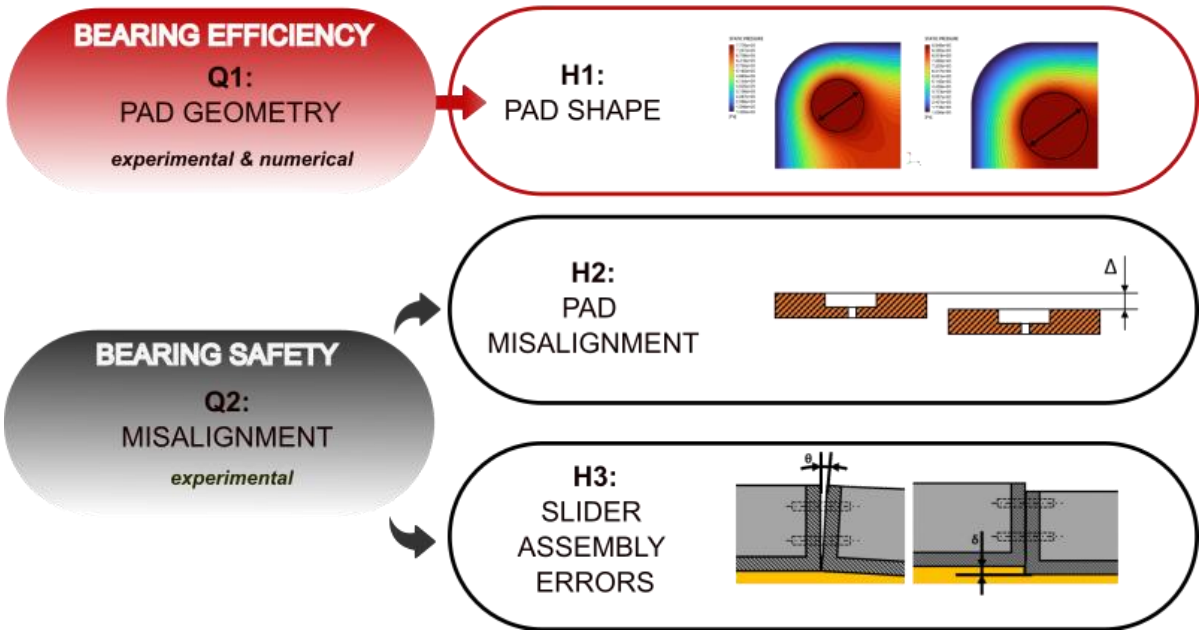

Figure 5 Thesis activities layout into bearing efficiency and bearing safety subcategories.

Bearing efficiency is linked with pad shape and the focus is aimed at pad geometry optimization, to reduce the power losses and thus energy consumption of the hydraulic pump. The first article [I] is focused on introducing a new two-parameter pad geometry optimization method based on CFD simulation. The second part is dealing with **bearing safety**, specifically pad and slider misalignment effect on the bearing performance. The second article [II] is focused on investigation of pad misalignment effect on the bearing performance, and the effects of compliant support on misalignment compensation. The last article [III] is focused on assessing assembly errors of segmented sliders in stationary and low-speed conditions.

I. MICHALEC, M., M. ONDRA, M. SVOBODA, J. CHMELÍK, P. ZEMAN, P. SVOBODA, R. L. JACKSON. A novel geometry optimization approach for multi-recess hydrostatic bearing pad operating in static and low-speed conditions using CFD simulation. *Tribology letters*, 2023, vol. 71, no. 2, p. 52. doi:10.1007/s11249-023-01726-3 [IF = 3.2]
(Author's contribution 65 %)

II. MICHALEC, M., V. POLNICKÝ, J. FOLTÝN, P. SVOBODA, P. ŠPERKA, J. HURNÍK. 2022. The prediction of large-scale hydrostatic bearing pad misalignment error and its compensation using compliant support. *Precision engineering*, 2022, vol. 75, pp.67-79. doi:10.1016/j.precisioneng.2022.01.011 [IF = 3.6]
(Author's contribution 40 %)

III. MICHALEC, M., J. FOLTÝN, T. DRYML, L. SNOPEK, D. JAVORSKÝ, M. ČUPR, P. SVOBODA. Assembly error tolerance estimation for large-scale hydrostatic bearing segmented sliders under static and low-speed conditions. *Machines*. MDPI, 2023, vol. 11, p.14. doi:10.3390/machines11111025 [IF = 2.6]
(Author's contribution 54 %)

5 MATERIALS AND METHODS

The performed literature review led to outlining the knowledge gap in the area of large-scale HSB. Based on the knowledge gap, scientific questions and hypotheses were formed. To investigate the scientific questions and hypotheses outlined in the previous chapters, experimental and numerical methods are employed in the presented study. The experimental and CFD simulation results were compared with analytical calculations to determine the precision of the measured and computed values, respectively. A schematical representation of the performed activities are shown in Figure 6. The employed experimental and numerical methods, methodology and experiment design are described in the following chapters in detail.

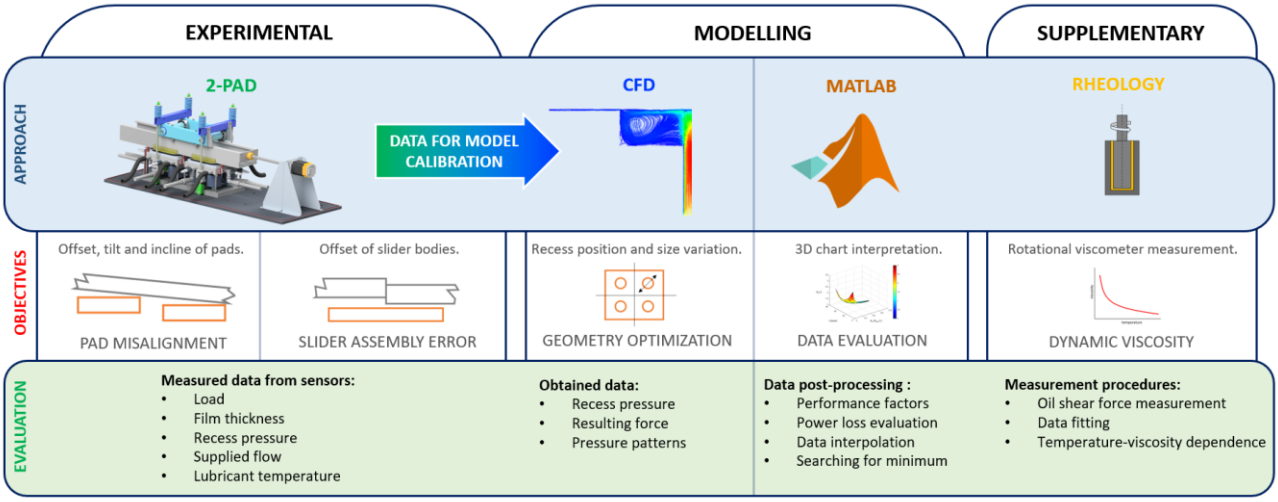

Figure 6 Schematical representation of the performed activities within the thesis.

5.1 Experimental devices

The experimental investigation was carried out on Dual-Pad Experimental HSB (2-PAD). To obtain inputs for the analytical calculation and CFD simulations, lubricant dynamic viscosity was measured using rotational viscometer.

5.1.1 Experimental hydrostatic bearing

The 2-PAD experimental device was designed at Institute of Machine and Industrial Design and introduced into function in 2020. 2-PAD consists of a loading frame that generates load on the slider, two HS pads mounted on pad supports with inlet channels. The slider can perform reciprocating motion driven by the electromotor.

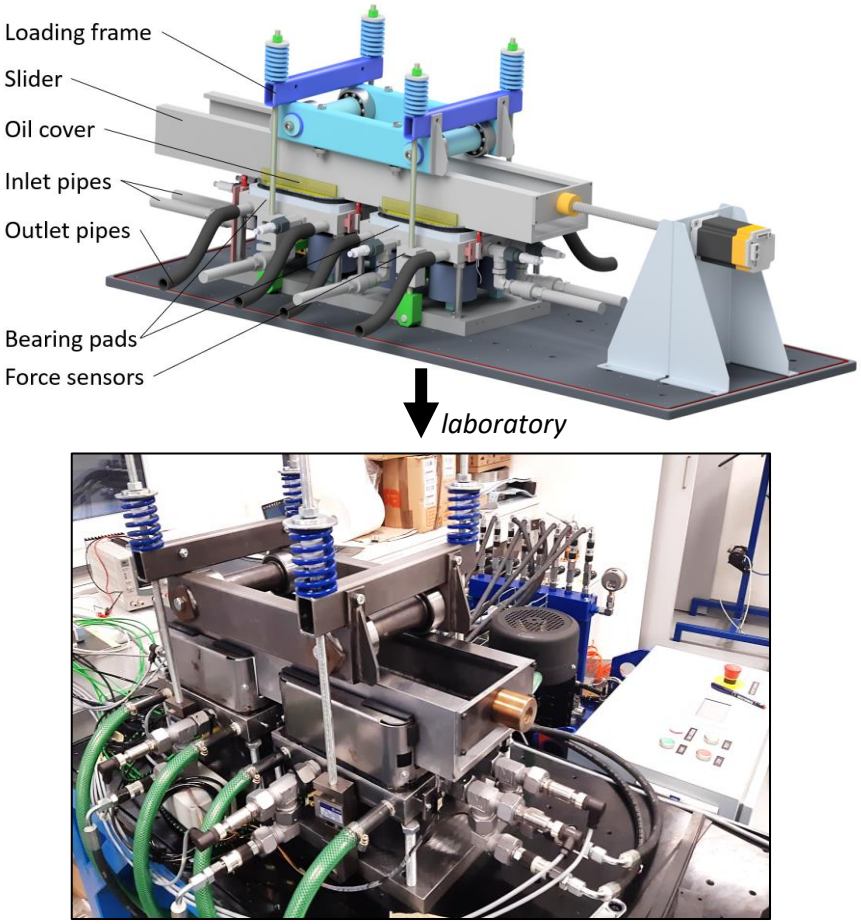

Figure 7 2-PAD experimental setup overview and laboratory view.

2-PAD was equipped with a variety of sensors (Figure 8) that allowed performing full online diagnostics of the bearing performance via controlling software build in the LabView environment. Proximity sensors mounted on pad supports provided direct measurement of the film thickness. Initially used contact proximity sensors with range of 3 mm and resolution of 0.02 mm were replaced with contactless sensors of 0.01 resolution and higher reliability. Four force sensors of range 10 kN and 2.5 N resolution allowed direct measurement of the applied load generated using threaded rods and compression springs. Temperature information from temperature sensors built in the recess were used to evaluate actual dynamic viscosity based on the viscosity-temperature dependence. Pressure sensors of 160 bar range and 0.5 bar resolution were used for obtaining information about the pressure in the recesses. The pad supports of 2-PAD were mounted on settings screws for the pad alignment based. For investigation of the compliant support, pads could be mounted on silentblocks with threaded ends instead.

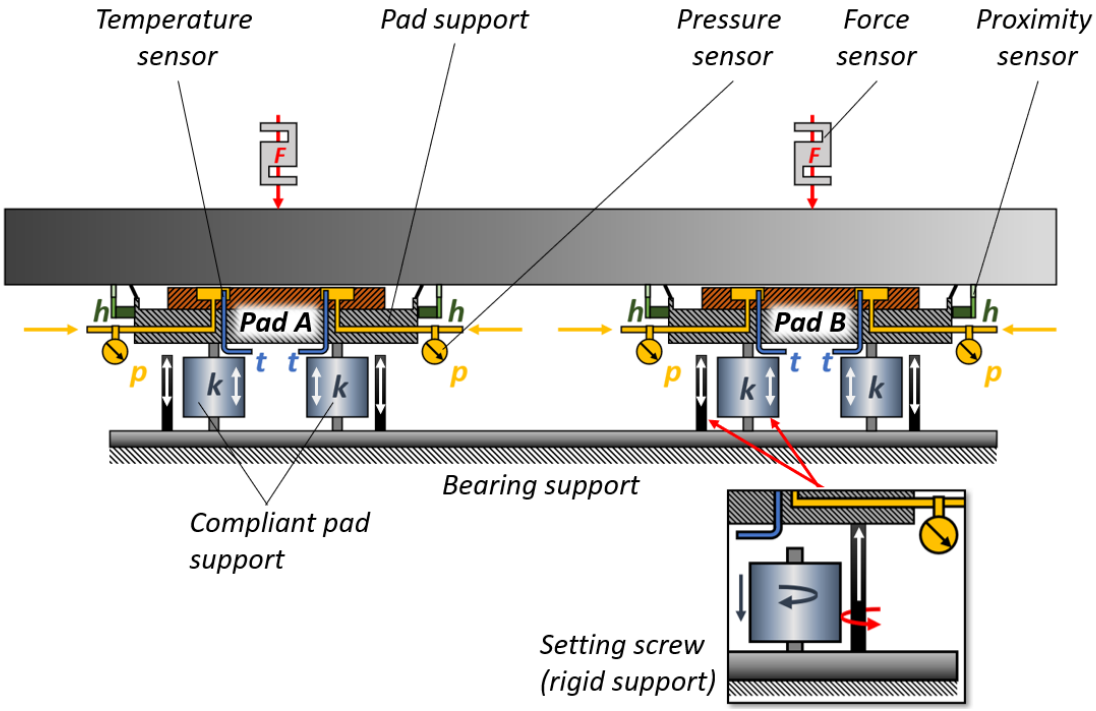

Figure 8 2-PAD sensor description and support type customization procedure.

The second, equally important part of the 2-PAD tester was the hydraulic circuit (Figure 9), which secures constant supply of the pressurized lubricant into the contact area and maintains lubricating film separating the sliding surfaces of slider and pad. The hydraulic circuit was designed as single-pump, thus restrictors had to be assumed to evenly distribute the supplied flow of the lubricant into the recesses. The hydraulic circuit was equipped with safety components, such as pressure relief valve, check valves. The supplied flow and supplied pressure information were displayed on the motor controller and logged via the LabView control program. The hydraulic circuit of the 2-PAD is open type; therefore, a filtering system was used to prevent damage of the hydraulic circuit parts. The information about the lubricant level and temperature were also displayed on the motor controller. The oil tank size was designed for 100 litres of oil, thus a cooler was not assumed, since the planned tests were primarily steady-state and short-term. The selected lubricant for the experimental device was ISO VG 46 grade oil.

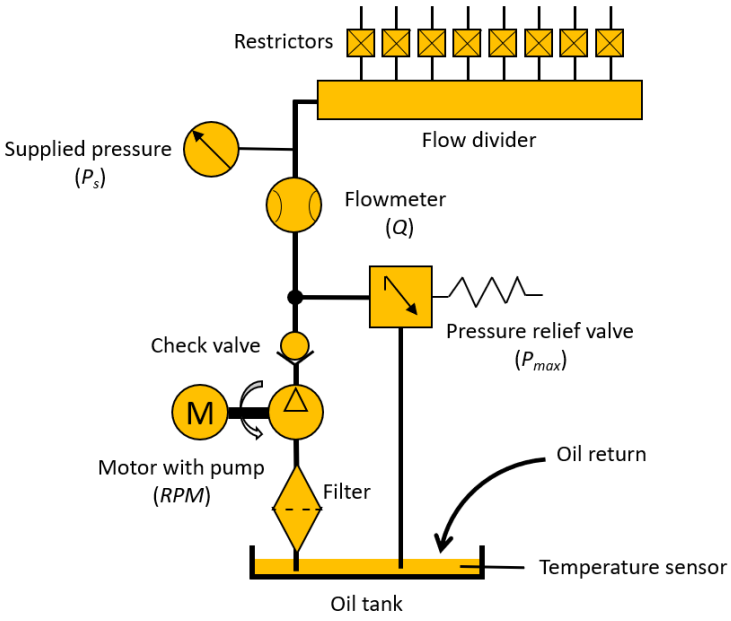

Figure 9 Hydraulic circuit scheme of the 2-PAD.

5.1.2 Viscometer

Dynamic viscosity is one of the primary variables that influence the bearing performance (Equation 1). Rotational viscosimeter HAAKE RotoVisco® 1 (PSL Systemtechnik, Germany) as shown in Figure 10 was used to obtain the lubricant dynamic viscosity dependency on temperature, thus actual viscosity could be evaluated in correspondence with the actual measured temperature in the recess region. The measured temperature was in range of 20 – 50 °C. The obtained coefficient for dependence were fitted using Vogel-Fulcher equation with R^2 = 99.87%. Final equation for dynamic viscosity evaluation was as follows:

$$\mu = 3.91 \cdot 10^{-5} \cdot e^{\left(\frac{1221}{T+131.5}\right)} \quad (1)$$

where T is lubricant temperature.

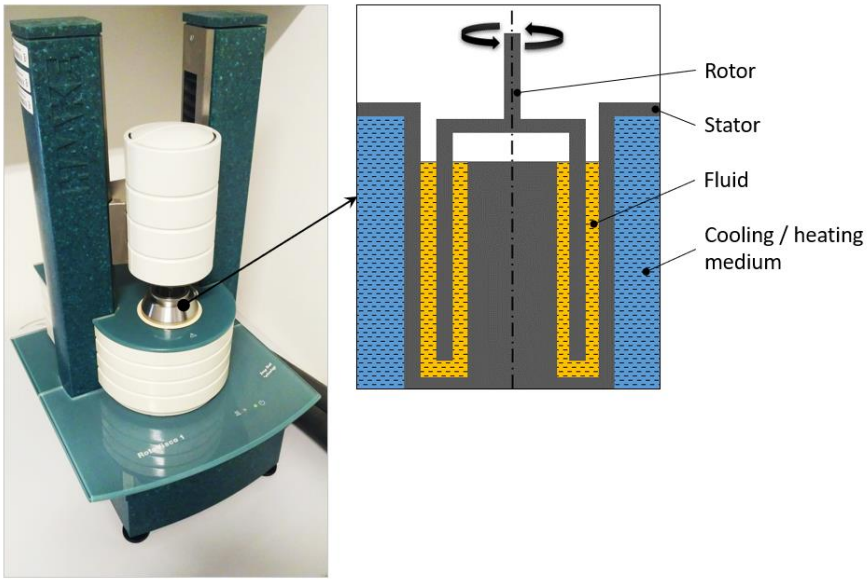

Figure 10 Rotational viscometer Haake Rotovisco 1 with schematical explanation of the working principle.

5.2 Numerical approach

Computational Fluid Dynamics (CFD) is a widely used method for analysis of fluid behaviour. Numerical analyses were performed using commercial software ANSYS Fluent 2021 R2 based on Finite Volume Method with Cell-Centered formulation. The calculation process could be divided into three main parts, as seen in Figure 11: pre-processing, solving and post-processing. Within the pre-processing stage, the 3D geometry was generated and transferred to discretization module Fluent Meshing. Subsequently, boundary conditions were set according to the experimentally obtained and measured data. Using the inputs, the case was solved until reached desired residual magnitude, and then the calculated case was used for results evaluation and flow analysis. The described procedure was performed for all design points according to the parametrization values, which can be found in article [I].

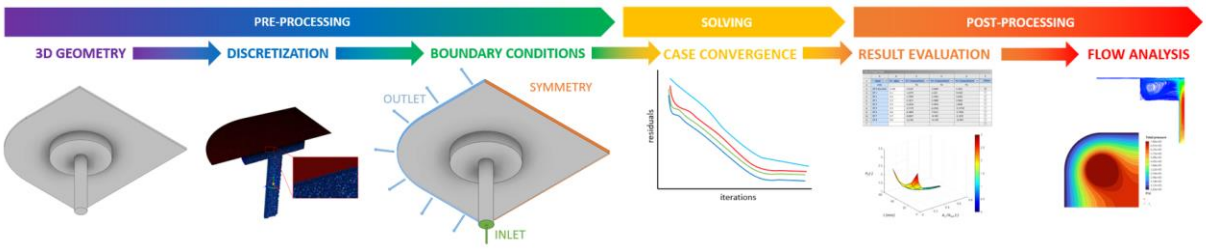

Figure 11 Schematical representation of the CFD solving processes.

After solving all parametrized design points in ANSYS Fluent, the data obtained from simulations were transferred to MATLAB for further evaluation. As seen in Figure 12, the classical 1-parameter optimization approach uses only one variable parameter, recess size *a*, or recess position/pad size *t*. The proposed 2-parameter approach works with two geometric parameters, recess position *p* and recess-to-pad size ratio A_r/A_{tot}, independently. The programmed MATLAB script generated 3D charts for each of the performance factors independently and then created the power loss factor interpolated surface, which was discretized into smaller areas to obtain more precise coordinates for minimal power loss factor H_f. Subsequently, using the coordinates, an optimized pad geometry could be created.

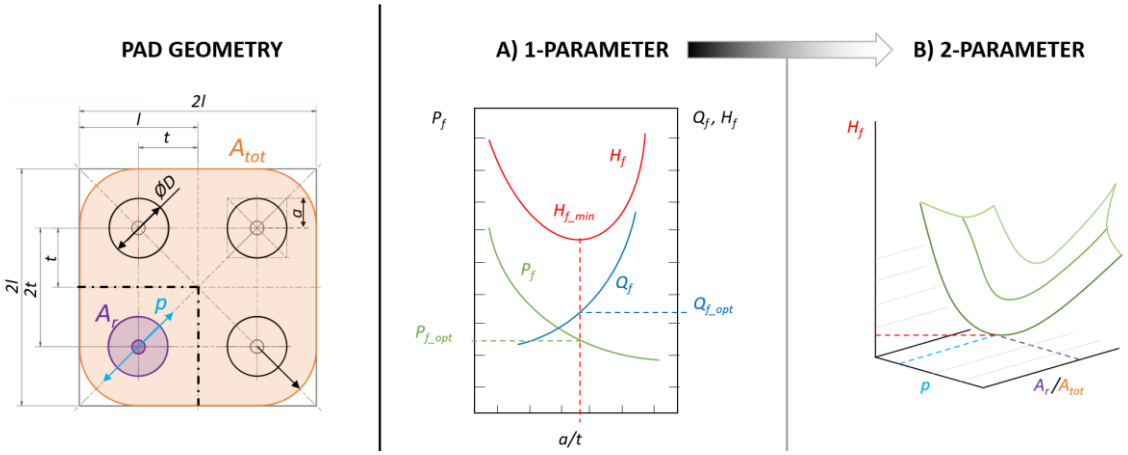

Figure 12 Schematical representation of A) classical 1-parameter approach and B) novel 2-parameter approach geometry optimization.

5.3 Methodology and experiment design

The methods used for the investigation of defined scientific questions and hypotheses were analytical, numerical and experimental. Firstly, the analytical formulation was employed to verify the results obtained from the remaining two approaches. The thesis investigation was divided into two main areas, namely bearing efficiency and bearing safety, respectively. Those areas are described in the following chapters in detail.

5.3.1 Bearing efficiency

The classical approach to HSB pad recess layout and size optimization is based on finding the minimal value of power loss factor, what is represented by an optimal ratio for the highest load capacity at lowest supplied flow. Then, an optimal ratio between recess radius and recess position (a/l) is determined. In case of pad geometry as shown in **Chyba! Nenalezen zdroj odkazů.**, an optimal a/l ratio is 0.4. Subsequently, the geometry is adjusted according to the obtained ratio. Nonetheless, the described classical approach constrains the two

geometrical parameters – recess size and recess position, together. Therefore, a numerical study was performed to investigate the bearing performance of the two geometric parameters, recess size and position, independently. In this approach, all three approaches (analytical, experimental and numerical) were combined to validate the numerical model result precision. As seen in Figure 13, the methodology steps were divided into four main parts: numerical model establishment (1.), domain discretization (2.), numerical model calibration (3.) and results evaluation (4.).

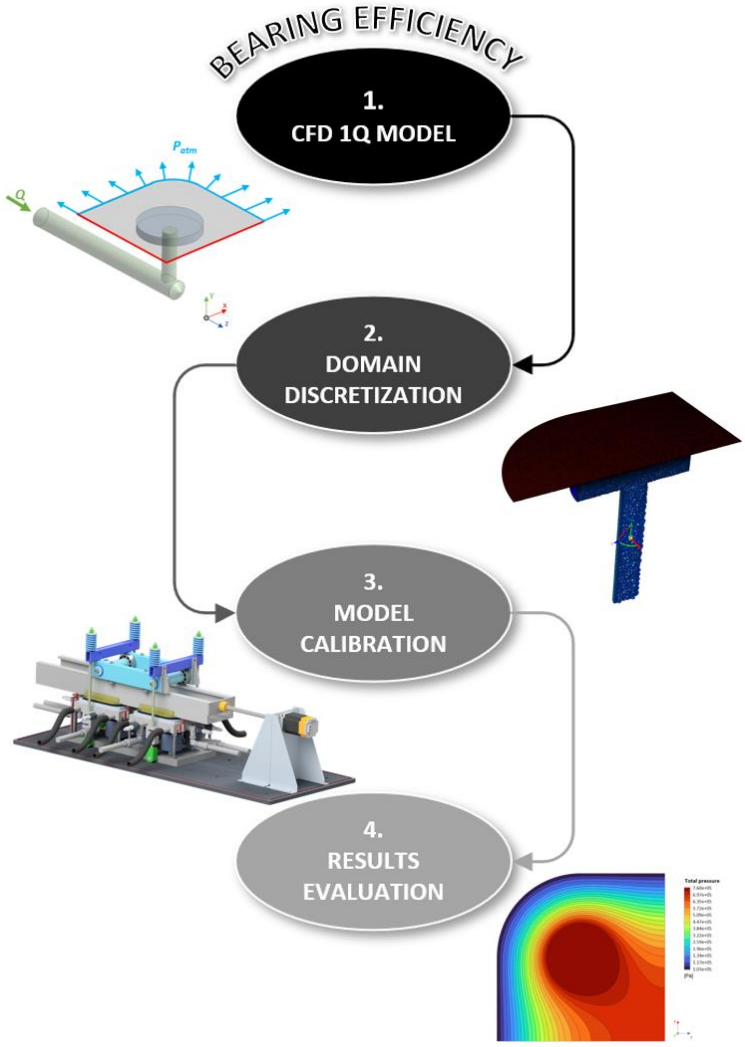

Figure 13 Bearing efficiency improvement methodology.

Firstly, a parametric 3D model was established for an automated geometry customization after each finished case calculation. To reduce the computational time and improve model

precision, one-quarter model was created using symmetry regions (as seen in Figure 14). Subsequently, the created domain was discretized using finite elements. Special attention was focused on smooth transition from the relatively small elements in the lubricating film region to the recess region. The mesh quality was assessed based on Richardson Extrapolation [44] for three sets of meshes. Upon reaching a satisfactory mesh quality, the boundary conditions were set according to the experimentally obtained results and the calculation was performed. Finally, the results for recess pressure, pressure contours and resulting force on the top plane were evaluated and discussed. More details can be found in the published paper [I], which is attached in the *Results and Discussion* section.

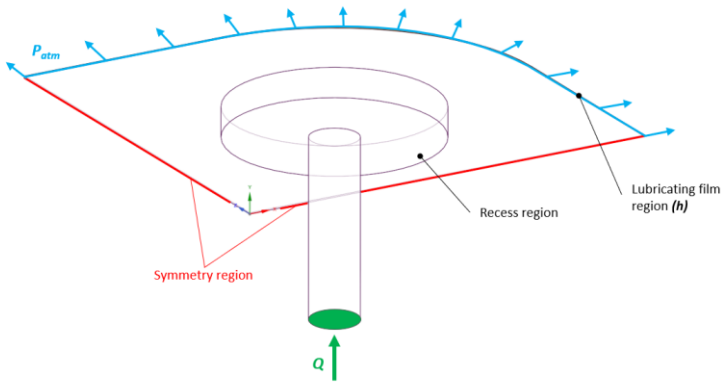

Figure 14 One-quarter model of the HSB pad with boundary conditions.

5.3.2 Bearing safety

The investigation of assembly errors was divided into two main branches – pad misalignment and slider segment misalignment, respectively. For those cases, only analytical and experimental methods were employed. The bearing performance and behaviour was judged based on experimental data, while the analytical approach served to check the generated data validity. The two investigated cases were described in detail in the published articles [II] and [III], respectively, which are attached in the *Results and Discussion* section.

Figure 15 Bearing safety testing methodology for A) pad misalignment and B) slider segment misalignment.

A) Pad misalignment

The investigation of maximal allowable misalignment errors of HSB pads was performed completely under static conditions. The first step was to identify the misalignment types that can occur during the assembly (Figure 16). Nonetheless, the misalignment had to be within the range of proximity sensors (0 – 3 mm). The misalignment errors were set using SKF calibrated shims. All pad misalignment types were measured for a range of error magnitudes with rigid support.

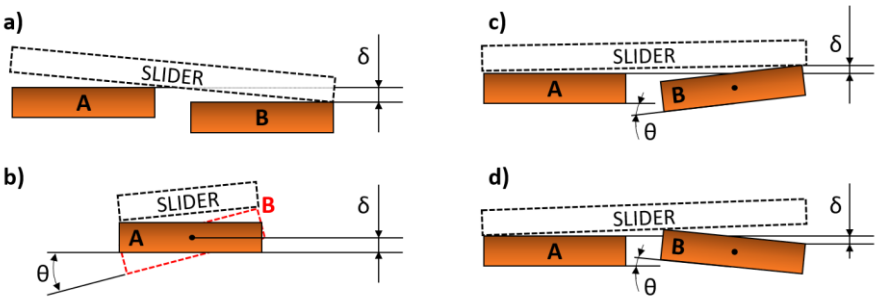

Figure 16 Pad misalignment error types: a) offset, b) inclination, c) tilt 1 and d) tilt 2.

Subsequently, a compliant support consisting of three silentblocks sets of different stiffness were measured (Figure 17). The stiffnesses were chosen according to the expected loads and the error compensation range. The ultimate goal of the compliant support was to deform and compensate the generated pad misalignment, thus creating an even pressure and film thickness distribution.

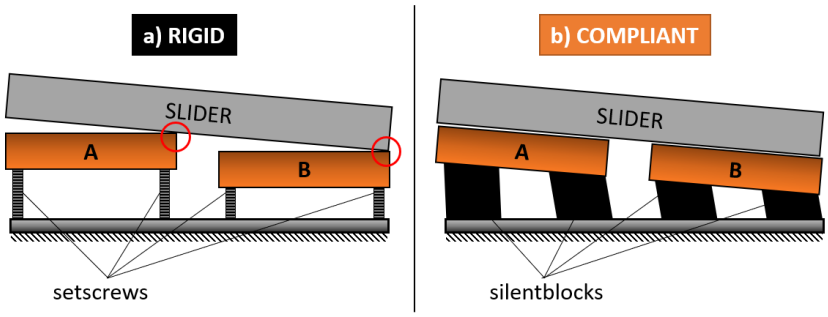

Figure 17 Comparison of a) rigid and b) compliant support type for HS pad.

B) Slider segment misalignment

The estimation of slider segment assembly error tolerance was carried out on the 2-PAD tester with a slider consisting of two parts with a bolted connection. The error was generated in the connection using SKF calibrated shims for two cases – offset and tilt, respectively (Figure 18). The error magnitudes were used in the error-to-film thickness ratio (*e/h*) for better transferability of obtained results for different scales. Firstly, static tests for offset and tilt error types were conducted to determine the critical error values. Subsequently, dynamic tests only for offset error type were performed. The "step-up" and "step-down" offset error types were investigated to determine the offset error type and critical error value for both directions of the slider movement. When the average recess pressure started to decrease, what signalized the loss of load carrying ability. The evaluation criteria for both, static and dynamic tests, respectively, were recess pressures and film thicknesses.

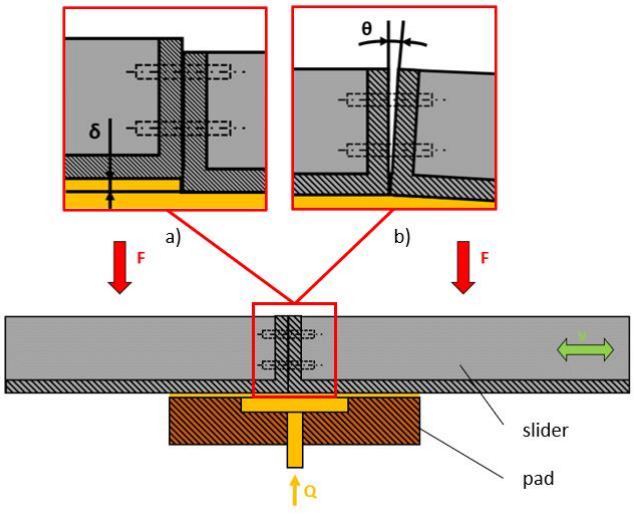

Figure 18 2-PAD Segmented slider error types a) offset and b) tilt.

6 RESULTS AND DISCUSSION

The state of the art was summarized in the review article entitled *"A review of the design and optimization of large-scale hydrostatic bearing systems"*. The conducted review was based on 209 references including original research articles, reviews and books on the topic of the HS lubrication and large-scale HSB. According to the analysed research, knowledge gaps in the investigated field were defined. The main aim of the doctoral thesis is to improve efficiency and safety of multi-recess large-scale HSB. The obtained results were described in the papers [I – III], which were published in peer-reviewed impacted journals. The HSB performance improvement based on CFD was published in paper [I]. The latter two articles [II & III] were focused on safety improvement of large-scale HSB, in terms of pad misalignment and segmented slider assembly errors, respectively.

The first paper [I] dealt with HSB pad geometry optimization based on CFD simulations. A novel method based on multi-parameter optimization of the recess size and position in a multi-recess HS pad was proposed. Unlike in the classical single-parameter approach, where the position of the recess is linked with its size, the novel method allows to separate the two parameters. The CFD model, assuming 3D quarter pad geometry, was calibrated based on analytical calculation and experimental data. Subsequently, the various positions and sizes were determined to proceed with a parametric study in the ANSYS Fluent software. The results from the CFD simulations – resulting load and recess pressure, respectively, were used to determine load and pressure factors. Those two parameters were combined to determine power loss factor, which is directly correlated with pumping power losses. The goal of the optimization was to achieve optimal ratio between load-carrying capacity and supplied flow. The obtained results were interpolated in the MATLAB environment to find the minimal value of power loss factor. Using the two-parameter optimization, the power losses can be reduced by 20 % compared to the classical single-parameter optimization approach.

The second paper [II] was focused on assessing compliant support effect on HSB performance for misaligned HS pads. The investigation was performed experimentally using 2-PAD device. Firstly, four pad misalignment types (offset, inclination, and two variations of tilt) were identified and described. Subsequently, HS lubrication performance criteria for bearing condition monitoring were introduced (normal operation, overload and failure). According to these criteria, the bearing performance in various types of misalignments was assessed. Each misalignment type was tested for rigid and compliant support, respectively. The results show that the compliant support deforms to compensate the pad misalignment and thus creates more evenly distributed oil pressure in recesses. This results in four to six times higher error allowance compared to the rigid support. The stiffness of the compliant support directly affects the magnitude of the misalignment that can be compensated to secure proper function of the HSB pads. Moreover, it has been observed that some types of

misalignments affect the performance more. Inclination seems to be the least dangerous, while on the other hand, tilting and offset of the pads are more critical. As concluded, compliant support allows higher magnitudes of pad misalignment, however, it is not suitable for high precision machines. Finally, a methodology for allowable error estimation for HSB was proposed as a tool for design engineers.

The third publication [III] was aimed at assembly error tolerance estimation for segmented sliders of large-scale HSB working under static and low-speed conditions. The study was performed on 2-PAD experimental device, which was capable of performing low-speed slider movements. Firstly, the expected assembly error types were defined and described in detail. Subsequently, measurements were carried out for each of the defined error types and error ranges. Recess pressure and film thickness were set as the judging criteria for performance evaluation, which were considered altogether to determine the bearing performance. To make the results applicable to wider range of film thicknesses, a ratio e/h (error magnitude to film thickness) was established. As the results obtained from static tests indicate, the allowable error ratio e/h for offset is 2.5. To determine allowable tilt errors, angular error was set as the evaluation criteria. The maximum error tolerance was considered as $\theta = 0.46$ ° for the tilt static tests. Finally, dynamic tests were performed to assess the lubricating film behaviour under low-speed conditions (38 mm/s). Two error types were investigated – "step-up" and "step-down", respectively. The "step-up" error type is less dangerous as no collision might occur. The critical value vas determined as $e/h = 1.5$. However, on the other hand, the "step-down" error type is far more dangerous and as the results show, the e/h ratio for this type of error must not exceed 1. If bi-directional movement is assumed for the HS bearing operation. The e/h ratio should be always smaller than 1.

Tribology Letters (2023) 71:52
https://doi.org/10.1007/s11249-023-01726-3

ORIGINAL PAPER

A Novel Geometry Optimization Approach for Multi-Recess Hydrostatic Bearing Pad Operating in Static and low-Speed Conditions Using CFD Simulation

Michal Michalec[1] · Martin Ondra[1] · Martin Svoboda[1] · Jiří Chmelík[1] · Petr Zeman[1] · Petr Svoboda[1] · Robert L. Jackson[2]

Received: 3 January 2023 / Accepted: 22 March 2023

Abstract
The design of a hydrostatic bearing pad is limited to simple geometry using analytical equations or one-parameter optimization based on experimental data. This study proposes and investigates a new two-parameter method for estimating optimal hydrostatic bearing pad proportions—recess area and position, using Computational Fluid Dynamics (CFD). In this study, 3D static CFD quarter model of a multi-recess hydrostatic bearing pad assuming laminar flow is used. The CFD model was calibrated based on experimentally obtained results and the literature. The recess pressure and resulting load are evaluated for a variety of recess positions and areas. Performance factors are calculated and interpolated in the MATLAB environment. Using the proposed novel two-parameter optimization, the energetic loss was reduced by 20% compared to the classical one-parameter approach. This methodology allows versatile and effective design of optimal hydrostatic bearings operating in low-speed conditions to achieve minimum energetic loss.

Keywords Hydrostatic lubrication · Computational fluid dynamics · Model validation · Optimization methodology

Nomenclature

W	Bearing load (N)
A_{tot}	Total pad area ($mm^{2)}$
A_r	Total recess area (mm^2)
a	Recess radius (mm)
D	Recess diameter (mm)
l	Quarter model edge length (mm)
t	Recess position from pad center (mm)
h	Film thickness (mm)
H_f	Power loss factor
Q_f	Flow factor
P_f	Load factor
P_r	Recess pressure (MPa)
P_{atm}	Atmospheric pressure (MPa)
Q	Supplied flow (L/min)
μ	Dynamic viscosity of lubricant Pa • s
η	Pump efficiency

✉ Michal Michalec
michal.michalec@vut.cz

[1] Institute of Machine and Industrial Design, Faculty of Mechanical Engineering, Brno University of Technology, Technická 2896/2, Brno 616 69, Czech Republic

[2] Department of Mechanical Engineering, Auburn University, Auburn, AL 36849, USA

1 Introduction

Hydrostatic (HS) bearings are a vital part of high-precision machines whose sizes range from millimeters up to tens of meters [1]. They are widely used in machining centers, guideways, turntables, space telescopes, and hydro-energetics [2–5]. The main advantages are operation at zero speed, very low friction, minimal wear, high stiffness, and good damping ability. The possibility to operate at zero speed creates a huge advantage for the operation of hydrodynamic bearings in low-speed conditions. Thus, they are frequently combined with HS bearings to improve the performance and reduce wear during low-speed operation and start and stop phases [6, 7]. Such bearings are called hybrid bearings. On the contrary, it is necessary to continuously supply the bearing with pressurized lubricant to maintain a uniform lubricating layer and proper function. The energetic requirements and initial costs are considerably higher than that for other bearing types. Nevertheless, interest in replacing large rotors

Published online: 06 April 2023

rolling bearings has been rising in recent years to reduce downtime and maintenance costs [8].

The working principle is shown in Fig. 1. Lubricant is supplied by a hydraulic circuit into the recesses of the pad. The generated pressure then lifts the load and separates the solid bodies of the bearing pad and turntable (in case of circular bearings) or slider (in case of guideways). Then, a lubricating film of thickness usually in the range of 10–100 µm is created. The lubricant outflowing from the narrow gap is returned to the hydraulic circuit. The restrictor plays an important role in achieving high stiffness, stability, and control. Many types of such devices have been proposed to improve the bearing performance, such as orifice [9, 10], membrane members [11], or feedback systems [12]. The lubricant supply is necessary for proper function while moving or until the required sliding speed is reached, in the case of hybrid bearings, for the hydrodynamic effect to occur and carry the load. Liu et al. [13] concluded that HS bearings have had an increasing trend of research interest over the last few years. Therefore, it is crucial to design the HS bearing pad for the best performance and minimal energetic demands, which are increasing with the size of the bearing. He and Wang [14] added that the implementation of the best available technology in the industry can reduce the total energy consumption in some fields by up to 20%, which is a significant amount of energy directly affecting the environment and the final product or service price.

The geometry of the hydrostatic bearing is one of the key parameters that affect the lubricant pressure distribution and the bearing resulting performance [15]. Loeb and Rippel [16] introduced the determination of the optimal pad

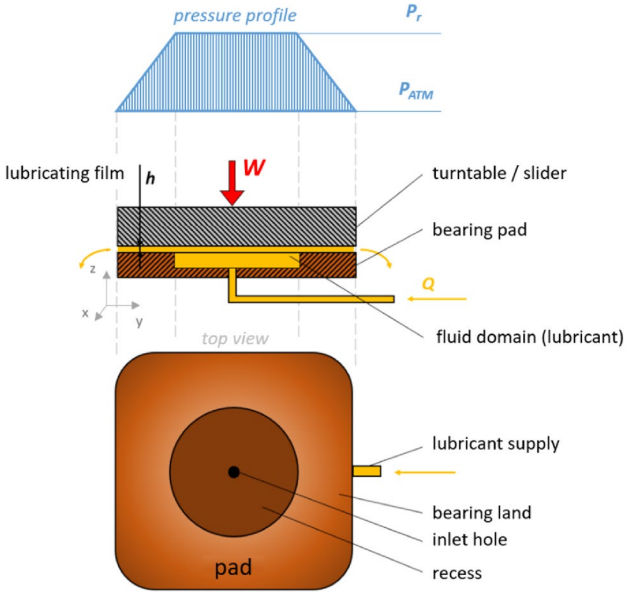

Fig. 1 Scheme of the bearing parts and working principle

shape using an electric field plotter analogy [17], where the optimal shape can be determined using performance factors for a variety of pad shapes using experimentally obtained curves. Subsequently, Rippel [18] published a design manual for HS bearings. Khonsari and Booser [19] published a book dealing with tribological aspects in engineering applications, including hydrostatic bearing shape optimization based on Loeb and Rippel [16] methodology. Based on previous research, Bassani and Piccigallo [20] presented a comprehensive methodology for the design of HS bearings describing the most important parameters and design considerations. Chikurov [21] later continued modeling HS bearings using the electric field analogy for possible simplification. A very important step in the HS bearing design process is optimization to achieve the best performance and reduce energetic demands as much as possible [22, 23]. This is especially crucial in large-scale HS bearings, where the energy consumption is significant [24]. To achieve the best performance and stability, a multicriterion optimization approach should be considered [25]. Simple pad geometries, such as circular pads and recesses, have been analytically derived [19]. However, in cases of complex and multi-recess pads, the analytical solution becomes very complicated, and the performance characteristics must be obtained experimentally or using a numerical approach.

Computational Fluid Dynamics (CFD) has been increasingly used in various applications over the past decade. One of the key advantages of this method is that it allows one to obtain many parameters and investigate flow characteristics in areas where it is extremely difficult or even impossible to implement sensors or use optical methods. CFD has already been used to study hydrodynamic, HS, and hybrid bearings [26–28]. Sharma et al. [29] conducted a numerical study to determine the performance of unconventional hybrid bearings. It has been shown that hybrid bearings perform with lower pressure and temperature peaks, which leads to higher bearing stability [30, 31]. However, it is crucial to determine the accuracy of the model. Cui et al. [32] investigated heavy HS bearing using a quarter CFD model and obtained errors under 10% compared to analytical approaches. Gao and colleagues [10] studied the effect of orifice length in HS bearings and compared the CFD model with experiments that reached errors under 1%. The experiments are crucial to CFD model validation, especially in cases where exact analytical approaches cannot be used. Wasilczuk et al. [33] concluded that the presence of HS pockets in hydrodynamic bearings reduces the temperature change and pressure peaks, leading to higher reliability of the hybrid bearing, but the drawback of the presence of the pocket is the larger friction losses due to the cooler oil. Wodtke et al. [34] carried out experimental validation for theoretical calculations and predictions of large hydrodynamic

thrust bearings and emphasized the necessity of experimental validation of numerical simulations, which are simplified and thus do not represent the real geometry and other influential effects. Helene et al. [35] conducted a parametric study of the flow pattern in the 2D recess of a hybrid bearing based on Navier–Stokes equations with the comparison of laminar and turbulent flow regimes. The authors concluded that the modeling of the turbulent flow regime could contribute to better understanding of the inertia and viscous effects in recess bearings. For that reason, turbulent models were later used by Ghezali et al. [36] and Gao et al. [10] in hydrostatic bearing orifice performance numerical investigation of flows of higher Reynolds numbers. Horvat and Braun [37] extended the study of numerical flow characteristics to 3D HS journal bearings with experimental validation using laser flow visualization of streamline maps at a high rotational speed. A similar study was later conducted on HS thrust bearings to investigate geometric patterns and different pad shapes, concluding that the presented model may be useful in HS bearing load-carrying capacity and stiffness of HS bearings for low-speed applications [38]. Du et al. [39] proposed an analytical model for the analysis of the pressure of tilted HS journal bearings validated using a CFD and experimental procedure. Guo et al. [40] performed a comparison of CFD codes for static and dynamic properties in hydrodynamic and HS bearing applications. The authors agree that CFD will play an important role in bearing and damper analysis in future research. The comparison of CFD standard code to a special one made for HS, hydrodynamic any hybrid bearing analyses showed good agreement, which leads to a conclusion that general codes might be used for the investigation of such bearings and their static and dynamic characteristics.

The CFD can significantly speed up the development, reduce costs, and provide detailed information about the flow character and many parameters. Although the CFD approach is widely adopted in various applications, including HS, hydrodynamic, and hybrid bearings, it is necessary to set appropriate boundary conditions and verify the results obtained with an experimental approach [41–43]. Moreover, many papers dealing with CFD analyses of HS bearings have been proposed over the last years, although only a few of them offered practical design recommendations. This article aims to optimize recess size and position in HS bearing pads to minimize energetic loss while achieving the best performance for static and low-speed conditions. The presented geometry optimization multi-parameter approach using area ratio and recess position has not yet been proposed.

2 Materials and Methods

Three approaches were used to verify the obtained results—analytical, experimental, and CFD. An integrated process was also followed to create and analyze the results using these three methods, as shown in Fig. 2. Based on the analytical calculation, experimental conditions were determined. Afterward, boundary conditions of the CFD analysis were set according to the resulting analytical results and experimental conditions. Subsequently, all results were compared and discussed.

2.1 Analytical Approach

Navier–Stokes equations play a significant role in the field of fluid mechanics. Nonetheless, due to the complexity of the Navier–Stokes equations, it is almost impossible to obtain

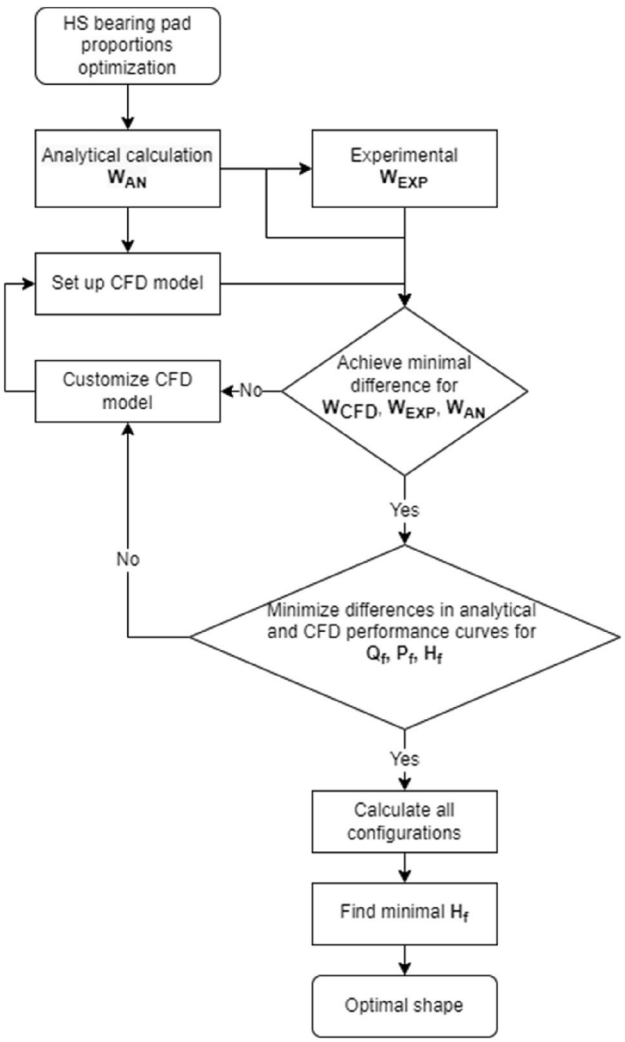

Fig. 2 Optimization flowchart used in the presented study

analytical expressions to calculate required flow characteristics. Therefore, certain assumptions can be considered to help to obtain a simpler form of equations. The assumptions are as follows:

1. Film thickness is constant and small compared to its size in other directions.
2. The fluid is Newtonian, incompressible, and isoviscous.
3. Inertia terms are negligible compared to the viscous forces.
4. No squeeze nor sliding exists and the bearing surfaces are stationary.
5. The pressure of lubricant is constant in the direction of the film thickness ($\partial p/\partial z = 0$).
6. There is a continuous supply of lubricant, and the flow is laminar.

Then, the Reynolds equation for computation of the pressure distribution in the simplified form is as follows:

$$\frac{\partial}{\partial x}\left(\frac{h^3}{12\mu}\frac{\partial}{\partial x}\right) + \frac{\partial}{\partial y}\left(\frac{h^3}{12\mu}\frac{\partial p}{\partial y}\right) = 0. \tag{1}$$

After obtaining the pressure distribution, the load-carrying capacity (or acting force) can be expressed as follows:

$$W = P_r \cdot A_{eff}, \tag{2}$$

where P_s is the recess pressure and A_{eff} is the effective area of the pad, which can be expressed from effective pad area proportion β ($\beta < 1$) and total area of the pad A_{tot}:

$$A_{eff} = \beta \cdot A_{tot}. \tag{3}$$

Eqs. (1–3) can be further customized and utilized to express required flow supply to the bearing as follows:

$$Q = Q_f \frac{W}{A_{tot}} \frac{h^3}{12 \cdot \mu}, \tag{4}$$

where h is the film thickness, μ is the dynamic viscosity of lubricant, and Q_f is the flow factor, dependent on the geometry and the effective area of the bearing.

Loeb [17] introduced a new methodology for estimating optimal proportions of the bearing pad and recess based on electric analog field plotter. Generalized analytical equations could be used to calculate the bearing performance using read values obtained from graphs, presented in Loeb and Rippel [16]. Similarly, the performance factors (Eq. 5–7) can be determined based on known values of bearing characteristics.

$$(a)\, pressure\, factor\, P_f = \frac{P_r \cdot A_{tot}}{W}, \tag{5}$$

$$(b)\, flow\, factor\, Q_f = \frac{12 \cdot \mu \cdot Q \cdot A_{tot}}{W \cdot h^3}, \tag{6}$$

$$(c)\, power\, loss\, factor\, H_f = \frac{P_f \cdot Q_f}{\eta}. \tag{7}$$

Eqs. (5, 6) can be transformed to obtain the required variable from the expression. An example of designing a HS bearing pad proportions using one-parameter optimization is shown in Fig. 3. The ratio *(a/l)* represents the characteristic dimension of the recess to the characteristic dimension of the pad, that is, the diameter of the recess to the pad edge length. One primary parameter is kept constant (usually recess size to retain the required lifting area), while the other is optimized. The aim of the pad geometry optimization is generally to achieve the best possible performance with minimal pumping power loss, in this case, the power loss factor—H_f. And for the

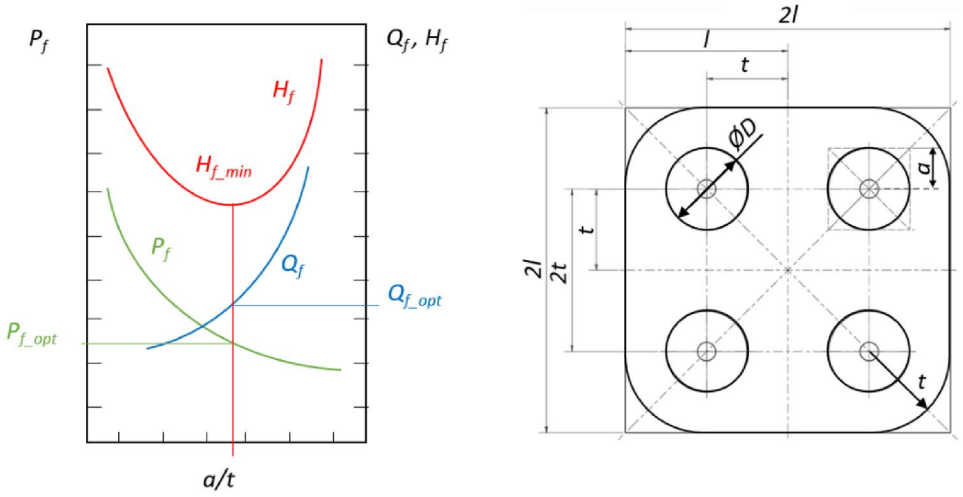

Fig. 3 An example design chart using one-parameter optimization with geometry description from Loeb and Rippel [16]

Table 1 Performance factors for experimental pad proportions read from Fig. 4 of [16]

Parameter	Label	Value
Pressure factor	P_f	1.52
Flow factor	Q_f	27.4
Power loss factor	H_f	41.65

(a/l) ratio of the minimum power loss factor, the values of optimal pressure (P_f) and flow (Q_f) factors are obtained, respectively. Performance factors for the experimental pad proportions can be found in (Table 1). This study assumes relative performance change independently on the pump efficiency, what is not the aim of this study, thus the parameter η was assumed as 1 for simplification.

In the basic approach, only one of the two parameters: a or l are used, while the recess position $(t = l)$ is assumed. The optimization approach using performance curves in a 2D graph utilizes $(l = 4a)$. However, we defined the new variable parameter (t) to describe the position of the recess. Thus, the proposed method uses two-parameter criteria, recess position (t), and recess area-to-total pad area ratio (A_r/A_{tot}) for performance optimization. The area and the position of the recess were chosen as the primary parameters because the recess shapes may be chosen to better accommodate the pad shape and thus improve the bearing performance. The length of the edge of the pad $(2\ l)$ remained constant, so the second variable assumed in this study was the recess radius (a). Attention should be paid to prevent exceeding the recess area out of the pad geometry, i.e., in case the pad has rounded corners.

2.2 Experimental Validation

2.2.1 Lubricant Viscosity

To obtain all the inputs required to build a relevant mathematical model, the dynamic viscosity measurement was performed on a rotational viscometer from HAAKE RotoVisco® 1 (PSL Systemtechnik, Germany). Measured data were filtered with 99.88% reliability using a Bingham rheological model. The dynamic viscosity of the used ISO VG 46 grade hydraulic oil was fitted using the Vogel–Fulcher equation with $R^2 = 99.89\%$. The experiments were carried in static conditions, with stable temperature 23 °C recorded using temperature sensors in the recess. The results showed very low temperature difference throughout the measurements, only ± 1 °C. Thus, constant viscosity of 0.104 Pa•s was considered in all simulations. It has been previously observed by Schmelzer et al. [44] that the pressure–viscosity dependence of liquids of constant composition is extremely small (around 2%) in the investigated pressure range (0–1 MPa). Therefore, the pressure–viscosity dependence was neglected in this study.

2.2.2 Two-Pad HS Experimental Bearing (2-PAD)

The experimental device used to obtain the measured data for evaluation is schematically shown in Fig. 4. It consists of two main parts, the bearing and the hydraulic circuit, which supplies pressurized lubricant with a pump powered by an electromotor. The hydraulic circuit is equipped with safety features, such as a check valve and a pressure relief valve.

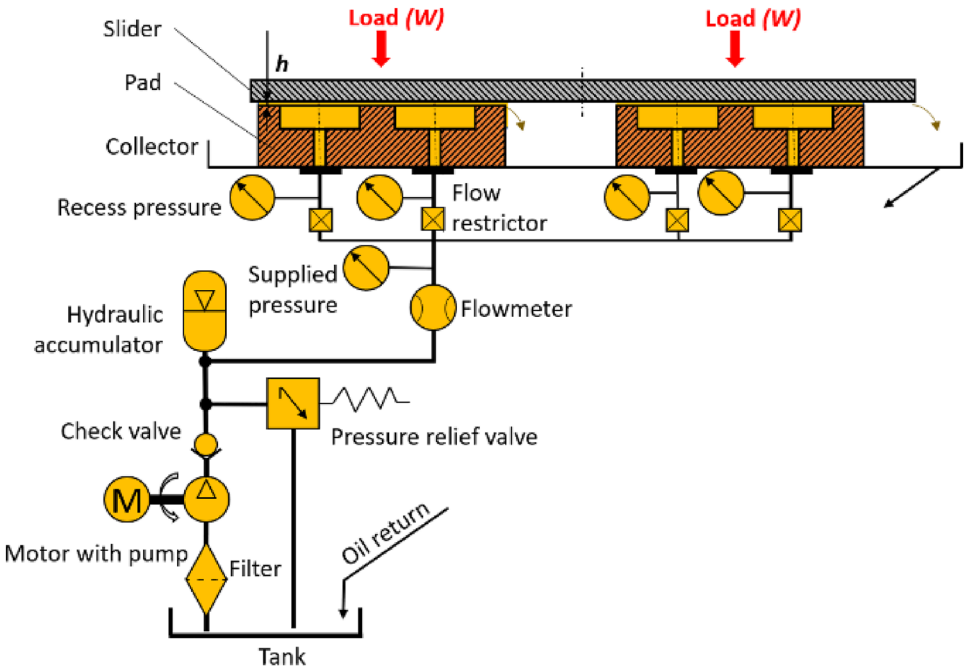

Fig. 4 Schematic representation of 2-PAD experimental device

The hydraulic accumulator minimizes the pressure spikes generated by the pump. The flowmeter measures the total supplied flow to the whole bearing. Flow restrictors (throttle valves) secure bearing stability in the event of asymmetrical load or misalignment. A pressure sensor of 0.25 bar precision is mounted on each of the inlets to the recess. The lubricant that flows out of the contact area to the collector is returned to the oil tank.

Three-contact potentiometer proximity sensors are mounted on each of the 2-PAD pads for obtaining film thickness with precision of 0.01 mm and range of 3 mm. To measure the actual temperature in the recess area, a thermometer is fitted in each of the recesses for calculation of the viscosity value of the lubricant. The load is created using four set screws, each mounted with a load cell with $\pm 5\ N$ precision, which provides a real-time measurement of the loading force. The experimental measurements were carried out three times after the temperature in the recess area stabilized at 23 °C (corresponding to a dynamic viscosity of 0.104 Pa•s). Since the hydraulic circuit has relatively large tank (100 l), no additional cooling was necessary. The experimental conditions were based on the previous test bearing comparison with analytical equations in ref. [45]. The total supplied flow into both pads was set to 8.5 l/min. A comparison of predicted and measured film thickness with variable load was presented in reference [45], where the highest precision was achieved at 16-kN load. Therefore, for all measurements, a total load of 16 kN were applied in this study. The resulting average film thickness was 0.197 mm. The pad size used in experiments was 140×140 mm with recess diameters of 35 mm and positions of $t = 35$ mm and recess depth was 5 mm. The inlet was 40 mm long and of 8 mm diameter (Fig. 5).

2.3 Numerical Approach

CFD analysis has become a favored method for the analysis of fluid dynamics. It provides a detailed understanding of the lubricant flow in hydrostatic bearings. In this study, the CFD analysis was done using commercial software ANSYS Fluent 2021 R2 based on the Finite Volume Method with Cell-Centered formulation. The code solves the conservation equations for mass (Eq. 8) and momentum (Eq. 9), respectively.

$$\nabla \cdot v = 0, \tag{8}$$

$$\rho(v \cdot \nabla)v = -\Delta p + \mu \nabla^2 v. \tag{9}$$

In this case, pressure-based steady-state incompressible flow with absolute velocity formulation was investigated without considering thermal effects and gravity. A uniform lubricant film was considered in all simulations. The Reynolds number estimation was below 10 and the laminar flow regime is expected in the film region, thus laminar model was selected. Because of relatively high film thickness and

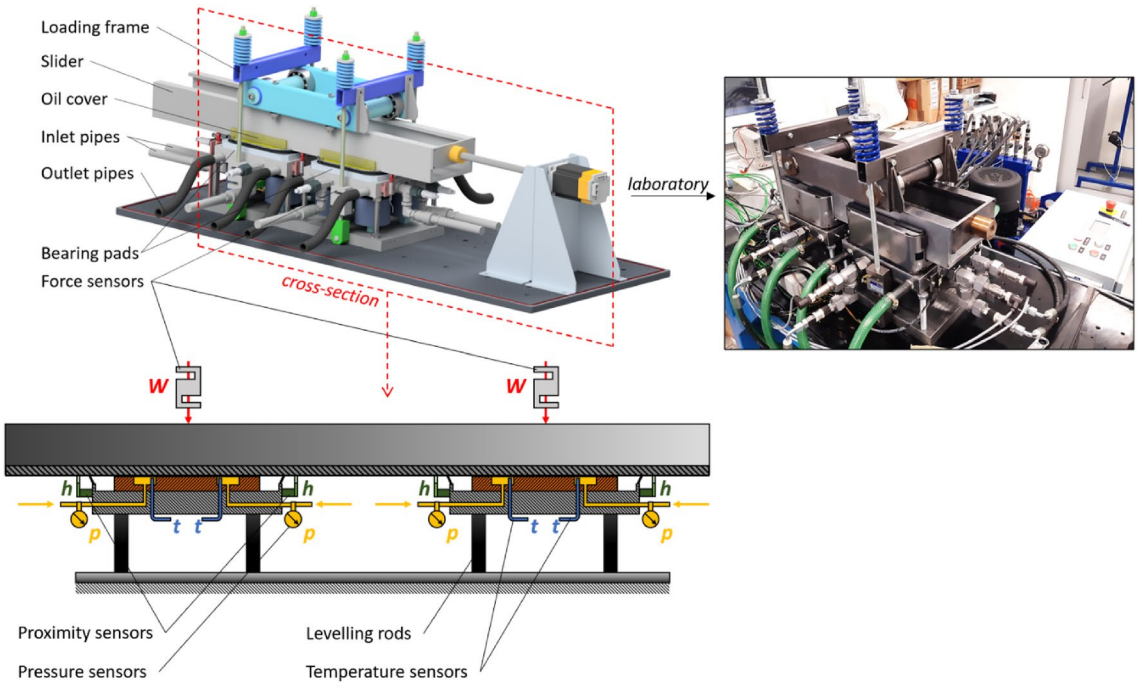

Fig. 5 Schematic representation of the 2-PAD hydrostatic test bearing with sensor description and photography of the assembled experimental device in the laboratory

Table 2 Combination table of variable parameters for simulation design points

Area ratio A_r/A_{tot} (−)	0.05	0.1	0.2	0.3	0.4	0.5	0.6	0.7
Recess diameter D (mm)	17.66	24.98	35.32	43.26	49.96	55.85	61.18	66.08
Recess position t (mm)	8.83	12.48	17.66	21.63	24.97	27.92	30.59	33.04
	19.29	21.49	24.59	26.97	28.98	30.75	32.35	33.82
	29.76	30.49	31.53	32.32	32.99	33.58	34.12	34.61
	40.23	39.50	38.46	37.67	37.01	36.41	35.88	35.39
	50.70	48.50	45.40	43.02	41.01	39.24	37.64	36.17

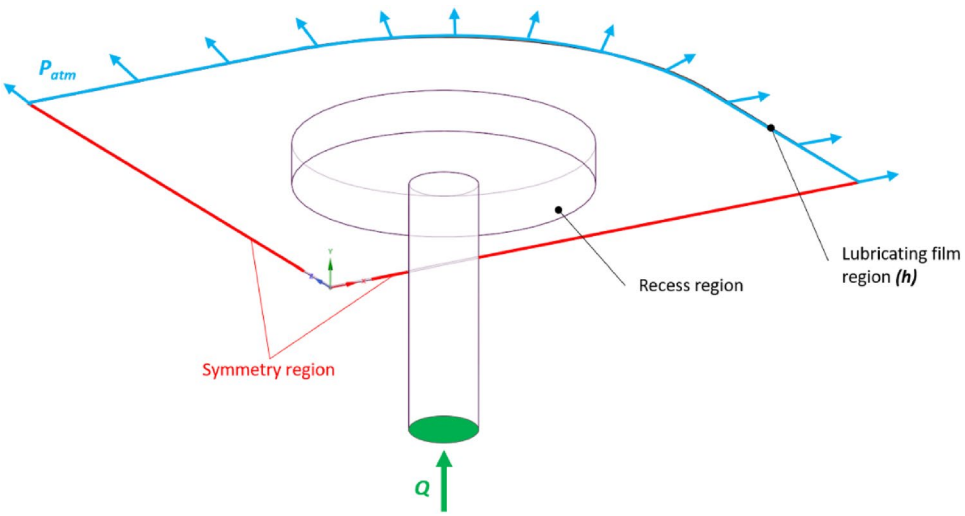

Fig. 6 Quarter model with boundary conditions used for the CFD analyses

low pressure were assumed for very short experimental tests isothermal conditions were assumed—constant viscosity (0.104 Pa•s) and density (875 kg/m^3) were established for all simulation design points. The operating conditions included an atmospheric pressure of 101.3 kPa to reflect the real conditions. The 3D geometry of the fluid domain was parametrized in 3D modeling software of the program. The variable parameters, recess position and diameter, are listed in Table 2. The simulation of all design points was conducted using the setting described below. An important rule to avoid the recess area outreaching the pad area must be checked before proceeding with the simulation parametrization.

The quarter model of the fluid domain was discretized into an unstructured polyhedral mesh in built-in ANSYS Fluent Meshing (* MERGEFORMAT Fig. 6). Mesh refinement was set on the top plane to enhance the results of the pressure and resulting forces acting on this plane. Three sets of meshes were compared using Richardson Extrapolation method [46]. Discretization error was calculated from a theoretical extrapolated value based on the results from the three sets of equally spaced meshes. Three boundary layers were added to the walls in the lubricating film region to enhance near wall fluid behavior in the top plane area, from which the results were evaluated. Due to the large difference between lubricating film height and recess depth, element growth rate was set to 1.05 to ensure slow transition of the

Table 3 Parameters of the three examined meshes

	Fine	Medium	Coarse
Resulting force – top plane (N)	1982.53	**1986.32**	1908.75
Refinement ratio	1	**1.25**	1.5
Discretization error (%)	0.02	**0.22**	3.7
Number of elements	3.92e + 6	**2.27e + 6**	1.09e + 6
Max. aspect ratio	21.7	**20.2**	23.3
Max. skewness	0.47	**0.43**	0.44
Min. orthogonal quality	0.21	**0.21**	0.21
Avg. total meshing time (min)	6.5	**4**	2
Avg. computational time (min)	30	**20**	12

elements. The final mesh selection was based on the results in Table 3. The precision of the model was also judged according to the analytically predicted and experimentally obtained results. It is also possible to optimize bearings with smaller film thickness using this method, but it may require longer computational times to secure smooth mesh element transition from the recess area to the film region.

A uniform film thickness of 0.197 mm, as obtained from experimental measurements, was used for all design points. The boundary conditions can be seen in Fig. 6. Starting with the mass flow inlet (Q) set at 0.015 kg/s on the face of 40-mm-long inlet pipe. Symmetry conditions

were employed on the symmetry planes of the quarter model and pressure outlet with atmospheric pressure operating condition (P_{atm}). Output parameters were the resulting force on the top plane of the bearing and average pressure over the recess area on the top plane.

The residuals of continuity and momentum equations condition were set below 10^{-4} to achieve convergence. Under relaxation factors for both velocity and pressure were set at 0.5 and 0.5, respectively, without any further need for adjustment. We used the coupled pressure–velocity coupling scheme, which should provide robust and high performance for steady-state flows compared to the segregated schemes available in ANSYS Fluent. The gradient least square-based spatial discretization method was used. The first-choice schemes—second order and second-order upwind were kept for pressure and momentum, respectively. Hybrid initialization was conducted to improve the convergence of each case. One case took approximately 20 min to discretize and solve with the used computer specifications: 12 physical cores of 3.47 GHz processor, 96 GB of RAM, and 1 TB SSD to store retained case data.

3 Results and Discussion

Firstly, the comparison of results obtained from experiments, calculations, and CFD simulations were performed to validate the CFD model precision. Subsequently, all design points were calculated and evaluated for the performance factors and shape optimization.

3.1 Model Calibration

The total load applied per pad was obtained based on three measurements using load cells with sensor precision of 3% and resulting average deviation under 0.5%. The recess pressure was obtained from pressure sensors in each of the recess with 5% sensor precision and resulting average deviation under 1% based on three measurements. The calculated load was obtained using information from sensors mounted on the pad. Then, a 3D CFD model was created and computed for the same geometry as on the experimental device. The results are shown in Fig. 7 for (a) load and (b) recess pressure. The CFD results for the load were obtained from resulting force acting on the top (contact) plane of the model. The weight of slider and loading frame was included in load evaluation. The experimental results show relatively good agreement with the calculation considering the precision of the used sensors. The recess depth influence on the performance might have affected the results as well, since analytical calculation does not assume this geometric parameter. The obtained difference from analytical calculation in load was − 3.2% for experimental results and + 0.65% for CFD, respectively. The difference in results of recess pressure compared to the analytical approach reached − 7.5% for experiments and + 5.3% for the CFD analysis. The values obtained experimentally exhibit lower values due to the simplifications that are assumed in analytical and CFD computation, respectively. Despite a constant viscosity was assumed in all simulations to determine optimal geometry, so that the comparison of various shapes was unaffected, additional influence of the results could be caused by the dynamic viscosity variation with temperature, which approximately changes by 5% for 1 °C. A minor contribution to the

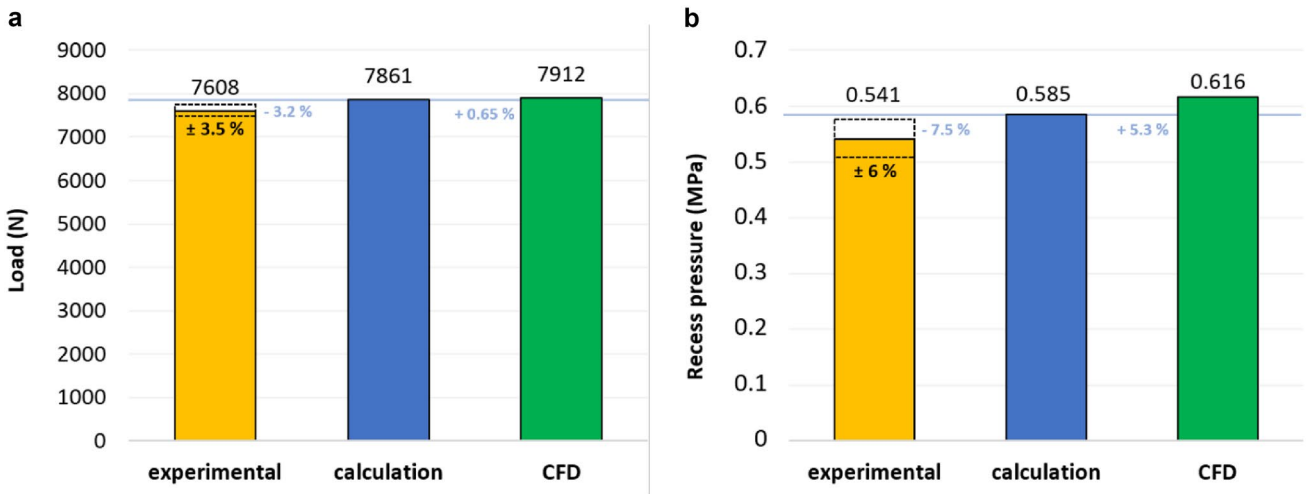

Fig. 7 Load (**a**) and recess pressure (**b**) comparison obtained from experimental measurements (including sensor error & measurement deviation), analytical calculation and CFD analysis for the initial pad geometry.

results difference could be caused by the geometry imperfections of the HS bearing (surface flatness and roughness) or the recess depth effect influence, which is in the case of analytical calculation neglected. Nonetheless, the obtained results were of satisfactory precision to carry on with the model parametrization.

3.2 Design Point Computation and Evaluation

After conducting the initial comparison of the different approaches, the numerical CFD study was solved for all the design points from Table 2. The performance factors P_f, Q_f, and H_f were calculated from the results obtained using Eqs. (5–7) for all design points. The results of all performance factors are shown in Figs. 8, 9, and 10 in the form of (a) 3D graphs with the variable recess on the y-axis and variable area ratio on the x-axis, forming the two-parameter approach and (b) area ratio sections for better readability of the obtained data. Generally, the optimization goal is to achieve the lowest P_f, Q_f, and H_f, assuming Eqs. (5–7). The load factor (Fig. 8) shows a similar trend as in the reference experimentally obtained 2D graph from [16], but in a different scale. The results for the load factor indicate that the load-carrying capacity decreases with increasing area ratio or position from the origin, separately and together. The larger the area ratio, the smaller the load factor. The lowest value of P_f can be found in the middle sector of the graph. Nonetheless, as seen in Fig. 11, the largest area ratio creates a very small sealing edge and thus is extremely sensitive to the pad misalignment and asymmetrical loading. In the case of flow factor (Fig. 9), it is obvious that the larger the area ratio or the farther the position of the recess from the center, the higher flow is required to sustain certain film thickness or load-carrying capacity. As for the flow factor, the closer to the pad center the recess is, the smaller the actual value. The smaller the area ratio is, the better performance will be achieved. Ultimately, the power loss factor (Fig. 10) expresses the overall performance—to secure an optimum between the highest load capacity and the lowest power requirements (as expressed in Fig. 3). Therefore, to achieve the lowest energy requirements, a minimal H_f should be considered.

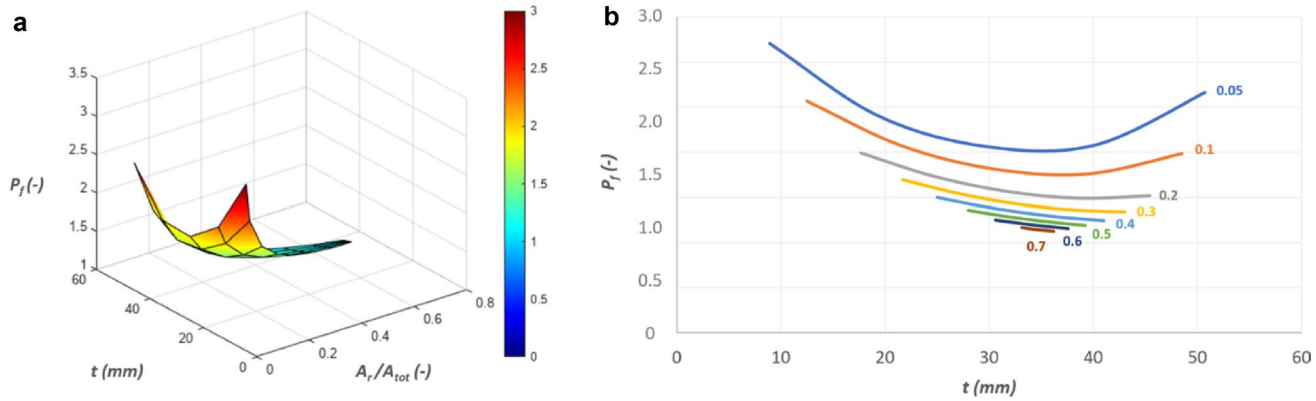

Fig. 8 Load factor **a** position and area ratio variation dependence and **b** area ratio sections obtained from CFD analysis

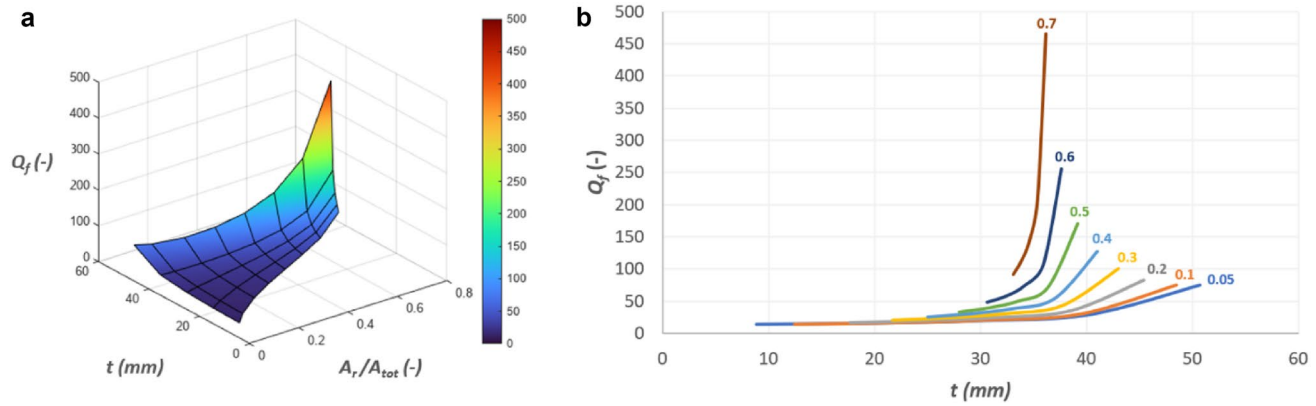

Fig. 9 Flow factor **a** position and area ratio variation dependence and **b** area ratio sections obtained from CFD analysis

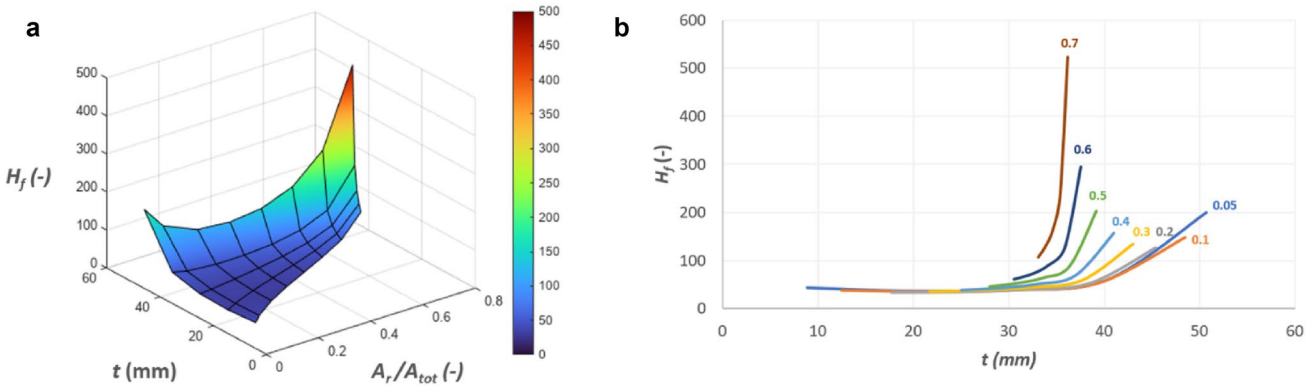

Fig. 10 Power loss factor **a** position and area ratio variation dependence and **b** area ratio sections obtained from CFD analysis

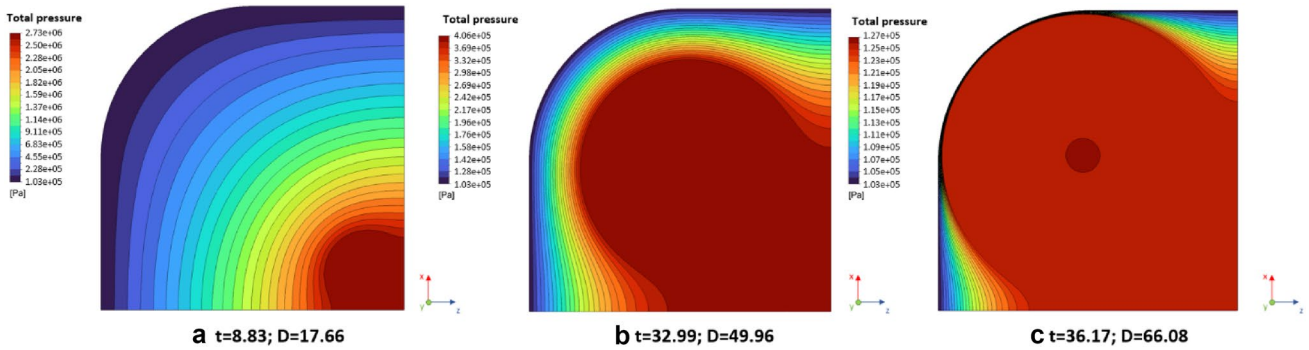

Fig. 11 Top plane pressure contours of static pressure for recess size and position: **a** smallest and closest to the center, **b** medium in the middle, and **c** largest and farthest from the pad center

In the case of open-type bearings (without counter pads, as explained in ref. [1]), the recess position should be chosen, also considering the ability of the bearing to manage asymmetrical loading and pad misalignment. This is another reason why the multi-parameter approach offers a more versatile design process compared to the classical one-parameter approach. For this reason, pressure contours of the various pad shapes from smallest and closest to the pad center, to the farthest and biggest (Fig. 11). It is obvious, that the larger the land area (as for the smallest area ratio), the higher the recess pressure. Nonetheless, the load capacity and ability to manage asymmetrical loading and misalignment are not desirable in this case (Fig. 11a). The recess pressure was gradually decreasing with increasing recess size and distance from the pad center (Fig. 11b). The highest ability to manage asymmetrical loading was achieved with largest recess size (Fig. 11c). The sealing edge is very small in this case and the pressure gradient is the steepest (Fig. 12) for this configuration, which makes the bearing extremely sensitive to pad misalignment. Even though the smallest load factor was obtained, the largest flow factor resulted for this case, which is undesirable.

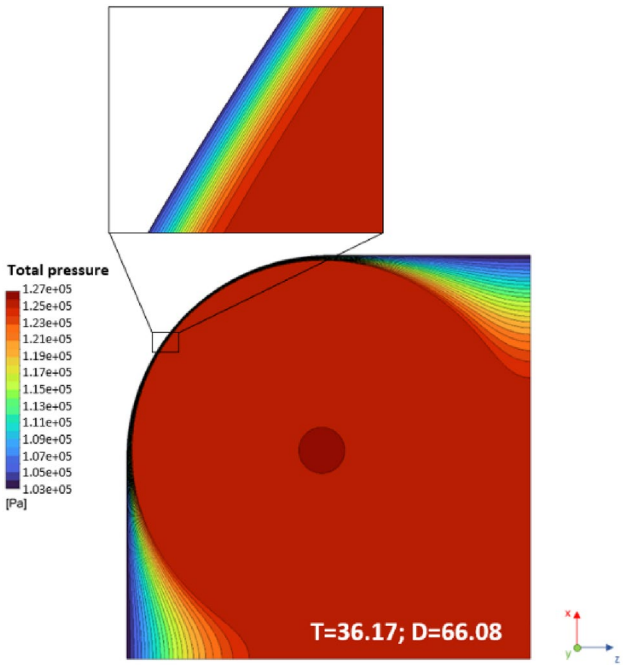

Fig. 12 Top plane pressure contour of static pressure for recess size of 68.4 mm diameter and position 35.48 mm from the pad center with detail on the sealing edge

3.3 Optimal Shape Determination

To determine the optimal shape of the bearing, the minimum power loss factor was searched for. To obtain a more accurate result, the minimum was not chosen from the calculated values of the design points, but using a cubic interpolated surface as seen in Fig. 13. This step allowed us to look for the minimum value of the power loss factor also between the calculated points. The calculated points were used to fit the cubic interpolated surface with normalization in MATLAB R2021a. It is also possible to use linear interpolation, which is simpler but does not capture the surface trend and curvature as well as the cubic interpolation. Subsequently, a minimum value of the power loss factor was found. Then, the coordinates of the minimum value expressed the optimal shape—the recess position and area ratio, respectively. The minimum value of the power loss factor, 30.66, obtained by CFD simulation was determined for the recess position 17.66 mm from the center and an area ratio of 0.2. In contrast, optimal value of the power loss factor obtained from the graph presented by Loeb and Rippel [16] is 38, with recess position of 35 mm and area ratio of 0.132. Compared to the basic approach using one-parameter criteria, a 20% reduction of the power loss factor was achieved. The investigated ranges of recess position and area ratio were chosen according to the pad size and computable geometry. The interpolated grid could be finer if even higher precision was required. The deformed grid areas on the left side of the 3D graph in Fig. 13 are only a graphical representation of the grid fitted over the sample points and thus are not evaluated.

Finally, we compared the pressure contours of the optimal shape obtained from the classical approach (Fig. 14a) and the presented two-parameter approach (Fig. 14b), respectively. The classical approach optimization resulted in smaller recess diameter and its farther position from the

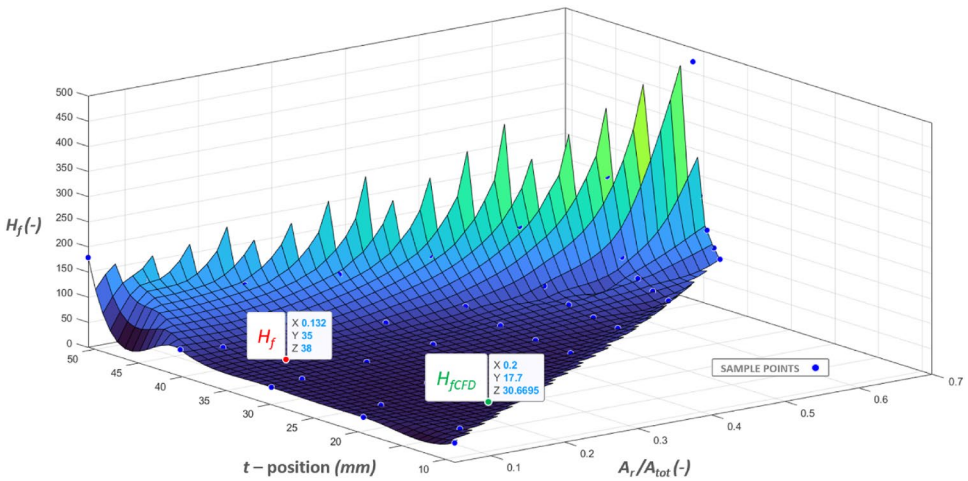

Fig. 13 Power loss factor cubic interpolation of results obtained from CFD analysis with highlighted minimal power loss factor for 2-parameter optimization (H_{fCFD}) and using 1-parameter optimization (H_f) based on [16]

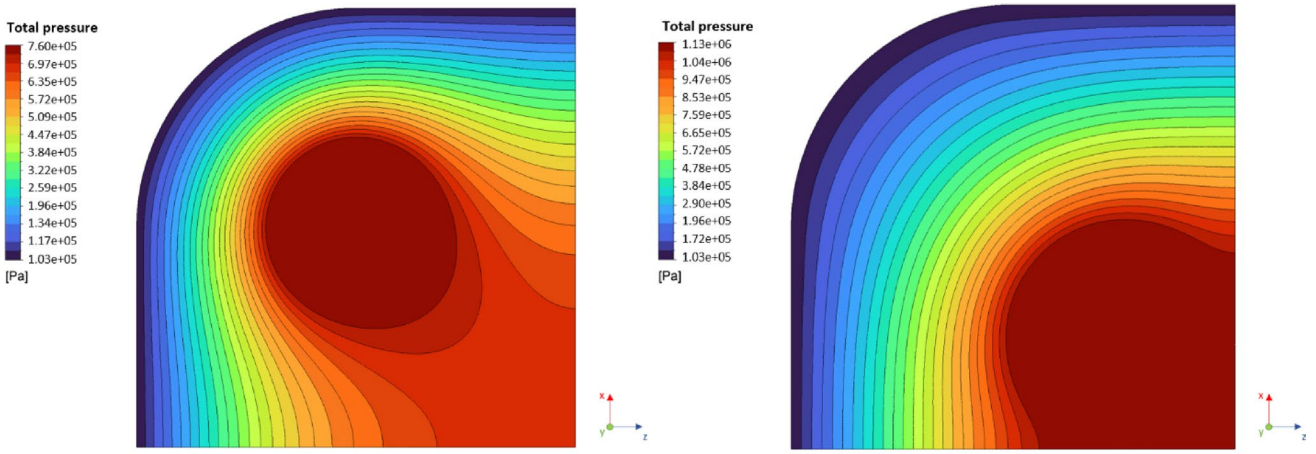

a t=35.00; D=28.00 **b** t=17.66; D=35.32

Fig. 14 Top plane static pressure contours of optimized pad shapes using **a** one-parameter approach and **b** novel two-parameter approach

pad center compared to the two-parameter approach, which also resulted in higher recess pressure due to larger sealing edge. As can be seen in the comparison of the two pressure contours (Fig. 14), the one-parameter approach performed with pressure decrease in the central area, while the two-parameter approach showed uniform pressure among the four recesses. This has also been observed in all two-parameter approach pressure contours as seen in Fig. 11. The results indicate that the proposed method provides more uniform pressure distribution and contributes to higher bearing load capacity, stiffness, and ability to carry asymmetrical loading and pad misalignment. The only drawback of this geometry might be worsened ability to assess the behavior of each of the recesses separately. Nonetheless, discharge grooves can be added to solve this issue [26].

4 Conclusion

This paper presents a novel approach to HS multi-recess thrust bearing pad geometry optimization using results based on CFD simulations. The precision of the CFD model was compared to the analytical and experimental results. The proposed two-parameter criterion was used to evaluate the optimal shape—recess position and recess area-to-pad area ratio. The obtained results from two-parameter optimization show a possible 20% power loss factor reduction, which is directly related to pumping power loss, compared to the case of conventionally used one-parameter criterion. Moreover, it has been observed that the position of the recess has a strong influence on the resulting performance and thus the size and position should be evaluated independently. The pressure contours indicate that the proposed two-parameter method provides more even pressure distribution in the central area of the pad, resulting in higher load capacity, stiffness, and ability to manage asymmetrical loading and pad misalignment. The optimization scheme tailored for best performance at lowest energetic requirements can be used for various shapes with custom defined geometric parameters. The proposed method might bring about a notable reduction in the energetic demands, especially for bearings of large-scale structures. Although in the presented study a cross-symmetrical four recess HS bearing pad geometry was optimized, this approach can be applied to any shape of HS bearing and a wide range of operating conditions—from very low to extremely high loads and recess pressures. It is necessary to determine the area ratio and position of the recess grooves first, then perform CFD analysis of selected design points, and find the minimal power loss factor. The drawback of the presented method is the computational time required to evaluate all design points, which nonetheless, depends on the machine used for simulations.

Further research might aim at full experimental evaluation of the presented 3D optimization graphs. The next steps might lead to the preparation of 3D optimization graphs for the mostly used bearing pad geometries to improve the design process of HS bearings. This approach could be used also for journal HS bearings. The precision of the model presented in this article could be further improved by considering the influence of sliding speed and thermal effects and sliding surface geometric precision (i.e., manufacturing and assembly errors). Very little attention has been paid to the structural deformation of the slider/turntable caused by the pressurized fluid flow. An experimental verification of real effects on bearing performance would provide valuable information for design engineers.

Author contributions M.M. wrote the main manuscript text and managed experiments. M.O. and J.Ch. prepared and carried out CFD analyses. M.S. and P.Z. carried out the experiments. P.S. supervised and managed the research. R.J. provided support in numerical modeling. All authors reviewed the manuscript.

Funding Open access publishing supported by the National Technical Library in Prague. This research was carried out under the project FW03010357 with financial support from the state budget by the Technology Agency of the Czech Republic and the Ministry of Industry and Trade within the TREND Program. Michal Michalec would like to thank Prof. Michel Fillon (University of Poitiers, FR) for assistance and comments that greatly improved the manuscript.

Declarations

Conflict of interest The authors declare no competing interests.

References

1. Michalec, M., Svoboda, P., Křupka, I., Hartl, M.: A review of the design and optimization of large-scale hydrostatic bearing systems. Eng. Sci. Technol. an Int. J. (2021). https://doi.org/10.1016/j.jestch.2021.01.010
2. Rowe, W.B.: Advances in hydrostatic and hybrid bearing technology. Proc. Inst. Mech Eng. Part C J. Mech. Eng. Sci. **203**, 225–242 (1989). https://doi.org/10.1243/PIME_PROC_1989_203_110_02
3. Sheehan, M., Gunnels, S., Hull, C., Kern, J., Smith, C., Johns, M., Shectman, S.: Progress on the structural and mechanical design

of the Giant Magellan Telescope. Ground-based Airborne Telesc. IV. **8444**, 84440N (2012). https://doi.org/10.1117/12.926469
4. Jang, S.-H., Choi, Y.-H., Kim, S.-T., An, H.-S., Choi, H.-B., Hong, J.-S.: Development of core technologies of multi-tasking machine tools for machining highly precision large parts. J. Korean Soc. Precis. Eng. **29**, 129–138 (2012). https://doi.org/10.7736/kspe.2012.29.2.129
5. Liming, Z., Yongyao, L., Zhengwei, W., Xin, L., Yexiang, X.: A review on the large tilting pad thrust bearings in the hydropower units. Renew. Sustain. Energy Rev. **69**, 1182–1198 (2017). https://doi.org/10.1016/j.rser.2016.09.140
6. De Pellegrin, D.V., Hargreaves, D.J.: An isoviscous, isothermal model investigating the influence of hydrostatic recesses on a spring-supported tilting pad thrust bearing. Tribol. Int. **51**, 25–35 (2012). https://doi.org/10.1016/j.triboint.2012.02.008
7. Bouyer, J., Wodtke, M., Fillon, M.: Experimental research on a hydrodynamic thrust bearing with hydrostatic lift pockets: Influence of lubrication modes on bearing performance. Tribol. Int. **165**, 107253 (2022). https://doi.org/10.1016/J.TRIBOINT.2021.107253
8. Dhanola, A., Garg, H.C.: Tribological challenges and advancements in wind turbine bearings: A review. Eng. Fail. Anal. **118**, 104885 (2020). https://doi.org/10.1016/j.engfailanal.2020.104885
9. Rajasekhar Nicodemus, E., Sharma, S.C.: Orifice compensated multirecess hydrostatic/hybrid journal bearing system of various geometric shapes of recess operating with micropolar lubricant. Tribol. Int. **44**, 284–296 (2011). https://doi.org/10.1016/j.triboint.2010.10.026
10. Gao, S., Shang, Y., Gao, Q., Lu, L., Zhu, M., Sun, Y., Yu, W.: CFD-based investigation on effects of orifice length–diameter ratio for the design of hydrostatic thrust bearings. Appl. Sci. (2021). https://doi.org/10.3390/app11030959
11. Chen, D.C., Chen, M.F., Pan, C.H., Pan, J.Y.: Study of membrane restrictors in hydrostatic bearing. Adv. Mech. Eng. (2018). https://doi.org/10.1177/1687814018799604
12. Rehman, W.U., Yuanxin, L., Guiyun, J., Yongqin, W., Yun, X., Iqbal, M.N., Zaheer, M.A., Azhar, I., Elahi, H., Xiaogao, Y. (2017) Control of an oil film thickness in a hydrostatic journal bearing under different dynamic conditions. Proc. 29th Chinese Control Decis. Conf. CCDC 2017. https://doi.org/10.1109/CCDC.2017.7979395
13. Liu, Z.F., Wang, Y.M., Cai, L.G., Zhao, Y.S., Cheng, Q., Dong, X.M.: A review of hydrostatic bearing system: Researches and applications. Adv. Mech. Eng (2017). https://doi.org/10.1177/1687814017730536
14. He, K., Wang, L.: A review of energy use and energy-efficient technologies for the iron and steel industry. Renew. Sustain. Energy Rev. **70**, 1022–1039 (2017). https://doi.org/10.1016/j.rser.2016.12.007
15. Okabe, E.P.: Analytical model of a tilting pad bearing including turbulence and fluid inertia effects. Tribol. Int. **114**, 245–256 (2017). https://doi.org/10.1016/j.triboint.2017.04.030
16. Loeb, A.M., Rippel, H.C.: Determination of optimum proportions for hydrostatic bearings. ASLE Trans. **1**, 241–247 (1958). https://doi.org/10.1080/05698195808972336
17. Loeb, A.M.: The determination of the characteristics of hydrostatic bearings through the use of the electric analog field plotter. A S L E Trans. **1**, 217–224 (1958). https://doi.org/10.1080/05698195808972333
18. Rippel, H.: Cast bronze hdyrostatic bearing design manual. Cast Bronze Institute, inc., Cleveland (1969)
19. Khonsari, M.M., Booser, R.E.: Applied tribology. (1970)
20. Bassani, R., Piccigallo, B.: Hydrostatic lubrication. Tribol. Ser. 22, (1992)
21. Chikurov, N.G.: Modeling of hydrostatic bearings by electrical analogy. Russ. Eng. Res. **37**, 517–522 (2017). https://doi.org/10.3103/S1068798X17060107
22. Fedorynenko, D., Sapon, S., Boyko, S., Urlina, A.: Increasing of energy efficiency of spindles with fluid bearings. Acta Mech. Autom. **11**, 204–209 (2017). https://doi.org/10.1515/ama-2017-0031
23. Doshi, N., Bambhania, M.: Optimization of Film thickness for hydrostatic circular pad bearing used in V-25 vertical turning machine. Int. J. Mech. Eng. Robot. (2013). https://doi.org/10.1453/IJMER/21
24. Li, X., Wang, X., Li, M., Ma, Y., Huang, Y.: The research status and progress of heavy/large hydrostatic thrust bearing. Adv. Mech. Eng. (2014). https://doi.org/10.1155/2014/982584
25. Solmaz, E., Babalik, F.C., Öztürk, F.: Multicriteria optimization approach for hydrostatic bearing design. Ind. Lubr. Tribol. **54**, 20–25 (2002). https://doi.org/10.1108/00368790210415338
26. Kozdera, M., Drbáková, S.: Numerical modelling of the flow in the annular multi-recess hydrostatic thrust bearing using CFD methods. EPJ Web Conf (2013). https://doi.org/10.1051/epjconf/20134501051
27. Xu, X., Shao, J., Yang, X., Zang, Y., Yu, X., Gao, B.: Simulation on multi-oil-cavity and multi-oil-pad hydrostatic bearings. Appl. Mech. Mater. **274**, 274–277 (2013). https://doi.org/10.4028/www.scientific.net/AMM.274.274
28. Snyder, T., Braun, M.: Comparison of perturbed Reynolds equation and CFD models for the prediction of dynamic Coefficients of sliding bearings. Lubricants (2018). https://doi.org/10.3390/lubricants6010005
29. Sharma, S.C., Sinhasan, R., Jain, S.C., Singh, N., Singh, S.K.: Performance of hydrostatic/hybrid journal bearings with unconventional recess geometries. Tribol. Trans. **41**, 375–381 (1998). https://doi.org/10.1080/10402009808983761
30. Fillon, M., Wodtke, M., Wasilczuk, M.: Effect of presence of lifting pocket on the THD performance of a large tilting-pad thrust bearing. Friction. **3**, 266–274 (2015). https://doi.org/10.1007/s40544-015-0092-4
31. Raud, X., Fillon, M., Helene, M.: Numerical modelling of hydrostatic lift pockets in hydrodynamic journal bearings—Application to low speed working conditions of highly loaded tilting pad journal bearings. Mech. Ind. **14**, 327–334 (2013). https://doi.org/10.1051/meca/2013073
32. Cui, C., Guo, T., Wang, Y., Dai, Q.: Research on carrying capacity of hydrostatic slideway on heavy-duty gantry CNC machine. AIP Conf. Proc. (2017). https://doi.org/10.1063/14982524
33. Wasilczuk, M., Wodtke, M., Dabrowski, L.: Field tests on hydrodynamic and hybrid operation of a bidirectional thrust bearing of a pump-turbine. Lubricants (2017). https://doi.org/10.3390/lubricants5040048
34. Wodtke, M., Schubert, A., Fillon, M., Wasilczuk, M., Pajaczkowski, P.: Large hydrodynamic thrust bearing: Comparison of the calculations and measurements. Proc. Inst Mech. Eng. Part J J. Eng. Tribol. **228**, 974–983 (2014). https://doi.org/10.1177/1350650114528317
35. Helene, M., Arghir, M., Frene, J.: Numerical study of the pressure pattern in a two-dimensional hybrid journal bearing recess, laminar, and turbulent flow results. J. Tribol. **125**, 283–290 (2003). https://doi.org/10.1115/1.1537233
36. Ghezali, F., Bouzidane, A., Thomas, M.: 3D Numerical investigation of pressure field of an orifice compensated hydrostatic bearing. Mech. Ind. (2017). https://doi.org/10.1051/meca/2016008
37. Horvat, F.E., Braun, M.J.: Comparative experimental and numerical analysis of flow and pressure fields inside deep and shallow pockets for a hydrostatic bearing. Tribol. Trans. **54**, 548–567 (2011). https://doi.org/10.1080/10402004.2011.575535

38. Shen, F., Chen, C.L., Liu, Z.M.: Effect of pocket geometry on the performance of a circular thrust pad hydrostatic bearing in machine tools. Tribol. Trans. **57**, 700–714 (2014). https://doi.org/10.1080/10402004.2014.906694
39. Du, Y., Mao, K., Liu, H., Mao, X., Li, Z.: A simplified analytical method for the pressure of tilt hydrostatic journal bearing. Ind. Lubr. Tribol. **70**, 993–1001 (2018). https://doi.org/10.1108/ILT-03-2017-0077
40. Guo, Z., Hirano, T., Kirk, R.G.: Application of CFD analysis for rotating machinery—Part I: Hydrodynamic, hydrostatic bearings and squeeze film damper. J. Eng. Gas Turbines Power. **127**, 445–451 (2005). https://doi.org/10.1115/1.1807415
41. Shao, J.-p, Liu, G.-d, Xiaodong, Y.: Simulation and experiment on pressure field characteristics of hydrostatic hydrodynamic hybrid thrust bearings. Ind. Lubr. Tribol. **71**, 102–108 (2019). https://doi.org/10.1108/ILT-02-2018-0063
42. Childs, D.W., Esser, P.: Measurements Versus predictions for a hybrid (Hydrostatic Plus Hydrodynamic) Thrust bearing for a range of orifice diameters. J. Eng. Gas Turbines Power-Trans. Asme. (2019). https://doi.org/10.1115/1.4042721
43. Fesanghary, M., Khonsari, M.M.: On the optimum groove shapes for load-carrying capacity enhancement in parallel flat surface bearings: Theory and experiment. Tribol. Int. **67**, 254–262 (2013). https://doi.org/10.1016/j.triboint.2013.08.001
44. Schmelzer, J.W.P., Zanotto, E.D., Fokin, V.M.: Pressure dependence of viscosity. J. Chem. Phys. (2005). https://doi.org/10.1063/11851510
45. Michalec, M., Polnický, V., Foltýn, J., Svoboda, P., Šperka, P., Hurník, J.: The prediction of large-scale hydrostatic bearing pad misalignment error and its compensation using compliant support. Precis. Eng. **75**, 67–79 (2022). https://doi.org/10.1016/j.precisioneng.2022.01.011
46. Richardson, L.F.: The approximate arithmetical solution by finite differences of physical problems involving differential equations, with an application to the stresses in a masonry dam. Philos. Trans. R. Soc. London. Ser. A, Contain Pap. a Math. or Phys. Character. **210**, 307–357 (1911). https://doi.org/10.1098/rsta.1911.0009

Precision Engineering 75 (2022) 67–79

Contents lists available at ScienceDirect

Precision Engineering

journal homepage: www.elsevier.com/locate/precision

The prediction of large-scale hydrostatic bearing pad misalignment error and its compensation using compliant support

Michal Michalec *, Vojtěch Polnický, Jan Foltýn, Petr Svoboda, Petr Šperka, Jakub Hurník

Institute of Machine and Industrial Design, Faculty of Mechanical Engineering, Brno University of Technology, Technická 2896/2, Brno, 616 69, Czech Republic

ARTICLE INFO

Keywords:
Hydrostatic lubrication
Multi-pad hydrostatic bearing
Large-scale bearings
Geometric errors
Compliant support
Support stiffness estimation

ABSTRACT

Hydrostatic bearings offer numerous advantages in large-scale moving mechanisms and structures. Nonetheless, the limits of manufacturing, transportation, and assembly in such scales are often encountered. The manufacturing and assembly errors significantly influence the hydrostatic bearing's overall performance. Therefore, it is desirable to compensate the resulting errors and pad misalignment of the hydrostatic multi-pad bearing. Previous research dealt with accuracy improvement and error prediction of small hydrostatic guideways. A little attention was aimed at the use of compliant materials for pads, but this area did not develop any further. The present study offers a methodology on how to estimate allowed assembly errors based on the analysis of the influence of manufacturing errors on the bearing's performance. Additionally, this article describes effects of the compliant support on assembly errors of hydrostatic multi-pad bearings. The proposed prediction is compared with experimental measurements on a hydrostatic bearing experimental rig. The effects of compliant support for a hydrostatic bearing can significantly increase the allowed error as compared to the usual rigid support. Furthermore, the experimental results indicate that the prediction of performance influence based on a known manufacturing error could be used for the hydrostatic bearing's performance improvement. The obtained results might help to enhance the design process of a hydrostatic bearing and improve its performance and extend the lifetime.

1. Introduction

The hydrostatic bearings have been known since 1851 when the first hydraulic bearing was introduced with the invention of L. D. Girard [1] – a pressurized water-fed bearing. By 1918, the equations for load, flow, and friction had been compiled by Lord Rayleigh [2]. In 1923, Hodgekinson [1] patented a bearing with pockets fed through restrictors. Recently, numerous investigations have been carried out to improve the performance of hydrostatic bearings, and the trend shows that it is still a topical issue [3,4]. Hydrostatic bearings operate on the principle of supplying pressurized fluid from an external source, a hydraulic pump, in between two sliding surfaces [5–7]. The hydrostatic bearing consists of a pad and equally important part – a hydraulic unit which secures a continuous supply of pressurized lubricant fed through inlet holes. The sliding surfaces are divided by a relatively small lubricating gap (Fig. 1), typically around 10–100 μm [6], and are completely separated at all speeds [8], even at standstill. This theoretically results in zero wear of the sliding surfaces [8] and a very low coefficient of friction, caused only by the viscous forces of the lubricant. The main disadvantage increasing the initial and operational cost is the need of an external hydraulic circuit and its regular maintenance.

The ability to transfer high loads, operate at zero speed, and vibration damping are highly desirable, and therefore, hydrostatic bearings are used in a wide range of industrial applications, ranging from large structures and machines to small ultraprecise mechanics [1]. Large-scale bearings diameters ranging from 2000 mm up to above 10 000 mm [2] are reaching the limit of technological possibilities due to manufacturing and transportation. The hydrostatic bearing offers high precision positioning of heavy structures since there is no solid-solid contact and thus no unwanted stick-slip effect [3,4]. Because of the high precision of hydrostatic bearings, they were used for nuclear structure analysers [5], antennas [1], large telescopes, such as the Giant Magellan Telescope [6], and hybrid bearings for water energetics [7]. This type of bearing provides high stiffness, low wear, and fair vibration isolation; therefore, hydrostatic bearings are also widely used in heavy machining tools [8,9]. Other applications might include turntables and rotary parts of large-scale machines, such as boring and digging machines or trains, stage and showroom rotation structures and guideways. The slider deformations under high loads of large-scale structures play a major role;

* Corresponding author.
E-mail address: michal.michalec@vut.cz (M. Michalec).

https://doi.org/10.1016/j.precisioneng.2022.01.011
Received 22 September 2021; Received in revised form 20 January 2022; Accepted 27 January 2022
Available online 29 January 2022

Nomenclature

A	cross section of pad
E	error
E_A	assembly errors
E_E	structural deformation caused by thermal effects
E_M	manufacturing errors
E_S	structural deformation caused by external forces
E_T	total errors
F	bearing load
N_p	number of pads of the bearing
N_{SB}	number of compliant supports supporting each pad
P_r	recess pressure
P_{atm}	atmospheric pressure
Q	supplied oil flow
h	film thickness
k	stiffness
k_{SB}	stiffness of silentblock
k_T	total stiffness of compliant HS pad
q_f	flow factor
x	deformation
x_A	maximum error tolerance
x_{AC}	maximum error tolerance of compliant support
x_{AR}	maximum error tolerance of rigid support
x_F	lubricating film maximum error tolerance
x_{SR}	rigid support maximum error tolerance
x_{SC}	compliant support maximum error tolerance
δ	height difference error
θ	angular error
μ	dynamic viscosity

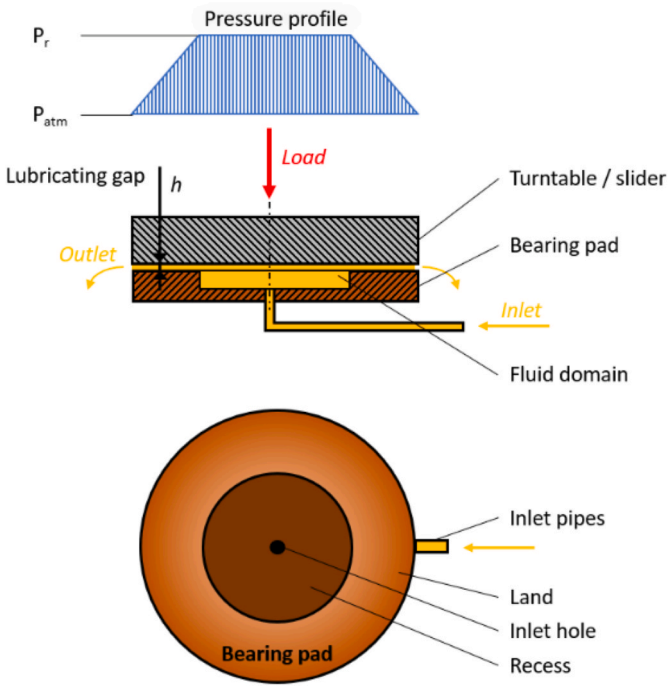

Fig. 1. Longitudinal cross section of the bearing (contact) with fluid pressure profile, and top view of the bearing pad.

thus the elastic and plastic structural deformation should not be neglected in the design process. Inaccuracies can be caused by dynamic or eccentric loading and local overloading (e.g., during machining) [10], uncontrolled lubricant temperature increase, workpiece heating [11] or dynamic ambient temperature change, and other effects, such as flow instability [12–15].

Widely used methods for the determination of the sliding surface structural deformations during the design process are fluid dynamics and fluid-structure interaction (FSI) [16]. An advancement to those methods is thermohydrodynamic (THD) that was used for the investigation of the bearing performance characteristics considering the manufacturing tolerances either for steady-state or dynamic analyses [17,18] of high-speed hydrodynamic (HD) applications as hydrostatic bearings are often used as hybrid bearings to achieve wear-free lift-off during the start and stop procedures in large HD bearings [19].

Geometric imperfections, such as manufacturing and assembly errors, significantly influence the bearing's performance [20]. For example, non-parallelism of the sliding surfaces might cause an uneven pressure distribution across the pad width or undesired film thickness decrease. Rajput and Sharma's [21] numerical investigation showed that the combined effect of shape and misalignment significantly contributed to film thickness reduction. Therefore, it is necessary to inspect the manufactured surfaces to avoid the undesired decrease of the bearing's performance [22]. Emerging trends in numerical compensation [23] provide higher accuracy and efficiency, especially in precision manufacturing. As Cappa et al. [24] proposed, the deviation could be reduced by increasing the number of feedholes, although the increased number of inlets might undesirably raise pressure losses. There have been proposed several models for numerical modelling of motion errors of hydrostatic bearings [25–27] that can be used for performance optimization. However, it is often problematic to determine the allowable manufacturing and assembly tolerances during the design stage of hydrostatic bearings to achieve the desired performance.

A discrete part tolerance analysis [28] might be useful to determine the worst-case scenario and it is preferred in small-scale manufacturing. However, statistical methods are highly emphasised [29] for the whole manufacturing process precision and efficiency improvement. Every tolerance analysis method has its pros and cons, but it is obvious that 3D tolerance analyses [30] allow an investigation of manufacturing deviations and more versatile postprocessing. Recent improvements in image processing allow a deviation investigation of sizeable sites [31] and large-scale structures [32] with satisfactory precision. Qi et al. [33] proposed a method for predicting the hydrostatic guide error based on the measured 3D profile, indicating that the part error might be processed with improved accuracy and more information about its shape.

Misalignment of the bearing pads might affect the performance significantly [20], which is greater in the case of non-recessed hydrostatic bearings [34]. However, the hydrostatic bearing pad misalignment is especially dangerous in large-scale structures. Although the misalignment of journal bearings might slightly improve the load-carrying capacity at higher speeds [35], it also decreases the film thickness dramatically. And it is even more dangerous in the case of low-speed hybrid bearings where the wedge can certainly not generate enough lifting force to make the lubricating film thicker, and the hydrostatic bearing misaligned surfaces cannot support the load equally to prevent the collision of the sliding surfaces. The effect of assembly errors might eventually lead to the sliding surfaces collision [36]. In the field of hydrostatic bearings, the latest improvements from the still-developing trend of Industry 4.0 and Internet of Things (IoT) [37–39] could be adapted. However, active regulation might significantly increase the initial cost and service demands. There are also different ways that allow tilting and height adjustment, such as a self-aligning hydrostatic bearing design [40], or a master-slave pad system [41], which also allow height adjustment or spherical mounting. These enable tilting according to

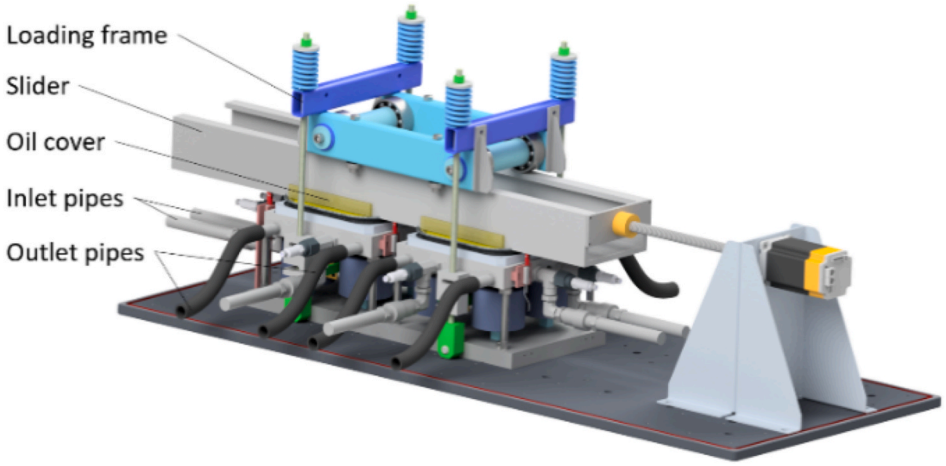

Fig. 2. Overview of the hydrostatic bearing experimental device.

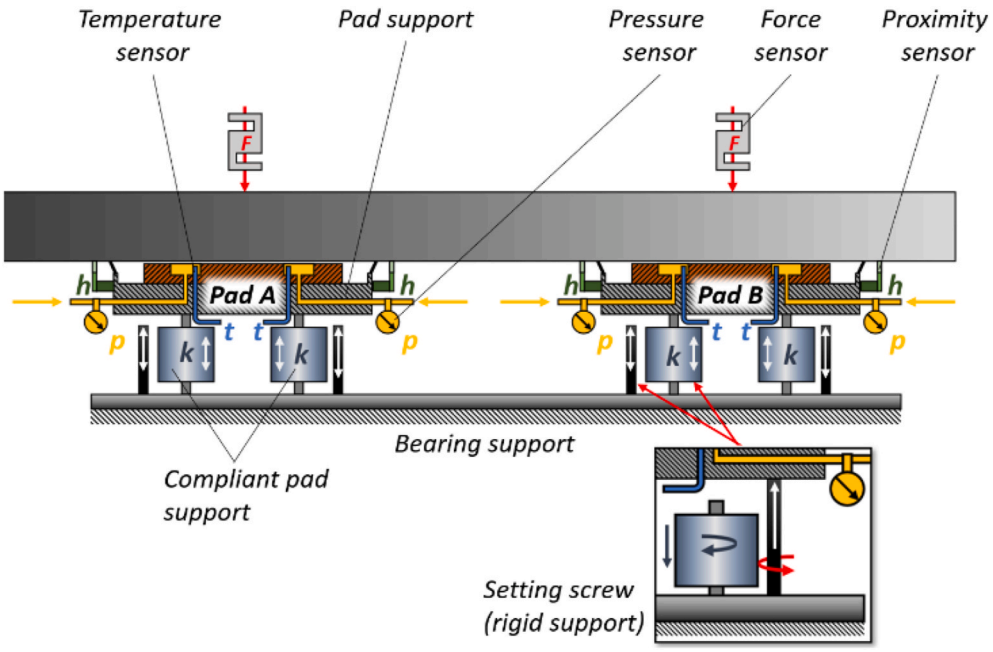

Fig. 3. Scheme of the whole hydrostatic bearing experimental device (cross section of the pad bodies).

slider shape and orientation. Nonetheless, the complexity of these systems could be significantly simplified by using elastic pad supports. The use of a compliant or elastic pad support [42] can improve the pressure profile even on non-parallel sliding surfaces. Van Beek et al. [43] studied the effect of the shape of the sliding elastic surface on the thickness of the lubricating film. Liang et al. [44] proposed an HD bearing with elastic support and verified the obtained experimental results with numerical simulations, which demonstrates the possibility of using the compliant support also for other types of bearings, including HD and plain bearings or sliding guideways. Lefanti et al. [45] studied the wear of elastomeric compliant pads at various loads and at various offsets. The results show that the critical factors determining the life of a compliant pad are the offset and the amount of deformation capacity for a given load, but its life can be increased by using a harder material. Frequently used natural rubber (NR) compliant pads provide low oil resistance [46]; nonetheless, oil resistance can be greatly improved by altering the chemical composition or careful sealing of possible oil leakage to achieve a proper and long-lasting function of the hydrostatic bearing.

This article aims at the issue of the effects of manufacturing and assembling large-scale axial hydrostatic bearings on their performance. Bearing pad misalignment and uneven pressure distribution can cause a decrease in load carrying capacity that might lead to sliding surface damage or eventually to failure. A possible solution to these problems could be the use of compliant support which enables misalignment compensation. However, it is crucial for the designer to determine the required stiffness of the compliant support for a certain load or what inaccuracies can be allowed for securing a proper function. The previous research aimed at hydrostatic bearing design and performance has not yet presented possible solutions to the above-mentioned issues; hence this article deals with answering these questions.

2. Materials and methods

In the following sections, the experimental setup and error measurements are described in detail. Subsequently, the allowable error estimation and compliant support stiffness calculation are presented and explained.

Table 1
Characteristics of used compliant pads.

Compliant pad	Stiffness
Soft	850 N/mm
Medium	1750 N/mm
Hard	3200 N/mm

2.1. Experimental setup

The experimental device (a dual-pad hydrostatic bearing tester) used for the investigation of the presented issue was developed at Tribology department of Institute of Machine and Industrial Design. The dual-pad tester shown in Fig. 2 is composed of two main parts – bearing pads and hydraulic supply. The hydrostatic bearing consists of a slider, a loading frame with springs to simulate the free weight, threaded rods with force sensors, oil inlet pipes from the hydraulic supply, outlet pipes for collected oil returning to an oil tank, and an oil cover with a compliant lip seal to prevent oil leakage. The dual-pad hydrostatic tester's maximum load capacity is 40 kN and it can also be used to perform dynamic tests (reciprocating motion). However, in this study only static tests were performed as we investigated the static performance of misaligned pads.

The dual-pad hydrostatic tester (Fig. 3) was specially designed for the experimental investigation of hydrostatic lubricating film behaviour between the slider and the misaligned pads. Both pads are mounted on the bearing support that is used for pad levelling and bedding of the loading frame. The pad misalignment can be created using setscrews or threaded ends of compliant pads. The reference height is set using 100 mm calibration rods with the precision of ±0.005 mm. The misalignment is created by adding normalised calibration plates.

Each of the hydrostatic bearing's pads could be supported by either a rigid base – a setting screw with large stiffness, or a compliant base made of four compliant pads with specific, much lower stiffness. The compliant support was made of compliant pads from natural rubber (NR) based on polyisoprene. Three sets of compliant pads with specific stiffnesses were used for the experiments (Table 1). The bearing pad levelling was performed before the experiment by threads on the compliant pad body or by the setting screw. The pads were loaded by the loading frame and threaded rods. The loading force was logged using four force sensors with 1 N resolution. The pressurized oil from the hydraulic supply was distributed to the recess by inlet holes in the pad support and its pressure was logged using pressure sensors with the resolution of 0.5 bar. The temperature of the lubricant significantly influences the resulting film thickness by the dynamic viscosity variation. Thus, temperature sensor probes were placed in each of the recesses of both pads, at such a height as to prevent a collision with the slider. The film thickness values were obtained using proximity sensors. Due to the relatively high misalignment in the range 0–4 mm, the resolution of proximity sensors was 0.01 mm.

All sensors are schematically shown in Fig. 4. There were four force sensors (F_1–F_4) on the threaded rods that allowed an accurate setting of

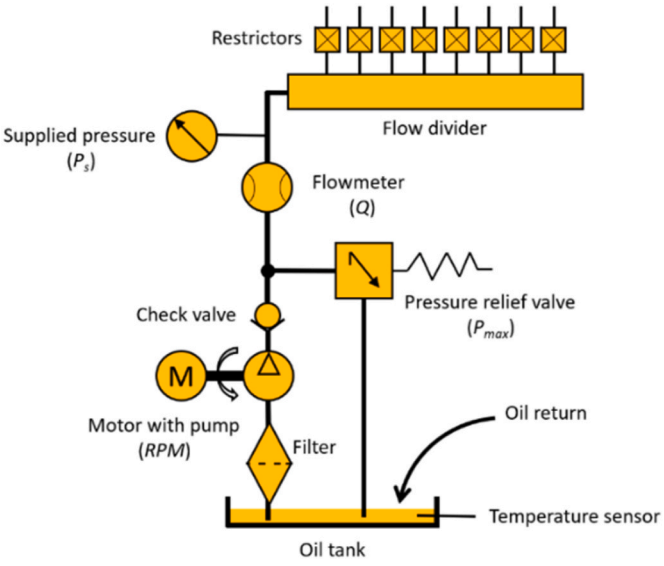

Fig. 5. Schematic representation of lubricant supply.

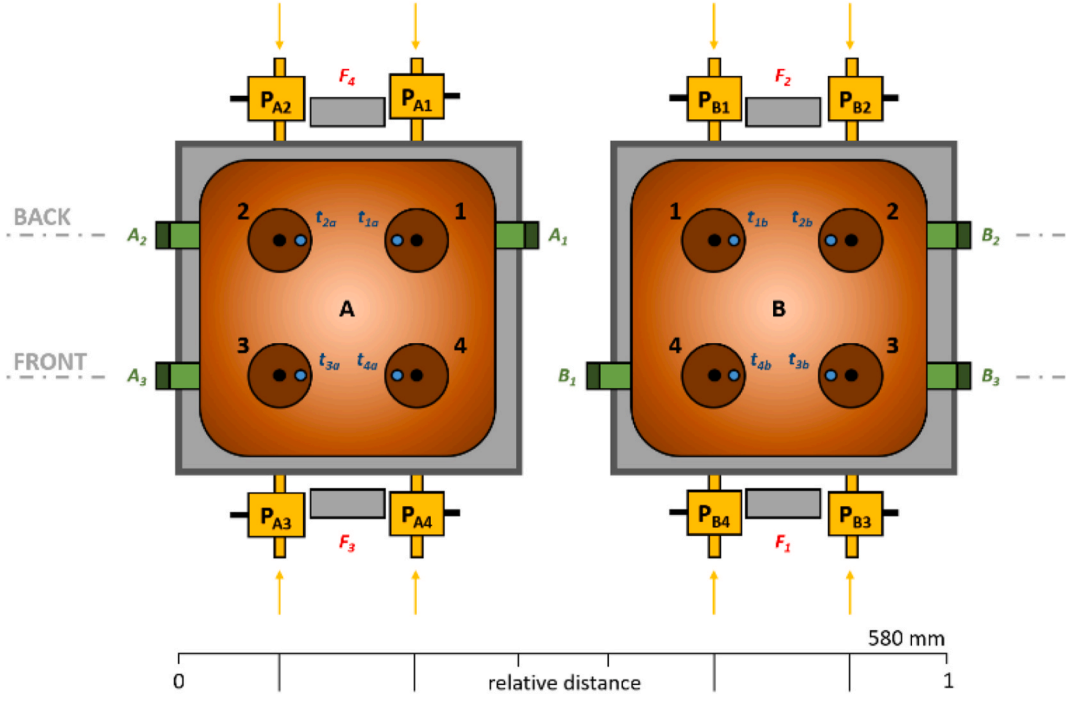

Fig. 4. Top view of hydrostatic pads with all sensors and relevant labels.

Table 2
Selected characteristics of hydraulic oil used in experiments.

Parameter	Range
Viscosity grade	ISO VG 46
Kinematic viscosity (at 40 °C)	46 mm/s^2
Density (at 15 °C)	875 kg/m^3
Dynamic viscosity (at 21 °C)	0.118 Pa s

the required loading force. The information about slider tilting was acquired by central proximity sensors (A_1 and B_1). The device was equipped with six proximity sensors, three on the left pad (A_1-A_3) and three on the right pad (B_1–B_3). The lubricant temperatures inside the recesses (1–4) of both left and right pads (t_{1a}-t_{4b}) provided the actual oil film temperature. The recess pressure was acquired using pressure sensors at the inlet of the recess, four for each pad (P_{A1}-P_{B4}). The total pad size was 180 × 180 mm with four recesses with the diameter of 36 mm and depth of 5 mm. Inlet holes with an 8 mm diameter are in the centres of each the recess grooves and are drilled onto a square 60 × 60 mm.

The hydraulic supply (Fig. 5) consisted of an oil tank with passive oil cooling. The oil was pumped through filters and the required flow was maintained using the motor rpm and a flowmeter. A pressure relief valve and a check valve were necessary safety elements. The supplied flow was distributed to each recess by a flow divider and an equally set needle restrictor for each of the recesses in both pads. The restrictor valves were all set to generate a pressure drop of approximately 1.5 bar per restrictor. The hydraulic supply working range was 0–20 l/min of total volumetric flow at the maximum pressure of 100 bar. After considering the experimental device operation range and the hydrostatic lubrication performance, sensor accuracy, and misalignment range, the hydraulic supply was set to the constant pressure inlet for 20 bar (primary condition) with an approximate 10 l/min total volumetric flow for both pads.

The lubricant used for the experiments was standard hydraulic oil of viscosity grade ISO VG 46 (Table 2). The selected oil was preferred due to its suitability for the hydraulic circuit and satisfactory characteristics for the overall hydrostatic bearing performance. The viscosity was measured using the HAAKE RotoVisco® 1 rotational viscosimeter (PSL Systemtechnik, Germany) filtered with 99.88% reliability using the Bingham rheological model. The dynamic viscosity dependence on the temperature shown in Fig. 6 was fitted using the Vogel-Fulcher equation with $R^2 = 99.89\%$.

2.2. Manufacturing error measurement

The slider's manufacturing imperfections were examined using the GOM ATOS III Triple Scan 8 MP optical 3D scanner (GOM – ZEISS

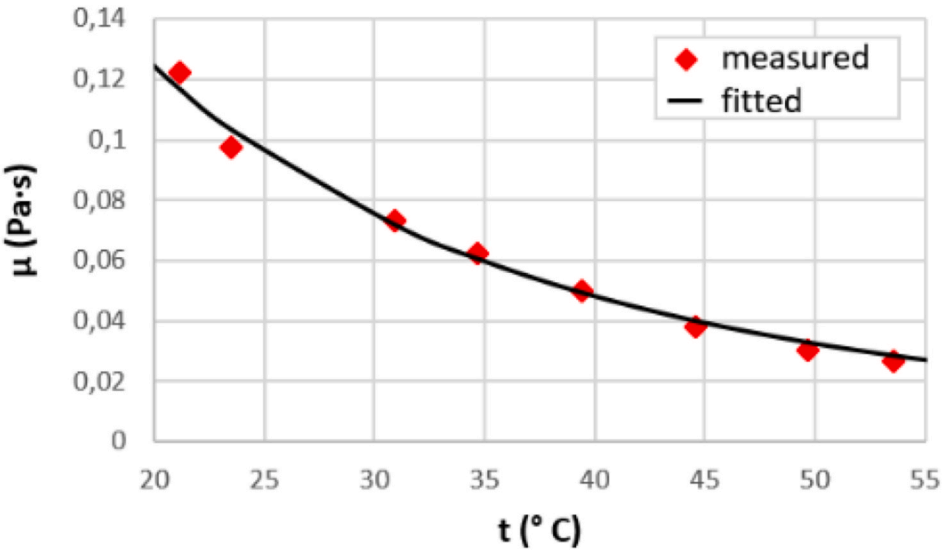

Fig. 6. Viscosity-temperature dependence of the used 46 viscosity grade hydraulic oil.

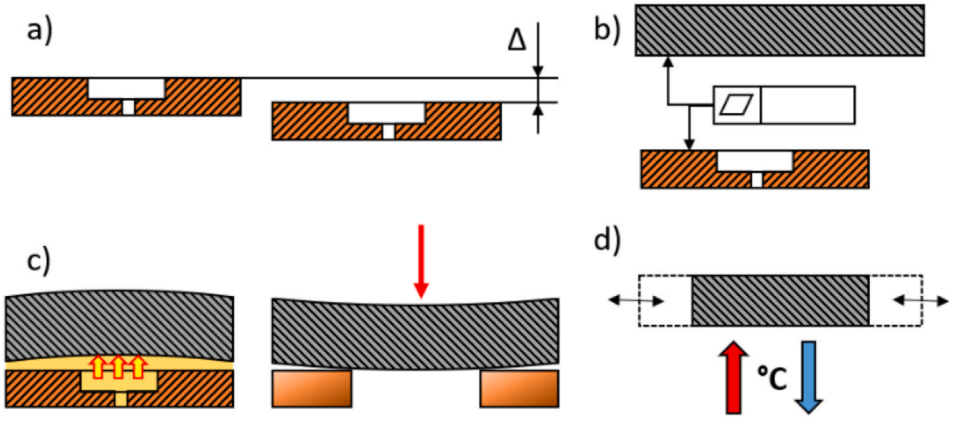

Fig. 7. Schematic representation of error types: a) assembly error represented as pad misalignment, b) contacting bodies flatness, c) slider deformation caused by pressurized fluid or local overload between pads, and d) thermal deformation of the slider.

Group, Germany). The scanner was used in an MV560 configuration (measurement volume 560 × 420 × 420 mm). According to the acceptance tests (VDI/VDE 2634 standard), the total maximum measurement errors were under 0.01 mm, which was satisfactory for this analysis. Before scanning, the part was covered with a thin titanium oxide layer to prevent reflection. The resulting mesh was refined and smoothed with a surface tolerance of less than 0.01 mm, which matches the scanner accuracy.

The pad sliding surface flatness was carried out using a digital micrometre with a 0.001 mm resolution. It is necessary to obtain the errors of contacting surfaces because the pads will be levelled on the sliding surfaces. However, the manufacturing errors of other parts and surfaces are not so important and therefore further not assumed in this study.

2.3. Allowable error estimation

To secure a proper function of the hydrostatic bearing, it is necessary to achieve high surface accuracy and flatness, and in case of multi-pad bearings the flatness among the pads as well. Additionally, other effects, such as structural deformation and environment dynamics, should not be neglected. The total error is then given as a sum of all expected errors:

$$E_T = \sum E \tag{1}$$

And if we assume the most frequent and significant errors, we get:

$$E_T = E_A + E_M + E_S + E_E \tag{2}$$

where:

***E_A* are assembly errors**, and the key parameter investigated in this study (Fig. 7 a), ***E_M* is an average manufacturing error of contacting surfaces** – slider and pad (Fig. 7 b), ***E_S* are structural deformations** caused by a local overload of the slider or by the pressurized fluid (Fig. 7 c), and.

***E_E* are deformations** caused by other effects, such as variable temperature (Fig. 7 d) of the environment.

The lubricating film and bodies of the pad must then be able to cover or compensate occurred total error E_T. To obtain a maximum error tolerance (the compensation range) value of the bearing, we can express it as a sum of the deformation of all bodies:

$$x_A = \sum x \tag{3}$$

The deformation of separate bodies can be obtained using the following formula:

$$x = \frac{F}{k} \tag{4}$$

where F is the local applied force per pad or the total applied force, and k is the stiffness of the body. Subsequently, the estimated value of the lubricating film stiffness can be obtained as change of the film thickness with the load change using eqn. (13). The resulting film stiffness is then as follows:

$$k = \frac{dF}{dh} \tag{5}$$

where dF is the force increment, and dh is the film thickness change. The maximum error tolerance for rigid support on setscrews:

$$x_{AR} = x_F + x_{SR} \tag{6}$$

where x_F is the lubricating film's maximum error tolerance (assumed as constant), and x_{SR} is the rigid support allowance (given by the setscrew). Then for the case of the experimental rig with compliant pads, we obtain the maximum error tolerance for compliant support as:

$$x_{AC} = x_F + x_{SC} \tag{7}$$

where x_{SC} is the compliant support maximum error tolerance (given by the compliant pad). And finally, a condition to determine whether the total error could be compensated:

$$x_A > E_T \tag{8}$$

The maximum error tolerance should be always higher than the total error to secure the proper function of the bearing and to prevent damage or failure. It is also possible to determine a specific error tolerance. For example, when we want to determine an approximate value of the maximum assembly error tolerance, we can express the equation to obtain the maximum assembly error tolerance in the following form:

$$E_A = \sum x - \sum E \tag{9}$$

$$E_A = x_A - (E_M + E_S + E_E) \tag{10}$$

2.4. Compliant support stiffness calculation

To be able to determine the stiffness of the compliant support, we can use the following expression:

$$k = \frac{F}{\delta} = \frac{F}{E_T} \tag{11}$$

where F is the applied force (including load given weight of the turntable) and δ is the required deformation that will compensate the occurred errors, in this case the total error (E_T). In the case of a pad supported by numerous supporting elements or rather compliant pads, the stiffness of one compliant pad can be estimated from the total required stiffness as follows:

$$k_{SB} = \frac{k_T}{N_P \cdot N_{SB}} \tag{12}$$

where N_P is the number of pads of the bearing and N_{SB} is the number of compliant pads supporting each pad.

A note for design engineers: it is necessary to consider the stroke of a deformed compliant pad in the loading direction in a some application to avoid malfunction because large deformations might occur at very high loads, especially in large-scale structures.

3. Results and discussion

Firstly, the initial measurements were conducted without any misalignment setup to determine the accuracy of the designed experimental device and compare it with the prediction. Then, measurements for all misalignment types that might occur were performed. And finally, the variations of the compliant pads' stiffnesses were compared.

3.1. Prediction evaluation

The film thickness prediction calculation was obtained using eqn. (13):

$$h = \sqrt[3]{\frac{12 \cdot Q \cdot \mu \cdot A}{F \cdot q_f}} \tag{13}$$

where h is the film thickness, Q is the lubricant flow to pad, μ is the dynamic viscosity, A the geometry coefficient, F is the applied load, and q_f is the flow factor (obtained from Ref. [47]). Because of the constant pressure at inlet condition, the feed volumetric flow decreased with the increasing load; therefore, the actual values obtained from the experimental device were used in the film thickness prediction calculation. The calculated values were compared with the experimental results that are shown in Fig. 8. The experiment was repeated six times to obtain

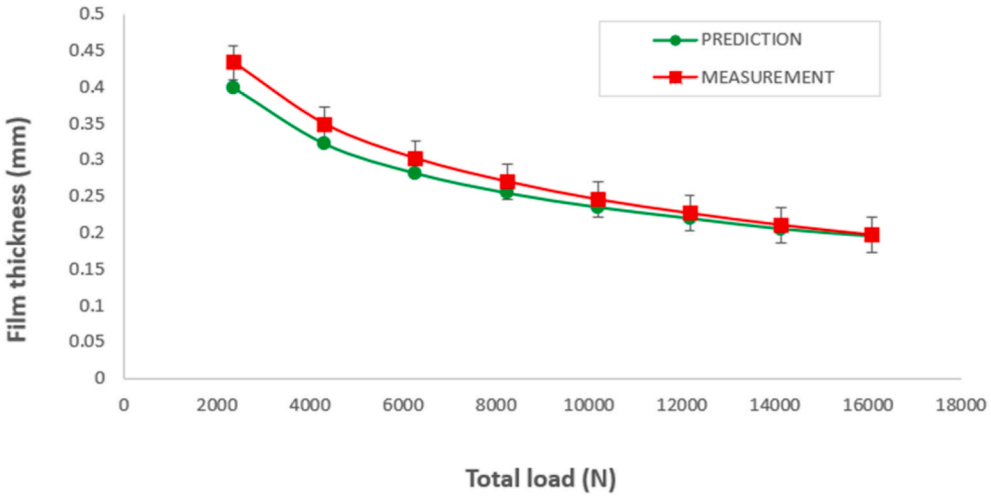

Fig. 8. Experimental and predicted film thickness dependence on total load.

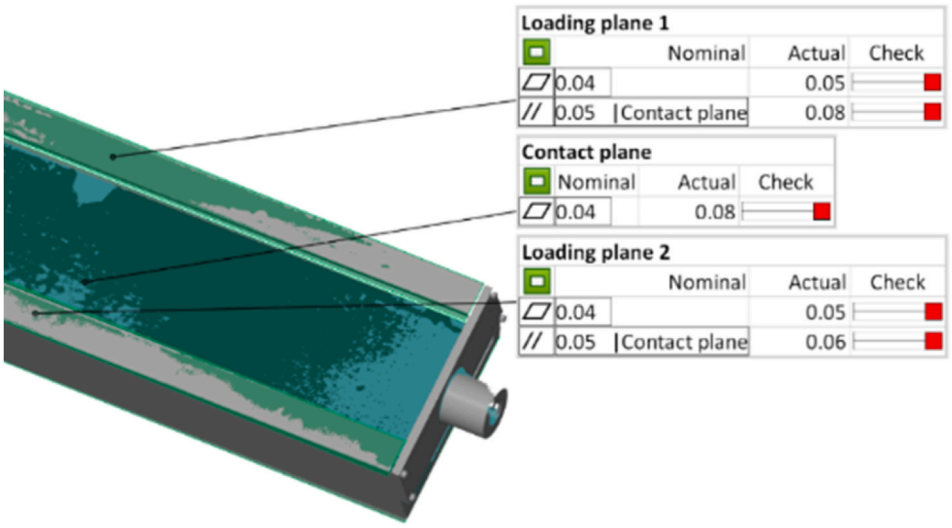

Fig. 9. Slider's manufacturing imperfections – nominal (demanded) tolerances and actual (measured, evaluated) values; red sign in "Check" column means that the actual value is out of tolerance. (For interpretation of the references to colour in this figure legend, the reader is referred to the Web version of this article.)

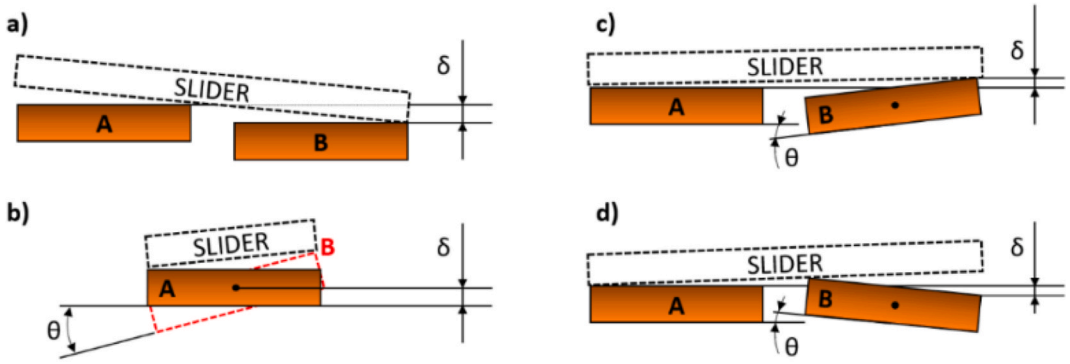

Fig. 10. Investigated misalignment error types: a) OFFSET, b) INCLINE, c) TILT1, and d) TILT2.

more reliable results, while the maximum standard deviation values reached 0.025 mm, which is in the range of the proximity sensor resolution. The measurement results show a good agreement with the predicted values of film thickness. The largest difference between the prediction and the measurement is visible in the range of lower loads, where the lubricating film demonstrated very low stiffness and pressure. Thus, the lubricating film between the sliding surfaces was probably not evenly distributed. However, around the load of 16 kN, the measurement results showed a good agreement with the prediction, and so this load was further applied in all xperiments.

Table 3
TILT and INCLINE rotation angle calculated from height difference.

δ [mm]	0.5	1	1.5	2	2.5	3	3.5	4
θ [°]	0.3	0.6	0.9	1.2	1.5	1.8	2.1	2.4

Table 4
Average recess pressure criteria values.

$$E_A = x_A - E_M \quad (14)$$

Bearing condition	Average recess pressure	Percentual value
Overload	5.67 bar	Higher than 102.5%
Normal	5.40 ± 0.135 bar	100% ± 2.5%
Failure	5.13 bar	Lower than 97.5%

For simplicity, E_S and E_E errors were not assumed in this study. The final estimated maximum assembly error tolerance was obtained as follows:

Table 5
Maximum allowed error according to the proposed prediction and experimental results for both MEDIUM compliant pad and RIGID supports.

Assembly error tolerance - E_A [mm]				
Error type	RIGID		COMPLIANT	
	Experimental	Prediction	Experimental	Prediction
OFFSET	max. 0.5	max. 0.05	max. 2.5	max. 1.72
INCLINE	max. 0.5		max. 3	
TILT 1	max. 0.35		1.5–2	
TILT 2	max. 0.4		1.5–2	

3.2. Manufacturing error measurement

The examined manufacturing imperfections are the contact plane flatness and the flatness and parallelism of loading planes. The parallelism of the mentioned planes was evaluated with respect to the contact plane. The resulting values were also compared with the demanded tolerances as shown in Fig. 9. The contact plane represents the sliding surface of a slider and loading planes transmit the applied load. The parallelism did not significantly affect the measurements because the springs mounted on the loading frame allow for an adjustment of the slider to the lubricating film layer. As for the contact plane, the actual flatness was smaller than the projected lubricating gap and its actual value (maximum deviation) 0.08 mm was considered in the total error calculation as the manufacturing error. The actual value of the pad's sliding surface flatness (maximum deviation) was 0.05 mm. The measured manufacturing errors of contacting surfaces were averaged, resulting in 0.065 mm manufacturing error that was used for the further calculations.

3.3. Assembly errors

When considering a multi-pad large-scale hydrostatic thrust bearing, several types of pad misalignment can emerge, mostly pad height difference and tilt. As seen in Fig. 10, several cases that we assume might be the most significant were selected. The first one is a pure height error – offset (Fig. 10 a), which must be set among all pads and cannot be fixed separately. Then, inclined pads (Fig. 10 b) in the perpendicular direction to the slider's moving direction. Finally, we investigated tilted pads in both senses of pad B's rotation (Fig. 10 c and d), which could cause a collision and a failure in the moving direction of the slider. In all experiments, pad A was the reference pad and pad B was misaligned towards pad A. Actual values of the rotation angles are listed in Table 3 for simpler determination of the angular misalignment errors – TILT and INCLINE.

The reference film thickness (h_0) without misalignment was set to approximately 0.15 mm (at least ten times the proximity sensor resolution). The supplied pressure was held constant at 20 bar as a primary condition of the hydraulics, thus forming constant pressure supply with a restricted flow. Considering that the load and supplied pressure are constant, the average recess pressure should not change. The reference operating recess pressure was chosen to be at least ten times the resolution of the pressure sensors. All measurements were repeated three times. The average recess pressure throughout all measurements was 5.4 bar with an average deviation of 0.012 bar. Thus, the evaluation criteria were set to average recess pressure of 5.4 bar ±2.5% (the reference pressure P_0), or a total of 5% of the total tolerance to cover the recess temperature that was in all experiments in the range of 25 ± 3 °C. The recess pressure increase would signal that the load is increasing. On the other hand, if the average recess pressure decreased under 97.5% of the normal value, this indicated that the load-carrying capacity was weakened and possibly the lubricating film might have started to collapse. Thus, the load could be partly carried by the hydrostatic pad edge in case of further decrease of the average recess pressure. All measurements were repeated four times, while the average deviation of the average recess pressure was under 2.5%. Therefore, if the average recess pressure value exceeded the 5% tolerance it was considered a failure. The actual value used for determining the hydrostatic bearing condition is listed in Table 4.

The predicted and experimentally obtained values of the maximum allowable error are listed in Table 5. The allowable error for rigid support was significantly lower compared to the compliant support with medium compliant pads. The experimental results show that the compliant support resulted in four to six times higher misalignment than the rigid support according to the average pressure evaluating criteria. The misalignment effect on performance might differ with the distance between the neighbouring pads – the larger the distance, the greater the misalignment. However, this could negatively influence the slider shape due to structural deformations.

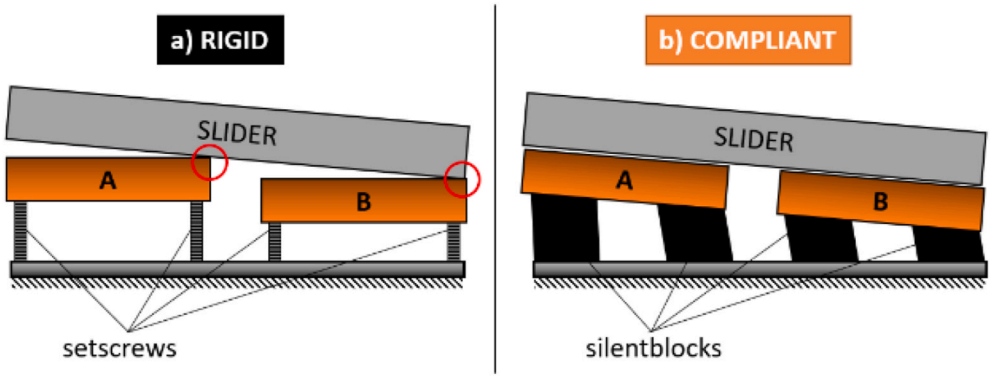

Fig. 11. Support behaviour of the misaligned hydrostatic pads with a) RIGID and b) COMPLIANT support.

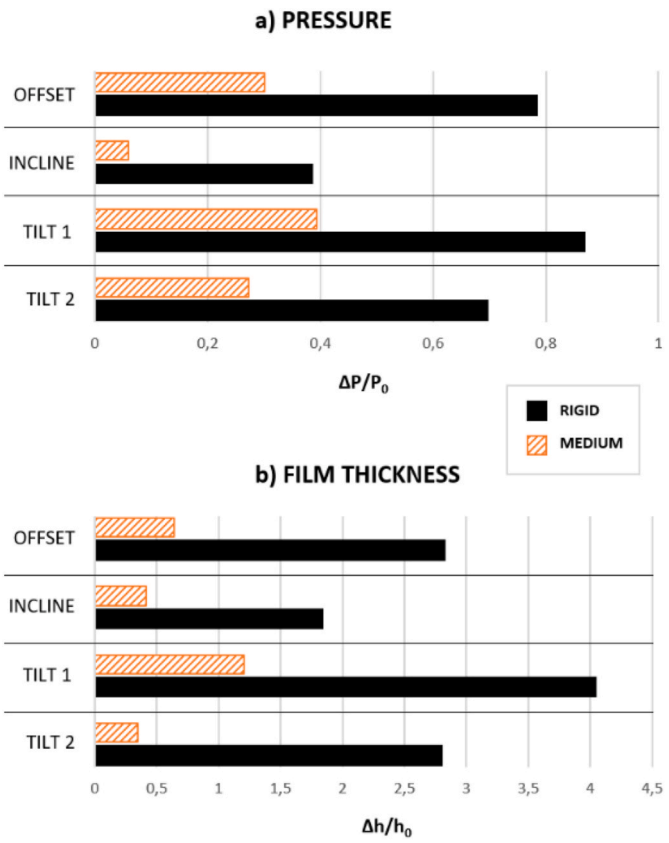

Fig. 12. Relative change of a) pressure and b) film thickness of rigid and compliant support (medium stiffness) for all studied misalignment types with 0.5 mm misalignment and 16 kN load.

The maximum allowed error of rigid support according to the prediction reached very low values compared to the experimental results, which was probably caused by considering the constant stiffness of the bolt. However, Lu et al. [48] proposed a new method for stiffness calculation considering the surface roughness where the stiffness increases gradually and approaches the traditional theory which assumes comparably higher values than the proposed method. Moreover, the rigid support was compensated with restrictors to some extent, and therefore the real allowed error was higher than predicted. However, the allowed error considering the restrictor depends on the operating conditions and was not investigated in this study. It is obvious that the maximum allowed error on compliant support is significantly higher either from the prediction or from the experimental measurement results. From the investigated error types, the INCLINE error seems to be less sensitive to the misalignment because effect on slider with is much smaller than along the slider between the two pads. The TILT and OFFSET errors might be a major issue for a moving slider in direction hitting the edge, either in hydrostatic or hybrid bearings during start and stop. From the obtained results, it is evident that in the compliant suport helps the pads to adjusts to the slider, as illustrated in Fig. 11.

The comparison of investigated misalignment types is shown in Fig. 12. To express the significance of the compliant support effect, the relative change of recess pressure to the initial recess pressure (with aligned sliding surfaces) was used as an evaluation criterion. Firstly, the difference was calculated for each sensor. Then the obtained values were divided by the initial film thickness, and then an average value was calculated. As shown in Fig. 12 a, the compliant pads adjusted to the occurred assembly error and caused a more even distribution of the pressurized fluid for at least twice in case of the TILT 2 error type, five times and eight times in case of the OFFSET and INCLINE errors respectively. TILT 1 did not show any significant difference with compliant pads in the recess pressure, which might be caused by a greater space for the slider deformation. A similar trend was observed with the film thickness relative change (Fig. 12 b). The INCLINE error type resulted in three times, TILT 2 3.8 times, TILT 1 twice, and the

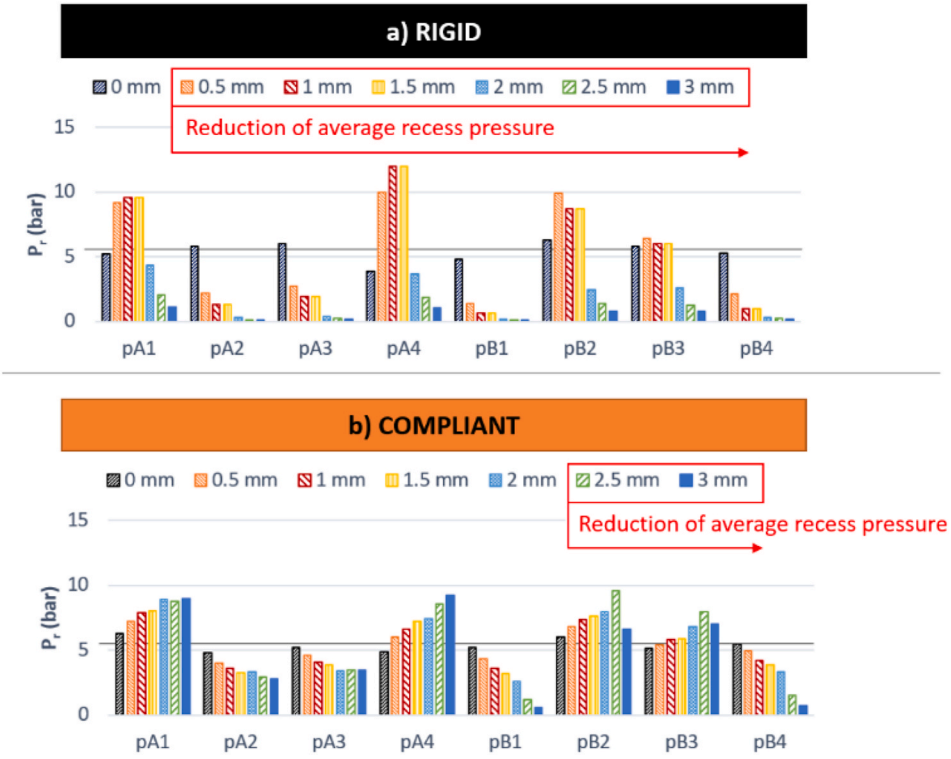

Fig. 13. Recess pressure values of OFFSET measurements for height difference δ (0, 0.5, 1, 1.5, 2, 2.5, and 3 mm) with a) RIGID and b) COMPLIANT (medium stiffness) support.

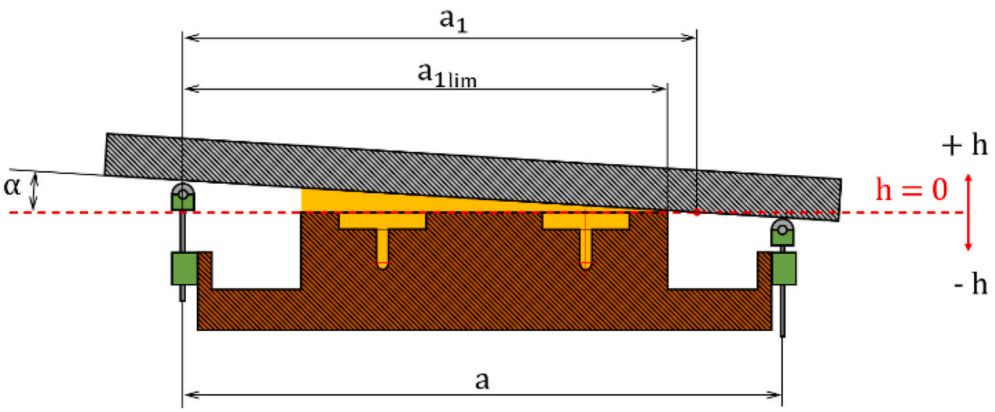

Fig. 14. Geometrical representation of the pad's geometry for film thickness evaluation (see Fig. 4. – front and back cross section).

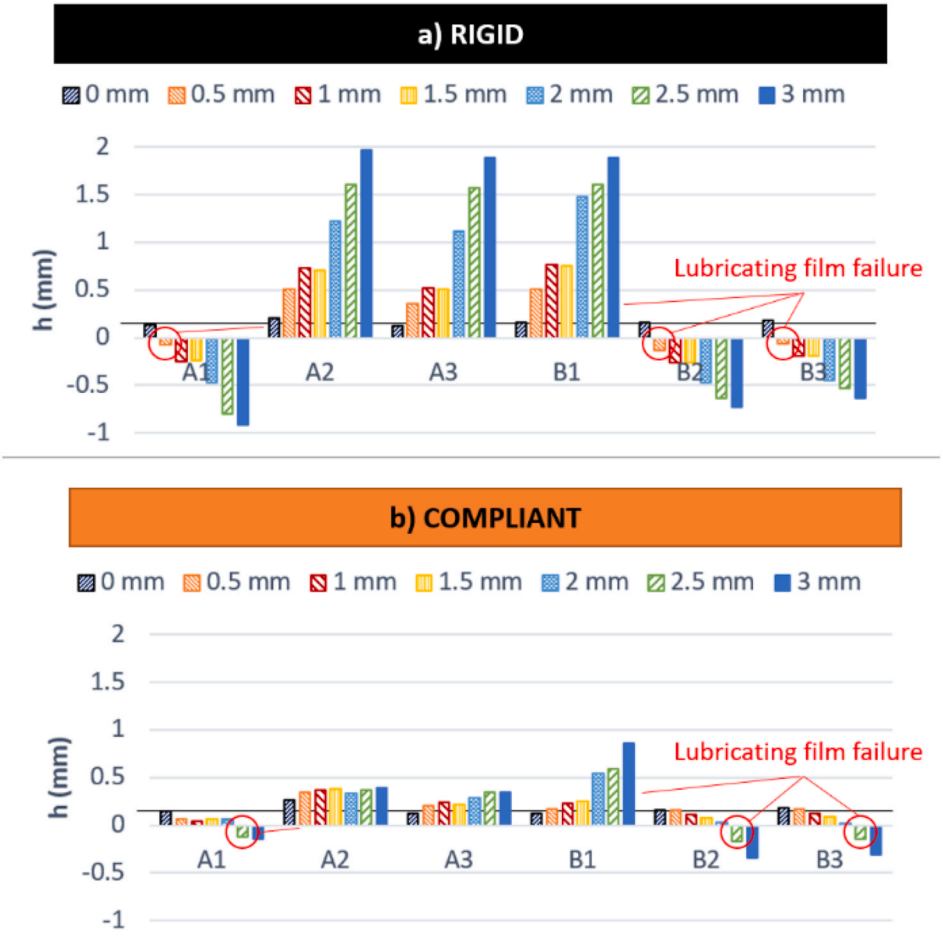

Fig. 15. Film thickness values of OFFSET measurements for height difference δ (0, 0.5, 1, 1.5, 2, 2.5, and 3 mm) with a) RIGID and b) COMPLIANT (medium stiffness) support.

OFFSET 5.3 times smaller relative film thickness change with medium compliant pads. The results clearly indicate that the compliant pads create more evenly distributed film thickness and pressure.

The obtained results show that the compliant support could provide a uniform film thickness along the slider and evenly distributed pressure in the recesses. To show the oil pressure distribution and film thickness, we selected only one misalignment type – OFFSET, which is probably the most problematic error from the presented ones because it is necessary to be set to all pads to achieve as high as possible sliding surface flatness. The obtained recess pressure values are shown in Fig. 13 for a) rigid support and b) compliant support with compliant pads of medium stiffness with the outlined average pressure values from Table 4. The rigidly supported hydrostatic bearing showed slightly higher local pressures (12 bar) compared to the compliant supported hydrostatic bearing (9.2 bar). However, the rigid support shows significantly greater differences in the recess pressure among all recesses, while the compliant support evidently distributes the lubricant pressure more evenly. The difference between the predicted and experimental values is most probably caused by a local increase and decrease in the lubricating film stiffness local according to the misalignment magnitude

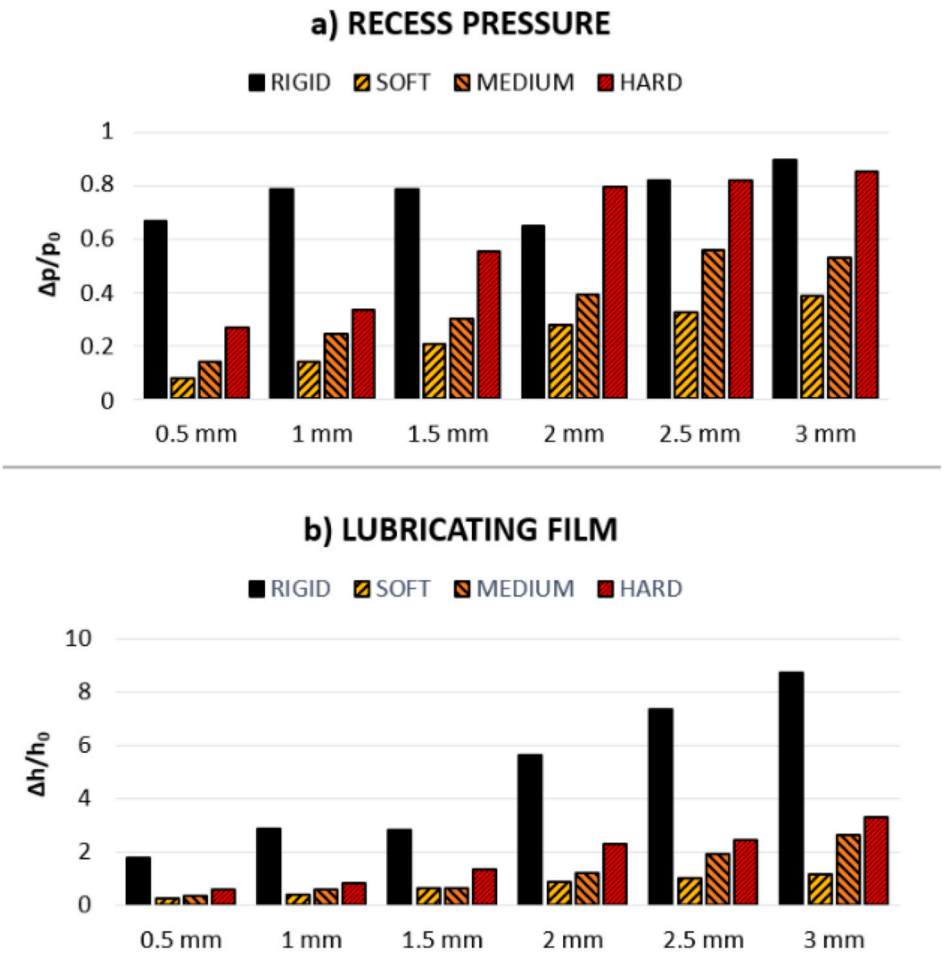

Fig. 16. Support stiffness comparison of the relative change to the initial value of a) recess pressure and b) lubricating film.

and slider position relative to the bearing pads. The local pressure decrease possibly causes the lubricating film stiffness to decrease and vice versa. Therefore, the load-carrying ability for certain misalignment types is higher than in the prediction.

The comparisons of lubricating film thickness are illustrated in Fig. 15 for a) rigid support and b) compliant support with a compliant pad of medium stiffness. The initial film thickness (h_0) of 0.16 mm is outlined in both figures. The negative values of film thickness represent the position of the slider's sliding surface relative to the pad's sliding surface because the proximity sensors are not located directly in the pad's sliding surface (see Fig. 4). The film thickness on the edge of the pad was calculated using values obtained from proximity sensors and their positions. Then the calculated film thickness was determined. When the value of film thickness reached 0 mm, a loss of the load-carrying ability occurred (as seen in Fig. 15). The negative film thicknes in Fig. 15 means that the slider came into contact with the pad, but the proximity sensor could still collect the data, as shown in Fig. 14. The results obtained from proximity sensors and pressure sensors correspond well, as the average recess pressure started to decrease with a 0.5 mm offset misalignment for rigid and a 2.5 mm offset misalignment respectively.

The results support the assumption that the compliant support significantly reduces the differences in the film thickness compared to the rigid support. The results show that a more than 50% smaller change of the film thickness was achieved using the compliant support. Therefore, the sensitivity to the misalignment error is greatly lower with the use of a compiant support for the hydrostatic bearing pads. The experimental results of film thickness indicate that the lubricating film stiffness is not constant along the slider in a misaligned bearing. Therefore, the maximum assembly error is actually higher than the predicted one as shown in Table 5, which emphasises the significance of the restrictor use in the hydrostatic bearing systems.

3.4. Compliant pad stiffness comparison

The compliant pad stiffness effect on the performance of the hydrostatic bearing with misaligned surfaces was investigated only for the OFFSET error. The recess pressure and film thickness relative change (Δp and Δh) with misaligned pads divided by the initial values (p_0 and h_0) obtained for levelled pads was used as the evaluation criteria. Hence, the relative change of the a) recess pressure and b) film thickness is shown in Fig. 16. It is evident that the hydrostatic bearing rigid support does not allow for even distribution of the pressure and uniform film thickness along the slider. The relative change of the film thickness is greater with increasing offset misalignment for all support types. In comparison with the rigid support, for the 3 mm offset a significant 56% reduction in recess pressure, and a 70% decrease in film thickness relative change were achieved using soft compliant pads. Therefore, it is evident that the lower support stiffness, the better the ability to adjust the pads' sliding surfaces to the slider. Thus, the bearing performance with compliant support shows significantly better performance and much lower sensitivity to the assembly errors. However, we want to emphasize that the use of compliant support for error compensation can only be used in applications that do not require high bearing stiffness, such as machining centres, precision guideways, or optical telescopes. On the contrary, it might be highly desirable in large-scale low-precision applications to reduce costs related to the manufacturing, assembly, and service.

4. Conclusions

In this article, we have reported an experimental investigation to verify the assumptions on the estimation of the allowable errors. We also demonstrated the hydrostatic bearing's compliant support effect and significance. Based on the obtained results, the following conclusions can be drawn:

- The proposed methodology can be used for hydrostatic bearing error estimation to achieve proper functioning and for assembly and manufacturing tolerance design approximation. This methodology can also be used for estimated compliant support (compliant pad) stiffness calculation according to the predicted assembly and manufacturing errors and errors caused by structural deformations of the slider, which could be obtained by numerical simulations.
- The compliant pads allow for an even distribution of the recess pressure in all recesses, and therefore maintain a uniform and stable lubricating film. The compliant pads can adjust the film thickness along the slider in case of misaligned hydrostatic pads during assembly when compared to rigid support. The compliant pads prevent the collision of the slider and misaligned pad surfaces four to six times more than the rigid support and work for either tilting or height difference compensation.
- In this article, natural rubber compliant pads were used. However, the compliant support material must be chosen according to the environment compatibility (sufficient oil resistance) or properly covered to prevent its degradation caused by oil leaks.
- The error prediction showed a relatively small assembly error allowance, which might be caused by neglecting the structural deformations of the slider and the restrictor compensation. However, the experimental results of the assembly error allowance for compliant support were at least four times higher than those of the rigid support. The predicted values were smaller than the experimentally obtained values from measurement, which indicates that this methodology could be used for hydrostatic bearing error estimation to prevent a collision of the sliding surfaces.
- The proposed way of error compensation using compliant support might be highly demanded to reduce the cost of large-scale low-precision structure positioning. However, it may not be suitable for applications that require high precision and high stiffness of the bearing.

Future work on this topic might focus on prediction accuracy improvement that includes structural deformation of the bodies caused by pressurized fluid force effects and thermal deformations. And possibly also the compensation range of restrictors and film stiffness change could be investigated and determined.

Declaration of competing interest

The authors declare that they have no known competing financial interests or personal relationships that could have appeared to influence the work reported in this paper.

Acknowledgements

This research was carried out under the project TN01000071 of National Competence Centre of Mechatronics and Smart Technologies for Mechanical Engineering, cofounded with the support of the Technology Agency of the Czech Republic, within the National Centres of Competence Programme and FSI–S-20-6443 with financial support from the Ministry of Education, Youth and Sports of the Czech Republic.

References

[1] Li X, Wang X, Li M, Ma Y, Huang Y. The research status and progress of heavy/large hydrostatic thrust bearing. Adv Mech Eng 2014;6:982584. https://doi.org/10.1155/2014/982584.
[2] Michalec M, Svoboda P, Křupka I, Hartl M. A review of the design and optimization of large-scale hydrostatic bearing systems. Eng Sci Technol an Int J 2021. https://doi.org/10.1016/j.jestch.2021.01.010.
[3] Awrejcewicz J, Olejnik P. The occurrence of stick-slip phenomenon. J Theor Appl Mech 2007;45:33–40.
[4] Mahdi R, Stephan K, Friedrich B. Experimental investigations on stick-slip phenomenon and friction characteristics of linear guides. Procedia Eng 2015;100:1023–31. https://doi.org/10.1016/j.proeng.2015.01.462.
[5] Rowe WB. Advances in hydrostatic and hybrid bearing technology. Proc Inst Mech Eng Part C J Mech Eng Sci 1989;203:225–42. https://doi.org/10.1243/PIME_PROC_1989_203_110_02.
[6] Bernstein RA, McCarthy PJ, Raybould K, Bigelow BC, Bouchez AH, Filgueira JM, et al. Overview and status of the giant magellan telescope project. Ground-Based Airborne Telesc; 2014. https://doi.org/10.1117/12.2055282. 9145:91451C.
[7] Wasilczuk M. Friction and lubrication of large tilting-pad thrust bearings. Lubricants 2015;3:164–80. https://doi.org/10.3390/lubricants3020164.
[8] Wang Y, Liu Z, Cheng Q, Zhao Y, Wang Y, Cai L. Analysis and optimization of nonlinear carrying performance of hydrostatic ram based on finite difference method and Runge–Kutta method. Adv Mech Eng 2019;11:1–12. https://doi.org/10.1177/1687814019856128.
[9] Jang S-H, Choi Y-H, Kim S-T, An H-S, Choi H-B, Hong J-S. Development of core Technologies of multi-tasking machine tools for machining highly precision large parts. J Korean Soc Precis Eng 2012;29:129–38. https://doi.org/10.7736/kspe.2012.29.2.129.
[10] Ramesh R, Mannan MA, Poo AN. Error compensation in machine tools - a review. Part I: geometric, cutting-force induced and fixture-dependent errors. Int J Mach Tool Manufact 2000;40:1235–56. https://doi.org/10.1016/S0890-6955(00)00009-2.
[11] Ramesh R, Mannan MA, Poo AN. Error compensation in machine tools- a review. Part II: thermal errors. Int J Mach Tool Manufact 2000;40:1257–84. https://doi.org/10.1016/S0890-6955(00)00010-9.
[12] San Andres L. The effect of journal misalignment on the operation of a turbulent flow hydrostatic bearing. J Tribol 1993;115:355–63. https://doi.org/10.1115/1.2921643.
[13] Okabe EP. Analytical model of a tilting pad bearing including turbulence and fluid inertia effects. Tribol Int 2017;114:245–56. https://doi.org/10.1016/j.triboint.2017.04.030.
[14] Shenoy BS, Pai R. Effect of turbulence on the static performance of a misaligned externally adjustable fluid film bearing lubricated with couple stress fluids. Tribol Int 2011;44:1774–81. https://doi.org/10.1016/j.triboint.2011.06.025.
[15] Ghezali F, Bouzidane A, Thomas M. 3D Numerical investigation of pressure field of an orifice compensated hydrostatic bearing. Mec Ind 2017;18. https://doi.org/10.1051/meca/2016008.
[16] Liu H, Xu H, Ellison PJ, Jin Z. Application of computational fluid dynamics and fluid-structure interaction method to the lubrication study of a rotor-bearing system. Tribol Lett 2010;38:325–36. https://doi.org/10.1007/s11249-010-9612-6.
[17] Fillon M, Dmochowski W, Dadouche A. Numerical study of the sensitivity of tilting pad journal bearing performance characteristics to manufacturing tolerances: steady-state analysis. Tribol Trans 2007;50:387–400. https://doi.org/10.1080/10402000701429246.
[18] Dmochowski W, Dadouche A, Fillon M. Numerical study of the sensitivity of tilting-pad journal bearing performance characteristics to manufacturing tolerances: dynamic analysis. Tribol Trans 2008;51:573–80. https://doi.org/10.1080/10402000801947709.
[19] Hagemann T, Pfeiffer P, Schwarze H. Measured and predicted operating characteristics of a tilting-pad journal bearing with jacking-oil device at hydrostatic, hybrid, and hydrodynamic operation. Lubricants 2018;6. https://doi.org/10.3390/lubricants6030081.
[20] Jang JY, Khonsari MM. On the characteristics of misaligned journal bearings. Lubricants 2015;3:27–53. https://doi.org/10.3390/lubricants3010027.
[21] Rajput AK, Sharma SC. Combined influence of geometric imperfections and misalignment of journal on the performance of four pocket hybrid journal bearing. Tribol Int 2016;97:59–70. https://doi.org/10.1016/j.triboint.2015.12.049.
[22] Bhat N, Barrans SM, Kumar AS. Performance analysis of Pareto optimal bearings subject to surface error variations. Tribol Int 2010;43:2240–9. https://doi.org/10.1016/j.triboint.2010.07.012.
[23] Schwenke H, Knapp W, Haitjema H, Weckenmann A, Schmitt R, Delbressine F. Geometric error measurement and compensation of machines-An update. CIRP Ann - Manuf Technol 2008;57:660–75. https://doi.org/10.1016/j.cirp.2008.09.008.
[24] Cappa S, Reynaerts D, Al-Bender F. Reducing the radial error motion of an aerostatic journal bearing to a nanometre level: theoretical modelling. Tribol Lett 2014;53:27–41. https://doi.org/10.1007/s11249-013-0241-8.
[25] Xue F, Zhao W, Chen Y, Wang Z. Research on error averaging effect of hydrostatic guideways. Precis Eng 2012;36:84–90. https://doi.org/10.1016/j.precisioneng.2011.07.007.
[26] Zhang P, Chen Y, Zhang C, Zha J, Wang T. Influence of geometric errors of guide rails and table on motion errors of hydrostatic guideways under quasi-static condition. Int J Mach Tool Manufact 2018;125:55–67. https://doi.org/10.1016/j.ijmachtools.2017.10.006.

[27] Zhang YT, Lu CH, Zhao HX, Shi WJ, Liang P. Error averaging effect of hydrostatic journal bearings considering the influences of shaft rotating speed and external load. Ieee Access 2019;7:106346–58. https://doi.org/10.1109/ACCESS.2019.2931948.
[28] Hoffmann P. Analysis of tolerances and process inaccuracies in discrete part manufacturing. Comput Des 1982;14:83–8. https://doi.org/10.1016/0010-4485(82)90172-5.
[29] Shan A, Roth RN, Wilson RJ. New approach to statistical geometrical tolerance analysis. Int J Adv Manuf Technol 1999;15:222–30. https://doi.org/10.1007/s001700050060.
[30] Shen Z, Ameta G, Shah JJ, Davidson JK. A comparative study of tolerance analysis methods. J Comput Inf Sci Eng 2005;5:247–56. https://doi.org/10.1115/1.1979509.
[31] Sapirstein P. Accurate measurement with photogrammetry at large sites. J Archaeol Sci 2016;66:137–45. https://doi.org/10.1016/j.jas.2016.01.002.
[32] Hurník J, Zatocilová A, Paloušek D. Camera calibration method of optical system for large field measurement of hot forgings in heavy industry. Proc SPIE 2019;11056. https://doi.org/10.1117/12.2527693.
[33] Qi E, Fang Z, Sun T, Chen J, Liu C, Wang J. A method for predicting hydrostatic guide error averaging effects based on three-dimensional profile error. Tribol Int 2016;95:279–89. https://doi.org/10.1016/j.triboint.2015.11.032.
[34] Jain SC, Sharma SC, Nagaraju T. Misaligned journal effects in liquid hydrostatic non-recessed journal bearings. Wear 1997;210:67–75. https://doi.org/10.1016/S0043-1648(97)00038-0.
[35] Lv F, Ta N, Rao Z. Analysis of equivalent supporting point location and carrying capacity of misaligned journal bearing. Tribol Int 2017;116:26–38. https://doi.org/10.1016/j.triboint.2017.06.034.
[36] Jang J, Khonsari M. On the characteristics of misaligned journal bearings. Lubricants 2015;3:27–53. https://doi.org/10.3390/lubricants3010027.
[37] Tang J, Huang XD, Fang CG. BP neural network in prediction of the constant-current hydrostatic bearing static stiffness. Adv Mater Res 2011;199–200:271–4. https://doi.org/10.4028/www.scientific.net/AMR.199-200.271.
[38] Liu ZF, Wang YM, Cai LG, Zhao YS, Cheng Q, Dong XM. A review of hydrostatic bearing system: researches and applications. Adv Mech Eng 2017;9. https://doi.org/10.1177/1687814017730536.
[39] Alcácer V, Cruz-Machado V. Scanning the industry 4.0: a literature review on Technologies for manufacturing systems. Eng Sci Technol an Int J 2019;22:899–919. https://doi.org/10.1016/j.jestch.2019.01.006.
[40] Abramovitz S. Fluid film bearings - fundamentals and design criteria and Pitfalls. Abramovitz Assoc Inc n.d.
[41] Bassani R, Piccigallo B. Hydrostatic lubrication. Tribol 1992;22.
[42] Van Beek A, Segal A. Rubber supported hydrostatic thrust bearings with rigid bearing surfaces. Tribol Int 1997;30:47–52. https://doi.org/10.1016/0301-679X(96)00021-7.
[43] Van Beek A, Lepic L. Rubber supported hydrostatic thrust bearings with elastic bearing surfaces of infinite length, vol. 201; 1996. p. 45–50.
[44] Wang L, Zeng Q, Lu C, Liang P. A numerical analysis and experimental investigation of three oil grooves sleeve bearing performance. Ind Lubric Tribol 2019;71:181–7. https://doi.org/10.1108/ILT-11-2017-0331.
[45] Lefanti R, Ando M, Sukumaran J. Fatigue and damage analysis of elastomeric silent block in light aircrafts. Mater Des 2013;52:384–92. https://doi.org/10.1016/j.matdes.2013.05.039.
[46] Chandrasekaran VC. Rubber seals for fluid and hydraulic systems. In: Chandrasekaran VCBT-RS for F and HS. Oxford: William Andrew Publishing; 2010. p. 7–22. https://doi.org/10.1016/B978-0-8155-2075-7.10002-4. Plast. Des. Libr.
[47] Khonsari MM, Booser RE. Appl Tribol 1970;3. https://doi.org/10.1016/0041-2678(70)90297-6.
[48] Lu SK, Hua DX, Li Y, Cui FY, Li PY. Stiffness calculation method and stiffness characteristic analysis of bolted connectors. Math Probl Eng 2019. https://doi.org/10.1155/2019/6206092. 2019.

machines

MDPI

Article

Assembly Error Tolerance Estimation for Large-Scale Hydrostatic Bearing Segmented Sliders under Static and Low-Speed Conditions

Michal Michalec, Jan Foltýn, Tomáš Dryml, Lukáš Snopek, Dominik Javorský, Martin Čupr and Petr Svoboda *

Institute of Machine and Industrial Design, Faculty of Mechanical Engineering, Brno University of Technology, 61669 Brno, Czech Republic; michal.michalec@vut.cz (M.M.); jan.foltyn@vut.cz (J.F.)
* Correspondence: petr.svoboda@vut.cz

Abstract: Hydrostatic bearings come with certain advantages over rolling bearings in moving large-scale structures. However, assembly errors are a serious matter on large scales. This study focuses on finding assembly error tolerances for the most common types in segmented errors of hydrostatic bearing sliders: tilt and offset. The experimental part was performed in the laboratory on a full diagnostic hydrostatic bearing testing rig. An investigation of the type of error on bearing performance was first conducted under static conditions. We identified the limiting error-to-film thickness ratio (e/h) for static offset error as 2.5 and the tilt angle as $\theta = 0.46^\circ$ for the investigated case. Subsequently, two types of offset error were investigated under slow-speed conditions at 38 mm/s. The limiting error for the offset error considering the relative bi-directional movement of the slider and the pad was determined as $e/h < 1$. The results further indicate that the error tolerance would further decrease with increasing speed. The experimental results of error tolerances can be used to determine the required film thickness or vice versa.

Keywords: tolerancing; error estimation; experimental investigation; hydrostatic lubrication; hydrostatic guideway

Citation: Michalec, M.; Foltýn, J.; Dryml, T.; Snopek, L.; Javorský, D.; Čupr, M.; Svoboda, P. Assembly Error Tolerance Estimation for Large-Scale Hydrostatic Bearing Segmented Sliders under Static and Low-Speed Conditions. *Machines* **2023**, *11*, 1025. https://doi.org/10.3390/machines11111025

Received: 20 October 2023
Revised: 9 November 2023
Accepted: 13 November 2023
Published: 15 November 2023

1. Introduction

Although rolling bearings are the most widely used type of bearing, their application becomes more challenging with increasing machine or structure size. When large structures need to be moved or rotated, hydrostatic (HS) bearings offer numerous advantages. The HS lubricating film is created between sliding surfaces by an external hydraulic supply. It secures the complete separation of conformal surfaces, resulting in very low friction, almost no wear, very high precision [1] without the appearance of a stick-slip effect, high stiffness, and vibration damping ability [2–4]. A great advantage of HS bearings consists of the possibility of active control implementation [5]. The use of fluid bearings could lead to higher energy efficiency compared to rolling or sliding bearings [6], although HS lubrication requires a continuous external supply of pressurized lubricant. HS lubrication is a unique type of lubrication regime that is suitable for a wide range of applications—from millimetres up to tens of metres [7]—for small ultra-precision machine tools [8], through medium-sized machining centres, or even for moving large structures, such as giant telescopes, radio antennas, or large-scale machining centres [9]. This type of bearing is frequently combined with hydrodynamic (HD) bearings to reduce wear in the start and stop phases [10,11]. In the case of such large scales, it is not possible to manufacture the slider and pad bodies in one piece because of manufacturing space, transportation, and assembly. The performance of the HS lubricating film is influenced by many factors, such as uneven loading, the elastic deformation of solid bodies, thermal effects [12], manufacturing precision, and, primarily in the case of large-scale bearing, assembly precision.

Geometric errors negatively influence the lubricating layer of sliding bearings, whose performance decreases with the magnitude of surface irregularities [13]. Two main types of geometric error that can be classified are manufacturing errors and assembly errors. This article focuses primarily on assembly errors. Misalignment causes serious problems leading to reduced bearing performance or even seizure [14]. The misalignment of the HD bearing strongly influences the lubricating film. HS bearings are often combined with HD bearings to reduce wear during the start and stop phase [15], compensate for misalignment, and are frequently mounted on the tilting support of the pad [16]. The HS lubrication regime increases the thickness of the film and improves circulation and cooling [17], thus improving its performance. This is one of the main reasons why HS lubrication is used as bearings on high-precision machines. However, HS bearings also have certain limits for geometric errors that could be compensated by the relatively thick lubricating film. The energetic demands needed to compensate for the geometric precision of the solid bodies surrounding the lubricating film [18] increase with the magnitude of the error. Restrictors are often used to control flow distribution into the pads and recesses in case of single-pump multi-pad HS bearings. They also serve as a safety element that helps to align the surfaces using the pressure difference they generate. There are various types, from basic, such as orifice (see [19,20] or [21]), to more sophisticated, including membranes [22] or controllable elements, such as electromagnetic valves [23,24]. Previous research aimed to compensate for pad misalignment using compliant support numerically [25,26] and experimentally [27], respectively.

Numerical modelling was used to investigate geometric errors. The model for the analysis of the motion error of closed guideways lubricated with the HS regime, based on the kinetic equilibrium of the table taking into account the effect of the squeeze film, was proposed by Wang et al. [28], who found that with increasing speed, the error is more significant but can be compensated for with higher lubricant supply. Rajput and Sharma [29] investigated different geometric imperfections of defined shapes and the misalignment of the HS-lubricated journal bearing using FEM formulation. All imperfections caused an observably lower minimal film thickness, whereas the minimal film thickness was twice as much lower in all cases with journal misalignment. As later observed by Zoupas et al. [30] using CFD analysis, different types of manufacturing error (convex, concave, and sine wave) have similar effects on HD thrust bearings, as in the case of journal bearings. Fedorynenko et al. [20] proposed a new design of adjustable HS bearing with improved precision [31]. Zhang et al. [32] presented a model based on formulations that describe the relationship between geometric errors and motion errors in bearings lubricated with the HS regime with experimental validation. Zha et al. [33] later proposed a tolerance design method for HS guideways based on the error averaging effect, considering geometric parameters of guide rails with experimental validation.

The certain misalignment of multi-pad HS bearing can be compensated by the lubricating film itself [27]; nonetheless, if the slider is assembled from smaller segments and is not aligned properly, it might result in edge collision and thus bearing failure. Compared to pad misalignment, slider segment misalignment is far more serious. This article focuses on assembly errors of segmented sliders, in which we identified two primary cases (Figure 1): offset (A) and tilt (B) of the neighbouring segments of the slider. Although a great deal of research work has focused on manufacturing errors in hydrostatic bearings and guideways, the following question remains unanswered: "What is the assembly error tolerance of a segmented hydrostatic bearing (guideway) slider?". This study will try to provide answers to this question.

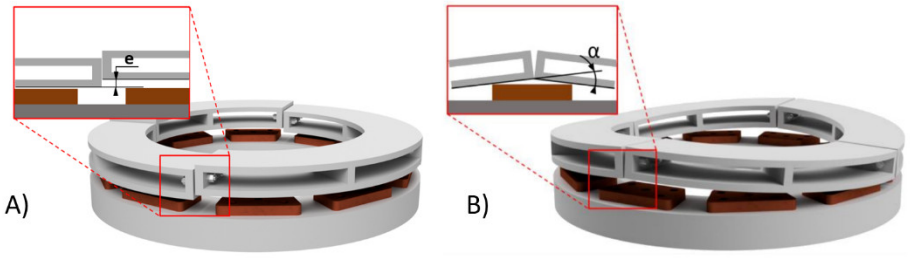

Figure 1. Schematic representation of two primary assembly errors of large-scale bearings: (**A**) offset and (**B**) tilt.

2. Materials and Methods

The dual pad experimental hydrostatic bearing (2PAD) was used for measuring the effect of assembly error on bearing performance. 2PAD (Figure 2) consists of two pads with oil inlets and outlets mounted on supports. The load was generated using four threaded rods and springs for even loading. Force sensors with a range of 10 kN mounted on each of the threaded rods were used to obtain loading force. The loading frame transferred the load through four ball bearings onto the slider. The slider was divided into two parts, which are assembled using four bolts, to simulate assembly error cases. The motion of the slider was secured by a ball screw and an electromotor.

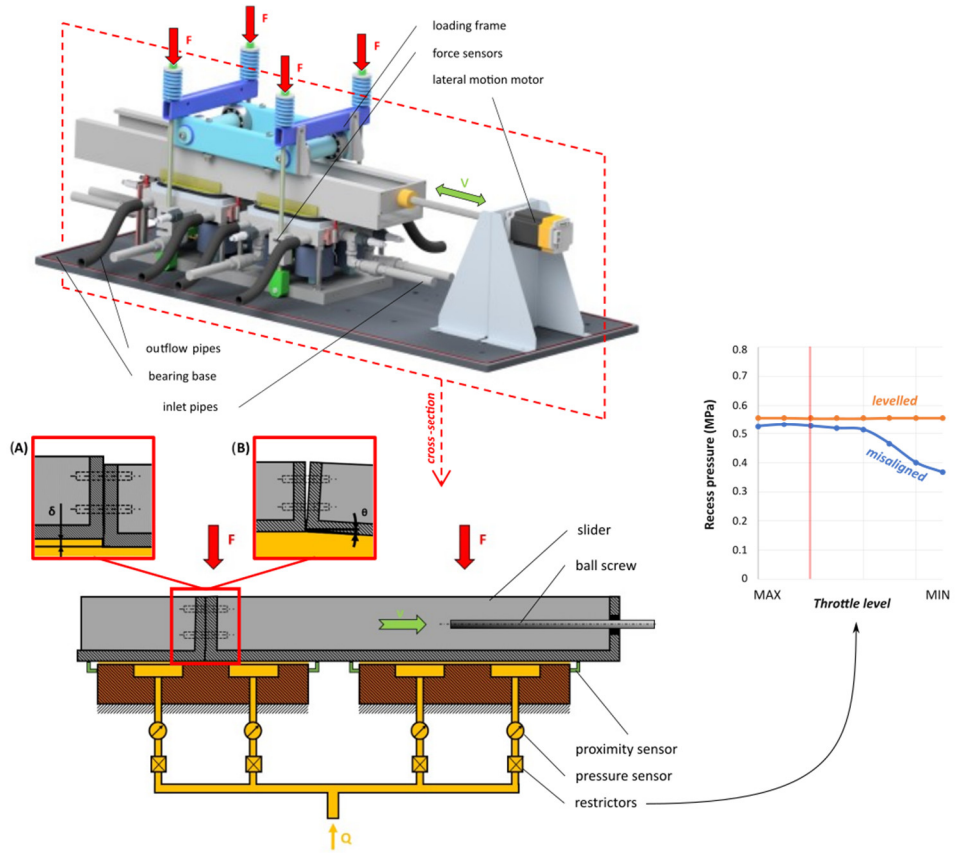

Figure 2. 2PAD experimental HS bearing setup, sensor description and assembly error setting for (**A**) offset (step) and (**B**) tilt.

During all experiments, ISO VG 46 grade oil was used, with measured temperature-viscosity dependence (0.104 mPa·s at 23 °C). The selected oil type is normally used for hydraulic systems, while the specific grade was chosen according to the environmental condition—room temperature. The oil flowed from the hydraulic pump into the recess and through the oil film gap in between the slider and the pad land to the collector and

then was returned to the tank. Excess oil was wiped using lip seal to prevent leakage and oil contamination outside the pad area. The oil temperature was obtained from the temperature sensor at the inlet of the bearing. The laboratory has its own air conditioning, and the tests were relatively short; therefore, the temperature was stable at 23 ± 0.5 °C during all experiments. A pressure sensor of precision ±0.056 MPa was mounted at each inlet to recess.

Since the 2PAD is a single-pump HS bearing, a restrictor (needle flow control valve) was mounted at each inlet into for recess to compensate the pressure differences in the recesses. The throttle level was the same for all valves and was determined in a misaligned pad case (Figure 2). The approximate pressure difference generated at each of the restrictors was 0.1 MPa. If there were no restrictors, the multi-recess pad would act as a single recess, and the pressure would be the same in each of the recess. Supplied oil flow was measured using flowmeter of range 15 L/min and precision 0.1 L/min.

Six contactless proximity sensors with a precision of ±0.01 mm were mounted on the pads to obtain information about the film's thickness. The sensor layout is shown in Figure 3, with details on proximity sensors mounted on pad supports. The four recesses in each pad secured an even pressure distribution over the pad area, while providing information about the pressure in each of the corners of the pad. In this study, pressure information in each recess and film thickness from proximity sensors were used as primary performance evaluation parameters. Secondary parameters, such as the load and flow supplied, were held constant. Pads were levelled using straight slider with a flatness of 0.02 mm, calibration rods with a precision of ±0.001 mm, and combined information from pressure and proximity sensors to achieve distribution of film thickness and recess pressure values that are as similar as possible. The 2PAD central distance of pads to pad size (length) ratio in the presented configuration was 2.3. This ratio is given by the design of the test rig that is based on a large hydrostatic bearing. Nonetheless, it must be carefully considered in actual design with respecting structural deformations of the slider, applied load, and required precision or stiffness.

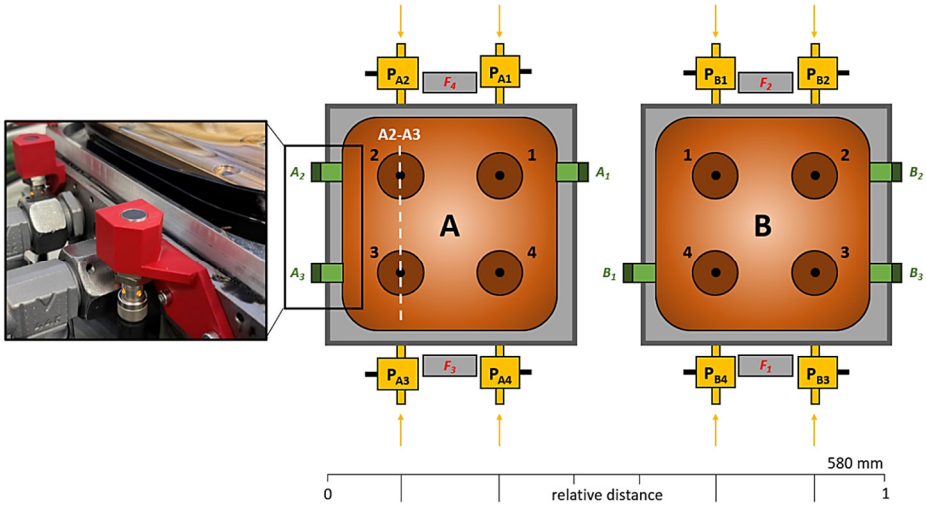

Figure 3. Pad shape and sensor composition on 2PAD with detail on proximity sensors.

2.1. Static Tests

An evaluation of static performance was performed for three possible scenarios that might emerge during the assembly process. The error was generated on the surface plate using SKF calibrated shims that were underlaid under one side of the slider. The offset error (Figure 4A) was assessed in the middle of pad A and in between the recesses. The tilt errors were investigated in two positions—in the middle of pad A (Figure 4B) and between the two pads (Figure 4C). Those two cases might occur when the slider connection is moving; thus, the two most critical scenarios were assessed.

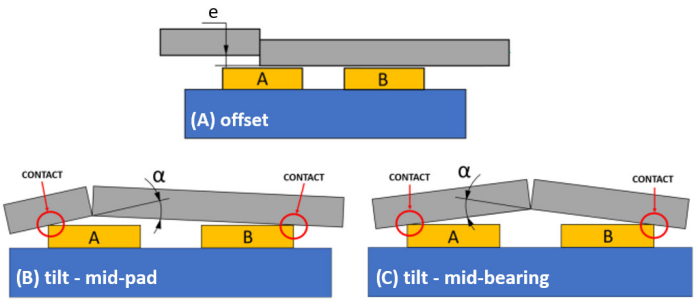

Figure 4. Schematical representation of the static error types assessed in this study for cases: (**A**) offset of slider bodies, (**B**) tilt positioned in the centre of pad A and (**C**) tilt positioned between the pads A and B.

2.2. Dynamic Tests

Dynamic tests were carried out only for offset errors. Two possible scenarios were identified: step-up (Figure 5A), with the second part of the slider offset upwards relative to the other, and step-down (Figure 5B), with the error created below the main slider. The latter is more dangerous since the collision of the slider and pad is inevitable for a certain error magnitude. This is the reason why the step-down dynamic experiment was conducted after all previous experiments were finished.

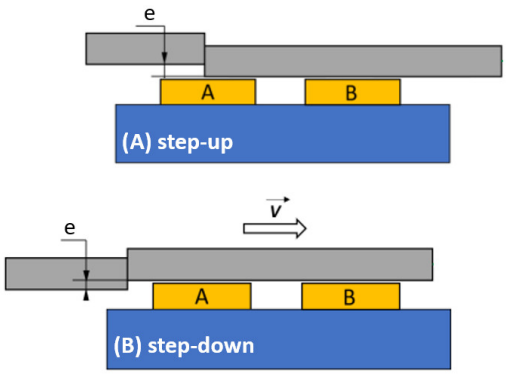

Figure 5. Error types assessed during the dynamic tests for offset cases: (**A**) step-up and (**B**) step-down.

3. Results and Discussion

Experimentally obtained results are described for the cases of assembly errors investigated. First, the static performance characteristics for offset and tilt are presented and assessed. Then, the effect of assembly error on dynamic performance is discussed. The experimental conditions chosen for the tests reflected service conditions of a hydrostatic turntable but on a smaller scale. The film thickness for the case without an assembly error was 0.13 mm with a total flow supplied to both pads of 4.3 L/min. The predicted value of film thickness for the geometry used and experimental conditions based on Rippel [34] was 0.14 mm. This value was used to validate the experimental setup and conditions. For all experiments, an evenly distributed constant 20 kN total load was applied. The load varied within 2% during experiments, thus was assumed as constant. The precision of the pressure sensor was considered in the performance evaluation and is highlighted in all graphs. We have set an additional 5% pressure difference that represents the critical pressure range. Within this range, the bearing can still perform normal functions, but it is necessary to proceed with caution. It can be also seen in Figure 6 that the pressure varied within this range. Especially in large HS bearings, the pressures might fluctuate due to manufacturing and assembly errors of higher magnitude. However, this could compromise the bearing precision and should be reflected in bearing performance requirements. The difference in the recess pressure can be caused by lubricant temperature change, variable

load, change in the supplied flow, or misalignment. The other effects were held constant throughout all measurements. Only the misalignment of the slider bodies, representing the assembly error, was varied.

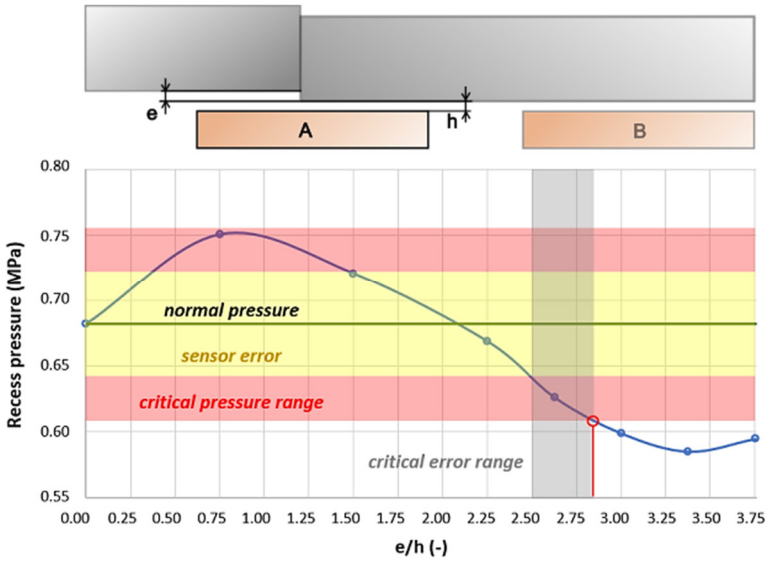

Figure 6. Recess pressure in pad A dependency on error-to-initial film thickness ratio.

3.1. Static Performance

The static performance of the assembly error was measured for both cases—the offset and tilt of the slider segments. To ensure the validity of the experimentally obtained data, all static measurements were repeated three times. Between each measurement, the bearing was turned off and back on. The loading frame and slider had to be disassembled with each error case. The repeatability of the static tests was within 2% error for pressure, 1% for film thickness, and 1% for load.

3.1.1. Offset of the Slider Bodies

The offset assembly error type was assessed only for the "step-up" configuration. The judging criteria were the average pressure of the pad A, pressure in recess A2 and A3, film thickness obtained from proximity sensor A1, and the initial film thickness of 0.13 mm at $e/h = 0$. The normal pressure for the supplied flow and load was 0.68 MPa. The dependence of the average pressure in pad A on the error magnitude to the film thickness ratio is drawn in Figure 6. An increase in the mean pressure was observed in pad A within the error ratio range $e/h = 0–0.75$. The overall average recess pressure rose by 0.03 MPa for this ratio, indicating that the slider might become slightly inclined due to the geometry change generated by the error. However, in the range of $e/h = 0–2.25$, the average pressure in pad A remained within the range of sensor error. The range of $e/h = 2.5–2.8$ was considered a critical error range because the average recess pressure in pad A fell into the critical pressure range, which was below the sensor error range. In this range, a contact between the solid bodies might occur since the load might not be carried only by the lubricating film. Therefore, the ratio $e/h = 2.5$ is considered as the limiting value in which the bearings can operate normally under static conditions. Regarding the ratio of $e/h = 3$ and higher, the contact of solid bodies was confirmed by the inability of the slider to move anymore.

As seen in Figure 7, the pressure decrease as the magnitude of the ratio increases. For the ratio $e/h = 3$, when a contact of solid bodies was confirmed, the average pressure in recesses pA2 and pA3 fell into the range of free outlet pressure. This means that those recesses did not carry load anymore, and that the remaining recesses could not sustain such load alone.

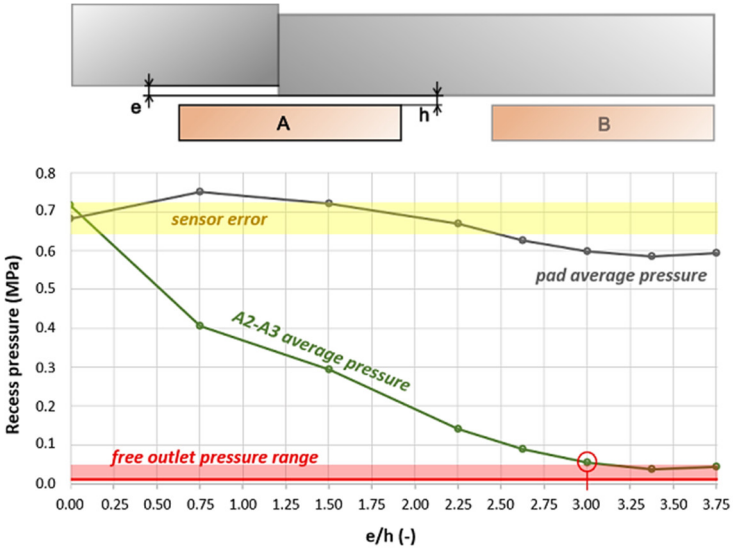

Figure 7. Recess pressure of pad A dependency on error-to-film-thickness ratio (grey) and average pressure in pockets 2 and 3 of pad A (green).

As observed from proximity sensors, the inclination of the slider, as shown in Figure 8 was more significant as the error magnitude increased. A film thickness of 0.06 mm was measured at proximity sensor A1 at the highest offset error magnitude. From Figure 3, it can be seen that the proximity sensor is not at the level of the edge of the pad, and therefore, a film thickness of 0.06 mm could already mean zero film thickness at the edge due to the slider inclination effect. Thus, during the offset static tests, the film thickness was considered as secondary criteria, and the main performance assessment criteria was the recess pressure in pad A.

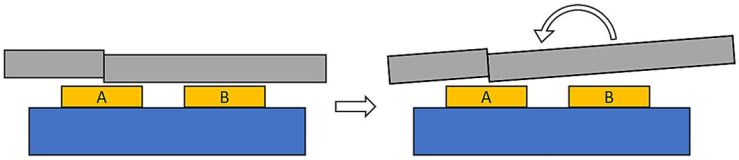

Figure 8. Schematical representation of slider inclination with increasing error magnitude.

3.1.2. Tilt

The tilt assembly error type was assessed for two positions—"mid-pad" (Figure 9A) and "mid-bearing" (Figure 9B) configurations. The judging criteria were the average pressure of both pads, pressure in all recesses, film thickness obtained from proximity sensors, and an initial film thickness of 0.13 mm at $\theta = 0°$. The normal pressure for the supplied flow and load was again 0.68 MPa. The bearing performed normal operation within the angular error of $\theta = 0–0.4°$. In the case of the "mid-pad", the average recess pressure slowly decreased, starting at $\theta = 0.2°$ until $\theta = 0.42°$. The range of $\theta = 0.46–0.5°$ was considered as the critical error range for the "mid-pad" error type. The limiting value that would allow the bearing to be functional was 0.5°. Regarding the "mid-bearing" error type, the average recess pressure was relatively stable until the tilt angular error reached a value of $\theta = 0.75°$. Any further added error caused the average recess pressure to rapidly decrease. Due to the rapid decrease in the average recess pressure with increased error value, the critical error range is relatively small, within $\theta = 0.78–0.8°$. Any error greater than $\theta = 0.8°$ would mean a loss of the load-carrying ability. However, a relative movement of the pad and slider bodies is required for proper bearing function. Therefore, the angular error of $\theta = 0.46°$ is considered the limit value for which the bearings can operate normally under static conditions in the two investigated positions. Considering that the slider will move during operation, the "mid-pad" error type allows for a smaller error tolerance. The

highest value of θ is 0.5°. Any higher error would lead to a contact of solid bodies for the tilt error type. The pads were positioned at ratio of pad centre distance to pad edge length of 2.3. Nonetheless, if the distance of the pads were greater, the angular tolerance would decrease.

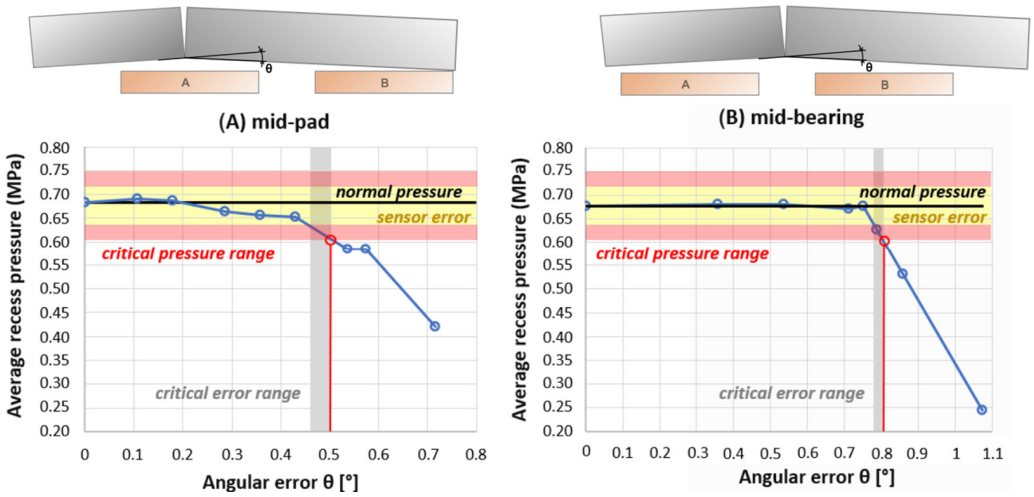

Figure 9. Average recess pressure dependency on angular error (tilt) of the slider bodies for cases (**A**) in the middle of pad A and (**B**) in between pads A and B.

3.2. Dynamic Performance

All dynamic tests were performed at a slider movement speed relative to the pads. To prove the repeatability of the dynamic tests, three initial measurements with 0.1 mm error ("STEP-UP" type) were carried out and compared. The following test were repeated three times as well, but only one run was plotted as they all exhibited high repeatability. As seen in Figure 10, the data obtained from the proximity sensors show the same trends for film thickness with very few differences, as shown in the detailed comparison for the proximity sensors (see the scheme in Figure 3). The repeatability of pressure sensors in all three measurements was within ±3%. For subsequent measurements, three measurements were carried out and thoroughly compared. All exhibited very high repeatability and the same deviation as in the initial experiment with 0.1 mm offset "step-up" type of error. The initial average film thickness was approximately 0.13 ±0.02 mm. A slightly higher deviation could be caused by the manufacturing error of the slider during movement compared to the static results.

3.2.1. Offset—"Step-Up"

The "step-up" dynamic tests were performed for a range of errors (e) from 0.05 to 0.3 mm with 0.05 increment, as seen in Figure 11. The average recess pressure trend was very similar for all cases; therefore, only runs of 0.1 mm, 0.2 mm, and 0.3 mm errors (e) are drawn in Figure 11. The measured data show an almost identical rise of the average recess pressure when the edge passes through the pad land area (between points I. and II.). This is caused by decreasing the effective area of pad A while carrying the same load; thus, the pressure increases. However, as soon as the slider step approaches the recess area (point II.), the pressure rapidly decreases, depending on the magnitude of the error. If the error (e) was within 0.05–0.015 mm, the pressure was still within the sensor error area and did not reach the critical pressure range. However, the pressure with a 0.2 mm error (equivalent to the ratio e/h = 1.5) has already entered the critical pressure range and is considered as the limiting value of error for the investigated movement speed. After the edge passed the recess area, the average pressure stabilized at a higher value in the case of smaller errors (e < 0.2 mm). The errors within the range of 0.2–0.3 mm (e/h = 1.5–2.3) exhibited average pressures below the critical pressure range. This is also a matter of the restrictor setup and

their performance. The test was terminated when the edge reached middle of the pad A (point IV).

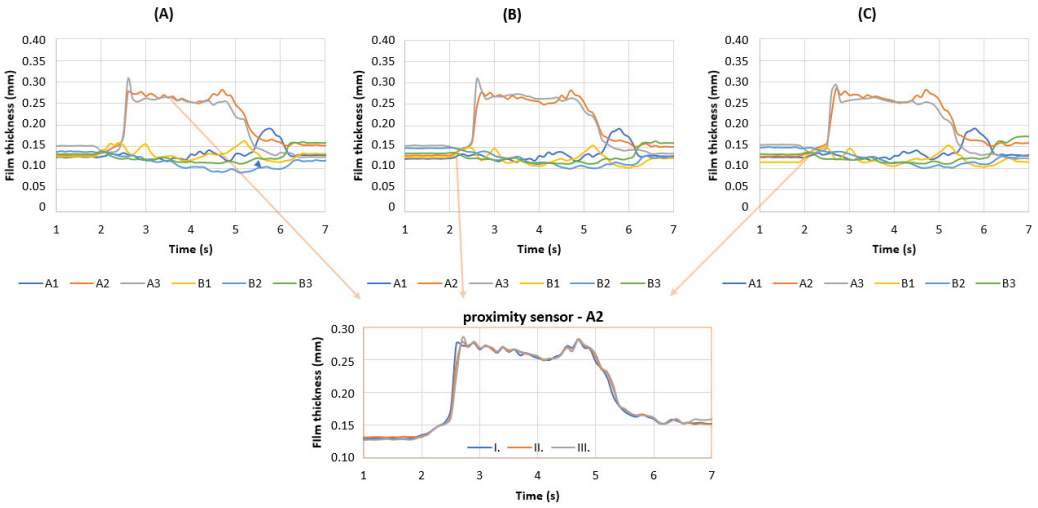

Figure 10. Film thickness charts comparison for three different measurements (**A**–**C**) of 0.1 mm "STEP-UP" type error with highlighted A2 sensor film thickness from all the three measurements.

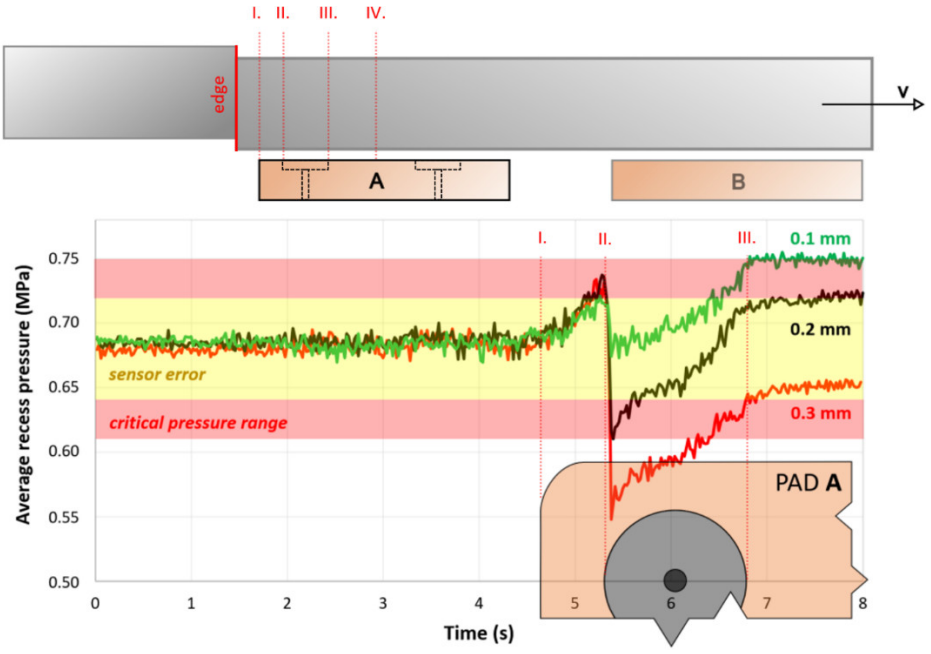

Figure 11. Average recess pressure value evolution in time for "step-up" error at 38 mm/s movement speed.

Although the returned pressure was above the critical pressure range, as in the case of a 0.3 mm error, the critical area when the slider is passing the edge and entering the bearing is more important. Furthermore, the precision is already compromised, because the thickness of the film becomes more non-uniform, as shown in Figure 12. A similar effect is expected to occur, as described in Figure 8. Nevertheless, the magnitude of error that the lubricating film can manage without suffering decreased performance would most likely be lower at higher movement speeds.

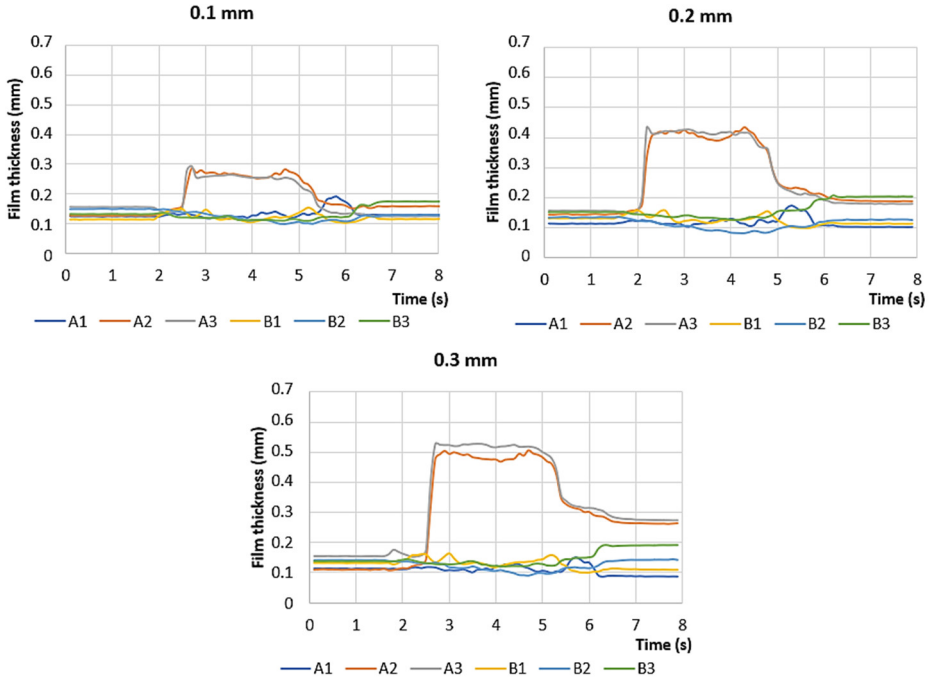

Figure 12. Film thickness evolution in time for the "step-up" error at 38 mm/s movement speed.

3.2.2. Offset—"Step-Down"

The "step-down" dynamic tests were also performed for a range of errors (e) of 0.05–0.3 mm with 0.05 mm increments, as seen in Figure 13. However, the average recess pressure trend was different from that in the previous investigated case. In the error range (e) of 0.05–0.15 mm (e/h = 0.38–1.15), the bearing could still operate normally and did not exhibit any form of collision. As seen in Figure 14, the assumed 0.15 mm error was smaller, approximately 0.1 mm instead of 0.15 mm. Moreover, the average recess pressure, as seen in Figure 13, was slightly higher than the critical pressure after passing the recess area (starting with point III.). It did not fall below the lower critical value; thus, we assumed normal operation. The tests were terminated when the edge reached the middle of the pad A (point IV.). An actual problem with the bearing performance started to arise at an error of 0.2 mm (e/h = 1.54), whose real value seems to be, according to the obtained data from sensors, 0.15 mm. As seen in Figure 13, the "0.2 mm" error exhibited a rapid decrease in the average pressure when the edge entered the pad area (point I.), but the bearing was able to react to the change with increased pressure. This type of error was not as sensitive to the average recess pressure (between points II. and III.) as the "step-up" type but was more dangerous from the film-thickness point of view. The bearing pad could not handle such an error at higher speeds. As expected, this type of offset error was more dangerous, and the slider and pad collision occurred at an error 0.25 mm (e/h = 1.92). The motor managed to pull the slider despite contact was observed (the slider stopped for a while and then continued with the movement). Therefore, the "step-down" tolerance must be within the film thickness height, and thus, the ratio e/h should be smaller than 1 to avoid the collision of the solid bodies. Although the average recess pressure almost did not reach the critical pressure area, the film thickness (Figure 14) was already around zero, which means that the slider error edge and pad were almost at the same level.

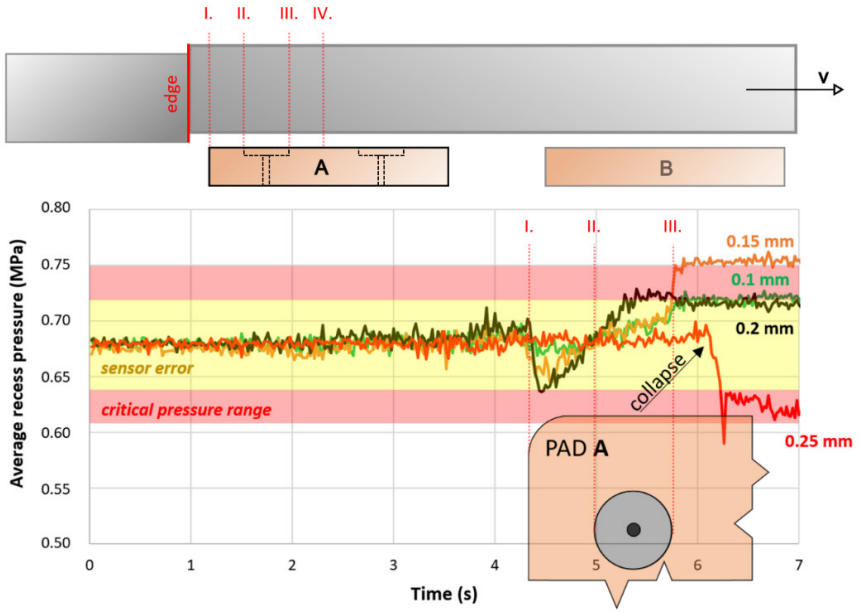

Figure 13. Average recess pressure value evolution in time for "step-down" error at 38 mm/s movement speed.

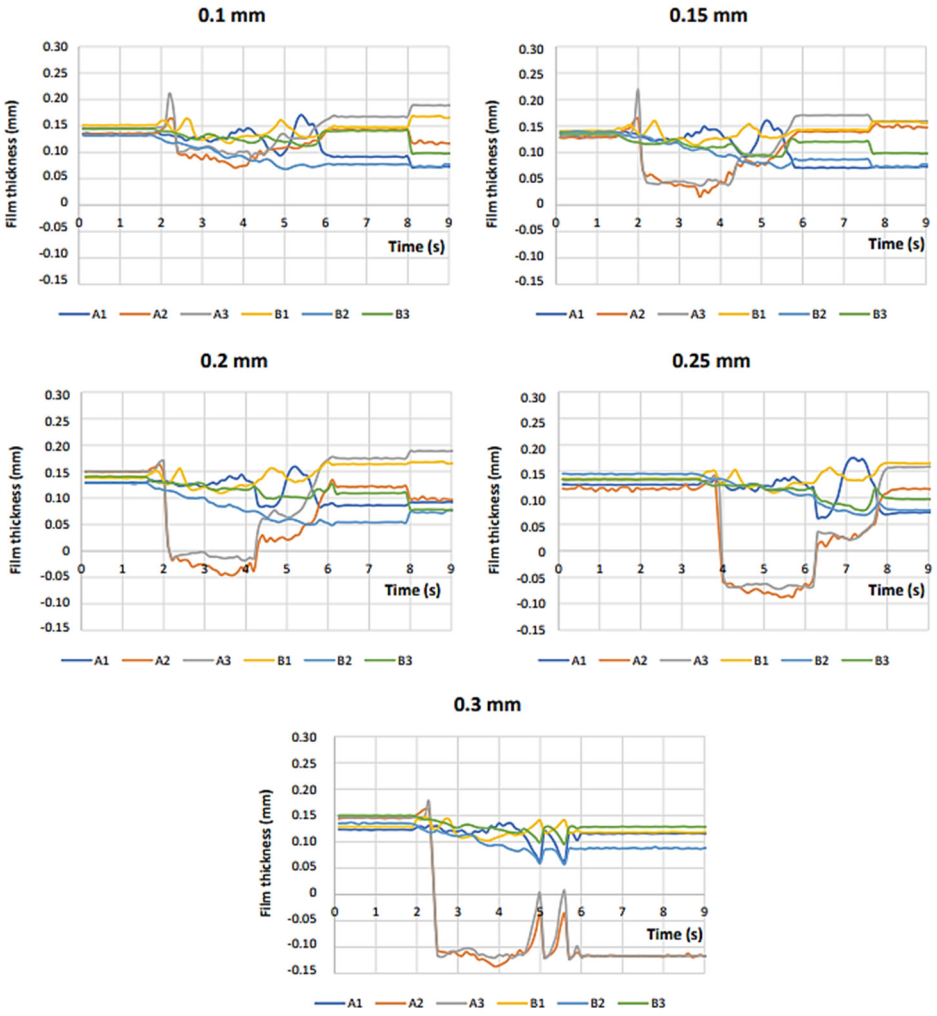

Figure 14. Film thickness evolution in time for the "step-down" error at 38 mm/s movement speed.

The error of 0.3 mm (e/h = 2.3) caused a total failure of the bearing. As seen in Figure 14, for this case, two sharp spikes were observed at sensors A2 and A3, respectively. The slider completely stopped its movement at the edge of the pad due to collision. The motor tried to pull the slider over the edge, which is what is explaining the two sharp spikes on the film thickness sensors, and then it was interrupted. The pads were manufactured without chamfers on the edges. This could surely help the bearing manage slightly higher assembly errors of the slider bodies but the contact of solid bodies would be inevitable. Considering the results obtained, we assume that the general recommendation for the offset error would be that the error value should be smaller than the film thickness, or rather, that the e/h ratio must be smaller than 1. The edge chamfer could help to avoid the impact, but most probably not the collision of the slider and pad bodies.

4. Conclusions

In this study, assembly error tolerance was assessed for large-scale HS bearings working under static and low-speed conditions. Two main types of errors were classified—offset and tilt. The study was carried out on an experimental HS bearing with complete performance diagnostics. The investigation was evaluated on information from pressure and distance sensors. Both types of errors were first investigated under static conditions. The maximum tolerance for offset error was found to be for the ratio of error-to-film-thickness of e/h = 2.5 for static conditions. Regarding tilt, two scenarios were tested: tilt centre in the middle of the pad and between the bearings. However, when assuming a movement of the slider, the maximum error tolerance was considered as $\theta = 0.46^{\circ}$ at the investigated distance. Thus, the greater the pad distance, the smaller the angular error tolerance. The angular error tolerance will decrease with increasing distance of the pads. Subsequently, the offset error was investigated under low-speed conditions (38 mm/s) for two cases—"step up" and "step down" error types. The critical error value was estimated for ratio e/h = 1.5 for "step-up" and e/h < 1 for "step-down", which means that the error tolerance is higher for static conditions, and that it is decreasing as the relative movement speed of the solid bodies increases. In case of bi-directional movement, the step-down error type should always be preferred, and the e/h ratio should not exceed 1 to avoid surface damage. The tolerance estimation approach provided in this study offers an experiment-based tool for design engineers and can help with assessment of the assembly process of such bearings on large scales. It can also be used to determine required film thickness for known magnitudes of error that occur in the final assembly, or to set limiting assembly errors based on the knowledge of the designed film thickness. Further research could aim to obtain error tolerance values depending on the relative speed of the solid bearing bodies. Numerical modelling of the case could provide insight into how the pressure field changes with different error magnitudes or during movement.

Author Contributions: Conceptualization, M.M. and P.S.; data curation, J.F.; formal analysis, T.D.; funding acquisition, P.S.; investigation, L.S. and D.J.; methodology, M.M.; project administration, P.S.; resources, M.Č.; software, T.D.; supervision, P.S.; validation, D.J. and M.Č.; Visualization, L.S.; writing—original draft, M.M.; writing—review and editing, J.F. All authors have read and agreed to the published version of the manuscript.

Funding: This research was carried out under the project FW03010357 with financial support from the state budget by the Technology Agency of the Czech Republic and the Ministry of Industry and Trade within the TREND Programme.

Data Availability Statement: The data presented in this study are available on request from the corresponding author.

Conflicts of Interest: The authors declare no conflict of interest.

References

1. Zha, J.; Chen, Y.; Zhang, P. Precision design of hydrostatic thrust bearing in rotary table and spindle. *Proc. Inst. Mech. Eng. Part B J. Eng. Manuf.* **2016**, *232*, 2044–2053. [CrossRef]
2. Bassani, R.; Piccigallo, B. *Hydrostatic Lubrication*, 22nd ed.; Elsevier B.V.: Amsterdam, The Netherlands, 1992.
3. Khonsari, M.M.; Booser, E.R. *Applied Tribology: Bearing Design and Lubrication*; John Wiley & Sons, Ltd.: Chichester, UK, 2017. [CrossRef]
4. Hamrock, B.J.; Schmid, S.R.; Jacobson, B.O. *Fundamentals of Fluid Film Lubrication*, 2nd ed.; Marcel Dekker: New York, NY, USA, 2004.
5. Breńkacz, Ł.; Witanowski, Ł.; Drosińska-Komor, M.; Szewczuk-Krypa, N. Research and applications of active bearings: A state-of-the-art review. *Mech. Syst. Signal. Process* **2021**, *151*, 107423. [CrossRef]
6. Fedorynenko, D.; Sapon, S.; Boyko, S.; Urlina, A. Increasing of energy efficiency of spindles with fluid bearings. *Acta Mech. Autom.* **2017**, *11*, 204–209. [CrossRef]
7. Michalec, M.; Svoboda, P.; Křupka, I.; Hartl, M. A review of the design and optimization of large-scale hydrostatic bearing systems. *Eng. Sci. Technol. Int. J.* **2021**, *24*, 936–958. [CrossRef]
8. Fedorynenko, D.; Kirigaya, R.; Nakao, Y. Dynamic characteristics of spindle with water-lubricated hydrostatic bearings for ultra-precision machine tools. *Precis. Eng.* **2020**, *63*, 187–196. [CrossRef]
9. Liu, Z.; Wang, Y.; Cai, L.; Zhao, Y.; Cheng, Q.; Dong, X. A review of hydrostatic bearing system: Researches and applications. *Adv. Mech. Eng.* **2017**, *9*, 1687814017730536. [CrossRef]
10. Liming, Z.; Yongyao, L.; Zhengwei, W.; Xin, L.; Yexiang, X. A review on the large tilting pad thrust bearings in the hydropower units. *Renew. Sustain. Energy Rev.* **2017**, *69*, 1182–1198. [CrossRef]
11. Bouyer, J.; Wodtke, M.; Fillon, M. Experimental research on a hydrodynamic thrust bearing with hydrostatic lift pockets: Influence of lubrication modes on bearing performance. *Tribol. Int.* **2022**, *165*, 107253. [CrossRef]
12. Stach, E.; Smolik, J.; Sulitka, M.; Lazak, T.; Divis, I.; Falta, J. Thermo-Mechanical Analysis of a Machine tool with Hydrostatic Bearings. *MM Sci. J.* **2022**, *2022*, 6180–6189. [CrossRef]
13. Jang, J.; Khonsari, M. On the Characteristics of Misaligned Journal Bearings. *Lubricants* **2015**, *3*, 27–53. [CrossRef]
14. Rowe, W.B. Advances in hydrostatic and hybrid bearing technology. *Proc. Inst. Mech. Eng. C J. Mech. Eng. Sci.* **1989**, *203*, 225–242. [CrossRef]
15. Fillon, M.; Wodtke, M.; Wasilczuk, M. Effect of presence of lifting pocket on the THD performance of a large tilting-pad thrust bearing. *Friction* **2015**, *3*, 266–274. [CrossRef]
16. Da Silva, H.A.P.; Nicoletti, R. Design of Tilting-Pad Journal Bearings Considering Bearing Clearance Uncertainty and Reliability Analysis. *J. Tribol.* **2019**, *141*, 011703. [CrossRef]
17. Wasilczuk, M.; Wodtke, M.; Dabrowski, L. Field tests on hydrodynamic and hybrid operation of a bidirectional thrust bearing of a pump-turbine. *Lubricants* **2017**, *5*, 48. [CrossRef]
18. Martinez Esparza, L.F.; Cervantes De Gortari, J.G.; Chicurel Uziel, E.J. Design of Hybrid Hydrostatic/Hydrodynamic Journal Bearings for Optimum Self-Compensation Under Misaligning External Loads. *J. Tribol.* **2015**, *139*, 041702. [CrossRef]
19. Ghezali, F.; Bouzidane, A.; Thomas, M. 3D Numerical investigation of pressure field of an orifice compensated hydrostatic bearing. *Mech. Ind.* **2017**, *18*, 101. [CrossRef]
20. Liu, Y.W.; Lin, S.C.; Chang, C.H.; Lan, P.-S. Design and test of hydrostatic built-in spindle compensated by orifice restrictors. In Proceedings of the 2018 IEEE International Conference on Advanced Manufacturing, ICAM 2018, Yunlin, Taiwan, 16–18 November 2019; pp. 302–305.
21. Khakse, P.G.; Phalle, V.M.; Mantha, S.S. Performance Analysis of a Nonrecessed Hybrid Conical Journal Bearing Compensated With Capillary Restrictors. *J. Tribol.* **2016**, *138*, 011703. [CrossRef]
22. Lin, S.C.; Lo, Y.H.; Lin, Y.H.; Tung, W.-T.; Lai, T.-H. Design and Performance Analysis of Dual Membrane Restrictor for Hydrostatic Bearing. *Lubricants* **2022**, *10*, 179. [CrossRef]
23. Rehman, W.U.R.; Luo, Y.X.; Wang, Y.Q.; Jiang, G.; Iqbal, N.; Rehman, S.U.; Bibi, S. Fuzzy logic-based intelligent control for hydrostatic journal bearing. *Meas. Control* **2019**, *52*, 229–243. [CrossRef]
24. Rehman, W.U.; Jiang, G.; Luo, Y.; Wang, Y.; Khan, W.; Rehman, S.U.; Iqbal, N. Control of active lubrication for hydrostatic journal bearing by monitoring bearing clearance. *Adv. Mech. Eng.* **2018**, *10*, 1687814018768142. [CrossRef]
25. Liang, X.; Yan, X.; Ouyang, W.; Wood, R.J.; Liu, Z. Thermo-Elasto-Hydrodynamic analysis and optimization of rubber-supported water-lubricated thrust bearings with polymer coated pads. *Tribol. Int.* **2019**, *138*, 365–379. [CrossRef]
26. Nijssen, J.; van Ostayen, R. Open Form Pressure Balancing for Compliant Hydrostatic Thrust Bearings. *Mech. Mach. Sci.* **2019**, *73*, 3965–3974.
27. Michalec, M.; Polnický, V.; Foltýn, J.; Svoboda, P.; Šperka, P.; Hurník, J. The prediction of large-scale hydrostatic bearing pad misalignment error and its compensation using compliant support. *Precis. Eng.* **2022**, *75*, 67–79. [CrossRef]
28. Wang, Z.; Zhao, W.; Chen, Y.; Lu, B. Prediction of the effect of speed on motion errors in hydrostatic guideways. *Int. J. Mach. Tools Manuf.* **2013**, *64*, 78–84. [CrossRef]
29. Rajput, A.K.; Sharma, S.C. Combined influence of geometric imperfections and misalignment of journal on the performance of four pocket hybrid journal bearing. *Tribol. Int.* **2016**, *97*, 59–70. [CrossRef]

30. Zoupas, L.; Wodtke, M.; Papadopoulos, C.I.; Wasilczuk, M. Effect of manufacturing errors of the pad sliding surface on the performance of the hydrodynamic thrust bearing. *Tribol. Int.* **2019**, *134*, 211–220. [CrossRef]
31. Fedorynenko, D.; Sapon, S.; Boyko, S. Accuracy of spindle units with hydrostatic bearings. *Acta Mech. Autom.* **2016**, *10*, 117–124. [CrossRef]
32. Zhang, P.H.; Chen, Y.L.; Zha, J. Relationship between geometric errors of thrust plates and error motions of hydrostatic thrust bearings under quasi-static condition. *Precis. Eng. J. Int. Soc. Precis. Eng. Nanotechnol.* **2017**, *50*, 119–131. [CrossRef]
33. Zha, J.; Chen, Y.; Wang, Z. A tolerance design method for hydrostatic guideways motion accuracy based on error averaging effect. *Procedia CIRP* **2018**, *75*, 196–201. [CrossRef]
34. Rippel, H. *Cast Bronze Hdyrostatic Bearing Design Manual*; Cast Bronze Institute, Inc.: Cleveland, OH, USA, 1969.

7 CONCLUSIONS

The dissertation thesis deals with large-scale HSB performance and safety improvement. The attention of research teams all over the world is mainly drawn by performance optimization and geometric error effect investigation on precision and bearing performance. Even though the HS lubrication was firstly demonstrated in the 19th century, the research interest in this lubrication regime has been rising over the years, and is still growing. Multiple approaches to design and optimization of such bearings were proposed over the years and a huge proportion of researchers and design engineers rely on them. Nonetheless, there are still some design aspects and procedures that are performed in an old-fashioned and not very effective way, or performed by estimation without an experimentally or numerically supported results. One of the primary factors of HS lubrication is the bearing geometry. The classical experimentally derived optimization method based on single-parameter pad shape optimization seems to serve well as a first iteration in design process, but further customization of the pad geometry might reduce the energy losses of the pump. The manufacturing precision and motion errors have been described in much detail, what allowed to improve the precision of HSB. Another very important factor is the precision of the HSB solid bodies, especially the assembly precision in the case of large-scale bearings. Pad misalignment was studied very briefly, with little attention paid to compliant support investigation. Segmented slider assembly errors have not yet been studied, even though large-scale HSB sliders are not possible to be manufactured in desirable precision for diameters exceeding tens of metres.

The first part of the thesis discusses all aspects of large-scale HSB design and optimization, including performance analyses, errors and materials. Subsequently, a novel approach to multi-recess pad geometry optimization using CFD is presented and validated based on experimental and analytical data. The latter part deals with pad and slider segment misalignment, based on experimental measurements.

The main aim of this thesis was to improve HSB performance and safety with the use of experimental and numerical methods. To be able to investigate the bearing performance in various cases and scenarios, an experimental HSB test rig was designed and developed as a part of the PhD thesis in collaboration with colleagues at the Institute of Machine and Industrial Design. The experimental rig data accuracy was validated against analytical data. Subsequently, methodological approach for geometry optimization using CFD simulation is presented and validated. Finally, allowed misalignment magnitudes of pad and slider segments are determined based on experimental data.

The presented thesis presents original results extending the knowledge in the area of hydrostatic bearing performance and safe operation. The results are confronted with previously published studies. The further step is to employ to develop a comprehensive

methodology for large-scale bearings working in the HS regime under real variable conditions.

The main contribution of the thesis can be summarized into the following points:

- A comprehensive summary of previously published research, current trends and future scope aimed at large-scale HSB design and optimization approaches was performed.
- A novel multi-recess pad shape optimization method of HSB based on CFD was developed.
- Experimental-based methodology for HSB compliant support design was suggested and compared with rigid support.
- For the first time, assembly errors of segmented sliders were assessed and experimentally investigated under static and low-speed conditions.

Regarding to scientific questions from chapter 4.1, the obtained knowledge can be summarized to the following concluding remarks:

A) Bearing performance

Q1: What is the influence of hydrostatic bearing recess position and size on the bearing performance?

H1: HYPOTHESIS WAS VERIFIED

- HSB pad geometry is one of the key parameters influencing its performance. Classical optimization approach is based on one parameter optimization of the recess size and position linked together. The proposed two parameter method shows that by adjusting recess size and position separately can influence the bearing performance and reduce energy losses up to 20 %.

B) Bearing safety:

Q2: How is the hydrostatic lubricating film affected by assembly errors of the bearing bodies?

H2: HYPOTHESIS WAS VERIFIED

- As the previous research indicated, compliant pad support for multi-pad HSB can help to compensate pad misalignment. Compared to the rigid support, compliant support allows 4 to 6 times larger misalignment depending on the misalignment type.

H3: HYPOTHESIS WAS VERIFIED

- The segmented slider errors, inclination and offset, have larger error tolerance under static conditions, depending on the distance between pads of multi-pad HSB when compared to the film thickness. As investigated the offset error under slow-speed conditions, the maximal allowed error to avoid solid bodies collision must be smaller than the film thickness.

8 LIST OF PUBLICATIONS & OUTCOMES

8.1 Publications related to the thesis topic

MICHALEC, M., P. SVOBODA, I. KŘUPKA, M. HARTL. A Review of the Design and Optimization of Large-scale Hydrostatic Bearing Systems. *Engineering Science and Technology, an International Journal*, 2021, vol. 24, issue 4, s. 936-958. ISSN: 2215-0986. [IF = 5.7] *(Author's contribution 70 %)*

MICHALEC, M., V. POLNICKÝ, J. FOLTÝN, P. SVOBODA, P. ŠPERKA, J. HURNÍK. The prediction of large-scale hydrostatic bearing pad misalignment error and its compensation using compliant support. *Precision engineering*. Elsevier, 2022, vol. 75, 67-79. doi:10.1016/j.precisioneng.2022.01.011 [IF = 3.6] *(Author's contribution 40 %)*

MICHALEC, M., J. HURNÍK, J. FOLTÝN, P. SVOBODA. Contactless measurement of hydrostatic bearing lubricating film using optical point tracking method. *Proceedings of the Institution of Mechanical Engineers, Part J: Journal of Engineering Tribology*, 2022, vol. 237, issue 1, 1-9. https://doi.org/10.1177/13506501221108138. [IF = 2.0] *(Author's contribution 40 %)*

MICHALEC, M., T. DRYML, D. JAVORSKÝ, L. SNOPEK, M. ČUPR, J. FOLTÝN, P. SVOBODA. Assembly error tolerance estimation for large-scale hydrostatic bearing segmented sliders under static and low speed conditions. *Machines*. MDPI, 2023, vol. 11, p.14. doi:10.3390/machines11111025 [IF = 2.6] *(Author's contribution 54 %)*

MICHALEC, M., M. ONDRA, M. SVOBODA, J. CHMELÍK, P. ZEMAN, P. SVOBODA, R. L. JACKSON. A novel geometry optimization approach for multi-recess hydrostatic bearing pad operating in static and low-speed conditions using CFD simulation. *Tribology Letters*. Elsevier, 2023, vol. 71, issue 52, p.14. doi:10.1016/j.precisioneng.2022.01.011 [IF = 3.2] *(Author's contribution 65 %)*

8.2 Other publications

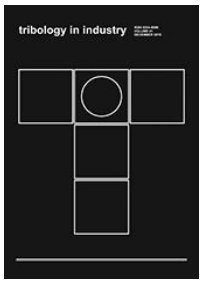

MICHALEC, M., P. SVOBODA, I. KŘUPKA, M. HARTL. Tribological behaviour of smart fluids influenced by magnetic and electric field – A review. *Tribology in Industry*, 2018, vol. 40, issue 4, pp. 515-528. ISSN: 0354-8996. [Citescore = 2.6]
(Author's contribution 65 %)

MICHALEC, M., P. SVOBODA, I. KRUPKA, M. HARTL a A. VENCL. Investigation of the tribological performance of ionic liquids in non-conformal EHL contacts under electric field activation. *Friction*, 2020, 8(5), 982-994. ISSN 2223-7690. Available from: doi:10.1007/s40544-019-0342-y [IF = 7.4]
(Author's contribution 65 %)

VENCL, A., M. KANDEVA, E. ZADOROZHNAYA, P. SVOBODA, M. MICHALEC, A. MILIVOJEVIĆ a U. TRDAN. Studies on structural, mechanical and erosive wear properties of ZA-27 alloy-based micro-nanocomposites. *Proceedings of the Institution of Mechanical Engineers, Part L: Journal of Materials: Design and Applications*, 2021. https://doi.org/10.1177/1464420721994870. [IF = 2.5]
(Author's contribution 5 %)

ČERNÁK, M., M. MICHALEC, M. VALENA, M. RANUŠA. Inlet shape optimization of pneumobil engine pneumatic cylinder using CFD analysis. Journal of Physics: Conference Series 1935. *Journal of Physics: Conference Series*, 2021. ISBN: 1742-6588. [Citescore = 0.7]
(Author's contribution 30 %)

8.3 Applied research outcomes

UTILITY MODELS

SVOBODA, P.; V. POLNICKÝ, M. MICHALEC, D. ROBENEK. Brno University of Technology, Antonínská 548/1, 60200 Brno, Veveří, Czech Republic, IČ: 216305 (40 %) Bosch Rexroth, spol. s r.o., Těžební 1238/2, 62700 Brno, Černovice, Czech Republic (60 %): Device for testing the operating conditions of segmental axial hydrostatic bearings. 35880, utility model (2022) URL:
https://isdv.upv.cz/doc/FullFiles/UtilityModels/FullDocuments/FDUM0035/uv035880.pdf

FUNCTIONAL SAMPLES

POLNICKÝ, V.; M. MICHALEC, P. SVOBODA, D. ROBENEK: Experimental stand for testing hydrostatic bearing of large structures in the area of special equipment. Laboratory A3/109 IMID, FME, BUT, Technická 2896/2 616 69 Brno, functional sample (2020). URL: https://intranet.ustavkonstruovani.cz/file-download/get-project-pdf/419

FOLTÝN, J.; POLNICKÝ, V.; MICHALEC, M.; SVOBODA, P.; MARTINEK, J.; ROBENEK, V.: Experimental device 3PAD; Hydrostatic bearing with feedback film thickness control. Laboratory B2/305 IMID, FME, BUT, Technická 2896/2 616 69 Brno, functional sample (2023). URL: https://intranet.ustavkonstruovani.cz/file-download/get-project-pdf/467.

8.4 Other outcomes

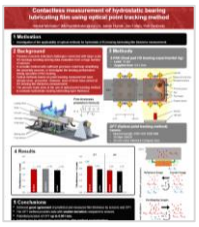

MICHALEC, M., J. HURNÍK, J. FOLTÝN, P. SVOBODA. Contactless measurement of hydrostatic bearing lubricating film using optical point tracking method. 7th World Tribology Congress 2022. 10.-15. 7. 2022 – Lyon, France. [Poster presentation].

9 LITERATURE

[1] Liu ZF, Wang YM, Cai LG, Zhao YS, Cheng Q, Dong XM. A review of hydrostatic bearing system: Researches and applications. Advances in Mechanical Engineering 2017;9. https://doi.org/10.1177/1687814017730536.

[2] Michalec M, Svoboda P, Křupka I, Hartl M. A review of the design and optimization of large-scale hydrostatic bearing systems. Engineering Science and Technology, an International Journal 2021. https://doi.org/10.1016/j.jestch.2021.01.010.

[3] Breńkacz Ł, Witanowski Ł, Drosińska-Komor M, Szewczuk-Krypa N. Research and applications of active bearings: A state-of-the-art review. Mech Syst Signal Process 2021;151:107423. https://doi.org/10.1016/j.ymssp.2020.107423.

[4] Bouyer J, Wodtke M, Fillon M. Experimental research on a hydrodynamic thrust bearing with hydrostatic lift pockets: Influence of lubrication modes on bearing performance. Tribol Int 2022;165:107253. https://doi.org/10.1016/J.TRIBOINT.2021.107253.

[5] Shang Y, Cheng K, Ding H, Chen S. Design of a Hydrostatic Spindle and Its Simulation Analysis with the Application to a High Precision Internal Grinding Machine. Machines 2022;10. https://doi.org/10.3390/machines10020127.

[6] Liu T, Li C, Duan R, Qu H, Chen F, Zhou Z, et al. Viscous Oil Film Thermal Modeling of Hydrostatic Bearings With a Rectangular Microgroove Surface. Front Energy Res 2022;10:1–11. https://doi.org/10.3389/fenrg.2022.891380.

[7] Li W, Wang G, Feng K, Zhang Y, Wang P. CFD-based investigation and experimental study on the performances of novel back-flow channel aerostatic bearings. Tribol Int 2022;165:107319. https://doi.org/10.1016/j.triboint.2021.107319.

[8] Helene M, Arghir M, Frene J. Numerical study of the pressure pattern in a two-dimensional hybrid journal bearing recess, laminar, and turbulent flow results. J Tribol 2003;125:283–90. https://doi.org/10.1115/1.1537233.

[9] Wang Y, Liu Z, Cheng Q, Zhao Y, Wang Y, Cai L. Analysis and optimization of nonlinear carrying performance of hydrostatic ram based on finite difference method and Runge–Kutta method. Advances in Mechanical Engineering 2019;11:1–12. https://doi.org/10.1177/1687814019856128.

[10] Cai LG, Wang YM, Liu ZF, Cheng Q. Carrying capacity analysis and optimizing of hydrostatic slider bearings under inertial force and vibration impact using finite difference method (FDM). Journal of Vibroengineering 2015;17:2781–94.

[11] Wang Y, Wu H, Rong Y. Analysis of Hydrostatic Bearings Based on a Unstructured Meshing Scheme and Turbulence Model 2022:1–18.

[12] Liu L, Lu L, Yu K, Gao Q, Zhao H, Chen W. A steady modeling method to study the effect of fluid–structure interaction on the thrust stiffness of an aerostatic spindle. Engineering Applications of Computational Fluid Mechanics 2022;16:453–68. https://doi.org/10.1080/19942060.2021.2024452.

[13] Fedorynenko D, Sapon S, Boyko S, Urlina A. Increasing of energy efficiency of spindles with fluid bearings. Acta Mechanica et Automatica 2017;11:204–9. https://doi.org/10.1515/AMA-2017-0031.

[14] Bassani R, Piccigallo B. Hydrostatic Lubrication. 1st ed. Elsevier Science & Technology; 1992.

[15] Jang J, Khonsari M. On the Characteristics of Misaligned Journal Bearings. Lubricants 2015;3:27–53. https://doi.org/10.3390/lubricants3010027.

[16] Fillon M, Wodtke M, Wasilczuk M. Effect of presence of lifting pocket on the THD performance of a large tilting-pad thrust bearing. Friction 2015;3:266–74. https://doi.org/10.1007/S40544-015-0092-4/METRICS.

[17] Da Silva HAP, Nicoletti R. Design of Tilting-Pad Journal Bearings Considering Bearing Clearance Uncertainty and Reliability Analysis. J Tribol 2019;141. https://doi.org/10.1115/1.4041021/401497.

[18] Wasilczuk M, Wodtke M, Dabrowski L. Field Tests on Hydrodynamic and Hybrid Operation of a Bidirectional Thrust Bearing of a Pump-Turbine. Lubricants 2017, Vol 5, Page 48 2017;5:48. https://doi.org/10.3390/LUBRICANTS5040048.

[19] Martinez Esparza LF, Cervantes De Gortari JG, Chicurel Uziel EJ. Design of Hybrid Hydrostatic/Hydrodynamic Journal Bearings for Optimum Self-Compensation Under Misaligning External Loads. J Tribol 2017;139. https://doi.org/10.1115/1.4035157.

[20] Beck A Van, Lepic L. Rubber supported hydrostatic thrust bearings with elastic bearing surfaces of infinite length 1996;201:45–50.

[21] Van Beek A, Segal A. Rubber supported hydrostatic thrust bearings with rigid bearing surfaces. Tribol Int 1997;30:47–52. https://doi.org/10.1016/0301-679X(96)00021-7.

[22] Liang X, Yan X, Ouyang W, Wood RJK, Liu Z. Thermo-Elasto-Hydrodynamic analysis and optimization of rubber-supported water-lubricated thrust bearings with polymer coated pads. Tribol Int 2019;138:365–79. https://doi.org/10.1016/j.triboint.2019.06.012.

[23] Wang Z, Zhao W, Chen Y, Lu B. Prediction of the effect of speed on motion errors in hydrostatic guideways. Int J Mach Tools Manuf 2013;64:78–84. https://doi.org/10.1016/J.IJMACHTOOLS.2012.07.011.

[24] Rajput AK, Sharma SC. Combined influence of geometric imperfections and misalignment of journal on the performance of four pocket hybrid journal bearing. Tribol Int 2016;97:59–70. https://doi.org/10.1016/J.TRIBOINT.2015.12.049.

[25] Zoupas L, Wodtke M, Papadopoulos CI, Wasilczuk M. Effect of manufacturing errors of the pad sliding surface on the performance of the hydrodynamic thrust bearing. Tribol Int 2019;134:211–20. https://doi.org/10.1016/j.triboint.2019.01.046.

[26] Fedorynenko D, Sapon S, Boyko S. Accuracy of spindle units with hydrostatic bearings. Acta Mechanica et Automatica 2016;10:117–24. https://doi.org/10.1515/ama-2016-0019.

[27] Zhang PH, Chen YL, Zha J. Relationship between geometric errors of thrust plates and error motions of hydrostatic thrust bearings under quasi-static condition. Precision Engineering-Journal of the International Societies For Precision Engineering and Nanotechnology 2017;50:119–31. https://doi.org/10.1016/j.precisioneng.2017.04.020.

[28] Zha J, Chen Y, Wang Z. A tolerance design method for hydrostatic guideways motion accuracy based on error averaging effect. Procedia CIRP 2018;75:196–201. https://doi.org/10.1016/j.procir.2018.04.054.

[29] Loeb AM, Rippel HC. Determination of optimum proportions for hydrostatic bearings. ASLE Transactions 1958;1:241–7. https://doi.org/10.1080/05698195808972336.

[30] Loeb AM. The Determination of the Characteristics of Hydrostatic Bearings through the use of the Electric Analog Field Plotter. A S L E Transactions 1958;1:217–24. https://doi.org/10.1080/05698195808972333.

[31] Khonsari MM, Booser ER. Applied Tribology: Bearing Design and Lubrication. vol. 3. Chichester, UK: John Wiley & Sons, Ltd; 2017. https://doi.org/10.1002/9781118700280.

[32] Yadav SK, Sharma SC. Performance of hydrostatic tilted thrust pad bearings of various recess shapes operating with non-Newtonian lubricant. Finite Elements in Analysis and Design 2014;87:43–55. https://doi.org/10.1016/j.finel.2014.04.009.

[33] Yadav SK, Sharma SC. Finite element analysis of tilted thrust pad bearings of various recesses shapes considering thrust pad flexibility. Proceedings of the Institution of Mechanical Engineers Part J-Journal of Engineering Tribology 2016;230:872–93. https://doi.org/10.1177/1350650115619610.

[34] Sharma SC, Jain SC, Bharuka DK. Influence of recess shape on the performance of a capillary compensated circular thrust pad hydrostatic bearing. Tribol Int 2002;35:347–56. https://doi.org/10.1016/S0301-679X(02)00013-0.

[35] Yu M, Yu X, Zheng X, Qu H, Yuan T, Li D. Influence of recess shape on comprehensive lubrication performance of high speed and heavy load hydrostatic thrust bearing. Industrial Lubrication and Tribology 2019;71:301–8. https://doi.org/10.1108/ILT-05-2018-0204.

[36] Rajasekhar Nicodemus E, Sharma SC. Orifice compensated multirecess hydrostatic/hybrid journal bearing system of various geometric shapes of recess operating with micropolar lubricant. Tribol Int 2011;44:284–96. https://doi.org/10.1016/j.triboint.2010.10.026.

[37] Yu MB, Yu XD, Zheng XH, Qu H, Yuan TF, Li DG. Influence of recess shape on comprehensive lubrication performance of high speed and heavy load hydrostatic thrust bearing. Industrial Lubrication and Tribology 2019;71:301–8. https://doi.org/10.1108/ILT-05-2018-0204.

[38] Khonsari MM, Booser RE. Applied tribology. vol. 3. 1970. https://doi.org/10.1016/0041-2678(70)90297-6.

[39] Rippel H. Cast Bronze Hdyrostatic Bearing Design Manual. Cleveland: Cast Bronze Institute, inc.; 1969.

[40] San Andres L. The Effect of Journal Misalignment on the Operation of a Turbulent Flow Hydrostatic Bearing. J Tribol 1993;115:355–63. https://doi.org/10.1115/1.2921643.

[41] Van Beek A, Segal A. Rubber supported hydrostatic thrust bearings with rigid bearing surfaces. Tribol Int 1997;30:47–52. https://doi.org/10.1016/0301-679X(96)00021-7.

[42] Xue F, Zhao W, Chen Y, Wang Z. Research on error averaging effect of hydrostatic guideways. Precis Eng 2012;36:84–90. https://doi.org/10.1016/j.precisioneng.2011.07.007.

[43] Zhang P, Chen Y, Liu X. Relationship between roundness errors of shaft and radial error motions of hydrostatic journal bearings under quasi-static condition. Precis Eng 2018;51:564–76. https://doi.org/10.1016/j.precisioneng.2017.10.012.

[44] Richardson LF. The approximate arithmetical solution by finite differences of physical problems involving differential equations, with an application to the stresses in a masonry dam. Philosophical Transactions of the Royal Society of London Series A, Containing Papers of a Mathematical or Physical Character 1911;210:307–57. https://doi.org/10.1098/rsta.1911.0009.

LIST OF FIGURES